Mathematics of biomimetics for active echo- and electro-sensing

Diss. ETH No. 27607

Mathematics of biomimetics for active echo- and electro-sensing

A thesis submitted to attain the degree of

DOCTOR OF SCIENCES of ETH ZURICH

(Dr. sc. ETH Zurich)

presented by

ANDREA SCAPIN

Laurea Magistrale in Matematica – Università degli Studi di Trieste

born July 8, 1990

citizen of Italy

accepted on the recommendation of

Prof. Dr. Habib Ammari, ETH Zurich, examiner

Prof. Dr. Elena Beretta, Politecnico di Milano, co-examiner

2021

Abstract

Active sensing animals may inspire the development of new technologies that mimic their sensing behavior. Electric fish, for instance, orient themselves at night in complete darkness by using their active electro-sensing system. They generate a stable, relatively high-frequency, weak electric field and perceive the transdermal potential modulations caused by nearby targets with different electromagnetic properties than the surrounding water. Since they have an electric sense that allows underwater navigation, target classification and intraspecific communication, they are privileged animals for bio-inspiring man-built autonomous systems. Bats, on the other hand, process the reflected echoes due to the presence of acoustic inclusions for echolocation. In general, they use acoustic waves for most of the perceptual tasks, that range from hunting to navigating.

This thesis introduces premier algorithms in electro-sensing and echo-sensing. The weakly electric fish is able to retrieve much more information about the target by approaching it. To mimic this behavior, an innovative (real-time) multi-scale method for target classification in electro-sensing is presented. The method is based on a family of transform-invariant shape descriptors computed from generalized polarization tensors (GPTs) reconstructed at multiple scales. The evidence provided by the different descriptors at each scale is fused using Dempster–Shafer Theory. Numerical simulations show that the recognition algorithm we proposed performs undoubtedly well and yields a robust classification. For real-world applications, inhomogeneous targets have to be identified. The shape descriptor-based classification algorithm is extended in order to consider inhomogenous material parameters. The approach is based on new invariants for the contracted generalized polarization tensors associated with inhomogeneous objects. The numerical simulations show that by comparing these invariants with those in a dictionary of precomputed homogeneous and inhomogeneous targets, one can successfully classify the inhomogeneous target.

Another problem concerns intraspecific electro-communication for weakly electric fish. In particular, a description on how the fish circumvent the jamming issue for both electro-communication and active electro-sensing is presented. The main result is a real-time tracking algorithm, which provides a new approach to the communication problem. It finds a natural application in robotics, where efficient communication strategies are needed to be implemented by bio-inspired underwater robots.

The concept of time-dependent polarization tensors (TDPTs) for the wave equation associated to a diametrically small acoustic inclusion, with constitutive parameters

different from those of the background and size smaller than the operating wavelength, is used to mimic the echo-sensing capabilities of a static bat. Firstly, the solution to the Helmholtz equation is considered, and a rigorous systematic derivation of a complete asymptotic expansion of the scattered field due to the presence of the inclusion is presented. Then, by applying the Fourier transform, the corresponding time-domain expansion is readily obtained after truncating the high frequencies. The new concept of TDPTs is shown to be promising for performing imaging. Numerical simulations are presented, showing that the TDPTs reconstructed from noisy measurements allow to image fine shape details of the inclusion.

Abstract (italian)

Animali che fanno *sensing* possono ispirare lo sviluppo di nuove tecnologie che mimichino le loro straordinarie abilità. I pesci elettrici, per esempio, si orientano di notte nella totale oscurità usando il loro *sensing* elettrico. Essi generano uno stabile e debole campo elettrico a frequenza relativamente alta, e percepiscono la modulazione di potenziale transdermico causata da oggetti dielettrici nelle vicinanze con proprietà materiali diverse da quelle dell'acqua. Possedendo un elettro-senso che permette loro la navigazione subacquea, classificazione di target e comunicazione intraspecifica, essi sono animali privilegiati per la costruzione di sistemi autonomi bio-ispirati. I pipistrelli, d'altra parte, elaborano l'eco riflesso originato dalla presenza di un'inclusione acustica per eco-localizzazione. In generale, essi sfruttano le onde acustiche per la maggior parte delle funzioni legate alla percezione, dal cacciare alla navigazione in volo.

In questa tesi si introducono algoritmi all'avanguardia nel campo del *sensing* elettrico ed acustico. Il pesce debolmente elettrico è in grado di recuperare molte più informazioni su un target avvicinandosi ad esso. Per mimare questo comportamento, viene presentato un innovativo metodo multi-scala per la classificazione dei target in tempo reale usando il *sensing* elettrico. Il metodo si basa su una famiglia di descrittori, invarianti per trasformazioni, che sono associati ai target dielettrici, e calcolati a partire dai tensori di polarizzazione generalizzati (GPTs) ricostruiti a diverse scale. L'evidenza data da differenti descrittori per ciascuna scala è fusa usando la teoria di Dempster–Shafer. Le simulazioni numeriche mostrano che l'algoritmo di riconoscimento proposto performa indubbiamente bene e fornisce una tecnica di classificazione robusta. D'altra parte, per applicazioni reali, è necessario essere in grado di identificare anche target che non sono omogenei. L'algoritmo di classificazione basato sui descrittori viene quindi esteso, in questa tesi, in modo da poter considerare anche parametri materiali eterogenei. L'approccio si basa su nuovi invarianti per i tensori (contratti) di polarizzazione generalizzati associati a oggetti eterogenei. Le simulazioni numeriche mostrano che è possibile identificare con successo un target comparandone gli invarianti con quelli appartenenti ad un dizionario di target omogenei e non.

Un altro problema riguarda l'elettro-comunicazione intraspecifica per il pesce debolmente elettrico. In particolare, viene presentata una descrizione su come il pesce possa aggirare il problema dell'interferenza per comunicare e per fare *sensing* attivo di un target. Il principale risultato è un algoritmo di tracking in tempo reale, il quale fornisce un nuovo approccio al problema della comunicazione. Ciò trova un naturale impiego in

robotica, dove robot subacquei hanno necessità di implementare efficienti strategie di comunicazione.

Il concetto di tensori di polarizzazione temporali (TDPTs) per l'equazione delle onde associati ad una inclusione acustica di piccolo diametro, con parametri materiali differenti da quelli del mezzo di background e taglia inferiore alla lunghezza d'onda operativa, può essere adoperato per mimare le capacità di *sensing* acustico di un pipistrello statico. Anzitutto, considerata la soluzione dell'equazione di Helmholtz, viene presentata una rigorosa e sistematica derivazione di una espansione asintotica completa del campo di scattering dovuto alla presenza dell'inclusione. Dopodiché, applicando la trasformata di Fourier, dopo aver troncato le alte frequenze, si ottiene la corrispondente espansione temporale. Il nuovo concetto di TDPTs appare di naturale impiego nei problemi di imaging. Vengono presentate simulazioni numeriche che mostrano come i TDPTs ricostruiti da misurazioni contaminate da rumore consentano di fare una ricostruzione di fini particolari dell'inclusione.

Contents

Introduction

In this thesis we present novel mathematical methods for bio-inspired imaging. In nature there exist some animals, such as weakly electric fish and bats, which possess extraordinary sensing abilities. While electric fish gather information on the surrounding waters by means of electrosensory organs, bats use their auditory system to perceive acoustic echoes and avoid obstacles. Taking inspiration from these biological observations, building improved autonomous robots that mimic their behavior is an intriguing challenge. This explains why active electro- and echo-sensing has motivated an increasing number of experimental, behavioral, biological, and computational studies.

Electric fish and electro-sensing

The biological behavior of weakly electric fish has been studied by scholars for years. These fish orient themselves at night in complete darkness by using electrosensory information, which makes these animals an ideal subject for developing bio-inspired imaging techniques. Such interest has motivated a huge number of studies addressing the active electro-sensing problem from many different perspectives since Lissmann and Machin's work [27, 28, 35, 54, 56, 55, 63, 75]. The growing interest in electro-sensing could be explained not only by the curiosity of discovering a sixth sense, electric perception, that is not one of our own senses, but also by potential bio-inspired applications in underwater robotics. Since they have an electric sense that allows underwater navigation, target classification and intraspecific communication, they are privileged animals for bio-inspiring man-built autonomous systems [37]. Building autonomous robots with electro-sensing technology may supply unexplored navigation, imaging and classification capabilities, especially when the sight is unreliable due to, for example, the turbidity of the surrounding waters or the poor lighting conditions [74, 39].

From the mathematical point of view, the electro-sensing problem is to detect and locate the dielectric target and to identify its shape and material parameters given the current distribution over the skin of the fish. The electric field perturbation due to the target is a complicated highly nonlinear function of its shape, electromagnetic parameters, and distance from the fish. Thus, understanding analytically this electric sensing is likely to give us insight in this regard [27, 28, 35, 56]. A simple physical model for the electric responses of the polarised targets has been proposed in [63]. The model shows that the target's position and size are intricately related in the measurements of the trans-cutaneous currents projected onto the skin. Numerical approaches have also been

driven for simplified geometries using a finite differences scheme in [46], a finite elements method in [49], and a boundary element method approach in [27]. The geometry of the fish is simplified by an ellipse and is divided into two areas: the thin skin with low conductivity and the interior of the body. In this simple model, the electric images projected onto the fish skin are fundamentally blurry and difficult to interpret [75, 76]. In [49], the skin's and body's conductivity values are optimized in order to approximate as well as possible the experimentally measured field. The result is that the optimal conductivity is not uniform, being higher in the tail region.

More recently, in [2], a rigorous model for the electro-location of a target around the fish has been derived. Using the fact that the electric current produced by the electric organ is time harmonic with a known fundamental frequency, a space-frequency location search algorithm has been introduced. Its robustness with respect to measurement noise and its sensitivity with respect to the number of frequencies, the number of sensors, and the distance to the target have been illustrated. In the case of disk- and ellipse-shaped targets, it has been shown that the conductivity, the permittivity, and the size of the targets can be reconstructed separately from multifrequency measurements. In [29], a capacitive sensing method has recently been implemented. It has been shown that the size of a capacitive sphere can be estimated from multifrequency electrosensory data. In [34], uniqueness and stability estimates to the considered electro-sensing inverse problem have been established. The electric current, which contains information on the target, is measured by a discrete number of receptors along the fish body. When enough measurements are collected, it is possible to recover the contracted generalized polarization tensors (CGPTs), which do encode information about the unknown target. One way in which the fish can acquire enough independent measurements is by exploiting the movement, i.e., by collecting several static measurements while swimming around the target [8]. In this way, it creates a synthetic-aperture view of the dielectric object that yields high-resolved reconstruction of its features. Although the inverse problem is severely ill-posed, classification works well. In [14] new shape descriptors, relying upon the CGPTs, which are invariant under rotations, translations, and scaling of the target, are found. In the previous works, a single circular trajectory around the target has been considered. In the two dimensional case, for small targets, the magnitude of the electric signal due to the presence of the target is of order ε^2, where ε is the length-scale, which is of the same order throughout the whole trajectory. In this type of setting it appears natural to reconstruct the target's features only up to some small order K^*, which is called the resolving order. These correspond to a finite number of Fourier modes of the signal. K^* is essentially determined by the signal-to-noise ratio (SNR), which sets a limit to the fineness of the reconstruction we are capable of; see, for instance, [6]. It has been shown that the reconstruction is accurate enough to perform a dictionary matching approach for homogeneous objects.

In Chapters 1 and 2 we investigate two significant extensions of the dictionary-based identification algorithm proposed in [6, 7].

In Chapter 1 we introduce a premier and innovative (real-time) multi-scale method

for target classification in electro-sensing. This is significant for instance for potential bio-inspired applications in underwater autonomous robotics, where it is important to improve the quality of the reconstruction of the features of a target by taking advantage of measurements which are at different length-scales. In particular, we aim at mimicking the behavior of the so-called weakly electric fish, which is able to retrieve much more information about the target when approaching it. We present a novel and complete analysis of the truncated acquisition operator, providing a full understanding of the reconstruction problem. In particular, our careful study of the reconstruction error boils down to the strategy of considering a multi-scale approach in order to design a classification algorithm that outperforms the single-scale ones. Based on this idea, evidence theory is applied to the electro-sensing problem in order to combine transform-invariant classifiers at multiple-scales. The expected enhancement of the recognition capabilities is corroborated by the numerical simulations.

In Chapter 2 we address the classification problem to make the algorithm applicable on more general targets rather than homogeneous. This extends the potential bio-inspired applications in underwater autonomous robotics. In real-life applications such devices could be surrounded by complex inhomogeneous objects and therefore they have to take into account the inhomogenities of the latters in the identification process. In this general context, a new multipole expansion is derived, showing that the generalized polarization tensors (GPTs) still appear as the natural quantities encoding the information about the small target. For such inhomogeneous GPTs new translation, rotation and scaling formulas are obtained. These formulas allow to build GPT-based transform invariants that can be used for performing a dictionary-matching algorithm for conductivity distributions identification. The good performance of the recognition procedure on a dictionary of coated/layered conductors when measurements are corrupted by noise is analyzed. Simulations show results which indicate that good recognition can be achieve with small noise-levels, even when the objects share a similar shape.

Besides electro-sensing, it is worth studying the behavior of two weakly electric fish when they populate the same environment. As a matter of fact, close-by active sensing animals may interfere with each other. For intraspecific electro-communication purposes, in processing sensory information, the fish has to separate feedback associated with their own signals from interfering sensations caused by signals from other animals. Wave and pulse species employ different mechanisms to minimize interference with electric organ discharges of conspecifics. It has been observed that certain wave species, having wave-type electric organ discharge (EOD) waveforms, such as Eigenmannia and Gymnarchus, reflexively shift their EOD frequency away from interfering frequencies of nearby conspecifics, in order to avoid "jamming" each others electrical signals. This phenomenon is known as *jamming avoidance response* (JAR) [36, 47, 48]. The electro-communication for the weakly electric fish has already been studied in the case of a simplified model consisting of a dipole-dipole interaction [78].

In Chapter 3 we aim at advancing the field of intraspecific electro-communication. In particular, we design and implement a real-time tracking algorithm for a fish to track another conspecific that is swimming nearby. In particular, we show that the following fish can sense the presence of the leading fish and can estimate its positions by using a MUSIC-type algorithm for searching its electric organ. The underlying idea is that a wave-type fish can passively communicate its own trajectory to fish populating the waters nearby. The capability of sensing each other movements is significant, for instance, for applications concerning robotics, where two or more underwater robots may implement such communication procedure to avoid collisions or to shoal. We also show that the fish can locate a small dielectric target which lies in its electro-sensing range even when another fish is swimming nearby, by filtering out its interfering signal and by applying the MUSIC-type algorithm developed in [2].

Bat and echo-sensing

Experimental data suggest that bats use temporal information for most, if not all, perceptual tasks. The bat perceives the phase of the sounds, which cover the 25- to 100-kilohertz frequency range, as these are represented in the auditory system after peripheral transformation. The acoustic image of a sonar target is apparently derived from time-domain or periodicity information processing by the nervous system [70, 71]. Echo-sensing is a form of acoustics that uses active sonar to locate and identify targets. Bats use this method to avoid collisions, to select, identify, and attack prey, and to navigate by emitting sounds and then analyzing the reflected waves. We aim at modeling perceptual and acoustic properties in echo-location. In [23], Ammari *et al.* introduced the concept of frequency-dependent polarization tensors (FDPTs) for a small inclusion. These tensors encode relevant information on the inclusion and appear naturally when we describe the perturbation of echoes emitted by animals such as bats [70, 71]. The extraction of the high-order FDPTs can be achieved from multi-static response (MSR) measurements [23, 25]. It appears natural to extend the shape reconstruction and classification methods for the frequency-domain proposed in [23, 25, 30] to the time-domain.

In Chapter 4 we model the problem of a static bat which is sending a wave and recording the scattering echoes due to the presence of an acoustic inclusion. We deal with the problem of reconstructing a small acoustic inclusion by using the new concept of time-dependent polarization tensors (TDPTs) for the wave equation. The TDPTs can be interpreted as an extension of the concept of the high-order FDPTs to the time-domain.

The results that are presented henceforth are published in [31, 67, 66, 32], each paper corresponding to a chapter of the thesis.

Part I.

Bio-inspired electro-sensing

1. Multi-scale classification for electro-sensing

Contents

1.1. Introduction

The results presented in this chapter are contained in [31]. The aim is to improve the recognition capabilities of the fish by acquiring measurements at different length-scales on multiple circular orbits around the target. The main advantage of the multi-scale configuration is that the descriptors introduced in [6] can be compared at different orders up to the resolving order, which is shown to be increasing with respect to the length-scale. This fact is revealed by a novel rigorous resolution analysis, which is an analysis of the condition number for the partial inversion of the acquisition operator. This also provides

a refined qualitative understanding of the fact that, when it comes to recovering coarse levels of information, the inverse problem becomes reasonably well-posed, and that one can progressively improve the reconstruction until the resolution reaches the maximum that data at different length-scales can provide [9, 10]. Ultimately, the aforementioned analysis leads to the idea of selecting different comparison orders, which produces different classifiers.

When many classifiers are available, the problem of combining them to enhance the classification capabilities naturally arises; see e.g. [80]. The approach we present in this chapter relies on the so-called Transferable Belief Model (TBM); see, for instance, [59]. The output of a scoring-classifier, i.e., a list of numerical scores (a score for each element of the dictionary) that corresponds to the evidence at hand, can be converted into a belief assignment. Following [50, 60], a natural way to translate the scores into beliefs is to consider the Shannon's entropy as a confidence factor associated to the evidence. Belief assignments are then combined by means of some combination rule, such as the Dempster–Shafer rule, in order to obtain a synthetized new belief that pulls together all the information. This approach is particularly suitable for the electro-sensing problem hereabove. Since the fish is able to retrieve much more information about its shape and material parameters when approaching it, the classification is expected to be more robust as soon as multiple circular orbits are considered.

The chapter is structured as follows. In Section 1.2, a preliminary description of the experimental design for electro-sensing is discussed. We show that the design matrix associated to the forward linear operator $\mathcal{L}$ defined in [7] can be expressed as a generalized block Kronecker product by vectorization; see [65, 57]. A reflexive minimum norm g-inverse of the acquisition operator, arising in a natural way from the block Kronecker structure, is also used. This has been recently introduced in [57] in the context of bivariate polynomial regression. Based on Greville's well known formulas in [42], this g-inverse provides a method to update recursively the estimates position after position right away.

In Section 1.3, a detailed analysis of the structure of the design matrix is carried out. In particular, the need of creating a synthetic-aperture view is readily understood by inspecting the rank of the design matrix. Assuming a circular acquisition setting, i.e., the fish collects the data swimming on a circular trajectory around the target, an estimate on the reconstruction error of the CGPTs is derived. The estimate has an upper bound depending on the length-scale, and it is formally equal to that given in [6]. Finally, issues related to limited-view data, i.e., data collected by receptors covering a limited angle of view, are discussed. In particular, a study of the spectrum of the matrix of receptors shows the impact of the angle of view on the reconstruction: the closer the angle of view is to 2π, the more informative the estimate becomes. Furthermore, if the reconstruction order is small, the limited-view configuration has a minor impact on the reconstructed CGPTs.

In Section 1.4, the classification problem based on a multi-scale acquisition setting is addressed. In particular, measurements at different length-scales are used to improve

the resolving power in the reconstruction of the CGPTs. As a matter of fact, the closer the orbit is to the target, the higher the SNR, and the higher the order of CGPTs-based descriptors that can be used in the comparison. A matching algorithm, which generalizes the one proposed in [7] to the case study we consider, is presented. First, a certain number of concentric orbits around the target are thoroughly chosen. On each orbit, a comparison between the theoretical and measured shape descriptors up to a properly chosen length-scale dependent order is required. Similarly to [7], the comparison is done by means of a given metric, and it yields a list of scores. The normalized list of scores produced on each orbit is converted into an evidence distribution, which is then stored. The Shannon's entropy is used as a confidence factor; see [50, 60]. The evidence distributions computed along different orbits are subsequently combined by using the TBM conjunctive rule introduced in [73].

In Section 1.5 we perform numerical simulations in order to test the performance of the recognition algorithm, introduced in Section 1.4, on a particular dictionary of dielectric targets. The reported results show an enhancement of the recognition rate, corroborating the idea that combining descriptors at different length-scales makes the classification more robust. Both the minimum norm reflexive generalized inverse and the Moore–Penrose inverse are used in the reconstruction.

1.2. Model specification for electro-sensing

Let us now briefly summarize the model of electro-sensing derived in [2]: the body of the fish is Ω, an open bounded set in $\mathbb{R}^2$, with smooth boundary $\partial\Omega$, and with outward normal unit vector denoted by ν. The electric organ is a dipole $f(x)$ inside Ω or a sum of point sources inside Ω satisfying the charge neutrality condition. The skin of the fish is very thin and highly resistive. Its effective thickness, that is, the skin thickness times the contrast between the water and the skin conductivities, is denoted by ξ, and it is much smaller than the fish size. We assume that the conductivity of the background medium is one. We consider a smooth bounded target $D = \delta B$, and B is a smooth bounded domain containing the origin. We assume that the conductivity of D is $0 < k \neq 1$, and we define the contrast $\lambda := (k+1)/(2(k-1))$. In the presence of D, the electric potential emitted by the fish is the solution to the following equations:

$$\begin{cases} \Delta u = f & \text{in } \Omega, \\ \nabla \cdot (1 + (k-1)\chi_D)\nabla u = 0 & \text{in } \mathbb{R}^2 \setminus \overline{\Omega}, \\ u|_+ - u|_- = \xi \left.\dfrac{\partial u}{\partial \nu}\right|_+ & \text{on } \partial\Omega, \\ \left.\dfrac{\partial u}{\partial \nu}\right|_- = 0 & \text{on } \partial\Omega, \\ |u(x)| = O(|x|^{-1}) & \text{as } |x| \to \infty. \end{cases} \tag{1.1}$$

Here, χ_D is the characteristic function of D, $\partial/\partial\nu$ is the normal derivative, and $|_\pm$ denotes the limits from, respectively, outside and inside Ω. Following [7], we introduce the function H defined as

$$H(x) := p(x) + \mathcal{S}_\Omega\left[\left.\frac{\partial u}{\partial \nu}\right|_+\right] - \xi\mathcal{D}_\Omega\left[\left.\frac{\partial u}{\partial \nu}\right|_+\right], \tag{1.2}$$

where $\Delta p = f$ on $\mathbb{R}^2$. $\mathcal{S}_\Omega$ and $\mathcal{D}_\Omega$ are the single- and double-layer potentials, respectively, defined in Appendix A.1. It is readily seen that the following representation formula holds:

$$u(x) - H(x) = \mathcal{S}_D(\lambda I - \mathcal{K}_D^*)^{-1}\left(\frac{\partial H}{\partial \nu}\right), \tag{1.3}$$

where I is the identity and $\mathcal{K}_D^*$ is the Neumann–Poincaré operator associated to the target D; see Appendix A.1.

1.2.1. Data acquisition system

In this section we aim at describing the data acquisition system, i.e., the experimental setting we shall adopt to solve the inverse problem.

As we briefly mentioned in the introduction, the fish use the movement in order to swim around the target, creating a synthetic aperture view.

Suppose that the scanning movement consists of a single circular orbit $\mathcal{O}$, with radius ρ, the target being located at its center. On each orbit only a discrete number of positions accounts for the data acquisition process. Precisely, M different positions are sampled along $\mathcal{O}$, and for each position s the corresponding electric signal $u^{(s)} - H^{(s)}$ is measured by N_r receptors on the skin, $\{x_r^{(s)}\}_{r=1}^{N_r}$. Here $u^{(s)}$ and $H^{(s)}$ denote the solution to (2.1) and the function defined by (1.2), associated to the position s, respectively.

This type of architecture resembles a multi-static single-input multi-output (SIMO) system.

Symbol	*Meaning*
Ω_s	Fish body
$\mathbf{p}_s$	dipole moment
ζ_s	electric organ
$x_r^{(s)}$	r-th receptor
$u^{(s)}$	electric potential solution to (2.1)
$H^{(s)}$	function defined in (1.2)
N_r	number of receptors
M	number of positions
$\mathcal{O}$	circular orbit

Table 1.1.: Notation referring to position $s \in \{1, \dots, M\}$ on the orbit $\mathcal{O}$.

For any orbit $\mathcal{O}$ we get an $N_r \times M$ matrix of data $\mathbf{Q}$, which is called multi-static response (MSR) matrix, whose (r, s)-entry is defined as

$$(\mathbf{Q})_{r,s} = u^{(s)}(x_r^{(s)}) - H^{(s)}(x_r^{(s)}). \tag{1.4}$$

Henceforth, we shall use the MATLAB colon notation for specifying submatrices of a given matrix. For instance, given matrix $\mathbf{X}$, we shall denote by $\mathbf{X}_{i,:}$ (resp. $\mathbf{X}_{:,j}$) the ith row (resp. the jth column) of $\mathbf{X}$.

1.2.2. Data acquisition operator

In order to simplify the notation, without loss of generality, we assume that the dielectric object is centered at the origin and that the impedance of the fish is $\xi = 0$.

We recall the following theorem which provides an expansion of (1.4); see [7].

Theorem 1.2.1 *Consider M different positions of the fish along the circular orbit $\mathcal{O}$ of radius ρ, with ρ large enough, indexed by $s = 1, \dots, M$. Let $\{x_r^{(s)}\}_{r=1}^{N_r}$ be a set of receptors distributed on $\partial\Omega_s$, the dipole located at $\zeta_s \in \mathcal{O}$ with dipole moment $\mathbf{p}_s$, and $K \geq 1$. Then the following expansion holds:*

$$u^{(s)}(x_r^{(s)}) - H^{(s)}(x_r^{(s)}) = \sum_{m+n=1}^{K+1} \underbrace{\begin{bmatrix} A_{s,m} & B_{s,m} \end{bmatrix}}_{\mathbf{S}_{s,m}} \underbrace{\begin{bmatrix} M_{mn}^{cc} & M_{mn}^{cs} \\ M_{mn}^{sc} & M_{mn}^{ss} \end{bmatrix}}_{\mathbf{M}_{mn}} \underbrace{\begin{bmatrix} \cos n\theta_{x_r^{(s)}} \\ \sin n\theta_{x_r^{(s)}} \end{bmatrix} \frac{-1}{2\pi n r^n_{x_r^{(s)}}}}_{\mathbf{G}_{rn}^{(s)\top}} + O(\delta^{K+2}), \tag{1.5}$$

where $M_{mn}^{cc}, M_{mn}^{cs}, M_{mn}^{sc}$ and M_{mn}^{ss} are as in Definition A.1.5, $r = 1, \dots, N_r$,

$$\begin{aligned} A_{s,m} &= -\frac{(-1)^m}{2\pi} \mathbf{p}_s \cdot \begin{bmatrix} \phi_{m+1}(\zeta_s) \\ \psi_{m+1}(\zeta_s) \end{bmatrix} - \frac{1}{2\pi m} \int_{\partial\Omega_s} \left. \frac{\partial u^{(s)}}{\partial \nu} \right|_+ (y) \phi_m(y) \, d\sigma_y, \\ B_{s,m} &= \frac{(-1)^m}{2\pi} \mathbf{p}_s \cdot \begin{bmatrix} -\psi_{m+1}(\zeta_s) \\ \phi_{m+1}(\zeta_s) \end{bmatrix} - \frac{1}{2\pi m} \int_{\partial\Omega_s} \left. \frac{\partial u^{(s)}}{\partial \nu} \right|_+ (y) \psi_m(y) \, d\sigma_y, \end{aligned} \tag{1.6}$$

$$\phi_m(x) = \frac{\cos(m\theta_x)}{r_x^m}, \qquad \psi_m(x) = \frac{\sin(m\theta_x)}{r_x^m},$$

and

$$\mathbb{M}^{(K)} = \mathbb{M} = \begin{bmatrix} \mathbf{M}_{11} & \mathbf{M}_{12} & \dots & \mathbf{M}_{1K} \\ \mathbf{M}_{21} & & \iddots & \mathbf{0} \\ \vdots & \iddots & \iddots & \vdots \\ \mathbf{M}_{K1} & \mathbf{0} & \dots & \mathbf{0} \end{bmatrix} \tag{1.7}$$

is the upper antidiagonal block matrix of the CGPTs of order $\leq K$*. Here,* $\top$ *denotes the transpose of a matrix.*

We define $\varepsilon = \delta/\rho$ as the length-scale associated to the orbit $\mathcal{O}$, i.e., the ratio between the size of the target and the distance ρ.

A more careful analysis of the reminder in formula (1.5) shows that the remainder can be expressed in terms of the length-scale ε, and written as $O(\varepsilon^{K+2})$. See Appendix A.3.

By Theorem 1.2.1, the rows of $\mathbf{Q}$ admit the following expansions:

$$(\mathbf{Q})_{:,s} = \mathcal{L}^{(s)}(\mathbb{M}^{(K)}) + \mathbf{E}_{:,s}, \qquad \|\mathbf{E}_{:,s}\|_\infty = O(\varepsilon^{K+2}), \qquad s = 1, ..., M, \tag{1.8}$$

where $\mathcal{L}^{(s)} : \mathcal{M}_{2K,2K} \longrightarrow \mathbb{R}^{N_r}$ is the linear map defined by (1.5), i.e., $\mathcal{L}^{(s)}(\mathbb{M}) = \mathbf{G}^{(s)}\,\mathbb{M}\,\mathbf{S}^\top_{s,:}$, K is the truncation order, and $\varepsilon = \delta/\rho$ is the length-scale associated to the orbit $\mathcal{O}$. Thus, we can write the expansion of the complete MSR matrix as follows:

$$\mathbf{Q} = \mathcal{L}(\mathbb{M}^{(K)}) + \mathbf{E}, \qquad \|\mathbf{E}\|_\infty = O(\varepsilon^{K+2}). \tag{1.9}$$

The linear map $\mathcal{L} : \Theta \subseteq \mathcal{M}_{2K,2K} \longrightarrow \mathcal{M}_{N_r,M}$ is the truncated output (or forward) operator.

The acquisition operator $\mathcal{L}(\mathbb{M})$ is defined by (1.5). More precisely, it can be written as

$$\mathcal{L}(\mathbb{M}) = \begin{bmatrix}\mathcal{L}^{(1)}(\mathbb{M}) & \mathcal{L}^{(2)}(\mathbb{M}) & \dots & \mathcal{L}^{(M)}(\mathbb{M})\end{bmatrix} = \begin{bmatrix}\mathbf{G}^{(1)}\,\mathbb{M}\,\mathbf{S}^\top_{1,:} & \dots & \mathbf{G}^{(M)}\,\mathbb{M}\,\mathbf{S}^\top_{M,:}\end{bmatrix},$$

where

$\mathcal{L}^{(s)}(\mathbb{M}) =$ 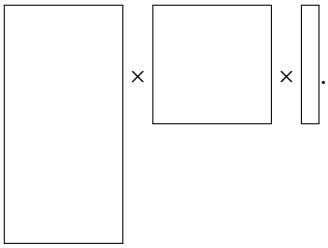 .

We define block matrices $\mathbf{G} \in \mathcal{M}_{M,1}(\mathcal{M}_{N_r,2K})$, $\mathbf{S} \in \mathcal{M}_{M,1}(\mathcal{M}_{1,2K})$ by vertically stacking the matrices, as in Figure 1.1.

We are interested in estimating the matrix parameter $\mathbb{M}$ from the MSR matrix $\mathbf{Q}$. Therefore, we aim at solving the following minimization problem

$$\min_{\mathbb{M} \perp \ker(\mathcal{L})} \|\mathcal{L}(\mathbb{M}) - \mathbf{Q}\|_{\mathrm{F}}, \tag{1.10}$$

where $\|\cdot\|_{\mathrm{F}}$ denotes the Frobenius norm of a matrix.

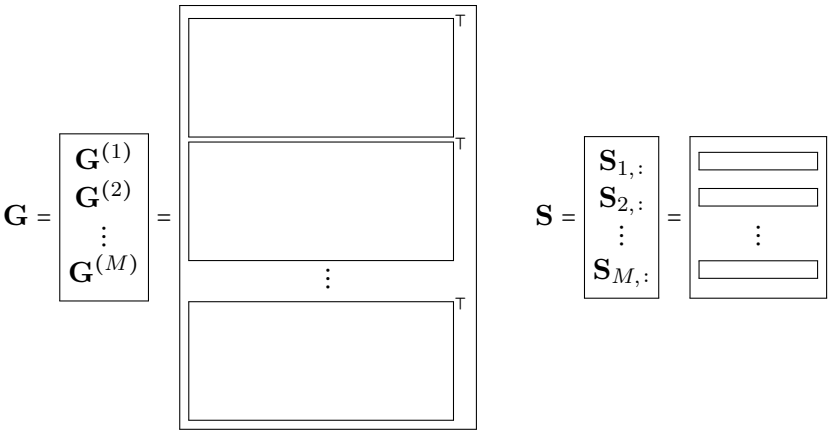

Figure 1.1.

1.2.3. Generalized Kronecker form of the forward operator

In this section we vectorize the data acquisition operator $\mathcal{L} : \mathcal{M}_{2K,2K} \longrightarrow \mathcal{M}_{N_r,M}$ in order to find a matrix representation.

Lemma 1.2.2 *The operator $\mathcal{L}$ defined by* (1.2.2) *can be represented in a vectorized form employing the product defined in Definition A.2.3:*

$$vec(\mathcal{L}(\mathbb{M})) = (\mathbf{S} \otimes \{\mathbf{G}^{(s)}\})\, vec(\mathbb{M}).$$

Proof. By definition,

$$\mathcal{L}(\mathbb{M}) = \left[\mathbf{G}^{(1)}\,\mathbb{M}\,\mathbf{S}_{1,:}^{\top} \quad \dots \quad \mathbf{G}^{(M)}\,\mathbb{M}\,\mathbf{S}_{M,:}^{\top}\right].$$

Therefore

$$\begin{aligned}
\operatorname{vec}(\mathcal{L}(\mathbb{M})) &= \operatorname{vec}\left[\mathbf{G}^{(1)}\,\mathbb{M}\,\mathbf{S}_{1,:}^{\top} \quad \dots \quad \mathbf{G}^{(M)}\,\mathbb{M}\,\mathbf{S}_{M,:}^{\top}\right] \\
&= \begin{bmatrix} \mathbf{G}^{(1)}\,\mathbb{M}\,\mathbf{S}_{1,:}^{\top} \\ \vdots \\ \mathbf{G}^{(M)}\,\mathbb{M}\,\mathbf{S}_{M,:}^{\top} \end{bmatrix} \\
&= \begin{bmatrix} (\mathbf{S}_{1,:} \otimes \mathbf{G}^{(1)})\operatorname{vec}(\mathbb{M}) \\ \vdots \\ (\mathbf{S}_{M,:} \otimes \mathbf{G}^{(M)})\operatorname{vec}(\mathbb{M}) \end{bmatrix} \\
&= \begin{bmatrix} \mathbf{S}_{1,:} \otimes \mathbf{G}^{(1)} \\ \vdots \\ \mathbf{S}_{M,:} \otimes \mathbf{G}^{(M)} \end{bmatrix} \operatorname{vec}(\mathbb{M}) \\
&= (\,\mathbf{S} \otimes \{\mathbf{G}^{(s)}\}\,)\operatorname{vec}(\mathbb{M}).
\end{aligned}$$

□

Notice that the matrix $\mathbf{L} \in \mathcal{M}_{MN_r,4K^2}$ defined by

$$\mathbf{L} := \mathbf{L}_{\mathcal{L}} = \mathbf{S} \otimes \{\mathbf{G}^{(s)}\} \tag{1.11}$$

is the unique $MN_r \times 4K^2$ matrix such that $\mathrm{vec}(\mathcal{L}(\mathbf{X})) = \mathbf{L}_{\mathcal{L}}\mathrm{vec}(\mathbf{X})$, for all $\mathbf{X} \in \mathcal{M}_{2K,2K}$.

Hence, minimization problem (1.10) assumes the following form

$$\min_{\mathbb{M}} \|\mathbf{L}_{\mathcal{L}}\mathrm{vec}(\mathbb{M}) - \mathrm{vec}(\mathbf{Q})\|_2. \tag{1.12}$$

We aim at seeking a vector $\mathrm{vec}(\widehat{\mathbb{M}})$ which is optimal in the least-squares sense.

As is well known, the standard least-squares estimator for (1.12) is given by the Moore-Penrose inverse of $\mathbf{L}$, denoted by $\mathbf{L}^{\dagger}$. If $\mathbf{L}$ is full column rank, than

$$\mathrm{vec}(\widehat{\mathbb{M}})_{MP} = \mathbf{L}^{\dagger}\mathrm{vec}(\mathbf{Q}) = (\mathbf{L}^{\top}\mathbf{L})^{-1}\mathbf{L}^{\top}\mathrm{vec}(\mathbf{Q}). \tag{1.13}$$

However, the special block Kronecker form of $\mathbf{L}$ suggests employing the following generalized inverse [57].

Theorem 1.2.3 *If* $\mathbf{S}$ *and* $\mathbf{G}^{(s)}$ *for* $s = 1, \ldots, M$*, are full column rank, then*

$$\mathfrak{L} := \mathbf{S}^{\dagger} \otimes_C \{\mathbf{G}^{(s)\dagger}\} \tag{1.14}$$

is a reflexive minimum norm g-inverse of $\mathbf{L}_{\mathcal{L}} = \mathbf{S} \otimes \{\mathbf{G}^{(s)}\}$*. Here* $\otimes_C$ *denotes the column-wise generalized Kronecker product defined in Definition A.2.4, and* † *denotes the Moore–Penrose inverse.*

Proof. The proof is readily obtained by noticing that

$$(\mathbf{S}^{\dagger} \otimes_C \{\mathbf{G}^{(s)\dagger}\})(\mathbf{S} \otimes \{\mathbf{G}^{(s)}\}) = \mathbf{I}_{4K^2}.$$

□

This particular generalized inverse is useful for solving (1.12) when $\mathrm{vec}(\mathbf{Q})$ lies in the range of $\mathbf{L}_{\mathcal{L}}$ [57]. Notice that $\mathfrak{L}$ is not the same as $\mathbf{L}^{\dagger}$ in general.

As we shall see later, the g-inverse given by (1.14) is particularly suitable for establishing a bound on the reconstruction error as well as for designing a recursive online estimation of the GPTs. Figure 1.2 schematically shows the computation of $\mathfrak{L}$.

1.2.4. Online reconstruction

In this section we propose very simple formulas to efficiently perform an online reconstruction of the features.

By inspecting the form of the g-inverse $\mathfrak{L}$ given by (1.14) it is easy to see that, when a new position becomes available, the pseudoinverse of the augmented source matrix $\mathbf{S}$ is the only term which needs to be recomputed. As shown in Figure 1.3, the pseudoinverses of the matrices $\mathbf{G}^{(s)}$ corresponding to different positions intervene in $\mathfrak{L}$ without interfering with each other. Therefore we have the following result.

Lemma 1.2.4 *Let us denote by $\mathfrak{L}_M$ the generalized inverse given by* (1.14) *for $M \gg 1$ positions, and let $\mathbf{S}_{M+1,:}$ be full column rank. Then*

$$\mathfrak{L}_{M+1} = \left[\mathbf{S}^{\dagger}_{1:M,:} - \mathbf{K}_{M+1}\mathbf{d}_{M+1} \quad | \quad \mathbf{K}_{M+1}\right] \otimes_C \{\mathbf{G}^{(s)\,\dagger}\}, \tag{1.15}$$

where

$$\mathbf{d}_{M+1} := \mathbf{S}_{M+1,:}\mathbf{S}^{\dagger}_{1:M,:},$$

and

$$\mathbf{K}_{M+1} := (1 + \mathbf{d}_{M+1}\mathbf{d}^{\top}_{M+1})^{-1}\mathbf{S}^{\dagger}_{1:M,:}\mathbf{d}^{\top}_{M+1}.$$

Proof. Appending new positions affects only the factor $\mathbf{S}$, which can be updated by means of Greville's recursive formula for the pseudoinverse; see [81]. □

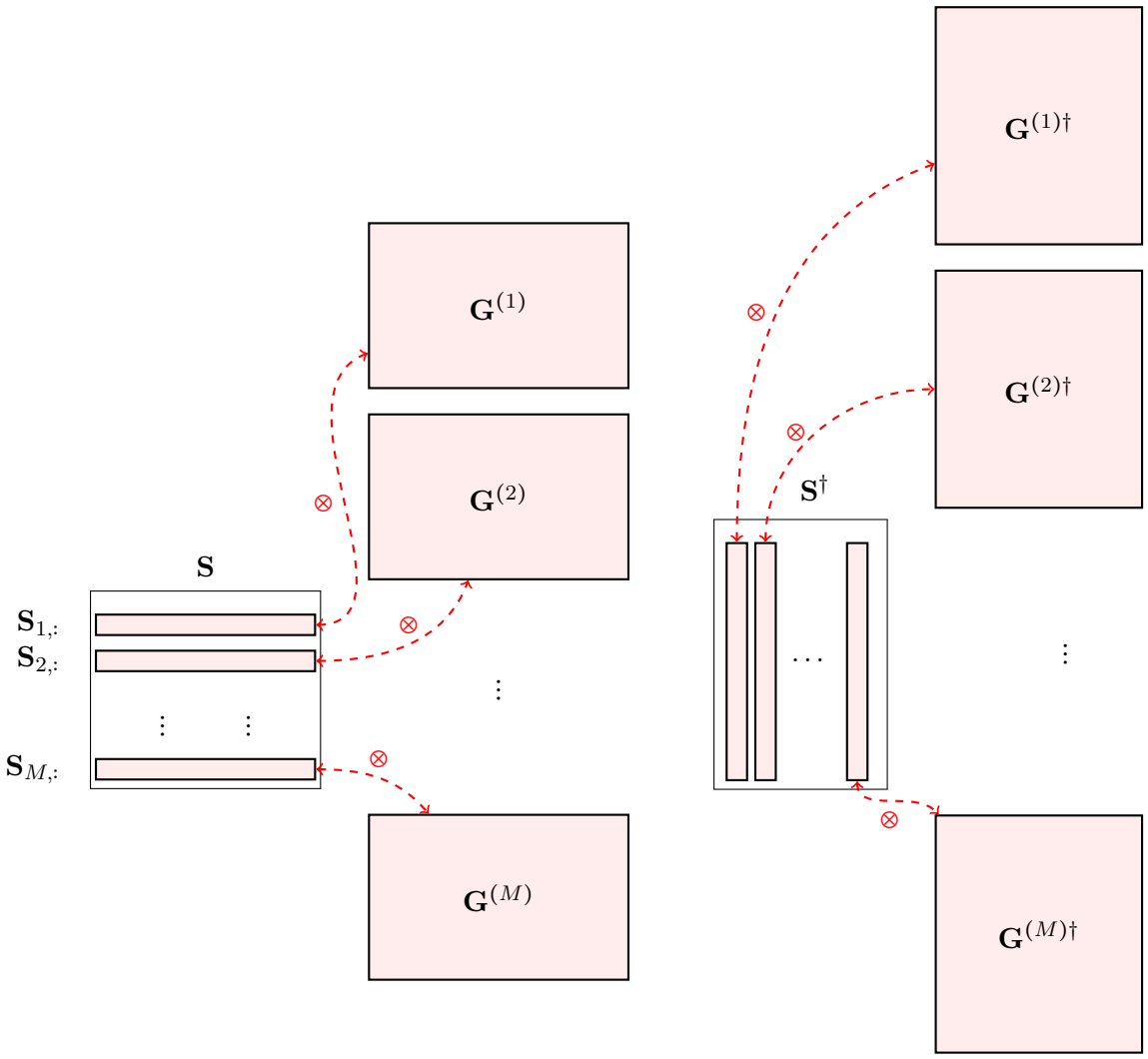

Figure 1.2.: On the left, the operator $\mathbf{L}$; on the right, its generalized inverse, i.e., $\mathfrak{L}$.

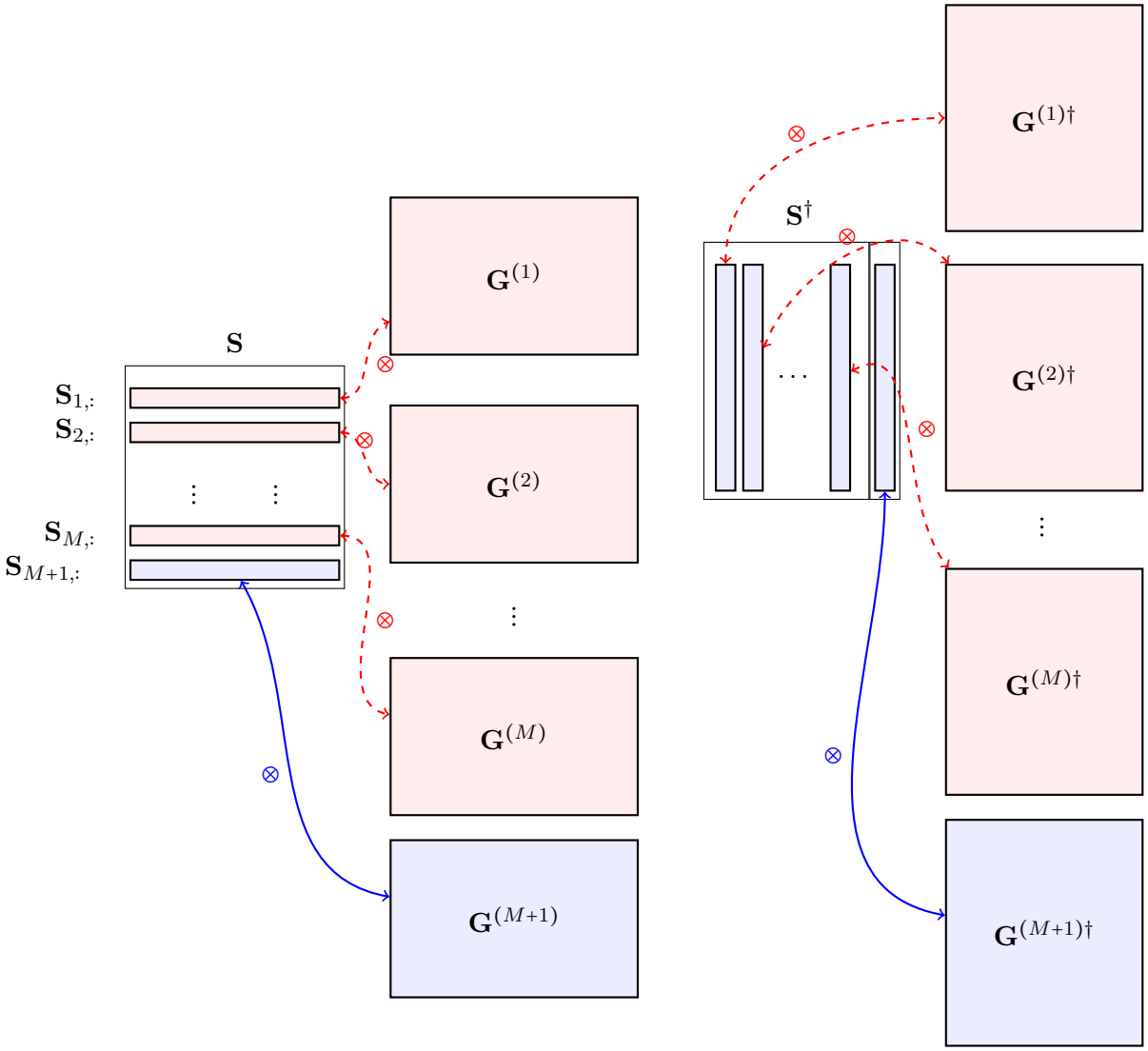

Figure 1.3.: On the left, the augmented operator $\mathbf{L}_{M+1}$; on the right: its generalized inverse, i.e., $\mathfrak{L}_{M+1}$. The parts which change are highlighted in blue.

1.3. Analysis of the design matrix

In this section we want to analyze in detail the form of the acquisition operator. As a result, we provide an in-depth study of the reconstruction.

Minimization problem (1.10) indicates that the null-space of the forward operator $\mathcal{L}_{\mathcal{L}}$ we studied so far is related to the capability of uniquely reconstructing the CGPTs, and, in the end, to the classification of a dielectric target.

1.3.1. Matrix of receptors

The matrix of receptors associated to the sth position is given by

$$\mathbf{G}^{(s)} = \begin{bmatrix} \frac{\cos(\theta_1)}{r_1} & \frac{\sin(\theta_1)}{r_1} & \frac{\cos(2\theta_1)}{2r_1^2} & \frac{\sin(2\theta_1)}{2r_1^2} & \cdots & \frac{\cos(K\theta_1)}{Kr_1^K} & \frac{\sin(K\theta_1)}{Kr_1^K} \\ \frac{\cos(\theta_2)}{r_2} & \frac{\sin(\theta_2)}{r_2} & \frac{\cos(2\theta_2)}{2r_2^2} & \frac{\sin(2\theta_2)}{2r_2^2} & \cdots & \frac{\cos(K\theta_2)}{Kr_2^K} & \frac{\sin(K\theta_2)}{Kr_2^K} \\ \vdots & & \vdots & & \ddots & & \vdots \\ \frac{\cos(\theta_{N_r})}{r_{N_r}} & \frac{\sin(\theta_{N_r})}{r_{N_r}} & \frac{\cos(2\theta_{N_r})}{2r_{N_r}^2} & \frac{\sin(2\theta_{N_r})}{2r_{N_r}^2} & \cdots & \frac{\cos(K\theta_{N_r})}{Kr_{N_r}^K} & \frac{\sin(K\theta_{N_r})}{Kr_{N_r}^K} \end{bmatrix}.$$

In Appendix A.4.1, we show that $\mathbf{G}^{(s)}$ is full column rank as soon as there are $2K \leq N_r$ distinct receptors that are a *general configuration* in the sense of Remark A.4.4. Furthermore, we have the following lemma [14].

Lemma 1.3.1 *$2K \leq N_r$ distinct points distributed along a circular arc are a general configuration.*

It is clear that a single position yields a design matrix $\mathbf{L}_{\mathcal{L}}$ which is not full column rank, no matter how many receptors are considered. However, collecting many electrostatic measurements at different positions ultimately enriches the column space of the matrix $\mathbf{S}$. As a matter of fact, if $\mathbf{S}$ and $\mathbf{G}^{(s)}$ for $s = 1, \ldots, M$, are full column rank, $\mathfrak{L}$ proves to be a left-inverse and thus $\mathbf{L}_{\mathcal{L}}$ is full column rank as well.

1.3.2. Source vector

The row vector $\mathbf{S}_{s,:}$, which refers to the source corresponding to the sth position, is defined by (1.5). For simplicity we consider the case $\xi = 0$; see (1.6).

Denote by

$$\mathbf{p}_s^{\perp} = \mathbf{p}_s \begin{bmatrix} 0 & 1 \\ -1 & 0 \end{bmatrix}$$

the unit vector orthogonal to the dipole moment $\mathbf{p}_s = [\cos\alpha, \sin\alpha]$, and let $\zeta_s = \rho e^{i\overline{\theta}_s}$ be the location of the dipole.

We can naturally split $\mathbf{S}_{s,:}$ into the pure dipole term and the distributed source term:

$$\mathbf{S}_{s,:} = (\mathbf{S}_{dip})_{s,:} + (\mathbf{S}_{SL})_{s,:}\,.$$

Here $\mathbf{S}_{dip}$ and $\mathbf{S}_{SL}$ are given as follows. Employing the product given in Definition A.3, define the block diagonal matrix

$$\mathbf{P}_K^{(s)} := \mathbf{I}_K \otimes \left\{ (-1)^\ell \begin{bmatrix} \mathbf{p}_s \\ \mathbf{p}_s^\perp \end{bmatrix} \right\},$$

the diagonal matrix

$$\mathbf{D}_{2,K+1} := \mathbf{I}_K \otimes \left\{ \rho^{-(\ell+1)} \mathbf{I}_2 \right\},$$

and the row vector

$$\mathbf{Z}_{s,:} := \begin{bmatrix} \cos(2\overline{\theta}_s) & \sin(2\overline{\theta}_s) & \cos(3\overline{\theta}_s) & \sin(3\overline{\theta}_s) & \dots & \cos((K+1)\overline{\theta}_s) & \sin((K+1)\overline{\theta}_s) \end{bmatrix}.$$

Then

$$(\mathbf{S}_{dip})_{s,:} = \mathbf{Z}_{s,:} \mathbf{P}_K^{(s)\top} \mathbf{D}_{2,K+1}.$$

On the other hand, given N points y_i uniformly distributed on $\partial\Omega_s$, we can discretize the integral defining $(\mathbf{S}_{SL})_{s,2k-1}$ and $(\mathbf{S}_{SL})_{s,2k}$ as follows

$$A_{s,k} = \int_{\partial\Omega_s} \left. \frac{\partial u^{(s)}}{\partial \nu} \right|_+ \frac{\cos(k\theta_y)}{k r_y^k} \, \mathrm{d}\sigma_y \approx \sum_{i=1}^N \frac{\partial u^{(s)}}{\partial \nu}(y_i) \frac{\cos(k\theta_{y_i})}{k r_i^k} \Delta y_i,$$

$$B_{s,k} = \int_{\partial\Omega_s} \left. \frac{\partial u^{(s)}}{\partial \nu} \right|_+ \frac{\sin(k\theta_y)}{k r_y^k} \, \mathrm{d}\sigma_y \approx \sum_{i=1}^N \frac{\partial u^{(s)}}{\partial \nu}(y_i) \frac{\sin(k\theta_{y_i})}{k r_i^k} \Delta y_i.$$

Consequently, defining the column vector

$$\mathbf{U}_{s,:} := \left(\frac{\partial u^{(s)}}{\partial \nu}(y_i) \Delta y_i \right)_{i=1}^N,$$

we get

$$(\mathbf{S}_{SL})_{s,:} = -\mathbf{U}_{s,:} \mathbf{G}_*^{(s)}.$$

Notice that $\mathbf{G}_*^{(s)}$ reduces to $\mathbf{G}^{(s)}$ if we choose the receptors as discretization points, i.e., $y_i = x_i^{(s)}$.

In the end, the source vector can be written in the following form:

$$\mathbf{S}_{s,:} = (\mathbf{S}_{dip})_{s,:} + (\mathbf{S}_{SL})_{s,:} = \mathbf{Z}_{s,:} \mathbf{P}_K^{(s)\top} \mathbf{D}_{2,\,K+1} - \mathbf{U}_{s,:} \mathbf{G}^{(s)}.$$

Let U be the background solution, i.e., the potential in the absence of any target. When $\rho \gg \delta$, the dipolar expansion derived in [2] yields

$$\mathbf{U}_{s,:} = \mathbf{u} + O(\delta^2), \tag{1.16}$$

where $\mathbf{u} := \left(\frac{\partial U}{\partial \nu}(y_i) \Delta y_i \right)_{i=1}^{N_r}$. Such first order approximation of $\mathbf{U}_{s,:}$ depends only on the geometry of the fish and on the position of the receptors.

1.3.3. Reconstruction error analysis

In this section we analyze the relative error in the reconstruction of the CGPTs when the g-inverse $\mathfrak{L}$ given by (1.14) is used, and the MSR data are acquired along a single circular orbit around the target.

Let $\mathbf{W}$ be a random matrix $N_r \times M$ with independent and identically distributed $\mathcal{N}(0, \sigma^2_{\text{noise}})$ entries. Let $\mathbf{E}$ be the matrix $N_r \times M$ of the truncation errors. Recall that the entries of $\mathbf{E}$ are of order ε^{K+2}; see (A.6).

The following multivariate multiple linear regression model for the measurements can be stated:

$$\mathbf{Q} = \mathcal{L}(\mathbb{M}) + \mathbf{E} + \mathbf{W}. \tag{1.17}$$

We restrict ourselves to the situation where the strength of the noise is enough to overpower the truncation error, which we disregard a posteriori for the rest of the analysis. More precisely, we assume that the strength of the noise satisfies

$$\varepsilon^{K+2} \ll \sigma^2_{\text{noise}} \ll \varepsilon^2. \tag{1.18}$$

We define the signal to noise ratio (SNR) associated to the orbit $\mathcal{O}$ as

$$\text{SNR} = \frac{\varepsilon^2}{\sigma^2_{\text{noise}}}.$$

Next, we vectorize (1.9). Define the vectorized error matrix

$$\text{vec}(\mathbf{W}) \sim \mathcal{N}(\mathbf{0}_{MN_r}, \sigma^2_{\text{noise}} \mathbf{I}_{MN_r}),$$

and the response matrix, which is a multivariate normal vector given $\mathbf{S}$ and $\mathbf{G}^{(s)}$ for $s = 1, \ldots, M$, namely,

$$\text{vec}(\mathbf{Q} \,|\, \{\mathbf{G}^{(s)}\}, \mathbf{S}) \sim \mathcal{N}(\text{vec}(\mathcal{L}(\mathbb{M})), \sigma^2_{\text{noise}} \mathbf{I}_{MN_r}).$$

Straightforward computations show that the covariance matrix of $\mathfrak{L}\,\text{vec}(\mathbf{W})$ can be written as

$$\begin{aligned} \text{Cov}(\mathfrak{L}\,\text{vec}(\mathbf{W})) &= \sigma^2_{\text{noise}} \sum_{s=1}^{M} \mathbf{S}^{\dagger}_{:,s} \mathbf{S}^{\dagger\top}_{:,s} \otimes \mathbf{G}^{(s)\dagger} \mathbf{G}^{(s)\dagger\top} \\ &= \sigma^2_{\text{noise}} \sum_{s=1}^{M} \begin{bmatrix} (\mathbf{S}^{\dagger}_{1,s})^2 \mathbf{G}^{(s)\dagger} \mathbf{G}^{(s)\dagger\top} & & * \\ & \ddots & \\ * & & (\mathbf{S}^{\dagger}_{2K,s})^2 \mathbf{G}^{(s)\dagger} \mathbf{G}^{(s)\dagger\top} \end{bmatrix}. \end{aligned} \tag{1.19}$$

Hereinafter, we assume that the N_r receptors of $\mathbf{G}^{(s)}$ are all distributed along one circular arc of radius ρ. This assumption is justified by the fact that if we model the fish skin by two close circular arcs of radius ρ and $\rho + \varepsilon$, with $N_r/2$ receptors on them, and we call $\mathbf{G}^{(s)}_{\varepsilon}$ its matrix of receptors, we can show that $\|\mathbf{G}^{(s)}_{\varepsilon} - \mathbf{G}^{(s)}\|_F \to 0$ as $\varepsilon \to 0$.

Theorem 1.3.2 *For j,k so that $(\mathbf{M})_{jk}$ is nonzero, the relative error on the reconstructed CGPT satisfies*

$$\sqrt{\frac{\mathbb{E}|(\mathbf{M}^{est})_{jk}-(\mathbf{M})_{jk}|^2}{|(\mathbf{M})_{jk}|^2}} \lesssim \sigma_{noise}\,\varepsilon^{-\lceil j/2\rceil-\lceil k/2\rceil}\left\lceil\frac{j}{2}\right\rceil\left\lceil\frac{k}{2}\right\rceil. \tag{1.20}$$

For vanishing $(\mathbf{M})_{jk}$, the error $\sqrt{\mathbb{E}|(\mathbf{M}^{est})_{jk}-(\mathbf{M})_{jk}|^2}$ can be bounded by the right-hand side above with ε replaced by ρ^{-1}.

Proof. We begin by observing that the absolute errors $\sqrt{\mathbb{E}|(\mathbf{M}^{\mathrm{est}})_{jk}-(\mathbf{M})_{jk}|^2}$ are the diagonal entries of $\mathrm{Cov}(\mathfrak{L}\mathbf{W})$. In particular, the (j,j)th entry of the kth block matrix of $\mathrm{Cov}(\mathfrak{L}\,\mathrm{vec}(\mathbf{W}))$ given by (1.19), i.e., $\sum_{s=1}^{M}(\mathbf{S}^{\dagger}_{k,s})^2(\mathbf{G}^{(s)\dagger}\mathbf{G}^{(s)\dagger\top})_{jj}$, corresponds to CGPT $(\mathbf{M})_{jk}$. Define $\mathcal{I}_{jk}\coloneqq(\mathbf{M}^{\mathrm{est}}-\mathbf{M})_{jk}$. By Lemma A.4.6 we have the inequality

$$|\mathbf{S}^{\dagger}_{k,s}|^2 \le \|\mathbf{S}^{\dagger}_{k,:}\|_F^2 \lesssim \frac{\rho^{2\lceil k/2\rceil}}{M}\left\lceil\frac{k}{2}\right\rceil^2.$$

On the other hand it is easy to show that

$$|(\mathbf{G}^{(s)\dagger}\mathbf{G}^{(s)\dagger\top})_{jj}| \lesssim \rho^{2\lceil j/2\rceil}\left\lceil\frac{j}{2}\right\rceil^2.$$

Therefore, we obtain the following estimate

$$\mathbb{E}(\mathcal{I}_{jk})^2=\sum_{s=1}^{M}(\mathbf{S}^{\dagger}_{k,s})^2(\mathbf{G}^{(s)\dagger}\mathbf{G}^{(s)\dagger\top})_{jj}\lesssim\rho^{2(\lceil j/2\rceil+\lceil k/2\rceil)}\left\lceil\frac{j}{2}\right\rceil^2\left\lceil\frac{k}{2}\right\rceil^2.$$

The scaling property

$$(\mathbf{M})_{jk}(\delta B)=\delta^{\lceil j/2\rceil+\lceil k/2\rceil}(\mathbf{M})_{jk}(B),$$

together with the above control on $\mathbb{E}(\mathcal{I}_{jk})^2$ show that the relative error satisfies (1.20).

□

Remark 1.3.3 *In the proof we used the following inequality:*

$$|(\mathbf{G}^{(s)\dagger}\mathbf{G}^{(s)\dagger\top})_{jj}| \lesssim \rho^{2\lceil j/2\rceil}\left\lceil\frac{j}{2}\right\rceil^2,$$

where the unspecified constant depends on the number of receptors N_r and the angle of view γ. In the next section we analyze such dependency in the limit as $N_r\to\infty$, observing that the upper bound in (1.20) *decays like $1/N_r$.*

Following [6], given the SNR and a tolerance level τ_0, the resolving order is defined as

$$K^*=\min\left\{1\le k\le K:\sqrt{\frac{\mathbb{E}|(\mathbf{M}^{\mathrm{est}})_{kk}-(\mathbf{M})_{kk}|^2}{|(\mathbf{M})_{kk}|^2}}\le\tau_0\right\}.$$

It is readily seen that the resolving order K^* satisfies

$$(K^*\varepsilon^{1-K^*})^2\simeq\tau_0\mathrm{SNR}. \tag{1.21}$$

1.3.4. Angular resolution

In this section we want to discuss the issues related to the limited-view configuration, which is an intrinsic feature of the fish geometry. In order to get an idea of how much the angle of view has an impact on the error estimate provided by Theorem 1.3.2, we restrict ourselves to a special configuration of receptors. In particular, we assume that there are N_r receptors evenly distributed on an arc of the unit circle, with aperture angle $\gamma \in (0, 2\pi)$, and we let N_r go to ∞.

Instead of studying the spectrum of $(\mathbf{G}^{(s)\mathsf{H}}\mathbf{G}^{(s)})^\dagger$ we shall equivalently consider that of $(\mathbf{V}_K^{\mathsf{H}}\mathbf{V}_K)^\dagger$, where $\mathbf{V}_K$ is as defined in Appendix A.4.1, and $\mathbf{V}_K^{\mathsf{H}}$ denotes the matrix $\overline{\mathbf{V}}_K^{\top}$. For the sake of notation we refer to $\mathbf{V}_K$ as the block matrix $\begin{bmatrix}\mathbf{W}_K & \overline{\mathbf{W}}_K\end{bmatrix}$, obtained from $\mathbf{V}_K$ by permuting the columns as in Appendix A.4.1. We are interested in the asymptotic expansion of $\mathbf{V}_K^{\mathsf{H}}\mathbf{V}_K$ as $N_r \to \infty$. Hereinafter, we denote $\lim_{N_r\to\infty} \frac{1}{N_r}\mathbf{A}$ by $(\mathbf{A})_\infty$.

With this particular geometry of receptors the limit matrix can be analytically computed:

$$(\mathbf{V}_K^{\mathsf{H}}\mathbf{V}_K)_\infty = \begin{bmatrix} (\overline{\mathbf{W}}_K^{\top}\mathbf{W}_K)_\infty & (\overline{\mathbf{W}}_K^{\top}\overline{\mathbf{W}}_K)_\infty \\ (\mathbf{W}_K^{\top}\mathbf{W}_K)_\infty & (\mathbf{W}_K^{\top}\overline{\mathbf{W}}_K)_\infty \end{bmatrix},$$

where

$$(\mathbf{W}_K^{\top}\mathbf{W}_K)_\infty = \begin{bmatrix} -\frac{1-e^{i2\gamma}}{2i\gamma} & -\frac{1-e^{i3\gamma}}{3i\gamma} & -\frac{1-e^{i4\gamma}}{4i\gamma} & \cdots & -\frac{1-e^{i(K+1)\gamma}}{(K+1)i\gamma} \\ -\frac{1-e^{i3\gamma}}{3i\gamma} & -\frac{1-e^{i4\gamma}}{4i\gamma} & -\frac{1-e^{i5\gamma}}{5i\gamma} & \cdots & -\frac{1-e^{i(K+2)\gamma}}{(K+2)i\gamma} \\ \vdots & \vdots & \vdots & & \vdots \\ -\frac{1-e^{i(K+1)\gamma}}{(K+1)i\gamma} & -\frac{1-e^{i(K+2)\gamma}}{(K+2)i\gamma} & -\frac{1-e^{i(K+3)\gamma}}{(K+3)i\gamma} & \cdots & -\frac{1-e^{2Ki\gamma}}{2Ki\gamma} \end{bmatrix},$$

$$(\overline{\mathbf{W}}_K^{\top}\mathbf{W}_K)_\infty = \begin{bmatrix} 1 & -\frac{1-e^{i\gamma}}{i\gamma} & -\frac{1-e^{i2\gamma}}{2i\gamma} & \cdots & -\frac{1-e^{i(K-1)\gamma}}{(K-1)i\gamma} \\ \frac{1-e^{-i\gamma}}{i\gamma} & 1 & -\frac{1-e^{i\gamma}}{i\gamma} & \cdots & -\frac{1-e^{i(K-2)\gamma}}{(K-2)i\gamma} \\ \frac{1-e^{-2i\gamma}}{2i\gamma} & \frac{1-e^{-i\gamma}}{i\gamma} & 1 & \cdots & -\frac{1-e^{i(K-3)\gamma}}{(K-3)i\gamma} \\ \vdots & \vdots & \vdots & & \vdots \\ \frac{1-e^{-i(K-1)\gamma}}{i(K-1)\gamma} & \frac{1-e^{-i(K-2)\gamma}}{i(K-2)\gamma} & \cdots & \frac{1-e^{-i\gamma}}{i\gamma} & 1 \end{bmatrix},$$

and $(\mathbf{W}_K^{\top}\overline{\mathbf{W}}_K)_\infty = \overline{(\overline{\mathbf{W}}_K^{\top}\mathbf{W}_K)_\infty}$, $(\overline{\mathbf{W}}_K^{\top}\overline{\mathbf{W}}_K)_\infty = \overline{(\mathbf{W}_K^{\top}\mathbf{W}_K)_\infty}$.

Hence,

$$\mathbf{V}_K^{\mathsf{H}}\mathbf{V}_K = N_r\left((\mathbf{V}_K^{\mathsf{H}}\mathbf{V}_K)_\infty + O\left(\frac{1}{N_r}\right)\right), \text{ as } N_r \to \infty.$$

Applying the results contained in [40] we obtain the following result.

Lemma 1.3.4 *For N_r large,*

$$(\mathbf{V}_K^{\mathsf{H}}\mathbf{V}_K)^{-1} = \frac{1}{N_r}\left((\mathbf{V}_K^{\mathsf{H}}\mathbf{V}_K)_\infty + O\left(\frac{1}{N_r}\right)\right)^{-1}, \tag{1.22}$$

where the entries of $(\mathbf{V}_K^{\mathsf{H}}\mathbf{V}_K)_\infty$ depend only on the angle of view γ and the truncation order K. Moreover, we have

$$\frac{1}{\widetilde{\sigma}_k} = \frac{1}{N_r}\left(\sigma_k + O\left(\frac{1}{N_r}\right)\right)^{-1}, \tag{1.23}$$

where $\widetilde{\sigma}_k$ (resp. σ_k) are the eigenvalues of the matrix $\mathbf{V}_K^{\mathsf{H}}\mathbf{V}_K$ (resp. $(\mathbf{V}_K^{\mathsf{H}}\mathbf{V}_K)_\infty$).

Remark 1.3.5 *Lemma 1.3.4 highlights the following facts. On one hand, as long as all the eigenvalues are away from zero, the reconstructed CGPTs have an upper bound on the relative error in* (1.20) *which decays like $1/N_r$. More precisely, $(\mathbf{G}^{(s)\dagger}\mathbf{G}^{(s)\dagger\mathsf{H}})_{jj} \lesssim 1/N_r \sum 1/|\sigma_k|$. On the other hand, when some eigenvalues are very small (e.g. $\sigma_l \leq 10^{-8}$), inequality* (1.20) *becomes uninformative, making us unable to predict the behavior of the relative error.*

Figure 1.4 provides the distribution of $\widetilde{\sigma}_k$, σ_k/N_r at different values of the reconstruction order K and angles of view γ, as $N_r \to \infty$. First, we clearly observe the asymptotic behavior of the spectrum stated by (1.23). Second, we notice that the effect of the limited-view configuration is reflected by the decaying of the eigenvalues of the matrix of receptors. As expected, the closer the angle of view is to 2π, the more informative estimate (1.20) becomes. Furthermore, if K is small, the angle of view has a minor impact on the reconstructed CGPTs.

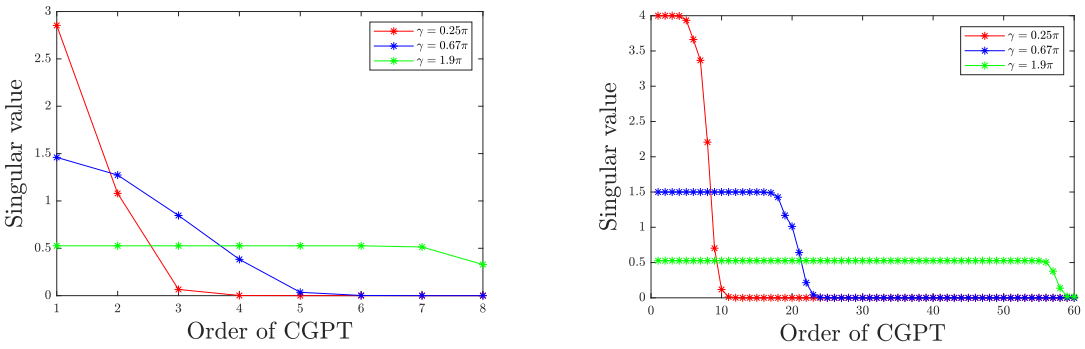

(a) $K = 4$ (b) $K = 30$

Figure 1.4.: The distribution of eigenvalues at different angles of view γ. The solid line corresponds to $\sigma(\mathbf{V}_K^{\mathsf{H}}\mathbf{V}_K/N_r)$, the starred line to $\sigma((\mathbf{V}_K^{\mathsf{H}}\mathbf{V}_K)_\infty)$. We use $N_r = 10^4$ receptors.

1.4. Recognition

In the previous section, we established an upper bound on the reconstruction error which essentially depends on the length-scale of the acquisition orbit. As a consequence, the closer the fish gets to the target, the higher the order of the features it can retrieve from the noisy measurements. This result suggests that, when it comes to classification, it is of preeminent importance to design recognition algorithms that exploit the information contained in measurements collected at multiple scales.

This section aims at presenting a novel multi-scale algorithm for target classification.

1.4.1. Complex CGPTs and shape descriptors

Let us briefly recall the definition of the shape descriptors.

We introduce convenient complex combinations of CGPTs. For any pair of indices $m, n = 1, 2, \dots$, we introduce the following quantities

$$\mathbf{N}^{(1)}_{mn}(\gamma, D) = (M^{cc}_{mn} - M^{ss}_{mn}) + i(M^{cs}_{mn} + M^{sc}_{mn}),$$
$$\mathbf{N}^{(2)}_{mn}(\gamma, D) = (M^{cc}_{mn} + M^{ss}_{mn}) + i(M^{cs}_{mn} - M^{sc}_{mn}).$$

We define the complex CGPT matrices by

$$\mathbf{N}^{(1)} := (\mathbf{N}^{(1)}_{mn})_{m,n}, \qquad \mathbf{N}^{(2)} := (\mathbf{N}^{(2)}_{mn})_{m,n}.$$

We call a dictionary $\mathcal{D}$ a collection of standard shapes B, centered at the origin, with characteristic size of order 1. We assume that a reference dictionary $\mathcal{D}$ is initially given. Furthermore, suppose we consider a shape D, which is unknown, that is obtained from an element $B \in \mathcal{D}$ by applying some unknown rotation θ and scaling s and translation z, i.e., $D = T_z s R_\theta B$.

Following [6], let $\eta = \frac{\mathbf{N}_{12}^{(2)}(D)}{2\mathbf{N}_{11}^{(2)}(D)}$. We define the following quantities

$$\mathcal{J}^{(1)}(D) = \mathbf{N}^{(1)}(T_{-\eta}D) = \mathbf{C}^{-\eta}\mathbf{N}^{(1)}(D)(\mathbf{C}^{-\eta})^T,$$

$$\mathcal{J}^{(2)}(D) = \mathbf{N}^{(2)}(T_{-\eta}D) = \overline{\mathbf{C}^{-\eta}}\mathbf{N}^{(2)}(D)(\mathbf{C}^{-\eta})^T,$$

where the matrix $\mathbf{C}^{-\eta}$ is a lower triangular matrix with the (m,n)th entry given by

$$\mathbf{C}_{mn}^{-\eta} = \binom{m}{n}(-\eta)^{m-n}.$$

These quantities are translation invariant.

From $\mathcal{J}^{(1)}(D) = (\mathcal{J}_{mn}^{(1)}(D))_{m,n}$, $\mathcal{J}^{(2)}(D) = (\mathcal{J}_{mn}^{(2)}(D))_{m,n}$, for each pair of indices m, n, we define the scaling invariant quantities:

$$\mathcal{S}_{mn}^{(1)}(D) = \frac{\mathcal{J}_{mn}^{(1)}(D)}{(\mathcal{J}_{mm}^{(2)}(D)\mathcal{J}_{nn}^{(2)}(D))^{1/2}}, \qquad \mathcal{S}_{mn}^{(2)}(D) = \frac{\mathcal{J}_{mn}^{(2)}(D)}{(\mathcal{J}_{mm}^{(2)}(D)\mathcal{J}_{nn}^{(2)}(D))^{1/2}}.$$

The CGPT-based shape descriptors $\mathcal{I}^{(1)} = (\mathcal{I}_{mn}^{(1)})_{m,n}$ and $\mathcal{I}^{(2)} = (\mathcal{I}_{mn}^{(2)})_{m,n}$ are defined as:

$$\mathcal{I}_{mn}^{(1)} = |\mathcal{S}_{mn}^{(1)}(\gamma, D)|, \qquad \mathcal{I}_{mn}^{(2)} = |\mathcal{S}_{mn}^{(2)}(\gamma, D)|,$$

where $|\cdot|$ denotes the modulus of a complex number. Recall that $\mathcal{I}^{(1)}$ and $\mathcal{I}^{(2)}$ are invariant under translation, rotation, and scaling.

The details of this construction can be found in [6].

1.4.2. Multi-scale acquisition setting

Suppose that the scanning movement consists of $\mathcal{M}$ concentric circular orbits $\mathcal{O}_1, \mathcal{O}_2, \ldots, \mathcal{O}_\mathcal{M}$, with radii $\rho_1 > \rho_2 > \cdots > \rho_\mathcal{M}$ respectively (ordered from the farthest to the nearest), the target being located at the common center. On each orbit only a discrete number of positions accounts for the data acquisition process, as described in Section 1.2.1. Precisely, M_j different positions are sampled along the orbit $\mathcal{O}_j$, and for each position s the corresponding electric signal $u_j^{(s)} - H_j^{(s)}$ is measured by N_r receptors on the skin, $\{x_{j,r}^{(s)}\}_{r=1}^{N_r}$.

Therefore, for any orbit $\mathcal{O}_j$ we get the $N_r \times M_j$ MSR matrix, whose (r,s)-entry is defined as

$$(\mathbf{Q}_{\mathcal{O}_j})_{r,s} = u_j^{(s)}(x_{j,r}^{(s)}) - H_j^{(s)}(x_{j,r}^{(s)}), \qquad j \in \{1,\dots,\mathcal{M}\}. \tag{1.24}$$

Notice that so far the setting described above is very general, as no restriction has been given on the radii of the orbits yet.

Since the orbits are at different length-scales, it is clear that the closer the orbit is to the center, the stronger the MSR signal is. However, resorting to the error estimate on the reconstruction order (1.20), we are able to choose the orbits in such a way that the resolving order is enhanced.

In the multi-scale setting described above, formula (1.21) reads

$$(K_j^* \varepsilon_j^{1-K_j^*})^2 \simeq \tau_0 \mathrm{SNR}_j, \tag{1.25}$$

where $\mathrm{SNR}_j = \frac{\varepsilon_j^2}{\sigma^2_{\mathrm{noise}}}$ is the SNR ratio associated to the jth orbit.

Thus, a length-scale dependent resolving order is introduced, and obviously $K_{j+1}^* \geq K_j^* \geq 2$.

The noisy MSR matrix is given by the following formula

$$\mathbf{Q}_{\mathcal{O}_j} = \mathcal{L}_j(\mathbb{M}^{(K_j)}) + \mathbf{E}_{\mathcal{O}_j} + \mathbf{W}. \tag{1.26}$$

On each orbit $\mathcal{O}_j$, the CGPTs can be retrieved from the data (1.26), for instance, by using either the classical Moore–Penrose inverse or the generalized inverse $\mathfrak{L}$ given by (1.14). Moreover, we denote by $(\mathcal{I}^{(1)}(D;\mathcal{O}_j), \mathcal{I}^{(2)}(D;\mathcal{O}_j))$ the measured descriptors associated to the small target D, which are computed from the reconstructed CGPTs $\mathbb{M}^{(K_j)}$.

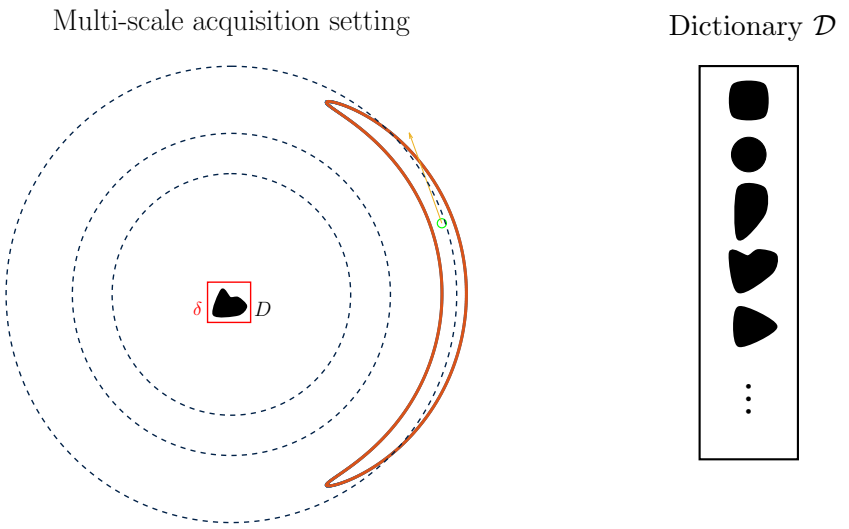

Figure 1.5.: Left: Multi-scale acquisition setting. Right: Dictionary $\mathcal{D}$. MSR data are collected by swimming along multiple concentric orbits as shown on the left. The classification problem is to use the features extracted from the data in order to classify, up to rotation and scaling, the small dielectric target D among the elements of a dictionary $\mathcal{D}$.

Given a dictionary $\mathcal{D}$ of N standard shapes, which are denoted by $B_1, B_2, \dots, B_N$, we want to design a matching algorithm, which generalizes the one proposed in [7] to a multi-scale configuration; see Figure 1.5. First, a matching procedure as in [7] is required on each orbit, which consists of a comparison between the theoretical shape descriptors $((\mathcal{I}^{(1)}(B_\kappa), \mathcal{I}^{(2)}(B_\kappa)))_{\kappa=1,\dots,N}$ and the measured ones $(\mathcal{I}^{(1)}(D;\mathcal{O}_j), \mathcal{I}^{(2)}(D;\mathcal{O}_j))$, up to a properly chosen length-scale dependent order K_j.

Let us define the following scores:

$$\Delta_j(B_\kappa, D) = \left(\|\mathcal{I}^{(1)}(B_\kappa) - \mathcal{I}^{(1)}(D;\mathcal{O}_j)\|_F^2 + \|\mathcal{I}^{(2)}(B_\kappa) - \mathcal{I}^{(2)}(D;\mathcal{O}_j)\|_F^2 \right)^{1/2}, \qquad (1.27)$$

where $\|\cdot\|_F$ denotes the Frobenius norm of matrices, $j = 1, \dots, \mathcal{M}$ and $\kappa = 1, \dots, N$.

For every j, the scores (1.27) are used to perform the (local) comparison. Precisely, let $\phi_j(D) \in \mathcal{D}^N$ be the vector formed by the elements of the dictionary, rearranged in ascending order according to Δ_j, i.e.,

$$\phi_j(D) = (B_{\sigma_j(1)}, \dots, B_{\sigma_j(N)}),$$

where σ_j is a permutation such that $\Delta_j(B_{\sigma_j(l')}, D) \le \Delta_j(B_{\sigma_j(l)}, D)$ for each $l < l'$.

Notice that, for efficiency reasons, it is convenient to cut the vector $\phi_j(D)$ retaining the first $n \le N$ components only, which are the elements of $\mathcal{D}$ that produce the lowest scores.

Thus far we have just sorted the elements of the dictionary by matching the descriptors on each orbit separately. Instead of simply returning $B_{\sigma_j(1)}$ for each j, that is, in fact, the algorithm in [6] applied on each orbit for a fixed reconstructing order K_j, we aim at fusing the descriptors at the score level. Of course, the scores corresponding to descriptors which have different orders are not directly comparable. The proposed approach is inspired by [60] and is based on the so-called Transferable Belief Model (TBM).

We consider, for every orbit $\mathcal{O}_j$, the evidence distribution

$$\pi_j := \pi_j(D) = (\eta_{j1}, \dots, \eta_{jn}),$$

where

$$\eta_{j\kappa} = \begin{cases} \varphi_j \left(\frac{\Delta_j(B_{\sigma_j(1)}, D)}{\Delta_j(B_\kappa, D)} \right)^\beta, & \text{if } \sigma_j(\kappa) \le n, \\ 0\,, & \text{otherwise.} \end{cases}$$

Here, φ_j is a normalization constant such that the integral of the evidence distribution π_j is 1, and β is a smoothing parameter.

Besides π_j, we may consider the Shannon's entropy as a confidence factor. Tracing [50], we define

$$c_j := c_j(D) = 1 - \frac{\mathcal{H}(\pi_j)}{\log(n)},$$

where $\mathcal{H}(\pi_j) = \sum_{\kappa=1}^{n} -\eta_{j\kappa} \log(\eta_{j\kappa})$ is the Shannon's entropy of the distribution π_j.

Then, for each j, we define the basic belief assignment (BBA)

$$\mathsf{m}_j := (\mathsf{m}_j(B_1), \dots, \mathsf{m}_j(B_N), \mathsf{m}_j(\mathcal{D})) \propto (\eta_{j1}, \dots, \eta_{jN}, c_j).$$

m_j quantifies the evidence given to each element of $\mathcal{D}$ by the comparison of the descriptors on the jth orbit.

There exist many ways to fuse the evidence which are expressed as BBAs. One of the simplest formulas is the TBM conjunctive rule (A.22), which is associative. Therefore, we start with blending m_1 in with m_2, obtaining $\mathsf{m}_{12} := \mathsf{m}_1 \textcircled{\cap} \mathsf{m}_2$. Then we combine m_{12} with m_3, obtaining

$$\mathsf{m}_{123} := (\mathsf{m}_1 \textcircled{\cap} \mathsf{m}_2) \textcircled{\cap} \mathsf{m}_3 = \mathsf{m}_1 \textcircled{\cap} \mathsf{m}_2 \textcircled{\cap} \mathsf{m}_3,$$

and so on, until we compute $\mathsf{m}_{12\dots\mathcal{M}}$.

Finally, from the fused BBAs we define the pignistic probability (A.23), which is used to select the best candidate among the elements of $\mathcal{D}$.

The procedure described hereabove is summarized in Algorithm 2. See also Figure 1.6.

Algorithm 1: Shape identification for a multi-scale setting based on transform invariant descriptors

Input : On each orbit $\mathcal{O}_j \in \{\mathcal{O}_1, \dots, \mathcal{O}_{\mathcal{M}}\}$, the first k-th order shape descriptors $\mathcal{I}^{(1)}(D, \mathcal{O}_j)$, $\mathcal{I}^{(2)}(D, \mathcal{O}_j)$ of an unknown target D.

for $\mathcal{O}_j \in \{\mathcal{O}_1, \dots, \mathcal{O}_{\mathcal{M}}\}$ **do**
  for $B_\kappa \in \{B_1, \dots, B_N\}$ **do**
    $\Delta_j(B_\kappa, D) \leftarrow$
    $\left(\|\mathcal{I}^{(1)}(B_\kappa) - \mathcal{I}^{(1)}(D; \mathcal{O}_j)\|_F^2 + \|\mathcal{I}^{(2)}(B_\kappa) - \mathcal{I}^{(2)}(D; \mathcal{O}_j)\|_F^2\right)^{1/2}$;
  end
  $\sigma_j(1) \leftarrow \operatorname{argmin}_\kappa \Delta_j(B_\kappa, D)$;
  for $B_\kappa \in \{B_1, \dots, B_N\}$ **do**
    $\eta_{j\kappa} \leftarrow \varphi_j\left(\frac{\Delta_j(B_{\sigma_j(1)}, D)}{\Delta_j(B_\kappa, D)}\right)^\beta$;
    $\mathsf{m}_j(B_\kappa) \leftarrow \eta_{j\kappa}$;
  end
  $c_j \leftarrow 1 - \frac{1}{\log(N)} \sum_{\kappa=1}^N -\eta_{j\kappa} \log(\eta_{j\kappa})$;
  $\mathsf{m}_j(\mathcal{D}) \leftarrow c_j$;
end
$\mathsf{m}_{1\dots\mathcal{M}} \leftarrow \mathsf{m}_1 \owedge \cdots \owedge \mathsf{m}_{\mathcal{M}}$;

Output : the best matching element of the dictionary $\kappa^* \leftarrow \operatorname{argmax}_\kappa \mathrm{BetP}(B_\kappa)$.

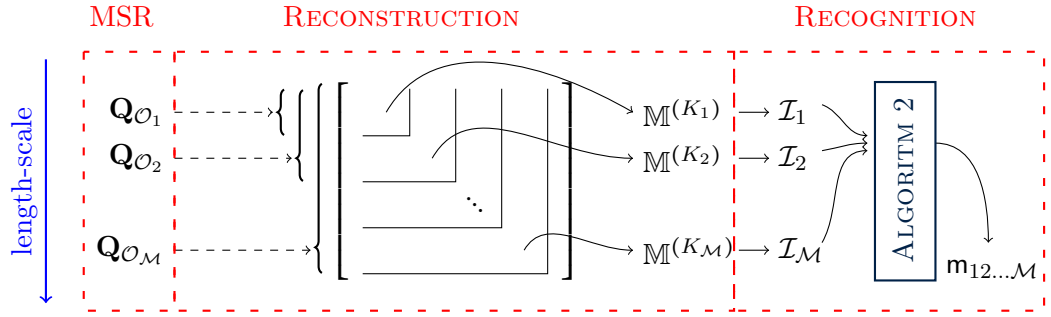

Figure 1.6.: Overview of the three relevant stages involved in our multi-scale approach. For conciseness, we denote $(\mathcal{I}^{(1)}(D; \mathcal{O}_j), \mathcal{I}^{(2)}(D; \mathcal{O}_j))$ by $\mathcal{I}_j$.

1.5. Numerical results

In this section, we show some numerical results which illustrate how Algorithm 2 can significantly improve the robustness of the recognition procedure.

1.5.1. Setting

Let $\mathcal{D}$ be a dictionary containing 8 standard shapes, as illustrated in Figure 2.1. Each solid shape is equipped with homogeneous conductivity having parameter $k = 3$ (Circle, Ellipse, Triangle, Bent Ellipse, Curved Triangle, Gingerbread Man, Drop), whereas the dashed one (Ellipse) has conductivity $k = 10$. All the shapes have the same characteristic size, which is of order one.

The targets D we are considering for the experiments are located at the origin as the standard shapes, and are obtained by scaling and rotating the elements of $\mathcal{D}$, with scaling coefficient and rotation angle chosen as $\delta = 0.2$ and $\theta = \pi/3$, respectively.

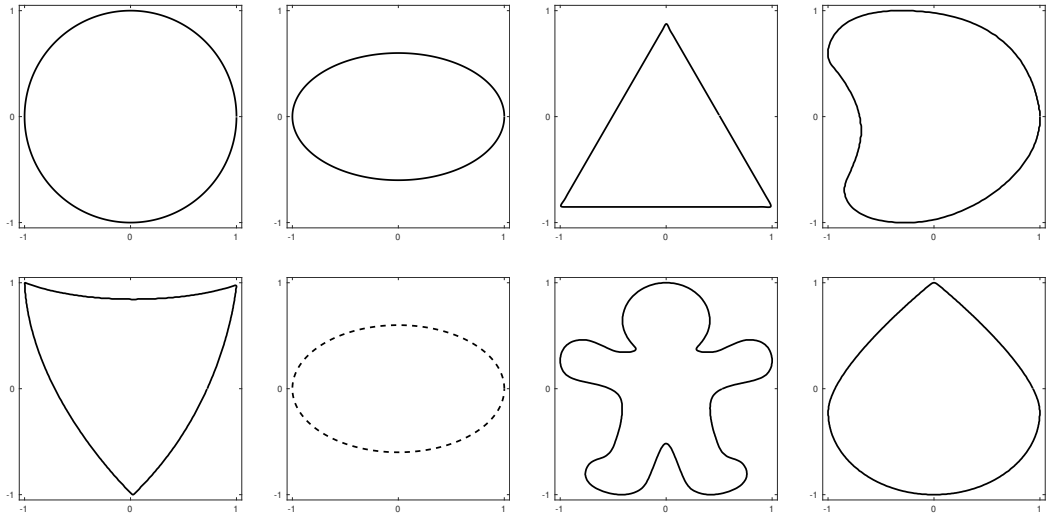

Figure 1.7.: Dictionary $\mathcal{D}$.

1.5.2. Experiment

The data are acquired as described in Section 1.4.2. Precisely, given $\mathcal{O}_1, \mathcal{O}_2$, and $\mathcal{O}_3$, three circular orbits around D of radii $\rho_1 = 1.6$, $\rho_2 = 1.1$, $\rho_3 = 0.9$, respectively, we sample $M_1 = M_2 = M_3 = 200$ positions on each trajectory and build the corresponding MSR matrices. We consider $N_r = 2^{10}$ receptors evenly distributed on the body of the fish. The acquisition setting is shown in Figure 1.8.

In the numerical experiments the MSR data are simulated using the code developed in [77].

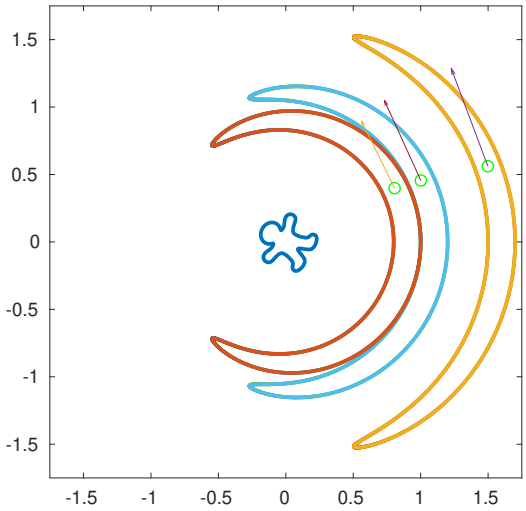

Figure 1.8.: A single position of the electric fish per orbit. The target is located at $(0, 0)$.

Remark 1.5.1 *In principle, the acquisition operator $\mathcal{L}$ depends on the measurements, which is not a desirable property. In order to overcome this difficulty, we perform the numerical simulations using the surrogate acquisition operator obtained from the dipolar approximation* (1.16).

The CGPTs are reconstructed on each orbit from the MSR matrix by exploiting either the g-inverse $\mathfrak{L}$ or the Moore–Penrose inverse $\mathbf{L}^{\dagger}$. The reconstruction orders are set as $K_1 = 2$ on $\mathcal{O}_1$, $K_2 = 3$ on $\mathcal{O}_2$, and $K_3 = 4$ on $\mathcal{O}_3$. The corresponding shape descriptors are then used as a rationale for building the BBAs $\mathsf{m}_1, \mathsf{m}_2$, and m_3, with parameter $\beta = 2$, as described in Section 1.4.2. For efficiency reasons, positive mass is given only to the first $n = 3$ best matching elements of $\mathcal{D}$.

We study the robustness of the fused descriptors given by Algorithm 2 with moderate noise in the measurements. Precisely, given a target D and $\sigma_{\text{noise}} \in [0.0025, 0.050]$, we test the recognition algorithm by considering 10^4 experiments and computing the frequencies.

The results arising from the beliefs produced on each orbit, i.e., $\mathsf{m}_1, \mathsf{m}_2$, and m_3, are compared with the ones obtained from the fused beliefs synthetized by the TBM conjunctive rule, i.e., $\mathsf{m}_{12} = \mathsf{m}_1 \textcircled{\cap} \mathsf{m}_2$ and $\mathsf{m}_{123} = \mathsf{m}_{12} \textcircled{\cap} \mathsf{m}_3$.

Reconstruction by the generalized inverse $\mathfrak{L}$

The results of this part are obtained by employing the reflexive minimum norm g-inverse $\mathfrak{L}$ of the acquisition operator given by (1.14) for the reconstruction of the CGPTs from the MSR data.

The frequencies are reported in Figures 1.9, 1.10, and 1.11.

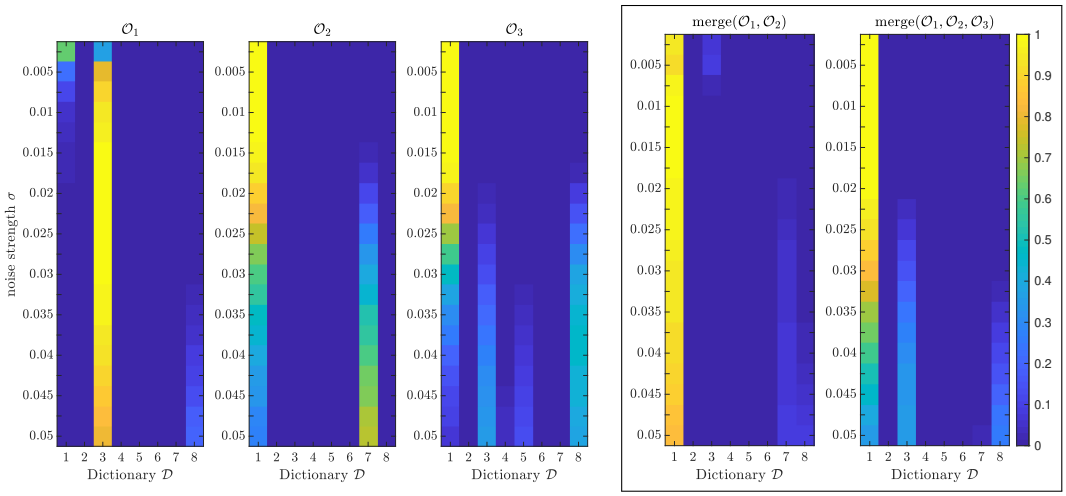

Figure 1.9.: Circle (1)

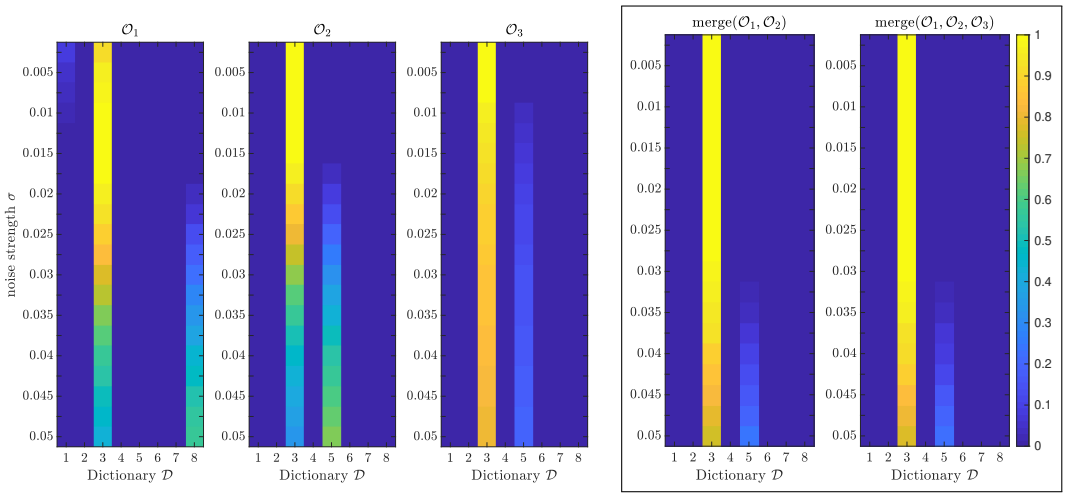

Figure 1.10.: Triangle (3)

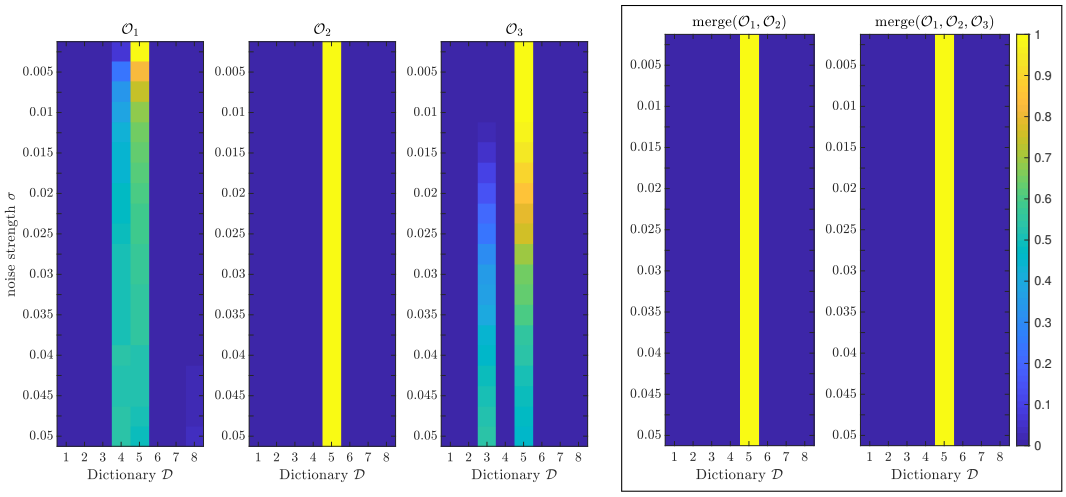

Figure 1.11.: Curved Triangle (5)

	1	2	3	4	5	6	7	8
m_1	0.0021	0	0.8029	0	0	0	0	0.1950
m_2	0.2805	0	0	0	0	0	0.7195	0
m_3	0.0728	0	0.3582	0.0381	0.1400	0	0.0088	0.3821
m_{12}	0.8288	0	0	0	0	0	0.0834	0.0878
m_{123}	0.3575	0	0.3585	0.0001	0.0013	0	0.0174	0.2652

Table 1.2.: Frequency table for the identification of the Circle (1) with the strongest noise, i.e., $\sigma = 0.05$. Each row displays the relative frequencies for all the elements of the dictionary corresponding to different BBAs.

Looking at Table 1.2, we can clearly see that the combination of classifiers outperforms each classifier. In particular, we can see that combining the classifiers on $\mathcal{O}_1$ and $\mathcal{O}_2$ yields a great improvement in the recognition already.

Tables 1.3 and 1.4 refer to the Triangle (3) and the Curved Triangle (5). Because of their similar silhouettes, they are troublesome from a dictionary approach point of view [66], and thus it is interesting to have a close look at what happens in both cases.

	1	2	3	4	5	6	7	8
m_1	0.0006	0	0.4229	0	0.0115	0	0	0.5650
m_2	0	0	0.3371	0	0.6629	0	0	0
m_3	0	0	0.8038	0	0.1962	0	0	0
m_{12}	0	0	0.7519	0	0.2382	0	0	0.0099
m_{123}	0	0	0.7702	0	0.2297	0	0	0.0001

Table 1.3.: Frequency table for the identification of the Triangle (3) with the strongest noise, i.e., $\sigma = 0.05$.

	1	2	3	4	5	6	7	8
m_1	0	0	0	0.5015	0.4650	0	0.0002	0.0333
m_2	0	0	0.0064	0	0.9936	0	0	0
m_3	0	0	0.5395	0	0.4605	0	0	0
m_{12}	0	0	0.0011	0.0016	0.9967	0	0	0.0006
m_{123}	0	0	0.0017	0	0.9983	0	0	0

Table 1.4.: Frequency table for the identification of the Curved Triangle (5) with the strongest noise, i.e., $\sigma = 0.05$.

It is worth noticing that in Table 1.3 the highest frequency is not attained by the fusion of the descriptors. Instead, the third orbit alone produces the best matching. However, merging all the three BBAs considerably enhances the classification success rate in the worst-case scenario, which is strikingly lower than the rate in the best case scenario.

Clearly, this is not a drawback of our method. As a matter of fact, since we don't know in advance which classifier performs the best, the above results indicate that using their combination is a valid –as well as natural– trade-off.

Reconstruction by the Moore-Penrose inverse

In this part we make use of the Moore-Penrose inverse to reconstruct the CGPTs from the MSR simulated data, as shown in (1.13). The frequencies are reported in Figures 1.12, 1.13, and 1.14.

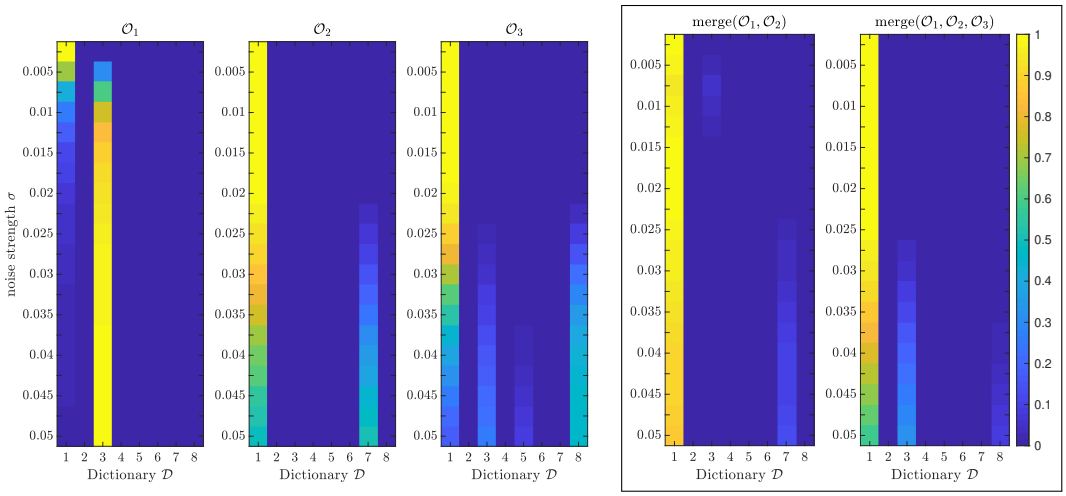

Figure 1.12.: Circle (1)

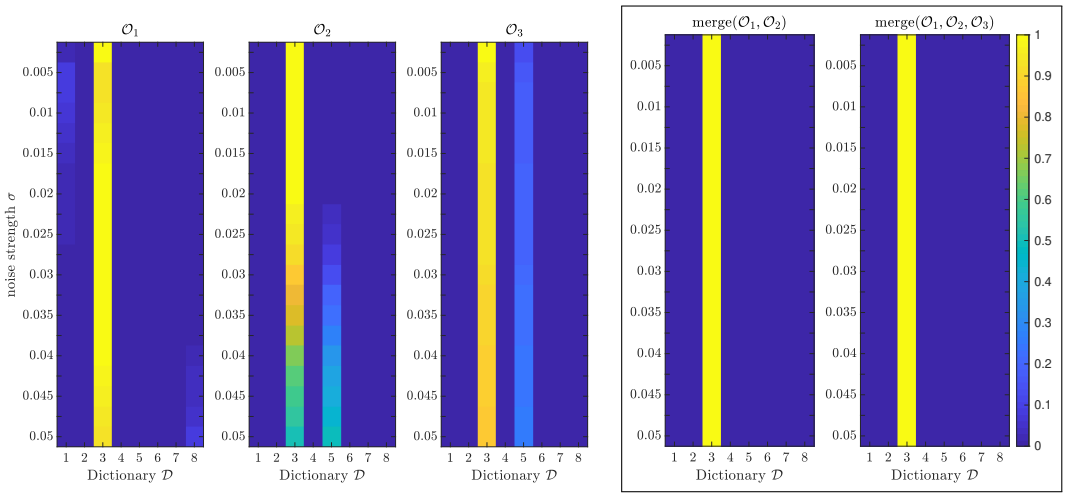

Figure 1.13.: Triangle (3)

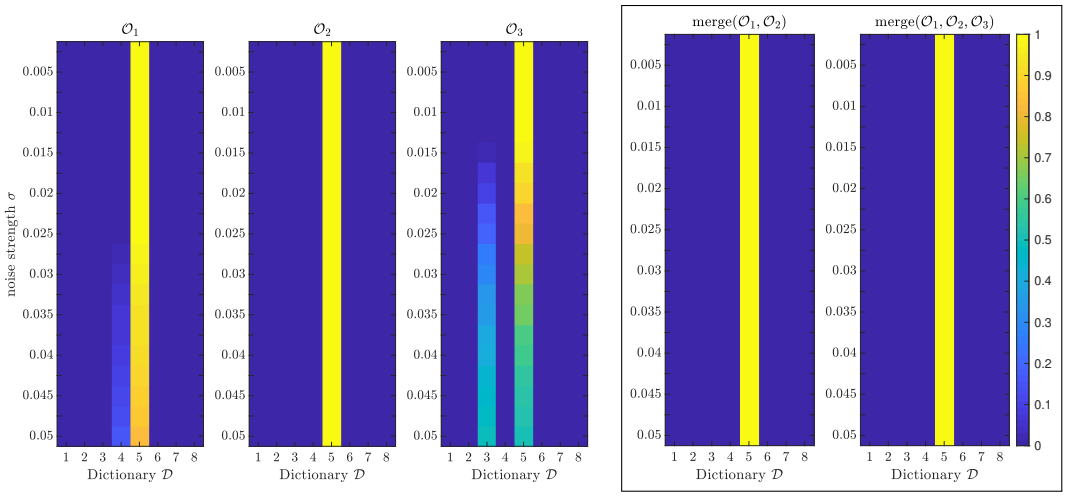

Figure 1.14.: Curved Triangle (5)

	1	2	3	4	5	6	7	8
m_1	0.0106	0	0.9885	0	0	0	0	0.0009
m_2	0.4889	0	0	0	0	0	0.5111	0
m_3	0.1784	0	0.2565	0.0138	0.0817	0	0.0021	0.4675
m_{12}	0.8729	0	0	0	0	0	0.1270	0.0001
m_{123}	0.5914	0	0.3185	0.0001	0.0016	0	0.0067	0.0817

Table 1.5.: Frequency table for the identification of the Circle (1) with the strongest noise, i.e., $\sigma = 0.05$. Each row displays the relative frequencies for all the elements of the dictionary corresponding to different BBAs.

	1	2	3	4	5	6	7	8
m_1	0.0033	0	0.9121	0	0	0	0	0.0846
m_2	0	0	0.5027	0	0.4973	0	0	0
m_3	0	0	0.7652	0	0.2346	0	0.0002	0
m_{12}	0	0	0.9933	0	0.0046	0	0	0.0021
m_{123}	0	0	0.9910	0	0.0090	0	0	0

Table 1.6.: Frequency table for the identification of the Triangle (3) with the strongest noise, i.e., $\sigma = 0.05$.

	1	2	3	4	5	6	7	8
m_1	0	0	0	0.1476	0.8512	0	0	0.0012
m_2	0	0	0.0013	0	0.9987	0	0	0
m_3	0	0	0.4855	0	0.5145	0	0	0
m_{12}	0	0	0	0.0008	0.9992	0	0	0
m_{123}	0	0	0.0001	0	0.9999	0	0	0

Table 1.7.: Frequency table for the identification of the Curved Triangle (5) with the strongest noise, i.e., $\sigma = 0.05$.

While the g-inverse $\mathfrak{L}$ lacks of the property of being a least-squares g-inverse, the Moore–Penrose $\mathbf{L}^\dagger$ provides the solution to the minimization problem (1.12). Therefore, it is not surprising that the classification rates obtained by using the latter are generally better than the ones resulting from using $\mathfrak{L}$.

1.6. Concluding remarks

In this chapter, we have presented a dictionary-matching approach for classification in electro-sensing that takes advantage of measurements at different length-scales. We have performed a careful analysis of the acquisition operator that was not available before now. In particular, by exploiting its peculiar block Kronecker form, we have studied its rank and established a length-scale dependent estimate on the reconstruction error. We have also discussed to what extent the limited-view configuration impacts prediction of the committed error.

2. Electro-sensing of inhomogeneous targets

Contents

2.1. Introduction

There are still many longstanding problems in electro-sensing. In particular, shape identification and classification are considered to be the most challenging ones. They have yet to be analyzed and understood. In [6, 7], two schemes that allow one to recognize and classify targets from measurements of the electric field perturbations induced by the targets have been presented and analyzed. The first algorithm is based on shape descriptors for nonbiological targets and the second one is based on spectral induced polarizations that can be used to image living biological targets, which have frequency-dependent electromagnetic parameters due to the capacitive effects induced by their cell membrane structures [13]. In [6], one first extracts the generalized (or high-order) polarization tensors of the target from the data. These tensors, first introduced in [22], are intrinsic geometric quantities and constitute the right class of features to represent the target shapes [6]. The shape features are encoded in the polarization tensors. The

extraction of the generalized polarization tensors can be achieved by a least-squares method.

Then from the extracted features one computes the invariants under rigid motion and scaling. Comparing these invariants with those in a dictionary of precomputed shapes, one can successfully classify the nonbiological target.

Since more complex objects may have arbitrary shapes and multiple layers of different dielectric materials warranting, a deeper analysis of the full response is required. It is the objective of the present chapter to extend the approach proposed in [6] to inhomogeneous targets.

The chapter is organized as follows. In Section 2.2, we derive a boundary integral representation for the perturbation of the potential due to the presence of the target. We introduce the GPTs associated with the inhomogeneous target D as the building blocks of the multipolar asymptotic expansion of the boundary measurements of $u|_+$ on $\partial\Omega$ in terms of the size of D. In Section 2.3, we consider a particular linear combination of the GPTs, called contracted generalized polarization tensors (CGPTs), and generalize the translation, rotation and scaling formulas for the contracted GPTs associated with homogeneous targets first derived in [6] to those associated with the inhomogeneous target D. Based on such formulas, we build transform invariants for the CGPTs and propose a matching algorithm for retrieving inhomogeneous targets. In Section 2.4, we present a variety of numerical simulations to illustrate the performance of the proposed matching algorithm. We aim at recognizing a specific inhomogeneous target by means of a dictionary-matching approach. The considered dictionary of targets contains both homogeneous and inhomogeneous objects. The latters are obtained by inserting inside the homogeneous targets inclusions with different conductivities. Similarily to what has been done in [6], the numerical simulations we perform confirm that extracting generalized polarization tensors of an inhomogeneous target from the data and comparing invariants with those of learned elements in a dictionary yields a classification procedure with a good performance in the full-view case and with small measurement noise level.

2.2. CGPTs for the weakly electric fish model

Let us now recall the model of electro-sensing derived in [2]: the body of the fish is Ω, an open bounded set in $\mathbb{R}^2$, with smooth boundary $\partial\Omega$, and with outward normal unit vector denoted by ν. The electric organ is a dipole $f(x)$ inside Ω or a sum of point sources inside Ω satisfying the charge neutrality condition. The skin of the fish is very thin and highly resistive. Its effective thickness, that is, the skin thickness times the contrast between the water and the skin conductivities, is denoted by ξ, and it is much smaller than the fish size. We assume that the conductivity of the background medium is one. We consider a smooth bounded target $D = z + \delta B$, where z is its location, and B is a smooth bounded domain containing the origin. We assume that the conductivity of D is a scalar function $\gamma(x) \neq 1$ for $x \in D$ with $\gamma(x) = \widetilde{\gamma}((x - z)/\delta)$. Also, let $\gamma \in L^\infty(\mathbb{R}^2)$ satisfies the uniform

ellipticity condition that for some $\lambda > 0$, $\lambda^{-1} \leq \gamma \leq \lambda$. In the presence of D, the electric potential emitted by the fish is the solution to the following equations:

$$\begin{cases} \Delta u = f & \text{in } \Omega, \\ \nabla \cdot (1 + (\gamma - 1)\chi_D)\nabla u = 0 & \text{in } \mathbb{R}^2 \setminus \overline{\Omega}, \\ u|_+ - u|_- = \xi \left.\dfrac{\partial u}{\partial \nu}\right|_+ & \text{on } \partial\Omega, \\ \left.\dfrac{\partial u}{\partial \nu}\right|_- = 0 & \text{on } \partial\Omega, \\ |u(x)| = O(|x|^{-1}) & \text{as } |x| \to \infty. \end{cases} \tag{2.1}$$

Here, χ_D is the characteristic function of D, $\partial/\partial\nu$ is the normal derivative, and $|_\pm$ denotes the limits from, respectively, outside and inside Ω. The static background potential U, i.e., the electric potential without any target, is the unique solution to (2.1) with a constant conductivity equal to 1 outside the body of the fish Ω:

$$\begin{cases} \Delta U = f & \text{in } \Omega, \\ \Delta U = 0 & \text{in } \mathbb{R}^2 \setminus \overline{\Omega}, \\ U|_+ - U|_- = \xi \left.\dfrac{\partial U}{\partial \nu}\right|_+ & \text{on } \partial\Omega, \\ \left.\dfrac{\partial U}{\partial \nu}\right|_- = 0 & \text{on } \partial\Omega, \\ |U(x)| = O(|x|^{-1}) & \text{as } |x| \to \infty. \end{cases} \tag{2.2}$$

A dipole approximation for small homogeneous targets away from the fish has been derived in [2]. It is given in terms of the generalized polarization tensors (GPTs). The concept of GPTs for an inhomogeneous target has been first considered in [11]. However in [11], a model much simpler then the weakly electric fish has been taken into account. The aim of the present chapter is to extend the notion of generalized polarization tensors (GPTs) to the fish model described above and to introduce an efficient shape descriptor-based classification for inhomogeneous targets from measurements of the potentials on the skin of the fish. The approach is based on new invariants for particular linear combinations of the GPTs associated with inhomogeneous objects.

2.2.1. Boundary integral representation

The two-dimensional model we want to study is (2.1) where the target D is assumed to be inhomogeneous.

First, we recall a boundary integral representation for the perturbation of the potential, namely $u - U$, where U and u are solutions to (2.2) and (2.1) respectively. Let Γ_R be the Green's function associated with Robin boundary conditions, that is defined for $x \in \mathbb{R}^2 \setminus \overline{\Omega}$ by

$$\begin{cases} -\Delta_y \Gamma_R(x,y) = \delta_x(y), & y \in \mathbb{R}^2 \setminus \overline{\Omega}, \\ \Gamma_R(x,y)|_+ - \xi \dfrac{\partial \Gamma_R}{\partial \nu_x}(x,y)\Big|_+ = 0, & y \in \partial\Omega, \\ \left|\Gamma_R(x,y) + \frac{1}{2\pi}\log|y|\right| = O(|y|^{-1}), & |y| \to \infty. \end{cases} \tag{2.3}$$

We consider the divergence-type equation in (2.1) posed on $\mathbb{R}^2 \setminus \overline{\Omega}$ and test it with the solution Γ_R to (3.8):

$$\Gamma_R(x,y)\, \nabla_y \cdot \gamma(y) \nabla_y u(y) = 0. \tag{2.4}$$

Let B_R be the two-dimensional ball centered at 0 of radius $R > 0$, large enough to enclose both Ω and D. Integrating (2.4) over $B_R \setminus (\overline{\Omega} \cup \overline{D})$, we get

$$\int_{B_R \setminus (\overline{\Omega} \cup \overline{D})} \Gamma_R(x,y) \nabla \cdot \gamma(y) \nabla_y u(y)\, \mathrm{d}y = \int_{B_R \setminus (\overline{\Omega} \cup \overline{D})} \Delta_y u(y)\, \Gamma_R(x,y) \mathrm{d}y = 0.$$

Applying Green's theorem we obtain

$$\begin{aligned} 0 &= \int_{B_R \setminus (\overline{\Omega} \cup \overline{D})} \Delta_y u(y)\, \Gamma_R(x,y) \mathrm{d}y \\ &= \int_{B_R \setminus (\overline{\Omega} \cup \overline{D})} u(y) \cdot (-\Delta_y \Gamma_R)(x,y)\, \mathrm{d}y + \int_{\partial (B_R \setminus (\overline{\Omega} \cup \overline{D}))} \left(\frac{\partial u}{\partial \nu_y}(y)\, \Gamma_R(x,y) - \frac{\partial \Gamma_R}{\partial \nu_y}\, u(y) \right) \mathrm{d}s_y \\ &= u(x) + \int_{\partial (B_R \setminus (\overline{\Omega} \cup \overline{D}))} \left(\frac{\partial u}{\partial \nu}\, \Gamma_R - \frac{\partial \Gamma_R}{\partial \nu_y}\, u \right) \mathrm{d}s. \end{aligned}$$

So, we have

$$\begin{aligned} u(x) &= \int_{\partial (B_R \setminus (\overline{\Omega} \cup \overline{D}))} \left(\frac{\partial \Gamma_R}{\partial \nu_y}\, u - \frac{\partial u}{\partial \nu}\, \Gamma_R \right) \mathrm{d}s \\ &= \int_{\partial B_R} \left(\frac{\partial \Gamma_R}{\partial \nu_y}\, u - \frac{\partial u}{\partial \nu}\, \Gamma_R \right) \mathrm{d}s - \int_{\partial \Omega} \left(\frac{\partial \Gamma_R}{\partial \nu_x}\, u - \frac{\partial u}{\partial \nu}\, \Gamma_R \right) \mathrm{d}s - \int_{\partial D} \left(\frac{\partial \Gamma_R}{\partial \nu_y}\, u - \frac{\partial u}{\partial \nu}\, \Gamma_R \right) \mathrm{d}s. \end{aligned}$$

Let U be the static background solution defined in (2.2). Then

$$\Delta U = 0 \qquad \text{in } \mathbb{R}^2 \setminus \overline{\Omega}.$$

Multiplying by Γ_R and integrating over $B_R \setminus \overline{\Omega}$ we get

$$U(x) = \int_{\partial B_R} \left(\frac{\partial \Gamma_R}{\partial \nu_y}\, U - \frac{\partial U}{\partial \nu}\, \Gamma_R \right) \mathrm{d}s - \int_{\partial \Omega} \left(\frac{\partial \Gamma_R}{\partial \nu_y}\, U - \frac{\partial U}{\partial \nu}\, \Gamma_R \right) \mathrm{d}s.$$

Omitting the contributions of the integrals on ∂B_R, that are negligible as $R \to +\infty$, we have that

$$u - U = \int_{\partial\Omega} \left(\frac{\partial \Gamma_R}{\partial \nu_y} U - \frac{\partial U}{\partial \nu} \Gamma_R \right) - \int_{\partial\Omega} \left(\frac{\partial \Gamma_R}{\partial \nu_y} u - \frac{\partial u}{\partial \nu} \Gamma_R \right) \mathrm{d}s - \int_{\partial D} \left(\frac{\partial \Gamma_R}{\partial \nu_y} u - \frac{\partial u}{\partial \nu} \Gamma_R \right) \mathrm{d}s$$
$$= \int_{\partial\Omega} \frac{\partial \Gamma_R}{\partial \nu_y} (U - u) - \Gamma_R \left(\frac{\partial U}{\partial \nu} - \frac{\partial u}{\partial \nu} \right) \mathrm{d}s - \int_{\partial D} \left(\frac{\partial \Gamma_R}{\partial \nu_y} u - \frac{\partial u}{\partial \nu} \Gamma_R \right) \mathrm{d}s.$$

Then, using the Robin's boundary conditions for Γ_R, U and u, we obtain that

$$= \int_{\partial\Omega} \frac{\partial \Gamma_R}{\partial \nu_y} \left(U_{|+} - u_{|+} \right) - \xi \frac{\partial \Gamma_R}{\partial \nu_y} \left(\frac{U_{|+} - U_{|-}}{\xi} - \frac{u_{|+} - u_{|-}}{\xi} \right) \mathrm{d}s - \int_{\partial D} \left(\frac{\partial \Gamma_R}{\partial \nu_y} u - \frac{\partial u}{\partial \nu} \Gamma_R \right) \mathrm{d}s.$$

Since $u_{|-} = U_{|-}$, we get

$$= \int_{\partial\Omega} \frac{\partial \Gamma_R}{\partial \nu_y} \left(U_{|+} - u_{|+} \right) - \frac{\partial \Gamma_R}{\partial \nu_y} \left(U_{|+} - u_{|+} \right) \mathrm{d}s - \int_{\partial D} \left(\frac{\partial \Gamma_R}{\partial \nu_y} u_{|+} - \left. \frac{\partial u}{\partial \nu} \right|_+ \Gamma_R \right) \mathrm{d}s \,.$$

Therefore,

$$(u - U)(x) = \int_{\partial D} \left(\left. \frac{\partial u}{\partial \nu} \right|_+ (y) \, \Gamma_R(x, y) - \frac{\partial \Gamma_R}{\partial \nu_x}(x, y) \, u_{|+}(y) \right) \mathrm{d}s_y \,. \tag{2.5}$$

Let us now define the Neumann–to–Dirichlet (NtD) map

$$\Lambda_\gamma \left[\gamma \left. \frac{\partial u}{\partial \nu} \right|_- \right] = u_{|\partial D}.$$

The transmission condition on ∂D

$$\gamma \left. \frac{\partial u}{\partial \nu} \right|_- = \left. \frac{\partial u}{\partial \nu} \right|_+$$

yields

$$(u - U)(x) = \int_{\partial D} g(y) \, \Gamma_R(x, y) \, \mathrm{d}s_y - \int_{\partial D} \frac{\partial \Gamma_R}{\partial \nu_y}(x, y) \, \Lambda_\gamma[g](y) \, \mathrm{d}s_y \,,$$

with $g = \partial u / \partial \nu|_+$.

For $x \in \mathbb{R}^2 \setminus (\overline{\Omega} \cup \overline{D})$,

$$\Lambda_1 \left(\frac{\partial \Gamma_R(x, \cdot)}{\partial \nu_y} \right) = \Gamma_R(x, \cdot) - \frac{1}{|\partial D|} \int_{\partial D} \Gamma_R(x, y) \, \mathrm{d}s_y \qquad \text{on } \partial D,$$

where $\Lambda_1 = \Lambda_{\gamma \equiv 1}$, and hence,

$$\frac{\partial \Gamma_R(x, \cdot)}{\partial \nu_y} = \Lambda_1^{-1} [\Gamma_R(x, \cdot)] \qquad \text{on } \partial D,$$

since $\Lambda_1 : H_0^{-1/2}(\partial D) \to H_0^{1/2}(\partial D)$ is invertible. Moreover, since $\Lambda_1 : H_0^{-1/2}(\partial D) \to H_0^{1/2}(\partial D)$ is self-adjoint, it follows that

$$\begin{aligned}(u-U)(x) &= \int_{\partial D} g(y)\,\Gamma_R(x,y)\,\mathrm{d}s_y - \int_{\partial D} \Lambda_1^{-1}[\Gamma_R(x,\cdot)](y)\,\Lambda_\gamma[g](y)\,\mathrm{d}s_y \\ &= \int_{\partial D} g(y)\,\Gamma_R(x,y)\,\mathrm{d}s_y - \int_{\partial D} \Gamma_R(x,y)\,\Lambda_1^{-1}\Lambda_\gamma[g](y)\,\mathrm{d}s_y \\ &= \int_{\partial D} \Gamma_R(x,y)(g(y) - \Lambda_1^{-1}\Lambda_\gamma[g](y))\,\mathrm{d}s_y \\ &= \int_{\partial D} \Gamma_R(x,y)(I - \Lambda_1^{-1}\Lambda_\gamma)[g](y)\,\mathrm{d}s_y \\ &= \int_{\partial D} \Gamma_R(x,y)\Lambda_1^{-1}(\Lambda_1 - \Lambda_\gamma)[g](y)\,\mathrm{d}s_y\,.\end{aligned}$$

Therefore, the following result holds.

Lemma 2.2.1 *For $x \in \mathbb{R}^2 \setminus (\overline{\Omega} \cup \overline{D})$, we have*

$$(u-U)(x) = \int_{\partial D} \Gamma_R(x,y)\Lambda_1^{-1}(\Lambda_1 - \Lambda_\gamma)[g](y)\; ds_y, \tag{2.6}$$

with $g = \partial u/\partial\nu|_+$.

Theorem 2.2.2 (Dipolar approximation) *If $D = z + \delta B$, with $dist(\partial\Omega, z) \gg 1$, $\delta \ll 1$ and B is a bounded open set, then for any $x \in \partial\Omega$,*

$$\left(\frac{\partial u}{\partial\nu} - \frac{\partial U}{\partial\nu}\right)(x) = -\delta^2 \nabla U(z)^T M(\widehat{\gamma}, B) \nabla_y \left(\left.\frac{\partial \Gamma_R}{\partial\nu}\right|_+\right)(x,z) + O(\delta^3), \tag{2.7}$$

where T denotes the transpose, $M(\widehat{\gamma}, B) = (m_{ij})_{i,j\in\{1,2\}}$ is the first-order polarization tensor associated with B and $\widehat{\gamma}$, given by

$$m_{ij} = \int_{\partial B} y_i \mathcal{T}_B \left(I - \left(\frac{I}{2} + \mathcal{K}_B^*\right)\mathcal{T}_B\right)^{-1} \left(\left.\frac{\partial x_j}{\partial\nu}\right|_{\partial B}\right)(y)\; ds_y, \tag{2.8}$$

where I is the identity operator, and $\mathcal{T}_B : H_0^{-1/2}(\partial B) \longrightarrow H_0^{-1/2}(\partial B)$ is the operator defined by $\mathcal{T}_B := \Lambda_1^{-1}(\Lambda_1 - \Lambda_{\widehat{\gamma}})$.

Proof. Let Γ be the fundamental solution of the Laplacian in $\mathbb{R}^2$. Following [18, 22], define

$$H = -\int_{\partial\Omega} \left(\frac{\partial\Gamma}{\partial\nu_y}\, u - \frac{\partial u}{\partial\nu}\,\Gamma\right)\mathrm{d}s = -\mathcal{D}_\Omega[u|_+] + \mathcal{S}_\Omega\left[\left.\frac{\partial u}{\partial\nu}\right|_+\right]. \tag{2.9}$$

Integration by parts and using the same arguments as those in the proof of Lemma 2.2.1 yields

$$(u-H)(x) = \int_{\partial D} \Gamma(x,y)\Lambda_1^{-1}(\Lambda_1 - \Lambda_\gamma)[g](y)\,\mathrm{d}s_y = \mathcal{S}_D\left[\mathcal{T}_D[g]\right](x), \tag{2.10}$$

where $\mathcal{T}_D := \Lambda_1^{-1}(\Lambda_1 - \Lambda_\gamma)$.

Taking the normal derivative on ∂D in (2.10) from outside and using the jump relations gives

$$g = \frac{\partial u}{\partial \nu}\bigg|_{+} = \frac{\partial H}{\partial \nu} + \left(\frac{I}{2} + \mathcal{K}_D^*\right)\mathcal{T}_D[g].$$

Hence,

$$g = \left(I - \left(\frac{I}{2} + \mathcal{K}_D^*\right)\mathcal{T}_D\right)^{-1}\left(\frac{\partial H}{\partial \nu}\bigg|_{\partial D}\right). \tag{2.11}$$

Substituting (2.11) into (2.6), we get

$$(u-U)(x) = \int_{\partial D} \Gamma_R(x,y)\mathcal{T}_D\left(I - \left(\frac{I}{2} + \mathcal{K}_D^*\right)\mathcal{T}_D\right)^{-1}\left(\frac{\partial H}{\partial \nu}\bigg|_{\partial D}\right)(y)\, \mathrm{d}s_y. \tag{2.12}$$

Following the same arguments as those in [18, 22], we can establish by using the scaling properties of $\mathcal{K}_D^*$ and $\mathcal{T}_D$ that $\|\nabla H - \nabla U\| = O(\delta^2)$; see [22]. Therefore, Taylor expanding $\Gamma_R(x,\cdot)$ and H at z and scaling the integral, we get the desired expression for the leading-order term of the small-volume expansion. □

Definition 2.2.3 *Let $\alpha, \beta \in \mathbb{N}^2$ be multi-indices. We define the generalized polarization tensors associated to the conductivity distribution $\widehat{\gamma}$ by*

$$M_{\alpha\beta}(\widehat{\gamma}, B) = \int_{\partial B} y^\alpha \mathcal{T}_B\left(I - \left(\frac{I}{2} + \mathcal{K}_B^*\right)\mathcal{T}_B\right)^{-1}\left(\frac{\partial x^\beta}{\partial \nu}\bigg|_{\partial B}\right)(y)\ ds_y. \tag{2.13}$$

We can also define the contracted generalized polarization tensors (CGPTs) as follows.

Definition 2.2.4 *Let $z = y_1 + iy_2$ and $\zeta = x_1 + ix_2$. For any pair of indices $m, n \in \mathbb{N}$, we define*

$$M_{mn}^{cc}(\widehat{\gamma}, B) := \int_{\partial B} Re(z^m)\mathcal{T}_B\left(I - \left(\frac{I}{2} + \mathcal{K}_B^*\right)\mathcal{T}_B\right)^{-1}[Re(\zeta^n)](y)\ ds_y,$$

$$M_{mn}^{cs}(\widehat{\gamma}, B) := \int_{\partial B} Re(z^m)\mathcal{T}_B\left(I - \left(\frac{I}{2} + \mathcal{K}_B^*\right)\mathcal{T}_B\right)^{-1}[Im(\zeta^n)](y)\ ds_y,$$

$$M_{mn}^{sc}(\widehat{\gamma}, B) := \int_{\partial B} Im(z^m)\mathcal{T}_B\left(I - \left(\frac{I}{2} + \mathcal{K}_B^*\right)\mathcal{T}_B\right)^{-1}[Re(\zeta^n)](y)\ ds_y,$$

$$M_{mn}^{ss}(\widehat{\gamma}, B) := \int_{\partial B} Im(z^m)\mathcal{T}_B\left(I - \left(\frac{I}{2} + \mathcal{K}_B^*\right)\mathcal{T}_B\right)^{-1}[Im(\zeta^n)](y)\ ds_y.$$

Note that the CGPTs introduced here coincide with those studied in [11].

Proposition 2.2.5 *Let u be the solution to*

$$\begin{cases} \nabla \cdot \gamma \nabla u = 0 & \text{in } \mathbb{R}^2, \\ u - h = O(|x|^{-1}) & \text{as } |x| \to +\infty, \end{cases} \tag{2.14}$$

where h is a harmonic function in $\mathbb{R}^2$. Then the following identity holds:

$$\gamma \frac{\partial u}{\partial \nu}\bigg|_- = \left(I - \left(\frac{I}{2} + \mathcal{K}_D^*\right)\mathcal{T}_D\right)^{-1}\left[\frac{\partial h}{\partial \nu}\right] \qquad \text{on } \partial D. \tag{2.15}$$

Proof. The solution u to (2.14) can be represented as

$$u = h + \mathcal{S}_D[\psi] \qquad \text{in } \mathbb{R}^2 \setminus \overline{D}, \tag{2.16}$$

for some $\psi \in L^2(\partial D)$. Therefore,

$$\frac{\partial u}{\partial \nu}\bigg|_+ = \frac{\partial h}{\partial \nu} + \left(\frac{I}{2} + \mathcal{K}_D^*\right)[\psi].$$

The transmission condition on ∂D

$$\frac{\partial u}{\partial \nu}\bigg|_+ = \gamma \frac{\partial u}{\partial \nu}\bigg|_-$$

leads to

$$\gamma \frac{\partial u}{\partial \nu}\bigg|_- = \frac{\partial h}{\partial \nu} + \left(\frac{I}{2} + \mathcal{K}_D^*\right)[\psi]. \tag{2.17}$$

Applying the map Λ_γ on both sides gives

$$\left(\frac{I}{2} + \mathcal{K}_D^*\right)[\psi] = u - \Lambda_\gamma\left[\frac{\partial h}{\partial \nu}\right].$$

Next, using the representation (2.16), we get

$$\Lambda_\gamma\left(\frac{I}{2} + \mathcal{K}_D^*\right)[\psi] = h + \mathcal{S}_D[\psi] - \Lambda_\gamma\left[\frac{\partial h}{\partial \nu}\right].$$

Applying Λ_1^{-1} and using the jump relations, we obtain

$$\Lambda_1^{-1}\Lambda_\gamma\left(\frac{I}{2} + \mathcal{K}_D^*\right)[\psi] = \frac{\partial h}{\partial \nu} + \left(-\frac{I}{2} + \mathcal{K}_D^*\right)[\psi] - \Lambda_1^{-1}\Lambda_\gamma\left[\frac{\partial h}{\partial \nu}\right].$$

Hence

$$\left[-\left(-\frac{I}{2} + \mathcal{K}_D^*\right) + \Lambda_1^{-1}\Lambda_\gamma\left(\frac{I}{2} + \mathcal{K}_D^*\right)\right][\psi] = \frac{\partial h}{\partial \nu} - \Lambda_1^{-1}\Lambda_\gamma\left[\frac{\partial h}{\partial \nu}\right],$$

$$\left[I - \left(\frac{I}{2} + \mathcal{K}_D^*\right) + \Lambda_1^{-1}\Lambda_\gamma\left(\frac{I}{2} + \mathcal{K}_D^*\right)\right][\psi] = \mathcal{T}_D\left[\frac{\partial h}{\partial \nu}\right],$$

$$\left[I - \mathcal{T}_D\left(\frac{I}{2} + \mathcal{K}_D^*\right)\right][\psi] = \mathcal{T}_D\left[\frac{\partial h}{\partial \nu}\right].$$

Therefore, we get the following expression of ψ:

$$\psi = \left(I - \mathcal{T}_D\left(\frac{I}{2} + \mathcal{K}_D^*\right)\right)^{-1}\left[\mathcal{T}_D\left[\frac{\partial h}{\partial \nu}\right]\right].$$

Substituting ψ into (2.17), we arrive at

$$\gamma \frac{\partial u}{\partial \nu}\bigg|_- = \frac{\partial h}{\partial \nu} + \left(\frac{I}{2} + \mathcal{K}_D^*\right)\left(I - \mathcal{T}_D\left(\frac{I}{2} + \mathcal{K}_D^*\right)\right)^{-1} \mathcal{T}_D\left[\frac{\partial h}{\partial \nu}\right],$$

or equivalently,

$$\gamma \frac{\partial u}{\partial \nu}\bigg|_- = \left[I - \left(I - \left(\left(\frac{I}{2} + \mathcal{K}_D^*\right)\mathcal{T}_D\right)^{-1}\right)^{-1}\right]\left[\frac{\partial h}{\partial \nu}\right], \tag{2.18}$$

which is equivalent to (2.15). □

The following result shows that the GPTs are the building blocks of the multipolar asymptotic expansion.

Theorem 2.2.6 (Multipolar approximation) *For every integer $K \geq 1$, the following expansion holds*

$$u(x) = H(x) + \delta^{d-2} \sum_{|\alpha|=1}^{K} \sum_{|\beta|=1}^{K-|\alpha|+1} \frac{(-1)^{|\beta|}\delta^{|\alpha|+|\beta|}}{\alpha!\beta!} \partial^\alpha H(z) M_{\alpha\beta}(\widehat{\gamma}, B) \partial_y^\beta \Gamma(x,z) + O(\delta^{2+K}), \tag{2.19}$$

uniformly for $x \in \partial\Omega$, where H is the function defined by (2.9).

Proof. The argument is the same used to prove the multipolar expansion in [7, Theorem 1]. For the sake of completeness, the adapted proof is reported below.

From (2.10) and (2.11) we get

$$u(x) = H(x) + \mathcal{S}_D[\phi](x), \quad x \in \mathbb{R}^2 \setminus (\overline{\Omega} \cup \overline{D}), \tag{2.20}$$

where $\phi := \mathcal{T}_D\left(I - \left(\frac{I}{2} + \mathcal{K}_D^*\right)\mathcal{T}_D\right)^{-1}\left(\frac{\partial H}{\partial \nu}|_{\partial D}\right)$. Denoting

$$H_K(x) = \sum_{|\alpha|=0}^{K} \frac{1}{\alpha!} \partial^\alpha H(z)(x-z)^\alpha, \tag{2.21}$$

a Taylor expansion implies

$$\left\| \frac{\partial H_K}{\partial \nu} - \frac{\partial H}{\partial \nu} \right\|_{L^2(\partial D)} \leq C\delta^K |\partial D|^{1/2}.$$

On the other hand, defining $\phi_K := \mathcal{T}_D\left(I - \left(\frac{I}{2} + \mathcal{K}_D^*\right)\mathcal{T}_D\right)^{-1}\left(\frac{\partial H_K}{\partial \nu}|_{\partial D}\right)$, the same argument as in [3, Section 4.2] leads to the following estimates: for any $x \in \partial\Omega$,

$$\begin{aligned} |\mathcal{S}_D(\phi - \phi_K)(x)| &= \left| \int_{\partial D} (\Gamma(x,y) - \Gamma(x,z))(\phi(y) - \phi_K(y)) \, \mathrm{d}s_y \right| \\ &\leq \int_{\partial D} |\Gamma(x,y) - \Gamma(x,z)||\phi(y) - \phi_K(y)| \, \mathrm{d}s_y \\ &\leq C'\delta |\partial D|^{1/2} \|\phi - \phi_K\|_{L^2(\partial D)}, \end{aligned}$$

whereas

$$\|\phi - \phi_K\|_{L^2(\partial D)} \leq C'' \left\| \frac{\partial H_K}{\partial \nu} - \frac{\partial H}{\partial \nu} \right\|_{L^2(\partial D)} \leq CC'' \delta^K |\partial D|^{1/2}.$$

Therefore

$$\|\mathcal{S}_D(\phi - \phi_K)\|_{L^\infty(\partial\Omega)} = O(\delta^{2+K}).$$

Thus, from (2.20) we immediately get

$$u(x) = H(x) + \mathcal{S}_D\left[\phi_K\right](x) + O(\delta^{2+K}). \tag{2.22}$$

Proceeding as in [5, Section 3], after plugging the Taylor expansion (2.21) of H into the expression of ϕ_K appearing in formula (2.22), by a change of variables $y' = (y - z)/\delta$ in the integral we obtain

$$u(x) = H(x) + \sum_{|\alpha|=0}^{K} \frac{1}{\alpha!} \partial^\alpha H(z) \delta^{|\alpha|} \int_{\partial B} \Gamma(x, z + \delta y') \psi_\alpha(y') \, \mathrm{d}s_{y'} + O(\delta^{2+K}), \tag{2.23}$$

where $\psi_\alpha = \mathcal{T}_B \left(I - \left(\frac{I}{2} + \mathcal{K}_B^* \right) \mathcal{T}_B \right)^{-1} (\nu \cdot \nabla \zeta^\alpha)$. Finally, expansion (2.19) follows by injecting a Taylor expansion of fundamental solution

$$\Gamma(x, z + \delta y') = \sum_{|\beta|=0}^{\infty} \frac{(-\delta)^{|\beta|}}{\beta!} \partial^\beta \Gamma(x, z) y^\beta,$$

into (2.23). □

Remark 2.2.7 *Observe that the terms $\partial^\alpha H(z)$ in the small-volume expansion stated above depend on δ. Even though (2.19) could have been derived in terms of U and its derivatives entirely, it is more convenient to keep the formula as it is. As a matter of fact $\partial^\alpha H(z)$ can be easily computed from the boundary measurements on $\partial\Omega$ once the center z is known and its simplicity makes it suitable to solve the inverse problem we are interested in.*

Remark 2.2.8 *In view of (2.19), the GPTs $M_{\alpha\beta}(\widehat{\gamma}, B)$ can be reconstructed from measurements of $(u - H)|_{\partial\Omega}$ corresponding to different positions of the fish. As in [6], the number of GPTs which can be reconstructed accurately for a given signal-to-noise ratio can be determined in terms of the ratio between the characteristic size of the target and its distance to the fish. The resolving formula derived in [6] holds. Moreover, it is worth mentioning that if the target is homogeneous, then the GPTs reduce to those first introduced and investigated in [18, 19]. In fact, if $\gamma|_D \equiv k$, $0 < k \neq 1 < +\infty$, then*

$$\begin{aligned} M_{\alpha\beta}(k, D) &= \int_{\partial D} y^\alpha \left(\mathcal{T}_D^{-1} - \left(\frac{I}{2} + \mathcal{K}_D^* \right) \right)^{-1} \left(\frac{\partial x^\beta}{\partial \nu} \bigg|_{\partial D} \right)(y) \, ds_y \\ &= \int_{\partial D} y^\alpha \left(\lambda I - \mathcal{K}_D^* \right)^{-1} \left(\frac{\partial x^\beta}{\partial \nu} \bigg|_{\partial D} \right)(y) \, ds_y, \end{aligned}$$

where $\lambda = \frac{k+1}{2(k-1)}$.

2.3. Properties of the CGPTs

The goal of this section is to provide transformation formulas for the contracted GPTs introduced in Definition 2.2.4.

2.3.1. Translation formula

We want to investigate how the quantity

$$M_{mn}^{cc}(\gamma, D) = M_{mn} = \int_{\partial D} \mathrm{Re}(z^m)\mathcal{T}_D[g_n^c](y)\ \mathrm{d}s_y \tag{2.24}$$

changes with respect to a translation of D.

We denote by $\widehat{x} = x + z$, $\widehat{D} := D + z$, $\widehat{1}(\widehat{x}) := 1$, and $\widehat{\gamma}(\widehat{x}) := \gamma(x)$. We want to relate $M_{mn}^{cc}(\gamma, D)$ with $M_{mn}^{cc}(\widehat{\gamma}, \widehat{D})$ defined by

$$M_{mn}^{cc}(\widehat{\gamma}, \widehat{D}) = \widehat{M}_{mn}^{cc} = \int_{\partial \widehat{D}} \mathrm{Re}(\widehat{x}^m)(\widehat{g}_n^c(\widehat{x}) - \Lambda_{\widehat{1}}^{-1}\Lambda_{\widehat{\gamma}}^{\widehat{D}}[\widehat{g}_n^c](\widehat{x}))\ \mathrm{d}s_{\widehat{x}}.$$

By the change of variables $\widehat{x} = x + z$, we obtain

$$M_{mn}^{cc}(\widehat{\gamma}, \widehat{D}) = \widehat{M}_{mn}^{cc} = \int_{\partial D} \mathrm{Re}((x+z)^m)(\widehat{g}_n^c(x+z) - \Lambda_{\widehat{1}}^{-1}\Lambda_{\widehat{\gamma}}^{\widehat{D}}[\widehat{g}_n^c](x+z))\ \mathrm{d}s_x\,. \tag{2.25}$$

Lemma 2.3.1 *We have*

$$\widehat{g}_n^c(x+z) = \sum_{k=1}^{n} \binom{n}{k} [g_k^c(x) r_z^{n-k} \cos((n-k)\theta_z) - g_k^s(x) r_z^{n-k} \sin((n-k)\theta_z)]\,, \tag{2.26}$$

and

$$\widehat{g}_n^s(x+z) = \sum_{k=1}^{n} \binom{n}{k} [g_k^s(x) r_z^{n-k} \cos((n-k)\theta_z) + g_k^c(x) r_z^{n-k} \sin((n-k)\theta_z)]\,, \tag{2.27}$$

where $z = r_z(\cos\theta_z, \sin\theta_z)$ in polar coordinates.

Proof. Let $\widehat{u}_n^c$ be the solution to

$$\begin{cases} \nabla_{\widehat{x}} \cdot \widehat{\gamma}(\widehat{x}) \nabla_{\widehat{x}} \widehat{u}_n^c(\widehat{x}) = 0 & \text{in } \mathbb{R}^2, \\ \widehat{u}_n^c(\widehat{x}) - \mathrm{Re}(\widehat{x}^n) = O(|\widehat{x}|^{-1}) & \text{as } |\widehat{x}| \to +\infty. \end{cases} \tag{2.28}$$

Then, by definition, $\widehat{g}_n^c := \widehat{\gamma}\dfrac{\partial \widehat{u}_n^c}{\partial \nu_{\widehat{x}}}$. Using the change of variables in (2.28) and setting $v_n^c(x) := \widehat{u}_n^c(x+z)$, we obtain

$$\begin{cases} \nabla_x \cdot \gamma(x) \nabla_x v_n^c(x) = 0 & \text{in } \mathbb{R}^2, \\ v_n^c(x) - \mathrm{Re}((x+z)^n) = O(|x|^{-1}) & \text{as } |x| \to +\infty. \end{cases}$$

From

$$\mathrm{Re}((x+z)^n) = \sum_{k=0}^{n} \binom{n}{k} r_x^k r_z^{n-k} [\cos(k\theta_x)\cos((n-k)\theta_z) - \sin(k\theta_x)\sin((n-k)\theta_z)],$$

it follows that

$$v_n^c(x) = \sum_{k=0}^{n} \binom{n}{k} [h_k^c(x) r_z^{n-k} \cos((n-k)\theta_z) - h_k^s(x) r_z^{n-k} \sin((n-k)\theta_z)].$$

Hence,

$$\widehat{g}_n^c(x+z) = \sum_{k=1}^{n} \binom{n}{k} [g_k^c(x) r_z^{n-k} \cos((n-k)\theta_z) - g_k^s(x) r_z^{n-k} \sin((n-k)\theta_z)].$$

Analogously we derive formula (2.27) for $\widehat{g}_n^s$. □

To relate (2.24) and (2.25) we consider the operator

$$\Lambda_1^{-1}\Lambda_\gamma^D : H_0^{-1/2}(\partial D) \longrightarrow H_0^{-1/2}(\partial D)$$

$$g_n^c \longmapsto \left.\frac{\partial h}{\partial \nu_x}\right|_-,$$

where h is the solution to the boundary value problem

$$\begin{cases} \Delta h = 0 & \text{in } D, \\ \nabla_x h \cdot \nu_x = g_n^c & \text{on } \partial D. \end{cases} \tag{2.29}$$

Let $y \in D$ and consider the corresponding Neumann function $N_1(x,y)$, that is, the solution to

$$\begin{cases} \Delta_x N_1(x,y) = -\delta_y(x), & x \in D, \\ \nabla_x N_1(x,y) \cdot \nu_x = \frac{1}{|\partial D|}, & x \in \partial D, \\ \displaystyle\int_{\partial D} N_1(x,y)\mathrm{d}s_x = 0. \end{cases} \tag{2.30}$$

Then the solution h of (2.29) can be represented by means of this Neumann function

$$h(y) = \int_{\partial D} N_1(x,y) g(x)\ \mathrm{d}s_x.$$

So, for $y \in \partial D$, we have

$$\Lambda_1^{-1}\Lambda_\gamma^D[g_n^c](y) = \nabla_y h(y) \cdot \nu_y|_{\partial D} = \int_{\partial D} \nabla_y N_1(x,y) \cdot \nu_y\, g_n^c(x)\ \mathrm{d}s_x. \tag{2.31}$$

Now we proceed similarly. We let the operator $\Lambda_{\widehat{1}}^{-1}\Lambda_{\widehat{\gamma}}^{\widehat{D}} : H_0^{-1/2}(\partial\widehat{D}) \longrightarrow H_0^{-1/2}(\partial\widehat{D})$ be defined by

$$\widehat{g}_n^c \longmapsto \left.\frac{\partial\widehat{h}}{\partial\nu_{\widehat{x}}}\right|_- ,$$

with $\widehat{h}$ being the solution of

$$\begin{cases} \Delta\widehat{h} = 0 & \text{in } \widehat{D}, \\ \nabla_{\widehat{x}}\widehat{h}\cdot\nu_{\widehat{x}} = \widehat{g}_n^c & \text{on } \partial\widehat{D}. \end{cases} \tag{2.32}$$

Let $\widehat{y} = y + z \in \widehat{D}$ and consider the corresponding Neumann function $\widehat{N}_1(\widehat{x},\widehat{y})$, that is, the solution to

$$\begin{cases} \Delta_{\widehat{x}}\widehat{N}_1(\widehat{x},\widehat{y}) = -\delta_{\widehat{y}}(\widehat{x}), & \widehat{x}\in\widehat{D}, \\ \nabla_{\widehat{x}}\widehat{N}_1(\widehat{x},\widehat{y})\cdot\nu_{\widehat{x}} = -\frac{1}{|\partial\widehat{D}|}, & \widehat{x}\in\partial\widehat{D}, \\ \displaystyle\int_{\partial\widehat{D}} \widehat{N}_1(\widehat{x},\widehat{y})\mathrm{d}s_{\widehat{x}} = 0, \end{cases}$$

that can be written as

$$\begin{cases} \Delta_x\widehat{N}_1(x+z,y+z) = -\delta_y(x), & x\in D, \\ \nabla_x\widehat{N}_1(x+z,y+z)\cdot\nu_x = -\frac{1}{|\partial D|}, & x\in\partial D, \\ \displaystyle\int_{\partial D} \widehat{N}_1(x+z,y+z)\mathrm{d}s_x = 0. \end{cases} \tag{2.33}$$

Comparing (2.33) and (2.30), we observe that $\widehat{N}_1(x+z,y+z)$ and $N_1(x,y)$ satisfy the same boundary value problem (2.30). The uniqueness of a solution to (2.30) yields

$$\widehat{N}_1(x+z,y+z) = N_1(x,y)\,. \tag{2.34}$$

The solution $\widehat{h}$ to (2.32) can be represented by means of the Neumann function $\widehat{N}_1$:

$$\widehat{h}(\widehat{y}) = \int_{\partial\widehat{D}} \widehat{N}_1(\widehat{x},\widehat{y})\,\widehat{g}_n^c(\widehat{x})\;\mathrm{d}s_{\widehat{x}}.$$

Moreover, for $y\in\partial D$, we have

$$\begin{aligned}
\Lambda_{\widehat{1}}^{-1}\Lambda_{\widehat{\gamma}}^{\widehat{D}}[\widehat{g}_n^c](\widehat{y}) &= \nabla_{\widehat{y}}\widehat{h}(\widehat{y})\cdot\nu_{\widehat{y}} \\
&= \int_{\partial\widehat{D}} (\nabla_{\widehat{y}}\widehat{N}_1)(\widehat{x},\widehat{y})\cdot\nu_{\widehat{y}}\,\widehat{g}_n^c(\widehat{x})\;\mathrm{d}s_{\widehat{x}} \\
&= \int_{\partial D} (\nabla_y\widehat{N}_1)(x+z,\widehat{y})\cdot\nu_y\,\widehat{g}_n^c(x+z)\;\mathrm{d}s_x \\
&= \int_{\partial D} (\nabla_y N_1)(x,y)\cdot\nu_y \sum_{k=1}^{n}\binom{n}{k}\left[g_k^c(x)r_z^{n-k}\cos((n-k)\theta_z) - g_k^s(x)r_z^{n-k}\sin((n-k)\theta_z)\right]\mathrm{d}s_x \\
&= \sum_{k=1}^{n}\binom{n}{k} r_z^{n-k}\Big[\cos((n-k)\theta_z)\int_{\partial D}(\nabla_y N_1)(x,y)\cdot\nu_y\,g_k^c(x)\;\mathrm{d}s_x \\
&\quad - \sin((n-k)\theta_z)\int_{\partial D}(\nabla_y N_1)(x,y)\cdot\nu_y\,g_k^s(x)\;\mathrm{d}s_x\Big] \\
&= \sum_{k=1}^{n}\binom{n}{k} r_z^{n-k}\left[\cos((n-k)\theta_z)\,\Lambda_1^{-1}\Lambda_\gamma^D[g_k^c](y) - \sin((n-k)\theta_z)\,\Lambda_1^{-1}\Lambda_\gamma^D[g_k^s](y)\right].
\end{aligned}$$

Here we have made the change of variables $\widehat{x} = x + z$ and used identity (2.34). Therefore, it follows that

$$\Lambda_{\widehat{1}}^{-1}\Lambda_{\widehat{\gamma}}^{\widehat{D}}[\widehat{g}](\widehat{y}) = \sum_{k=1}^{n}\binom{n}{k} r_z^{n-k}\left[\cos((n-k)\theta_z)\,\Lambda_1^{-1}\Lambda_\gamma^D[g_k^c](y) - \sin((n-k)\theta_z)\,\Lambda_1^{-1}\Lambda_\gamma^D[g_k^s](y)\right]. \tag{2.35}$$

Hence

$$M_{mn}^{cc}(\widehat{\gamma},\widehat{D}) = \int_{\partial D}\mathrm{Re}((x+z)^m)(g_n^c(x) - \Lambda_1^{-1}\Lambda_\gamma^D[g_n^c](x))\,\mathrm{d}s_x.$$

Using the identity

$$\mathrm{Re}((x+z)^m) = \sum_{k=0}^{m}\binom{m}{k} r_x^k r_z^{m-k}[\cos(k\theta_x)\cos((m-k)\theta_z) - \sin(k\theta_x)\sin((m-k)\theta_z)],$$

we get

$$\begin{aligned} M_{mn}^{cc}(\widehat{\gamma},\widehat{D}) &= \int_{\partial D}\mathrm{Re}((x+z)^m)(\widehat{g}_n^c(x+z) - \Lambda_{\widehat{1}}^{-1}\Lambda_{\widehat{\gamma}}^{\widehat{D}}[\widehat{g}_n^c](x+z))\,\mathrm{d}s_x \\ &= \sum_{k=1}^{m} r_z^{m-k}\binom{m}{k}\Big[\cos((m-k)\theta_z)\int_{\partial D} r_x^k\cos(k\theta_x)(\widehat{g}_n^c(x+z) - \Lambda_{\widehat{1}}^{-1}\Lambda_{\widehat{\gamma}}^{\widehat{D}}[\widehat{g}_n^c](x+z))\,\mathrm{d}s_x \\ &\quad - \sin((m-k)\theta_z)\int_{\partial D} r_x^k\sin(k\theta_x)(\widehat{g}_n^c(x+z) - \Lambda_{\widehat{1}}^{-1}\Lambda_{\widehat{\gamma}}^{\widehat{D}}[\widehat{g}_n^c](x+z))\,\mathrm{d}s_x\Big]. \end{aligned} \tag{2.36}$$

From Lemma 2.3.1 and formula (2.35), we obtain

$$\begin{aligned} \widehat{g}_n^c(x+z) - \Lambda_{\widehat{1}}^{-1}\Lambda_{\widehat{\gamma}}^{\widehat{D}}[\widehat{g}_n^c](x+z) &= \sum_{r=1}^{n}\binom{n}{r} r_z^{n-r}[g_r^c(x)\cos((n-r)\theta_z) - g_r^s(x)\sin((n-r)\theta_z)] \\ &\quad - \sum_{r=1}^{n}\binom{n}{r} r_z^{n-r}\left[\cos((n-r)\theta_z)\,\Lambda_1^{-1}\Lambda_\gamma^D[g_r^c](x) - \sin((n-r)\theta_z)\,\Lambda_1^{-1}\Lambda_\gamma^D[g_r^s](x)\right] \\ &= \sum_{r=1}^{n}\binom{n}{r} r_z^{n-r}\,[g_r^c(x)\cos((n-r)\theta_z) - g_r^s(x)\sin((n-r)\theta_z) \\ &\quad -(\cos((n-r)\theta_z)\,\Lambda_1^{-1}\Lambda_\gamma^D[g_r^c](x) - \sin((n-r)\theta_z)\,\Lambda_1^{-1}\Lambda_\gamma^D[g_r^s](x))\big] \\ &= \sum_{r=1}^{n}\binom{n}{r} r_z^{n-r}\left[(g_r^c(x) - \Lambda_1^{-1}\Lambda_\gamma^D[g_r^c](x))\cos((n-r)\theta_z) - (g_r^s(x) - \Lambda_1^{-1}\Lambda_\gamma^D[g_r^s](x))\sin((n-r)\theta_z)\right]. \end{aligned}$$

So

$$\begin{aligned} &\int_{\partial D} r_x^k\cos(k\theta_x)(\widehat{g}_n^c(x+z) - \Lambda_{\widehat{1}}^{-1}\Lambda_{\widehat{\gamma}}^{\widehat{D}}[\widehat{g}_n^c](x+z))\,\mathrm{d}s_x \\ &= \sum_{r=1}^{n}\binom{n}{r} r_z^{n-r}\left[\cos((n-r)\theta_z)M_{kr}^{cc} - \sin((n-r)\theta_z)M_{kr}^{cs}\right], \end{aligned} \tag{2.37}$$

and

$$\begin{aligned} &\int_{\partial D} r_x^k\sin(k\theta_x)(\widehat{g}_n^c(x+z) - \Lambda_{\widehat{1}}^{-1}\Lambda_{\widehat{\gamma}}^{\widehat{D}}[\widehat{g}_n^c](x+z))\,\mathrm{d}s_x \\ &= \sum_{r=1}^{n}\binom{n}{r} r_z^{n-r}\left[\cos((n-r)\theta_z)M_{kr}^{sc} - \sin((n-r)\theta_z)M_{kr}^{ss}\right]. \end{aligned} \tag{2.38}$$

Plugging (2.37) and (2.38) into formula (2.36), we arrive at

$$\begin{aligned}M^{cc}_{mn}(\widehat{\gamma},\widehat{D}) = \sum_{k=1}^{m}\sum_{r=1}^{n}\binom{n}{r}\binom{m}{k} r_z^{n-r} r_z^{m-k} \{&\cos((m-k)\theta_z)\,[\cos((n-r)\theta_z)M^{cc}_{kr} - \sin((n-r)\theta_z)M^{cs}_{kr}]\\ &-\sin((m-k)\theta_z)\;\,[\cos((n-r)\theta_z)M^{sc}_{kr} - \sin((n-r)\theta_z)M^{ss}_{kr}]\}\,.\end{aligned}$$

Analogously, we readily get

$$\begin{aligned}M^{sc}_{mn}(\widehat{\gamma},\widehat{D}) = \sum_{k=1}^{m}\sum_{r=1}^{n}\binom{n}{r}\binom{m}{k} r_z^{n-r} r_z^{m-k} \{&\cos((m-k)\theta_z)\,[\cos((n-r)\theta_z)M^{sc}_{kr} - \sin((n-r)\theta_z)M^{ss}_{kr}]\\ &+\sin((m-k)\theta_z)\,[\cos((n-r)\theta_z)M^{cc}_{kr} - \sin((n-r)\theta_z)M^{cs}_{kr}]\}\,,\end{aligned}$$

$$\begin{aligned}M^{cs}_{mn}(\widehat{\gamma},\widehat{D}) = \sum_{k=1}^{m}\sum_{r=1}^{n}\binom{n}{r}\binom{m}{k} r_z^{n-r} r_z^{m-k} \{&\cos((m-k)\theta_z)\,[\cos((n-r)\theta_z)M^{cs}_{kr} + \sin((n-r)\theta_z)M^{cc}_{kr}]\\ &-\sin((m-k)\theta_z)\;\,[\cos((n-r)\theta_z)M^{ss}_{kr} + \sin((n-r)\theta_z)M^{sc}_{kr}]\}\,,\end{aligned}$$

$$\begin{aligned}M^{ss}_{mn}(\widehat{\gamma},\widehat{D}) = \sum_{k=1}^{m}\sum_{r=1}^{n}\binom{n}{r}\binom{m}{k} r_z^{n-r} r_z^{m-k} \{&\cos((m-k)\theta_z)\,[\cos((n-r)\theta_z)M^{ss}_{kr} + \sin((n-r)\theta_z)M^{sc}_{kr}]\\ &+\sin((m-k)\theta_z)\;\,[\cos((n-r)\theta_z)M^{cs}_{kr} + \sin((n-r)\theta_z)M^{cc}_{kr}]\}\,.\end{aligned}$$

We write these formulas compactly in a matrix form as follows:

$$\begin{bmatrix}\widehat{M}^{cc}_{mn} & \widehat{M}^{sc}_{mn}\\ \widehat{M}^{cs}_{mn} & \widehat{M}^{ss}_{mn}\end{bmatrix} = \sum_{k=1}^{m}\sum_{r=1}^{n} r_z^{m-k} r_z^{n-r}\binom{m}{k}\binom{n}{r}\mathbf{R}((n-r)\theta_z)\begin{bmatrix}M^{cc}_{kr} & M^{sc}_{kr}\\ M^{cs}_{kr} & M^{ss}_{kr}\end{bmatrix}\cdot\mathbf{R}((m-k)\theta_z)^T\,,$$

where $\mathbf{R}(\theta)$ is the matrix associated with the rotation by θ, i.e.,

$$\mathbf{R}(\theta) := \begin{bmatrix}\cos\theta & -\sin\theta\\ \sin\theta & \cos\theta\end{bmatrix}. \tag{2.39}$$

2.3.2. Rotation formula

We want to investigate how M_{mn} changes with respect to a rotation of D by an angle θ.

Let $\theta \in [0, 2\pi)$ and let $\mathbf{R} \in \mathbb{R}^{2\times 2}$ be the matrix associated with the rotation

$$\mathbf{R} := \mathbf{R}(\theta) = \begin{bmatrix}\cos\theta & -\sin\theta\\ \sin\theta & \cos\theta\end{bmatrix}.$$

Let us define $\Phi_{\mathbf{R}}(x) := \mathbf{R}x = e^{i\theta}x$.

We denote $\widehat{x} = \mathbf{R}x$, $\widehat{D} := \Phi_{\mathbf{R}}(D)$ and $\widehat{\gamma}(\widehat{x}) := \gamma(x)$. We want to relate $M_{mn}^{cc}(\gamma, D)$ with $M_{mn}^{cc}(\widehat{\gamma}, \widehat{D})$ defined by

$$M_{mn}^{cc}(\widehat{\gamma}, \widehat{D}) = \widehat{M}_{mn}^{cc} = \int_{\partial\widehat{D}} \mathrm{Re}(\widehat{x}^m)(\widehat{g}_n^c(\widehat{x}) - \Lambda_{\widehat{1}}^{-1}\Lambda_{\widehat{\gamma}}^{\widehat{D}}[\widehat{g}_n^c](\widehat{x}))\, \mathrm{d}s_{\widehat{x}}. \tag{2.40}$$

By the change of variables $\widehat{x} = \mathbf{R}x$, we obtain

$$M_{mn}^{cc}(\widehat{\gamma}, \widehat{D}) = \widehat{M}_{mn}^{cc} = \int_{\partial D} r_x^m \cos(m(\theta_x + \theta))\, (\widehat{g}_n^c(\mathbf{R}x) - \Lambda_{\widehat{1}}^{-1}\Lambda_{\widehat{\gamma}}^{\widehat{D}}[\widehat{g}_n^c](\mathbf{R}x))\, \mathrm{d}s_x\,. \tag{2.41}$$

Lemma 2.3.2 *We have*

$$\widehat{g}_n^c(\mathbf{R}x) = \cos n\theta\, g_n^c(x) - \sin n\theta\, g_n^s(x)\,, \tag{2.42}$$

and

$$\widehat{g}_n^s(\mathbf{R}x) = \cos n\theta\, g_n^s(x) + \sin n\theta\, g_n^c(x)\,. \tag{2.43}$$

Proof. Let $\widehat{u}_n^c$ be the solution to

$$\begin{cases} \nabla_{\widehat{x}} \cdot \widehat{\gamma}(\widehat{x}) \nabla_{\widehat{x}} \widehat{u}_n^c(\widehat{x}) = 0 & \text{in } \mathbb{R}^2, \\ \widehat{u}_n^c(\widehat{x}) - r_{\widehat{x}}^n \cos(n\theta_{\widehat{x}}) = O(r_{\widehat{x}}^{-1}) & \text{as } |\widehat{x}| \to +\infty. \end{cases} \tag{2.44}$$

Then, by definition, we have $\widehat{g}_n^c := \left.\dfrac{\partial \widehat{u}_n^c}{\partial \nu_{\widehat{x}}}\right|_+$. By a change of variables in (2.44) and by setting $v_n^c(x) := \widehat{u}_n^c(\mathbf{R}x)$, we obtain

$$\begin{cases} \nabla_x \cdot \gamma(x) \nabla_x v_n^c(x) = 0 & \text{in } \mathbb{R}^2, \\ v_n^c(x) - r_x^n \cos(n(\theta_x + \theta)) = O(r_x^{-1}) & \text{as } |x| \to +\infty. \end{cases}$$

Hence,

$$\begin{cases} \nabla_x \cdot \gamma(x) \nabla_x v_n^c(x) = 0 & \text{in } \mathbb{R}^2, \\ v_n^c(x) - (r_x^n \cos n\theta_x \cos n\theta - r_x^n \sin n\theta_x \sin n\theta) = O(r_x^{-1}) & \text{as } |x| \to +\infty, \end{cases}$$

or equivalently,

$$\begin{cases} \nabla_x \cdot \gamma(x) \nabla_x v_n^c(x) = 0 & \text{in } \mathbb{R}^2, \\ v_n^c(x) - (h_n^c(x)\theta_x \cos n\theta - h_n^s(x) \sin n\theta) = O(r_x^{-1}) & \text{as } |x| \to +\infty. \end{cases}$$

Therefore,

$$v_n^c(x) = \cos n\theta\, u_n^c(x) - \sin n\theta\, u_n^s(x).$$

Analogously we derive formula (2.43) for $\widehat{g}_n^s$. □

In order to relate (2.24) and (2.41) we need to have a better understanding of the boundary operator that we are integrating. We have already written an integral representation for the operator $\Lambda_1^{-1}\Lambda_\gamma^D : H_0^{-1/2}(\partial D) \longrightarrow H_0^{-1/2}(\partial D)$ in the previous subsection (see (2.31)). Now, we proceed similarly for the operator that plays a role in the rotated problem:

$$\Lambda_{\widehat{1}}^{-1}\Lambda_{\widehat{\gamma}}^{\widehat{D}} : H_0^{-1/2}(\partial\widehat{D}) \longrightarrow H_0^{-1/2}(\partial\widehat{D})$$
$$\widehat{g}_n^c \longmapsto \left.\frac{\partial\widehat{h}}{\partial\nu_{\widehat{x}}}\right|_- ,$$

where $\widehat{h}$ is the solution to the boundary value problem

$$\begin{cases} \Delta\widehat{h} = 0 & \text{in } \widehat{D}, \\ \nabla_{\widehat{x}}\widehat{h}\cdot\nu_{\widehat{x}} = \widehat{g}_n^c & \text{on } \partial\widehat{D}. \end{cases} \tag{2.45}$$

Let $\widehat{y} = \mathbf{R}y \in \widehat{D}$ and consider the corresponding Neumann function $\widehat{N}_1(\widehat{x},\widehat{y})$, that is, the solution to

$$\begin{cases} \Delta_{\widehat{x}}\widehat{N}_1(\widehat{x},\widehat{y}) = -\delta_{\widehat{y}}(\widehat{x}), & \widehat{x}\in\widehat{D}, \\ \nabla_{\widehat{x}}\widehat{N}_1(\widehat{x},\widehat{y})\cdot\nu_{\widehat{x}} = -\frac{1}{|\partial\widehat{D}|}, & \widehat{x}\in\partial\widehat{D}, \\ \int_{\partial\widehat{D}}\widehat{N}_1(\widehat{x},\widehat{y})\mathrm{d}s_{\widehat{x}} = 0. \end{cases}$$

Exploiting the rotational invariance of the Laplacian gives

$$\begin{cases} (\Delta_x\widehat{N}_1\circ\Phi_{\mathbf{R}})(x,\mathbf{R}y) = -\delta_{\mathbf{R}y}(\mathbf{R}x) = -\delta_y(x), & x\in D, \\ \mathbf{R}(\nabla_x\widehat{N}_1\circ\Phi_{\mathbf{R}})(x,\mathbf{R}y)\cdot(\mathbf{R}\nu_x) = -\frac{1}{|\partial D|}, & x\in\partial D, \\ \int_{\partial D}\widehat{N}_1(\mathbf{R}x,\widehat{y})\mathrm{d}s_x = 0. \end{cases}$$

Therefore,

$$\begin{cases} (\Delta_x\widehat{N}_1\circ\Phi_{\mathbf{R}})(x,\mathbf{R}y) = -\delta_{\mathbf{R}y}(\mathbf{R}x) = -\delta_y(x), & x\in D, \\ (\nabla_x\widehat{N}_1\circ\Phi_{\mathbf{R}})(x,\mathbf{R}y)\cdot\nu_x = -\frac{1}{|\partial D|}, & x\in\partial D, \\ \int_{\partial D}\widehat{N}_1(\mathbf{R}x,\mathbf{R}y)\mathrm{d}s_x = 0. \end{cases}$$

One can easily see that $\widehat{N}_1(\mathbf{R}x,\mathbf{R}y)$ and $N_1(x,y)$ satisfy exactly the same boundary value problem (2.30). The uniqueness of a solution to (2.30) yields

$$\widehat{N}_1(\mathbf{R}x,\mathbf{R}y) = N_1(x,y)\,. \tag{2.46}$$

Since the solution $\widehat{h}$ to (2.45) can be represented by means of the Neumann function $\widehat{N}_1$:

$$\widehat{h}(\widehat{y}) = \int_{\partial\widehat{D}}\widehat{N}_1(\widehat{x},\widehat{y})\,\widehat{g}_n^c(\widehat{x})\;\mathrm{d}s_{\widehat{x}}\,,$$

we have, for $y \in \partial D$,

$$\begin{aligned}
\Lambda_{\widehat{1}}^{-1}\Lambda_{\widehat{\gamma}}^{\widehat{D}}[\widehat{g}_n^c](\widehat{y}) &= \nabla_{\widehat{y}}\widehat{h}(\widehat{y})\cdot\nu_{\widehat{y}} \\
&= \int_{\partial\widehat{D}} (\nabla_{\widehat{y}}\widehat{N}_1)(\widehat{x},\widehat{y})\cdot\nu_{\widehat{y}}\,\widehat{g}_n^c(\widehat{x})\,\mathrm{d}s_{\widehat{x}} \\
&= \int_{\partial D} (\nabla_{\widehat{y}}\widehat{N}_1)(\mathbf{R}x,\widehat{y})\cdot\nu_{\widehat{y}}\,\widehat{g}_n^c(\mathbf{R}x)\,\mathrm{d}s_x \\
&= \int_{\partial D} \mathbf{R}(\nabla_y \widehat{N}_1(\mathbf{R}x,\mathbf{R}\cdot))(\mathbf{R}x,y)\cdot\mathbf{R}\,\nu_y\,(\cos n\theta\, g_n^c(x) - \sin n\theta\, g_n^s(x))\,\mathrm{d}s_x \\
&= \int_{\partial D} (\nabla_y N_1)(x,y)\cdot\nu_y\,(\cos n\theta\, g_n^c(x) - \sin n\theta\, g_n^s(x))\,\mathrm{d}s_x \\
&= \cos n\theta \int_{\partial D} (\nabla_y N_1)(x,y)\cdot\nu_y\, g_n^c(x)\,\mathrm{d}s_x - \sin n\theta \int_{\partial D} (\nabla_y N_1)(x,y)\cdot\nu_y\, g_n^s(x)\,\mathrm{d}s_x\,.
\end{aligned}$$

Here, we have made the change of variables $\widehat{x} = \mathbf{R}x$ and used identity (2.46). Therefore, it follows that

$$\Lambda_{\widehat{1}}^{-1}\Lambda_{\widehat{\gamma}}^{\widehat{D}}[\widehat{g}_n^c](\mathbf{R}x) = \cos n\theta\,\Lambda_1^{-1}\Lambda_\gamma^D[g_n^c](x) - \sin n\theta\,\Lambda_1^{-1}\Lambda_\gamma^D[g_n^s](x)\,. \tag{2.47}$$

Hence, from Lemma 2.3.2 and (2.47), we get

$$\begin{aligned}
\widehat{g}_n^c(\mathbf{R}x) - \Lambda_{\widehat{1}}^{-1}\Lambda_{\widehat{\gamma}}^{\widehat{D}}[\widehat{g}_n^c](\mathbf{R}x) &= \cos n\theta\, g_n^c(x) - \sin n\theta\, g_n^s(x) - \cos n\theta\,\Lambda_1^{-1}\Lambda_\gamma^D[g_n^c](x) + \sin n\theta\,\Lambda_1^{-1}\Lambda_\gamma^D[g_n^s](x) \\
&= \cos n\theta\,(g_n^c(x) - \Lambda_1^{-1}\Lambda_\gamma^D[g_n^c](x)) - \sin n\theta\,(g_n^s(x) - \Lambda_1^{-1}\Lambda_\gamma^D[g_n^s](x))\,.
\end{aligned}$$

$$\begin{aligned}
M_{mn}^{cc}(\widehat{\gamma},\widehat{D}) &= \int_{\partial D} r_x^m \cos(m(\theta_x+\theta))\,(\widehat{g}_n^c(\mathbf{R}x) - \Lambda_{\widehat{1}}^{-1}\Lambda_{\widehat{\gamma}}^{\widehat{D}}[\widehat{g}_n^c](\mathbf{R}x))\,\mathrm{d}s_x \\
&= \int_{\partial D} [r_x^m\cos(m\theta_x)\cos(m\theta) - r_x^m\sin(m\theta_x)\sin(m\theta)](\widehat{g}_n^c(\mathbf{R}x) - \Lambda_{\widehat{1}}^{-1}\Lambda_{\widehat{\gamma}}^{\widehat{D}}[\widehat{g}_n^c](\mathbf{R}x))\,\mathrm{d}s_x \\
&= \cos(m\theta)\cos(n\theta)\int_{\partial D} r_x^m\cos(m\theta_x)(g_n^c(x) - \Lambda_1^{-1}\Lambda_\gamma^D[g_n^c](x))\,\mathrm{d}s_x \\
&- \cos(m\theta)\sin(n\theta)\int_{\partial D} r_x^m\cos(m\theta_x)(g_n^s(x) - \Lambda_1^{-1}\Lambda_\gamma^D[g_n^s](x))\,\mathrm{d}s_x \\
&- \sin(m\theta)\cos(n\theta)\int_{\partial D} r_x^m\sin(m\theta_x)(g_n^c(x) - \Lambda_1^{-1}\Lambda_\gamma^D[g_n^c](x))\,\mathrm{d}s_x \\
&+ \sin(m\theta)\sin(n\theta)\int_{\partial D} r_x^m\sin(m\theta_x)(g_n^s(x) - \Lambda_1^{-1}\Lambda_\gamma^D[g_n^s](x))\,\mathrm{d}s_x \\
&= \cos(m\theta)\cos(n\theta)M_{mn}^{cc} - \cos(m\theta)\sin(n\theta)M_{mn}^{cs} \\
&- \sin(m\theta)\cos(n\theta)M_{mn}^{sc} + \sin(m\theta)\sin(n\theta)M_{mn}^{ss}\,.
\end{aligned}$$

Similar computations lead to the rotation formulas for the others CGPTs $\widehat{M}_{mn}^{cs}, \widehat{M}_{mn}^{sc}$ and $\widehat{M}_{mn}^{ss}$. All these formulas can be written in a matrix form:

$$\begin{bmatrix} \widehat{M}_{mn}^{cc} & \widehat{M}_{mn}^{sc} \\ \widehat{M}_{mn}^{cs} & \widehat{M}_{mn}^{ss} \end{bmatrix} = \mathbf{R}(n\theta)\cdot\begin{bmatrix} M_{mn}^{cc} & M_{mn}^{sc} \\ M_{mn}^{cs} & M_{mn}^{ss} \end{bmatrix}\cdot\mathbf{R}(m\theta)^T\,,$$

where $\mathbf{R}(\theta)$ is defined in (2.39).

2.3.3. Scaling formula

Similarly to what we have done for translations and rotations we want to investigate how M_{mn} changes with respect to a scaling of D.

Let $s > 0$ and assume that $z = 0$. We denote $\widehat{x} = sx$, $\widehat{D} := sD$ and $\widehat{\gamma}(\widehat{x}) := \gamma(x)$. We want to relate $M^{cc}_{mn}(\gamma, D)$ with $M^{cc}_{mn}(\widehat{\gamma}, \widehat{D})$ given by

$$M^{cc}_{mn}(\widehat{\gamma}, \widehat{D}) = \widehat{M}_{mn} = \int_{\partial \widehat{D}} \mathrm{Re}(\widehat{x}^m)(\widehat{g}^c_n(\widehat{x}) - \Lambda^{-1}_{\widehat{1}} \Lambda^{\widehat{D}}_{\widehat{\gamma}}[\widehat{g}^c_n](\widehat{x}))\, \mathrm{d}s_{\widehat{x}}\,.$$

By the change of variables $\widehat{x} = sx$, we obtain

$$M^{cc}_{mn}(\widehat{\gamma}, \widehat{D}) = \widehat{M}_{mn} = s^{m+1} \int_{\partial D} \mathrm{Re}(x^m)(\widehat{g}^c_n(sx) - \Lambda^{-1}_{\widehat{1}} \Lambda^{\widehat{D}}_{\widehat{\gamma}}[\widehat{g}^c_n](sx))\, \mathrm{d}s_x. \tag{2.48}$$

Lemma 2.3.3 *We have*

$$\widehat{g}^c_n(sx) = s^{n-1} g^c_n(x)\,, \tag{2.49}$$

and

$$\widehat{g}^s_n(sx) = s^{n-1} g^s_n(x)\,. \tag{2.50}$$

Proof. We show the first identity. The one for $\widehat{g}^s_n$ can be proved in the same way. Let $\widehat{u}^c_n$ be the solution to

$$\begin{cases} \nabla_{\widehat{x}} \cdot \widehat{\gamma}(\widehat{x}) \nabla_{\widehat{x}} \widehat{u}^c_n(\widehat{x}) = 0 & \text{in } \mathbb{R}^2, \\ \widehat{u}^c_n(\widehat{x}) - r^n_{\widehat{x}} \cos(n\theta_{\widehat{x}}) = O(r^{-1}_{\widehat{x}}) & \text{as } |\widehat{x}| \to +\infty. \end{cases} \tag{2.51}$$

Then $\widehat{g}^c_n := \widehat{\gamma} \dfrac{\partial \widehat{u}^c_n}{\partial \nu_{\widehat{x}}}$. By a change of variables in (2.51) and by setting $v^c_n(x) := \widehat{u}^c_n(sx)$, we obtain

$$\begin{cases} \nabla_x \cdot \gamma(x) \nabla_x v^c_n(x) = 0 & \text{in } \mathbb{R}^2, \\ s(v^c_n(x) - s^n r^n_x \cos(n\theta_x)) = O(r^{-1}_x) & \text{as } |\widehat{x}| \to +\infty. \end{cases}$$

Therefore, $s^n v^c_n(x)$ solves the same problem as $u^c_n(x)$. By the uniqueness of a solution, we get

$$s^{-n} v^c_n(x) = u^c_n(x).$$

So

$$\nabla_x u^c_n(x) = s^{-n} \nabla_x v^c_n(x) = s^{-n+1} \nabla_{\widehat{x}} \widehat{u}^c_n(\widehat{x})\,.$$

Hence,

$$g^c_n(x) = s^{-n+1} \widehat{g}^c_n(\widehat{x}).$$

□

We want to relate (2.24) and (2.48). We refer to (2.31) for an integral representation of the operator $\Lambda_1^{-1}\Lambda_\gamma^D$.

Now we proceed similarly for the operator that plays a role in the scaled problem:

$$\Lambda_{\widehat{1}}^{-1}\Lambda_{\widehat{\gamma}}^{\widehat{D}} : H_0^{-1/2}(\partial\widehat{D}) \longrightarrow H_0^{-1/2}(\partial\widehat{D})$$

$$\widehat{g}_n^c \longmapsto \left.\frac{\partial\widehat{h}}{\partial\nu_{\widehat{x}}}\right|_- ,$$

where $\widehat{h}$ is the solution to the boundary value problem

$$\begin{cases} \Delta\widehat{h} = 0 & \text{in } \widehat{D}, \\ \nabla_{\widehat{x}}\widehat{h}\cdot\nu_{\widehat{x}} = \widehat{g}_n^c & \text{on } \partial\widehat{D}\,. \end{cases} \tag{2.52}$$

Let $\widehat{y} = sy \in \widehat{D}$ and consider the corresponding Neumann function $\widehat{N}_1(\widehat{x},\widehat{y})$, that is, the solution to

$$\begin{cases} \Delta_{\widehat{x}}\widehat{N}_1(\widehat{x},\widehat{y}) = -\delta_{\widehat{y}}(\widehat{x}), & \widehat{x}\in\widehat{D}, \\ \nabla_{\widehat{x}}\widehat{N}_1(\widehat{x},\widehat{y})\cdot\nu_{\widehat{x}} = -\frac{1}{|\partial\widehat{D}|}, & \widehat{x}\in\partial\widehat{D}, \\ \int_{\partial\widehat{D}}\widehat{N}_1(\widehat{x},\widehat{y})\mathrm{d}s_{\widehat{x}} = 0. \end{cases}$$

Then,

$$\begin{cases} \frac{1}{s^2}\,\Delta_x\widehat{N}_1(sx,sy) = -\delta_{sy}(sx) = -\delta_0(s(x-y)) = -\frac{1}{s^2}\delta_y(x), & x\in D, \\ \frac{1}{s}\,\nabla_x\widehat{N}_1(sx,sy)\cdot\nu_x = -\frac{1}{s|\partial D|}, & x\in\partial D, \\ \int_{\partial D}\widehat{N}_1(sx,\widehat{y})\mathrm{d}s_x = 0, \end{cases}$$

which shows that

$$\begin{cases} \Delta_x\widehat{N}_1(sx,sy) = -\delta_y(x), & x\in D, \\ \nabla_x\widehat{N}_1(sx,sy)\cdot\nu_x = -\frac{1}{|\partial D|}, & x\in\partial D, \\ \int_{\partial D}\widehat{N}_1(sx,sy)\mathrm{d}s_x = 0. \end{cases}$$

One can easily see that $\widehat{N}_1(sx,sy)$ and $N_1(x,y)$ satisfy exactly the same boundary value problem (2.30). Therefore,

$$\widehat{N}_1(sx,sy) = N_1(x,y)\,. \tag{2.53}$$

The solution $\widehat{h}$ to (2.52) can be represented by means of the Neumann function $\widehat{N}_1$:

$$\widehat{h}(\widehat{y}) = \int_{\partial\widehat{D}}\widehat{N}_1(\widehat{x},\widehat{y})\,\widehat{g}_n^c(\widehat{x})\;\mathrm{d}s_{\widehat{x}}\,,$$

and so, for $y \in \partial D$, we have

$$\begin{aligned}
\Lambda_{\widehat{1}}^{-1}\Lambda_{\widehat{\gamma}}^{\widehat{D}}[\widehat{g}](\widehat{y}) &= \nabla_{\widehat{y}}\widehat{h}(\widehat{y})\cdot\nu_{\widehat{y}} \\
&= \int_{\partial\widehat{D}}(\nabla_{\widehat{y}}\widehat{N}_1)(\widehat{x},\widehat{y})\cdot\nu_{\widehat{y}}\,\widehat{g}_n^c(\widehat{x})\,\mathrm{d}s_{\widehat{x}} \\
&= \int_{\partial D}(\nabla_{\widehat{y}}\widehat{N}_1)(sx,\widehat{y})\cdot\nu_y\, s^{n-1}\, g_n^c(x)\, s\,\mathrm{d}s_x \\
&= s^{n-1}\int_{\partial D}(\nabla_y \widehat{N}_1(sx,s\cdot))(sx,y)\cdot\nu_y\, g_n^c(x)\,\mathrm{d}s_x \\
&= s^{n-1}\int_{\partial D}(\nabla_y N_1)(x,y)\cdot\nu_y\, g_n^c(x)\,\mathrm{d}s_x.
\end{aligned}$$

Here, we have made the change of variables $\widehat{x} = sx$ and used identity (2.53). Therefore, it follows that

$$\Lambda_{\widehat{1}}^{-1}\Lambda_{\widehat{\gamma}}^{\widehat{D}}[\widehat{g}](\widehat{y}) = s^{n-1}\,\Lambda_1^{-1}\Lambda_\gamma^D[g](y).$$

Then

$$\begin{aligned}
M_{mn}^{cc}(\widehat{\gamma},\widehat{D}) &= s^{m+1}\int_{\partial D}\mathrm{Re}(x^m)(s^{n-1}g_n^c(x) - s^{n-1}\Lambda_1^{-1}\Lambda_\gamma^D[g_n^c](x))\,\mathrm{d}s_x \\
&= s^{m+n}\int_{\partial D}\mathrm{Re}(x^m)(g_n^c(x) - \Lambda_1^{-1}\Lambda_\gamma^D[g_n^c](x))\,\mathrm{d}s_x \\
&= s^{m+n}\,M_{mn}^{cc}(\gamma,D).
\end{aligned}$$

Hence, we obtain the following scaling formula

$$M_{mn}^{cc}(\widehat{\gamma},\widehat{D}) = s^{m+n}\,M_{mn}^{cc}(\gamma,D)\,.$$

Analogously, we get

$$\begin{aligned}
M_{mn}^{cs}(\widehat{\gamma},\widehat{D}) &= s^{m+n}\,M_{mn}^{cs}(\gamma,D), \\
M_{mn}^{sc}(\widehat{\gamma},\widehat{D}) &= s^{m+n}\,M_{mn}^{sc}(\gamma,D), \\
M_{mn}^{ss}(\widehat{\gamma},\widehat{D}) &= s^{m+n}\,M_{mn}^{ss}(\gamma,D).
\end{aligned}$$

In order to simplify the notation, for any pair of indices m,n, we denote by $\mathbf{M}_{mn} := \begin{bmatrix} M_{mn}^{cc} & M_{mn}^{sc} \\ M_{mn}^{cs} & M_{mn}^{ss}\end{bmatrix}$ and $\widehat{\mathbf{M}}_{mn} := \begin{bmatrix} \widehat{M}_{mn}^{cc} & \widehat{M}_{mn}^{sc} \\ \widehat{M}_{mn}^{cs} & \widehat{M}_{mn}^{ss}\end{bmatrix}$. We introduce also the following notation:

- $T_z D = \{x + z,\ \text{for } x \in D\}$, $(T_z \star \gamma)(x) = \gamma(x - z)$, for $z \in \mathbb{R}^2$;

- $R_\theta D = \{e^{i\theta}x,\ \text{for } x \in D\}$, $(R_\theta \star \gamma)(x) = \gamma(e^{-i\theta}x)$, for $\theta \in [0, 2\pi)$;

- $sD = \{sx,\ \text{for } x \in D\}$, $(s \star \gamma)(x) = \gamma(s^{-1}x)$, for $s > 0$,

where D is an open set and γ is a conductivity distribution in the plane.

We summarize the formulas that we obtained so far in the following theorem.

Proposition 2.3.4 *For any pair m, n of indices, $m, n = 1, 2, \ldots$, the following transformation formulas hold true:*

$$\mathbf{M}_{mn}(T_z \star \gamma, T_z D) = \sum_{k=1}^{m}\sum_{r=1}^{n} r_z^{m-k} r_z^{n-r} \binom{m}{k}\binom{n}{r} \mathbf{R}((n-r)\theta_z)\mathbf{M}_{kr}(\gamma, D)\mathbf{R}((m-k)\theta_z)^T,$$
$$\mathbf{M}_{mn}(R_\theta \star \gamma, R_\theta D) = \mathbf{R}(n\theta)\mathbf{M}_{mn}(\gamma, D)\mathbf{R}(m\theta)^T,$$

and

$$\mathbf{M}_{mn}(s \star \gamma, sD) = s^{m+n}\,\mathbf{M}_{mn}(\gamma, D).$$

2.3.4. Complex CGPTs

As observed in [6], it is convenient to consider complex combinations of CGPTs. For a pair of indices $m, n = 1, 2, \ldots$, we introduce the following quantities

$$\begin{aligned} \mathbf{N}^{(1)}_{mn}(\gamma, D) &= (M^{cc}_{mn} - M^{ss}_{mn}) + i(M^{cs}_{mn} + M^{sc}_{mn}), \\ \mathbf{N}^{(2)}_{mn}(\gamma, D) &= (M^{cc}_{mn} + M^{ss}_{mn}) + i(M^{cs}_{mn} - M^{sc}_{mn}). \end{aligned} \tag{2.54}$$

Using relations of Proposition 2.3.4 it is straightforward to prove similar rules than those derived in [6] for the complex CGPTs (2.54).

Proposition 2.3.5 *For all integers m, n, and geometric parameters θ, s and z, the following holds:*

$$\mathbf{N}^{(1)}_{mn}(R_\theta \star \gamma, R_\theta D) = e^{i(m+n)}\mathbf{N}^{(1)}_{mn}(\gamma, D), \qquad \mathbf{N}^{(2)}_{mn}(R_\theta \star \gamma, R_\theta D) = e^{i(n-m)}\mathbf{N}^{(2)}_{mn}(\gamma, D), \tag{2.55}$$

$$\mathbf{N}^{(1)}_{mn}(s \star \gamma, sD) = s^{m+n}\mathbf{N}^{(1)}_{mn}(\gamma, D), \qquad \mathbf{N}^{(2)}_{mn}(s \star \gamma, sD) = s^{m+n}\mathbf{N}^{(2)}_{mn}(\gamma, D), \tag{2.56}$$

and

$$\mathbf{N}^{(1)}_{mn}(T_z \star \gamma, T_z D) = \sum_{l=1}^{m}\sum_{k=1}^{n} \mathbf{C}^z_{ml}\mathbf{N}^{(1)}_{lk}(\gamma, D)\mathbf{C}^z_{nk}, \qquad \mathbf{N}^{(2)}_{mn}(T_z \star \gamma, T_z D) = \sum_{l=1}^{m}\sum_{k=1}^{n} \overline{\mathbf{C}^z_{ml}}\mathbf{N}^{(2)}_{lk}(\gamma, D)\mathbf{C}^z_{nk}, \tag{2.57}$$

where $\mathbf{C}^z$ is a lower triangular matrix with the m, n-th entry given by

$$\mathbf{C}^z_{mn} = \binom{m}{n} z^{m-n}.$$

We define the complex CGPT matrices by

$$\mathbf{N}^{(1)} := (\mathbf{N}^{(1)}_{mn})_{m,n}, \qquad \mathbf{N}^{(2)} := (\mathbf{N}^{(2)}_{mn})_{m,n}.$$

Setting $w = se^{i\theta}$ we introduce the diagonal matrix $\mathbf{G}^w$ with m-th diagonal entry given by $s^m e^{im\theta}$.

Applying one after the other the properties of Proposition 2.3.5 we immediately get the following relations:

$$\mathbf{N}^{(1)}(T_z \star (s \star (R_\theta \star \gamma)), T_z s R_\theta D) = \mathbf{C}^z \mathbf{G}^w \mathbf{N}^{(1)}(\gamma, D) \mathbf{G}^w (\mathbf{C}^z)^T, \tag{2.58}$$

$$\mathbf{N}^{(2)}(T_z \star (s \star (R_\theta \star \sigma)), T_z s R_\theta D) = \overline{\mathbf{C}^z \mathbf{G}^w} \mathbf{N}^{(2)}(\gamma, D) \mathbf{G}^w (\mathbf{C}^z)^T. \tag{2.59}$$

Relations (2.58) and (2.59) still hold for the truncated CGPTs of finite order, due to the triangular shape of the matrix $\mathbf{C}^z$.

We call a dictionary $\mathcal{D}$ a collection of pairs (σ, B), where B is a standard shape centered at the origin, with characteristic size of order 1, and σ is a conductivity distribution such that $\mathrm{supp}(\sigma - 1) = \overline{B}$.

We assume that a reference dictionary $\mathcal{D}$ is initially given. Furthermore, suppose to consider a pair (γ, D), which is unknow, that is obtained from an element $(\sigma, B) \in \mathcal{D}$ by applying some unknown rotation θ, scaling s and translation z, i.e., $D = T_z s R_\theta B$ and $\gamma = T_z \star (s \star (R_\theta \star \sigma))$.

2.3.5. Conductivity descriptors

If $D = T_z s R_\theta B$ and $\gamma = T_z \star (s \star (R_\theta \star \sigma))$ then the following identities hold true:

$$\mathbf{N}^{(1)}_{11}(\gamma, D) = w^2 \mathbf{N}^{(1)}_{11}(\sigma, B), \tag{2.60}$$

$$\mathbf{N}^{(1)}_{12}(\gamma, D) = 2\mathbf{N}^{(1)}_{11}(\gamma, D) z + w^3 \mathbf{N}^{(1)}_{12}(\sigma, B), \tag{2.61}$$

$$\mathbf{N}^{(2)}_{11}(\gamma, D) = s^2 \mathbf{N}^{(2)}_{11}(\sigma, B), \tag{2.62}$$

$$\mathbf{N}^{(2)}_{12}(\gamma, D) = 2\mathbf{N}^{(2)}_{11}(\gamma, D) z + s^2 w \mathbf{N}^{(2)}_{12}(\sigma, B), \tag{2.63}$$

where $w = se^{i\theta}$.

From identities (2.62) and (2.63) we obtain the relation:

$$\frac{\mathbf{N}^{(2)}_{12}(\gamma, D)}{2\mathbf{N}^{(2)}_{11}(\gamma, D)} = z + se^{i\theta} \frac{\mathbf{N}^{(2)}_{12}(\sigma, B)}{2\mathbf{N}^{(2)}_{11}(\sigma, B)}. \tag{2.64}$$

Following [6], let $\eta = \frac{\mathbf{N}_{12}^{(2)}(\gamma,D)}{2\mathbf{N}_{11}^{(2)}(\gamma,D)}$. We define the following quantities

$$\mathcal{J}^{(1)}(\gamma,D) = \mathbf{N}^{(1)}(T_{-\eta}\star\gamma, T_{-\eta}D) = \mathbf{C}^{-\eta}\mathbf{N}^{(1)}(\gamma,D)(\mathbf{C}^{-\eta})^T, \tag{2.65}$$

$$\mathcal{J}^{(2)}(\gamma,D) = \mathbf{N}^{(2)}(T_{-\eta}\star\gamma, T_{-\eta}D) = \overline{\mathbf{C}^{-\eta}}\mathbf{N}^{(2)}(\gamma,D)(\mathbf{C}^{-\eta})^T, \tag{2.66}$$

where the matrix $\mathbf{C}^{-\eta}$ has been previously defined in Proposition 2.3.5. These quantities are translation invariant.

From $\mathcal{J}^{(1)}(\gamma,D) = (\mathcal{J}_{mn}^{(1)}(\gamma,D))_{m,n}$, $\mathcal{J}^{(2)}(\gamma,D) = (\mathcal{J}_{mn}^{(2)}(\gamma,D))_{m,n}$, for each pair of indices m,n, we define the scaling invariant quantities:

$$\mathcal{S}_{mn}^{(1)}(\gamma,D) = \frac{\mathcal{J}_{mn}^{(1)}(\gamma,D)}{(\mathcal{J}_{mm}^{(2)}(\gamma,D)\mathcal{J}_{nn}^{(2)}(\gamma,D))^{1/2}}, \qquad \mathcal{S}_{mn}^{(2)}(\gamma,D) = \frac{\mathcal{J}_{mn}^{(2)}(\gamma,D)}{(\mathcal{J}_{mm}^{(2)}(\gamma,D)\mathcal{J}_{nn}^{(2)}(\gamma,D))^{1/2}}. \tag{2.67}$$

Finally, we introduce the CGPT-based shape descriptors $\mathcal{I}^{(1)} = (\mathcal{I}_{mn}^{(1)})_{m,n}$ and $\mathcal{I}^{(2)} = (\mathcal{I}_{mn}^{(2)})_{m,n}$:

$$\mathcal{I}_{mn}^{(1)} = |\mathcal{S}_{mn}^{(1)}(\gamma,D)|, \qquad \mathcal{I}_{mn}^{(2)} = |\mathcal{S}_{mn}^{(2)}(\gamma,D)|,$$

where $|\cdot|$ denotes the modulus of a complex number. It is clear, by construction, that $\mathcal{I}^{(1)}$ and $\mathcal{I}^{(2)}$ are invariant under translation, rotation, and scaling.

The matching algorithm we refer to is rather simple; see Algorithm 2. This approach has been presented previously by Ammari et al. in [7], where shape descriptors have been exploited for dealing with homogeneous conductivities.

Algorithm 2: Shape identification based on transform invariant descriptors

Input : the first k-th order shape descriptors $\mathcal{I}^{(1)}(D)$, $\mathcal{I}^{(2)}(D)$ of an unknown shape D.

for $B_n \in \mathcal{D}$ **do**

  $e_n \leftarrow \left(\|\mathcal{I}^{(1)}(B_n) - \mathcal{I}^{(1)}(D)\|_F^2 + \|\mathcal{I}^{(2)}(B_n) - \mathcal{I}^{(2)}(D)\|_F^2\right)^{1/2}$;

  $n \leftarrow n+1$;

end

Output : the true dictionary element $n^* \leftarrow \mathrm{argmin}_n e_n$.

$\|\cdot\|_F$ denotes the Frobenius norm of matrices.

Remark 2.3.6 *It is easy to see that all the radially symmetric conductivities possess the same conductivity descriptors $\mathcal{I}^{(1)}$ and $\mathcal{I}^{(2)}$. This is a consequence of the following identities:*

$$M_{mn}^{cs} = M_{mn}^{sc} = 0 \quad \text{for all } m,n,$$
$$M_{mn}^{cc} = M_{mn}^{ss} = 0 \quad \text{if } m \neq n,$$
$$M_{mm}^{cc} = M_{mm}^{ss} \quad \text{if } m = n.$$

2.4. Numerical results

In this section, we show some proof-of-concept numerical simulations about the dictionary-matching approach. Henceforth, we will restrict ourselves to piecewise constant distributions only.

2.4.1. Setting

Let $\mathcal{D}$ be the dictionary containing 10 standard conductivity distributions, as illustrated in Figure 2.1. Each one of the 5 shapes in the row a is equipped with homogeneous conductivity having parameter $k = 2$ (Triangle, Ellipse, Bean, Shield and Triangular Shield) whereas each coated shape in the row b is equipped with an inhomogeneous conductivity distribution having value $k_1 = 2$ in the outer coating and having value $k_2 = 4$ in the inner coating. All the shapes have the same characteristic size, which is of order one.

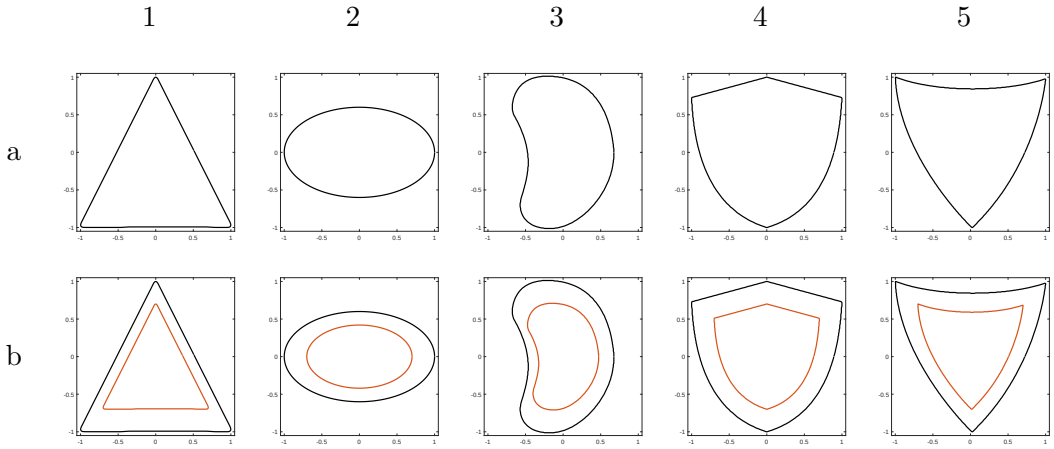

Figure 2.1.: Dictionary $\mathcal{D}$.

Our aim is to numerically simulate the mechanism of sensing a specific target (γ, D) which is obtained starting from a standard element of the dictionary $(\sigma, B) \in \mathcal{D}$, applying a scaling by a parameter $s > 0$ and a rotation by an angle $\theta \in [0, 2\pi)$. For doing so, we generalize the code developed in [77] for homogeneous targets to piecewise inhomogeneous ones.

The targets we are considering for the experiments are located at the origin as the standard shapes. The scaling coefficient and the rotation angle are $s = 0.5$ and $\theta = \pi/3$, respectively. On the other hand, we consider the full-view setting. We assume that the fish is a banana-shaped fish that swims around the target along a circular trajectory whose curvature center is located at the origin $(0, 0)$ and the radius is $R = 1.5 \times \text{diameter}(D)$. We set the impedance of the skin $\xi = 0$. See for instance Figure 2.2.

2.4.2. Experiment

The experiment is as follows. As the fish swims around the target, a series of 512 equispaced receptors on its skin collects the measurements for 500 different positions, so that the resulting multi-static response (MSR) matrix is a 500×512 matrix. From this acquisition procedure, we reconstruct the CGPTs of the target up to a certain order K and use a proper subset of them to compute approximately some distribution descriptors. The descriptors obtained in this manner are then compared to the precomputed theoretical descriptors of the standard distributions of $\mathcal{D}$. We select the best matching conductivity as the standard conductivity that corresponds to the minimal error, in the noiseless case, or to the minimal mean error, when the measurements are corrupted by noise.

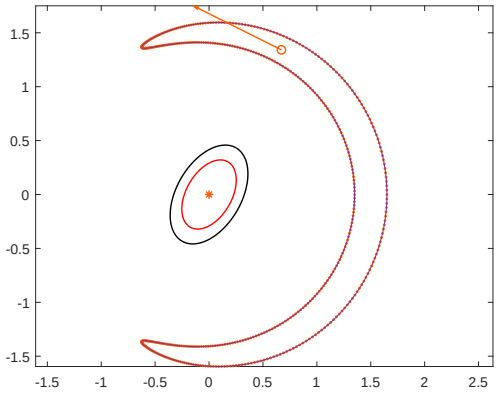

Figure 2.2.: Banana-shaped fish drawn at a fixed position, while swimming along a circular trajectory centered at the origin and collecting measurements for sensing the inhomogeneous target 2b.

We observe from Figure 2.3 that the conductivities of the dictionary $\mathcal{D}$ can be both theoretically and experimentally well-distinguished by means of their second-order descriptors $\left(\mathcal{I}^{(1)}_{mn}\right)_{m,n=1,2}, \left(\mathcal{I}^{(2)}_{mn}\right)_{m,n=1,2}$.

For each noise-level, we repeat the same experiment $N = 10^4$ times and compute the probability of identification. The results are shown in Figure 2.4. We report in Table 2.1 some additional data concerning the identification that performs relatively badly, i.e., that of the target 1a.

The results reveal that the mismatching happens more frequently between conductivities for which the corresponding geometric shapes share the same kind of high-frequency components; see [16]. In particular, depending on the strength of the noise that is considered, the pairs of conductivities 1a-b,4a-b and 5a-b are frequently confused with each other, due to the presence of corners and are rarely confused with the pairs 2a-b,3a-b. This mismatching pattern is confirmed by Figure 2.3c, where third-order descriptors qualitatively highlight such similarities.

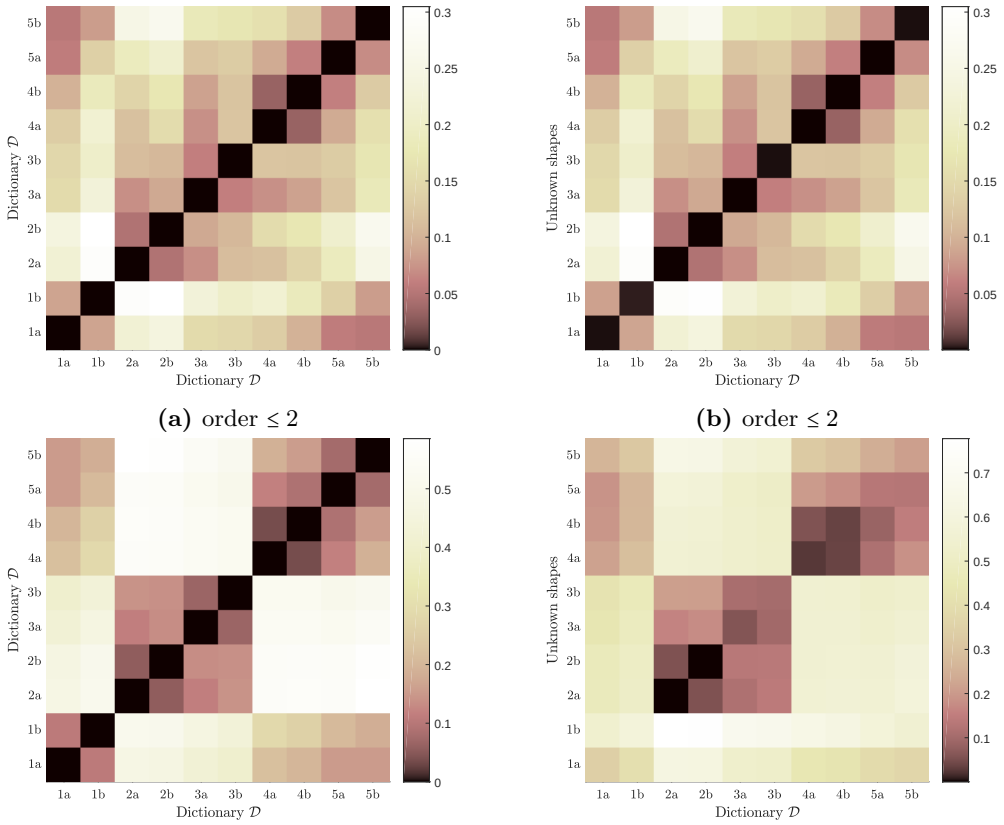

(a) order ≤ 2 **(b)** order ≤ 2

(c) order ≤ 3 **(d)** order ≤ 3

Figure 2.3.: Figure 2.3a and Figure 2.3c show the discrepancy between the theoretical descriptors, wheras Figure 2.3b and Figure 2.3d show the discrepancy between the theoretical descriptors and the ones obtained from the reconstructed CGPTs at noise-level $\sigma_0 = 0$.

We also exhibit some plots showing the mean errors resulting from the identification procedure for two different conductivities; see Figure 2.5 and Figure 2.6. In this case the experiment has been repeated for 5000 times, using independent draws of white noise, and the results are the mean values of all experiments.

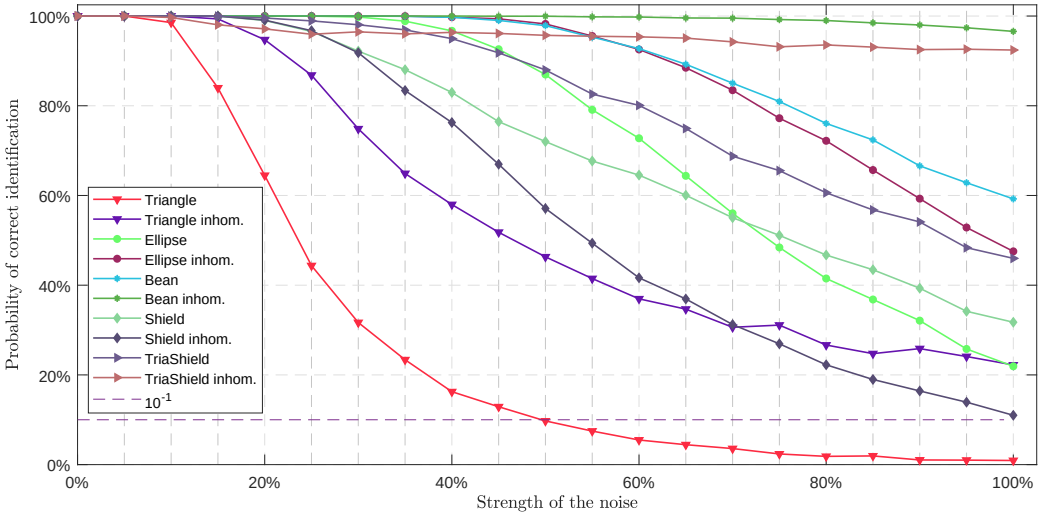

Figure 2.4.: Stability of classification based on second-order descriptors. For each level of noise $N = 10^4$ experiments have been driven. The location of the target is supposed to be known.

	1a	1b	2a	2b	3a	3b	4a	4b	5a	5b
0.1	0.9854	0	0	0	0	0	0	0	0.0004	0.0142
0.2	0.6448	0	0	0	0	0	0	0	0.0514	0.3038
0.3	0.3168	0	0	0	0	0	0	0	0.1252	0.558
0.4	0.1626	0.0006	0	0	0	0	0	0	0.1584	0.6784
0.5	0.0974	0.0012	0	0	0	0	0	0	0.1712	0.7302

Table 2.1.: Frequency table for the identification of the conductivity 1a, i.e., the homogeneous Triangle, at different small noise-levels. Each row contains the relative frequencies for all the elements of the dictionary at a fixed noise-level.

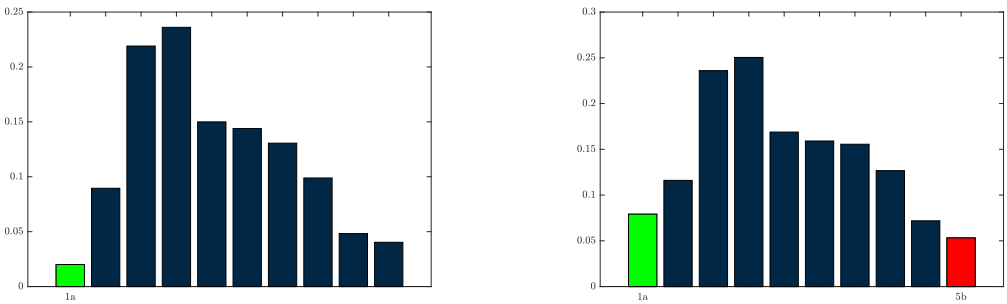

(a) $\sigma_0 = 0.15$. **(b)** $\sigma_0 = 0.50$.

Figure 2.5.: Errors concerning the identification of the homogeneous Triangle 1a at different noise-levels. Each bar refers to a different element of $\mathcal{D}$.

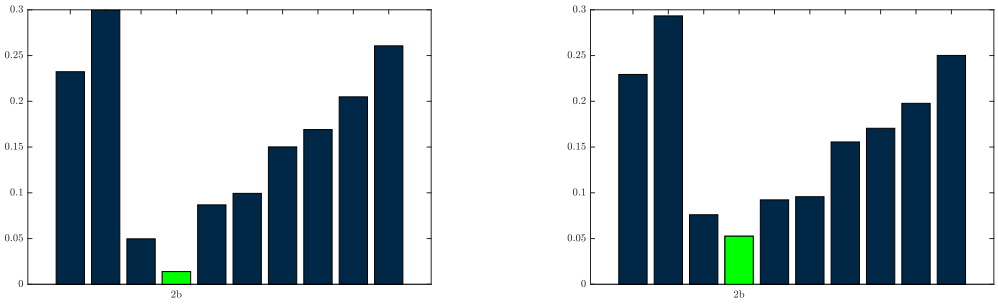

(a) $\sigma_0 = 0.15$. **(b)** $\sigma_0 = 0.50$.

Figure 2.6.: Identification of the inhomogeneous Ellipse 2b at different noise-levels. Each bar refers to a different element of $\mathcal{D}$.

2.4.3. Robustness of the reconstruction

We numerically reconstructed the CGPTs from the measurements, i.e., from the MSR matrix. This reconstruction turns out to be robust when we add some noise to the simulated data. Fixing the truncation order in the reconstruction at $K = 5$, the relative error of the reconstructed CGPTs of orders k for $k \leq 5$ is illustrated in Figure 2.7. For the noisy case, the experiment has been repeated 100 times, using independent draws of white noise and the reconstructed CGPT is taken as the average of the CGPTs.

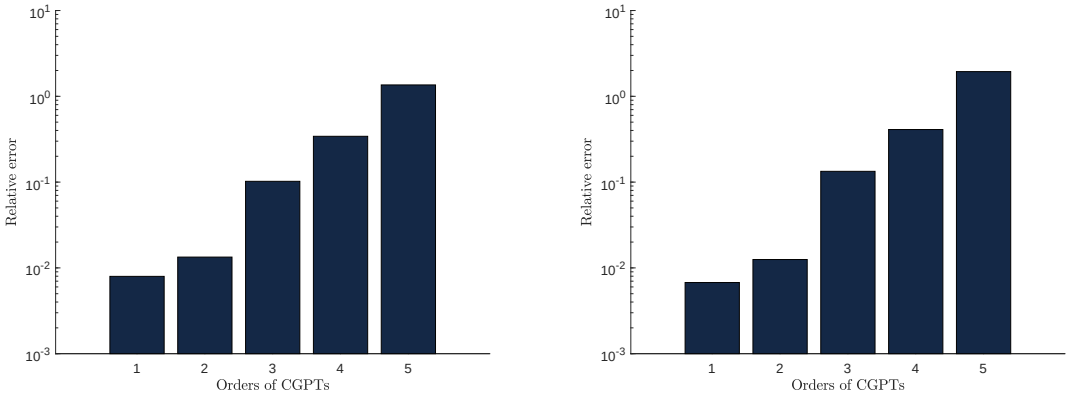

(a) $\sigma_0 = 0$. **(b)** $\sigma_0 = 0.2$.

Figure 2.7.: Relative error $\|\mathbf{M}-\mathbf{M}_{\text{recon}}\|_F/\|\mathbf{M}\|_F$ of the reconstruction of the CGPTs throughout the acquisition procedure described previously in 2.4.1 for the conductivity 1b, the inhomogeneous Triangle.

2.5. Concluding remarks

In this chapter, we have extended the dictionary-matching approach for classification in electro-sensing to inhomogeneous targets. We have established translation, rotation, and scaling formulas for particular linear combinations of the generalized polarization tensors associated with inhomogeneous targets. We have derived new invariants and tested their performance for recognizing inhomogeneous targets inside a dictionary of homogeneous and inhomogeneous conductivity distributions. In a forthcoming work, we plan to combine our present approach together with the multi-frequency approach introduced in [7] to enhance the classification capabilities of the proposed method and its stability.

3. Electro-communication

Contents

3.1. Introduction

The results of this chapter are presented in [67]. We propose a real-time tracking algorithm for a fish to track another conspecific that is swimming nearby. In particular, we show that the following fish can sense the presence of the leading fish and can estimate its positions by using a MUSIC-type algorithm for searching its electric organ. The underlying idea is that a wave-type fish can passively communicate its own trajectory to fish populating the waters nearby. The capability of sensing each other movements is significant, for instance, for applications concerning robotics, where two or more underwater robots may implement such communication procedure to avoid collisions or to shoal. We also showed that the fish can locate a small dielectric target which lies in its electro-sensing range even when another fish is swimming nearby, by filtering out its interfering signal and by applying the MUSIC-type algorithm developed in [2].

The chapter is organized as follows. In Section 3.2, starting from Maxwell's equations in time domain we adapt the mathematical model of the electric fish proposed in [2] in order to be able to consider many fish with EOD working at possibly different frequencies. We give a decomposition formula for the potential and, as a consequence, we decouple the dipolar signals of the two fish when they have different EOD fundamental frequencies.

The amplitude of each signal can be retrieved from the measurements using Fourier analysis techniques.

In Section 3.3, which is the core of this chapter, we consider a new approach to the communication problem, which is based on a non-iterative MUSIC-type dipole search algorithm. The MUSIC-type algorithm tackles the problem in the frequency domain, and it allows us to elaborate the main result, which is a real-time algorithm for a fish to track another fish of the same species by means of subsequent multi-static measurements.

In Section 3.4, we provide a method for a fish to electro-sense a small dielectric target in the presence of many conspecifics. The aim of this section is to locate the target by making use of the dipolar approximation of the transdermal potential modulations. We show that the multi-frequency MUSIC-type algorithm in [8] is still applicable after decomposing the total signal.

In Section 3.5, many numerical simulations are driven. The performances of the real-time tracking algorithm are reported. We show that the algorithms work well even when the measurements are corrupted by noise.

3.2. The two-fish model and the jamming avoidance response

For the sake of simplicity, we consider the case of two weakly electric fish $\mathfrak{F}_1$ and $\mathfrak{F}_2$. The extension to the case of many fish is immediate.

Starting from Maxwell's equations in time domain we derive

$$\nabla \cdot (\sigma + \varepsilon \partial_t) E = -\nabla \cdot j_s \quad \text{in } \mathbb{R}^2,$$

where σ is the conductivity of the medium, ε is the electric permittivity, E is the electric field, j_s is a source of current. Let ω_1 and ω_2 be the fundamental frequencies associated to the oscillations of the electric organ discharge (EOD) of the two fish $\mathfrak{F}_1$ and $\mathfrak{F}_2$, respectively. We consider a source term which is of the form

$$-\nabla \cdot j_s = e^{i\omega_1 t} f_1(x) + e^{i\omega_2 t} f_2(x),$$

where $f_1 = \sum \alpha_j^{(1)} \delta_{x_j^{(1)}}$ and $f_2 = \sum \alpha_j^{(2)} \delta_{x_j^{(2)}}$ are the spatial dipoles located inside Ω_1 and Ω_2, respectively. Throughout this chapter we assume that the dipoles f_1 and f_2 satisfy the local charge neutrality conditions:

$$\alpha_1^{(i)} + \alpha_2^{(i)} = 0 \quad \text{for } i = 1;$$

see [2]. Considering the boundary conditions as in [2], we get the following system of equations:

$$\begin{cases} \Delta u(x,t) = f_1(x)h_1(t) & \text{in } \Omega_1 \times \mathbb{R}^+, \\ \Delta u(x,t) = f_2(x)h_2(t) & \text{in } \Omega_2 \times \mathbb{R}^+, \\ \nabla \cdot (\sigma(x) + \varepsilon(x)\partial_t)\nabla u(x,t) = 0 & \text{in } (\mathbb{R}^2 \setminus \overline{\Omega_1 \cup \Omega_2}) \times \mathbb{R}^+, \\ u|_+ - u|_- = \xi_1 \dfrac{\partial u}{\partial \nu}\Big|_+ & \text{on } \partial\Omega_1 \times \mathbb{R}^+, \\ u|_+ - u|_- = \xi_2 \dfrac{\partial u}{\partial \nu}\Big|_+ & \text{on } \partial\Omega_2 \times \mathbb{R}^+, \\ \dfrac{\partial u}{\partial \nu}\Big|_- = 0 & \text{on } \partial\Omega_1 \times \mathbb{R}^+, \partial\Omega_2 \times \mathbb{R}^+, \\ |u(x,t)| = O(|x|^{-1}) & \text{as } |x| \to \infty,\ t \in \mathbb{R}^+, \end{cases} \tag{3.1}$$

where σ_0, ε_0 are the material parameters of the target D, and ξ_1 and ξ_2 are the effective skin thickness parameters of $\mathfrak{F}_1$ and $\mathfrak{F}_2$, respectively. Here, h_1 and h_2 encode the type of signal generated by the fish.

3.2.1. Wave-type fish

For the wave-type fish we have $h_1(t) = e^{i\omega_1 t}$ and $h_2(t) = e^{i\omega_2 t}$.

When $\omega_1 \neq \omega_2$ the overall signal is the superposition of two periodic signals oscillating at different frequencies.

Proposition 3.2.1 *If $\omega_1 \neq \omega_2$ such that $\omega_1, \omega_2 \neq 0$, then the solution u to the equations* (3.1) *can be represented as*

$$u(x,t) = u_1(x)e^{i\omega_1 t} + u_2(x)e^{i\omega_2 t}, \tag{3.2}$$

where u_1, u_2 satisfy the following transmission problems:

$$\begin{cases} \Delta u_1(x) = f_1(x) & \text{in } \Omega_1, \\ \Delta u_1(x) = 0 & \text{in } \Omega_2, \\ \nabla \cdot (\sigma(x) + i\omega_1\varepsilon(x))\nabla u_1(x) = 0 & \text{in } \mathbb{R}^2 \setminus \overline{\Omega_1 \cup \Omega_2}, \\ u_1|_+ - u_1|_- = \xi_1 \dfrac{\partial u_1}{\partial \nu}\Big|_+ & \text{on } \partial\Omega_1, \\ u_1|_+ - u_1|_- = \xi_2 \dfrac{\partial u_1}{\partial \nu}\Big|_+ & \text{on } \partial\Omega_2, \\ \dfrac{\partial u_1}{\partial \nu}\Big|_- = 0 & \text{on } \partial\Omega_1, \partial\Omega_2, \\ |u_1(x)| = O(|x|^{-1}) & \text{as } |x| \to \infty, \end{cases} \tag{3.3}$$

and

$$\begin{cases} \Delta u_2(x) = 0 & \text{in } \Omega_1, \\ \Delta u_2(x) = f_2(x) & \text{in } \Omega_2, \\ \nabla \cdot (\sigma(x) + i\omega_2 \varepsilon(x)) \nabla u_2(x) = 0 & \text{in } \mathbb{R}^2 \setminus \overline{\Omega_1 \cup \Omega_2}, \\ u_2|_+ - u_2|_- = \xi_1 \dfrac{\partial u_2}{\partial \nu}\Big|_+ & \text{on } \partial\Omega_1, \\ u_2|_+ - u_2|_- = \xi_2 \dfrac{\partial u_2}{\partial \nu}\Big|_+ & \text{on } \partial\Omega_2, \\ \dfrac{\partial u_2}{\partial \nu}\Big|_- = 0 & \text{on } \partial\Omega_1, \partial\Omega_2, \\ |u_2(x)| = O(|x|^{-1}) & \text{as } |x| \to \infty. \end{cases} \tag{3.4}$$

Proof. We substitute (3.2) into (3.1). Considering the equation in $\Omega_1 \times \mathbb{R}^+$ we get

$$e^{i\omega_1 t}\Delta u_1 + e^{i\omega_2 t}\Delta u_2 = e^{i\omega_1 t} f_1.$$

Thus

$$(\Delta u_1 - f_1) + e^{i(\omega_2 - \omega_1)t}\Delta u_2 = 0,$$

which yields $\Delta u_1 - f_1 = 0$ in Ω_1 and $\Delta u_2 = 0$ in Ω_1.

In the same manner, we get the equations satisfied by u_1 and u_2 in Ω_2.

Outside the fish bodies, we have

$$\nabla \cdot (\sigma + \varepsilon\partial_t)\nabla e^{i\omega_1 t} u_1 + \nabla \cdot (\sigma + \varepsilon\partial_t)\nabla e^{i\omega_2 t} u_2 = 0,$$

$$e^{i\omega_1 t}\nabla \cdot (\sigma + i\omega_1\varepsilon)\nabla u_1 + e^{i\omega_2 t}\nabla \cdot (\sigma + i\omega_2\varepsilon)\nabla u_2 = 0,$$

which yields $\nabla \cdot (\sigma + i\omega_1\varepsilon)\nabla u_1 = 0$ in $\mathbb{R}^2 \setminus (\overline{\Omega_1 \cup \Omega_2})$ and $\nabla \cdot (\sigma + i\omega_2\varepsilon)\nabla u_2 = 0$ in $\mathbb{R}^2 \setminus (\overline{\Omega_1 \cup \Omega_2})$.

Finally it is easy to check that the boundary conditions remain unchanged because the time dependency does not appear explicitly.

□

Remark 3.2.2 *The potentials u_1 and u_2, that respectively solve* (3.3) *and* (3.4)*, have a meaningful interpretation that is based on two different sub-modalities of the electroreception. As a matter of fact, u_1 can be viewed as the potential when the fish $\mathfrak{F}_1$ is active and $\mathfrak{F}_2$ is passive, whereas u_2 can be viewed as the potential when the fish $\mathfrak{F}_1$ is passive and $\mathfrak{F}_2$ is active; see [62].*

Formula (3.2) *tells us that it is possible to study the total field looking separately at these two different oscillating regimes.*

The idea is to separate the two signals from the measurements of their superposition. This can be done easily by using signal analysis techniques; see [38].

Figure 3.3 illustrates the potential before the jamming avoidance response, when the fish emit signals at a certain common frequency, whereas Figure 3.4 depicts the two submodalities contained in the total signal $u(x,t)$ after they have switched their EOD frequencies.

3.2.2. Pulse-type fish

For the pulse-type fish we have that $h_1(t)$ and $h_2(t)$ are pulse wave. We can assume that they both can be obtained from a standard pulse shape $h(t)$ (see Figure Figure 3.1) by means of translation and scaling, i.e.,

$$h_1(t) = h(\eta_1 t - T_1),$$

$$h_2(t) = h(\eta_2 t - T_2).$$

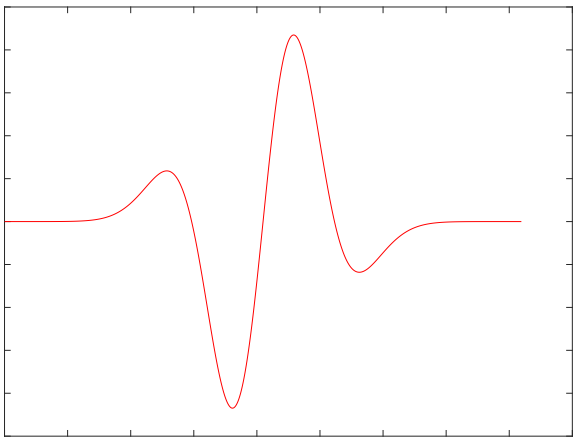

Figure 3.1.: Standard shape of the pulse wave $h(t)$.

For some pulse-type species, as Gymnotoid, the jamming avoidance response is obtained by shortening the duration of the emitted pulse; see [48]. In this way, they minimize the chance of pulse coincidence by transient accelerations (decelerations) of their EOD rate. For $\eta_1, \eta_2 > 0$ large enough such that $\operatorname{supp}(h_1) \cap \operatorname{supp}(h_2) = \varnothing$.

Thus, for $t_1, t_2 > 0$ such that $h_1(t_1) \neq 0$ and $h_2(t_2) \neq 0$ we can consider $u_1(x) := u(x,t_1)$ and $u_2(x) := u(x,t_2)$. These time-slices have the following property:

$$\begin{cases} \Delta u_1(x) = f_1(x)h_1(t_1), & x \in \Omega_1 \\ \Delta u_1(x) = 0, & x \in \Omega_2, \end{cases} \quad \begin{cases} \Delta u_2(x) = 0, & x \in \Omega_1 \\ \Delta u_2(x) = f_2(x)h_2(t_2), & x \in \Omega_2 \end{cases}.$$

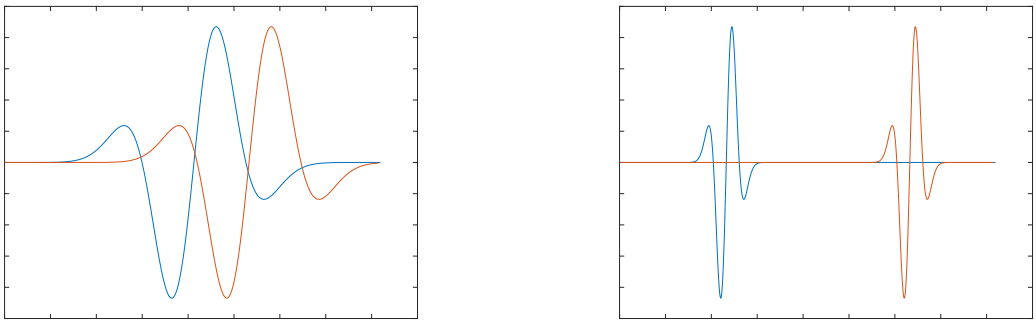

(a) Before the JAR the two pulse signals may interfere with each other.

(b) By shortening the duration of the pulse it is possible to identify two non-overlapping time-windows I_1 and I_2 corresponding to the signal emitted by the fish $\mathfrak{F}_1$ and $\mathfrak{F}_2$, respectively.

Figure 3.2.

Hence we can achieve a separation of signals.

In the next sections, we will see an important consequence of Proposition 3.2.1. As a matter of fact $\mathfrak{F}_1$ can track $\mathfrak{F}_2$ by using the measurements of $u_2|_{\partial\Omega_1}$, solution to (3.4), and can detect a small target D by using the measurements of $u_1|_{\partial\Omega_1}$.

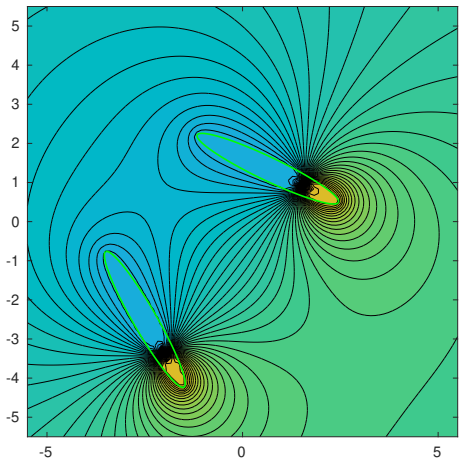

Figure 3.3.: Before the JAR (the EOD frequencies of the two fish are the same). Plot of $u(x) = u_1(x) + u_2(x)$, where $u(x,t) = u(x)e^{i\omega_0 t}$.

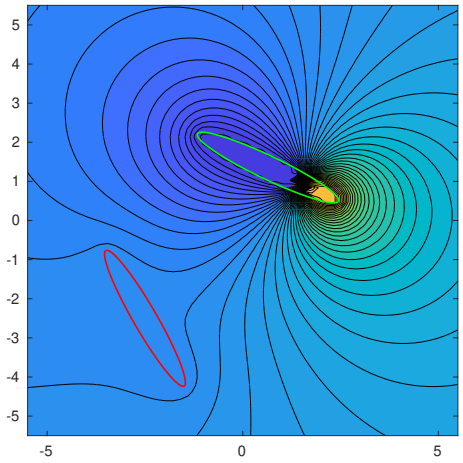

(a) Plot of u_2. Ω_1 (red) is passive and Ω_2 (green) is active.

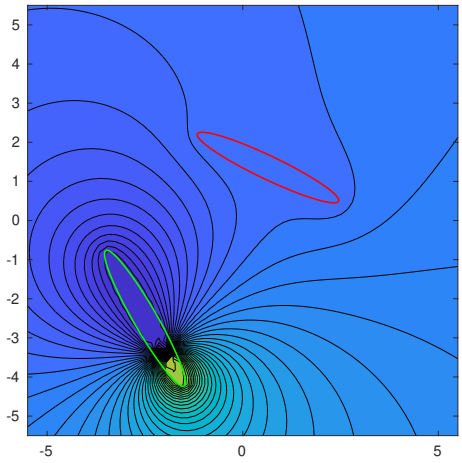

(b) Plot of u_1. Ω_1 (green) is active and Ω_2 (red) is passive.

Figure 3.4.: After the JAR (the EOD frequencies ω_1 and ω_2 of the two fish are apart from each other).

3.3. Electro–communication

The aim of this section is to give a mathematical procedure to model the communication abilities of the weakly electric fish, i.e., the capability of a fish to perceive a conspecific nearby. Assume, for instance, the point of view of the fish $\mathfrak{F}_1$. We want $\mathfrak{F}_1$ to estimate some basic features of $\mathfrak{F}_2$, such as the position of its electric organ. More importantly, by using subsequent estimates, we want to design an algorithm for $\mathfrak{F}_1$ to track $\mathfrak{F}_2$.

For the sake of clarity, we consider the case without the small dielectric target. It is worth emphasizing that the presence of the target is not troublesome since its effect on the tracking procedure is negligible even when the fish are swimming nearby.

When $\mathfrak{F}_1$ gets close to $\mathfrak{F}_2$, both $\mathfrak{F}_1$ and $\mathfrak{F}_2$ experiment the so-called jamming avoidance response and thus their electric organ discharge (EOD) frequencies switch. When the EOD frequencies ω_1 and ω_2 are apart from each other, Proposition 3.2.1 can be applied.

Let u_2 be the solution to the transmission problem (3.4). As previously mentioned, the function u_2 can be extracted from the total signal $u(x,t)$ using signal analysis techniques.

We define

$$H^{u_2}(x) = (\mathcal{S}_{\Omega_1} - \xi_1 \mathcal{D}_{\Omega_1}) \left[\left. \frac{\partial u_2}{\partial \nu} \right|_+ \right](x).$$

Let us recall the following boundary integral representation: for each $x \in \mathbb{R}^2 \setminus (\overline{\Omega_1 \cup \Omega_2})$,

$$(u_2 - H^{u_2})(x) = \int_{\partial\Omega_2} \left(\left.\frac{\partial u_2}{\partial \nu}\right|_+ (y)\, \Gamma(x,y) - \frac{\partial \Gamma}{\partial \nu_y}(x,y)\, u_2|_+(y) \right) \mathrm{d}s_y \,.$$

Making use of the Robin boundary condition on $\partial\Omega_2$ and integration by parts yields

$$\begin{aligned}
(u_2 - H^{u_2})(x) &= \int_{\partial\Omega_2} \left(\left.\frac{\partial u_2}{\partial \nu}\right|_+ (y)\, \Gamma(x,y) - \frac{\partial \Gamma}{\partial \nu_y}(x,y)\, u_2|_+(y) \right) \mathrm{d}s_y \\
&= \int_{\partial\Omega_2} \left(\left.\frac{\partial u_2}{\partial \nu}\right|_+ (y)\, \Gamma(x,y) - \frac{\partial \Gamma}{\partial \nu_y}(x,y) \left(\xi_2 \left.\frac{\partial u_2}{\partial \nu}\right|_+ (y) + u_2|_-(y) \right) \right) \mathrm{d}s_y \\
&= \int_{\partial\Omega_2} \left.\frac{\partial u_2}{\partial \nu}\right|_+ (y) \left(\Gamma(x,y) - \xi_2 \frac{\partial \Gamma}{\partial \nu_y}(x,y) \right) \mathrm{d}s_y - \int_{\partial\Omega_2} \frac{\partial \Gamma}{\partial \nu_y}(x,y) u_2|_-(y)\, \mathrm{d}s_y \\
&= \int_{\partial\Omega_2} \left.\frac{\partial u_2}{\partial \nu}\right|_+ \left(\Gamma - \xi_2 \frac{\partial \Gamma}{\partial \nu} \right) \mathrm{d}s \pm \alpha \left[\Gamma(x - x_1^{(2)}) - \Gamma(x - x_2^{(2)}) \right] .
\end{aligned}$$

Therefore, we obtain

$$(u_2 - H^{u_2})(x) = \int_{\partial\Omega_2} \left.\frac{\partial u_2}{\partial \nu}\right|_+ \left(\Gamma - \xi_2 \frac{\partial \Gamma}{\partial \nu} \right) \mathrm{d}s \pm \alpha \left[\Gamma(x - x_1^{(2)}) - \Gamma(x - x_2^{(2)}) \right] . \tag{3.5}$$

Observe that, for x away from the $x_1^{(i)}$, we can approximate $\Gamma(x - x_2^{(2)}) - \Gamma(x - x_1^{(2)})$ as follows:

$$\left[\Gamma(x - x_2^{(2)}) - \Gamma(x - x_1^{(2)}) \right] \approx \pm \nabla\Gamma(x - x_1^{(2)}) \cdot (x_2^{(2)} - x_1^{(2)}) = \frac{(x - x_1^{(2)}) \cdot (x_2^{(2)} - x_1^{(2)})}{\|x - x_1^{(2)}\|^2} .$$

Consider an array of receptors $(x_l)_{l=1}^M$ on $\partial\Omega_1$. We aim at solving the inverse source problem of determining the dipole, of $\mathfrak{F}_2$ from the knowledge of the measurements on the skin of $\mathfrak{F}_1$:

$$\{ (u_2 - H^{u_2})(x_l) \ : \ \text{for } l = 1, \dots, N \} . \tag{3.6}$$

In order to estimate the dipole, we assume that the following single-dipole approximation holds:

$$(u_2 - H^{u_2})(x_l) \approx \frac{(x_l - \widehat{z}) \cdot \widehat{\mathbf{p}}}{\|x_l - \widehat{z}\|^2}, \tag{3.7}$$

where $\widehat{\mathbf{p}}$ and $\widehat{z}$ denote respectively the moment and the center of the equivalent dipolar source.

Remark 3.3.1 *The single-dipole approximation* (3.7) *is an equivalent representation of a spread source. However, in the presence of several well-separated sources, such approximation is not trustworthy anymore [45]. In the case of $P \geq 3$ conspecifics we would extract $u_1, \dots, u_P$ components from the total signal, and the single-dipole approximation remains applicable to each one of the components $u_2, \dots, u_P$.*

3.4. Electro–sensing

Now, suppose to have $\mathfrak{F}_1, \mathfrak{F}_2$ as before and a target close to $\mathfrak{F}_1$.

Let u_1 be the solution to the transmission problem (3.3), that is,

$$\begin{cases} \Delta u_1(x) = f_1(x) & \text{in } \Omega_1, \\ \Delta u_1(x) = 0 & \text{in } \Omega_2, \\ \nabla \cdot (\sigma(x) + i\omega_1 \varepsilon(x)) \nabla u_1(x) = 0 & \text{in } \mathbb{R}^2 \setminus \overline{\Omega_1 \cup \Omega_2}, \\ u_1|_+ - u_1|_- = \xi_1 \dfrac{\partial u_1}{\partial \nu}\Big|_+ & \text{on } \partial\Omega_1, \\ u_1|_+ - u_1|_- = \xi_2 \dfrac{\partial u_1}{\partial \nu}\Big|_+ & \text{on } \partial\Omega_2, \\ \dfrac{\partial u_1}{\partial \nu}\Big|_- = 0 & \text{on } \partial\Omega_1, \partial\Omega_2, \\ |u_1(x)| = O(|x|^{-1}) & \text{as } |x| \to \infty, \end{cases}$$

and let U_1 be the background solution, that solves the problem

$$\begin{cases} \Delta U_1(x) = f_1(x) & \text{in } \Omega_1, \\ \Delta U_1(x) = 0 & \text{in } \Omega_2, \\ \Delta U_1(x) = 0 & \text{in } \mathbb{R}^2 \setminus \overline{\Omega_1 \cup \Omega_2}, \\ U_1|_+ - U_1|_- = \xi_1 \dfrac{\partial U_1}{\partial \nu}\Big|_+ & \text{on } \partial\Omega_1, \\ U_1|_+ - U_1|_- = \xi_2 \dfrac{\partial U_1}{\partial \nu}\Big|_+ & \text{on } \partial\Omega_2, \\ \dfrac{\partial U_1}{\partial \nu}\Big|_- = 0 & \text{on } \partial\Omega_1, \partial\Omega_2, \\ |U_1(x)| = O(|x|^{-1}) & \text{as } |x| \to \infty. \end{cases}$$

Consider $\Gamma_R^{(1,2)}$ the Green's function associated with Robin boundary conditions, that is defined for $x \in \mathbb{R}^2 \setminus (\overline{\Omega_1 \cup \Omega_2})$ by

$$\begin{cases} -\Delta_y \Gamma_R^{(1,2)}(x,y) = \delta_x(y), & y \in \mathbb{R}^2 \setminus \overline{\Omega_1 \cup \Omega_2}, \\ \Gamma_R^{(1,2)}(x,y)|_+ - \xi_1 \dfrac{\partial \Gamma_R^{(1,2)}}{\partial \nu_x}(x,y)\Big|_+ = 0, & y \in \partial\Omega_1, \\ \Gamma_R^{(1,2)}(x,y)|_+ - \xi_2 \dfrac{\partial \Gamma_R^{(1,2)}}{\partial \nu_x}(x,y)\Big|_+ = 0, & y \in \partial\Omega_2, \\ \left|\Gamma_R^{(1,2)}(x,y) + \frac{1}{2\pi}\log|y|\right| = O(|y|^{-1}), & |y| \to \infty. \end{cases} \tag{3.8}$$

Recall the following boundary integral equation: for each $x \in \mathbb{R}^2 \setminus (\overline{\Omega_1 \cup \Omega_2 \cup D})$,

$$(u_1 - U_1)(x) = \int_{\partial D} \left(\frac{\partial u}{\partial \nu}\Big|_+ (y)\, \Gamma_R^{(1,2)}(x,y) - \frac{\partial \Gamma_R^{(1,2)}}{\partial \nu_y}(x,y)\, u|_+(y) \right) \mathrm{d}s_y,$$

where U_1 is the background solution, i.e., the solution without the inhomogeneity D, when the only dipolar source lies inside the body of $\mathfrak{F}_1$; see Figure 3.4b.

$$(u_1 - U_1)(x) = \frac{(k-1)}{k} \int_{\partial D} \left(\frac{\partial u}{\partial \nu}\bigg|_+ (y)\, \Gamma_R^{(1,2)}(x,y) \right) \mathrm{d}s_y.$$

Let B be a bounded open set with characteristic size 1. Assume that $D = z + \delta B$, i.e., D is a target located at z which has characteristic size δ. With the same argument as in [2], we obtain the following small volume approximation.

Theorem 3.4.1 (Dipolar approximation) *Suppose dist$(\partial\Omega_1, z) \gg 1$ and $\delta \ll 1$. Then for any $x \in \partial\Omega_1$,*

$$\left(\frac{\partial u_1}{\partial \nu} - \frac{\partial U_1}{\partial \nu} \right)(x) = -\delta^2 \nabla U_1(z)^T M(\lambda, B) \nabla_y \left(\frac{\partial \Gamma_R^{(1,2)}}{\partial \nu}\bigg|_+ \right)(x,z) + O(\delta^3), \tag{3.9}$$

where T denotes the transpose, $M(\lambda, B) = (m_{ij})_{i,j\in\{1,2\}}$ is the first-order polarization tensor associated with B and contrast parameter λ, given by

$$m_{ij} = \int_{\partial B} y_i \left(\lambda I - \mathcal{K}_B^*\right)^{-1} \left(\frac{\partial x_j}{\partial \nu}\bigg|_{\partial B} \right)(y)\ ds_y. \tag{3.10}$$

Note that, since the background potential is real, for $x \in \partial\Omega_1$ we have

$$\mathrm{Im}\left(\frac{\partial u_1}{\partial \nu} \right)(x) \approx -\delta^2 \nabla U_1(z)^T\, \mathrm{Im}\, M(\lambda, B) \nabla_y \left(\frac{\partial \Gamma_R^{(1,2)}}{\partial \nu}\bigg|_+ \right)(x,z). \tag{3.11}$$

This last step is crucial to locate the target because U_1 is only approximately known from the measurements and even a very small displacement in the location of $\mathfrak{F}_2$ can cause an error on the background potential U_1, which is of the same order as the contribution of the target.

On the other hand, when z is not too close to $\partial\Omega_2$, the contribution of $\mathfrak{F}_2$ contained into $\nabla U_1(z)$ is negligible. Therefore, we approximate $\nabla U_1(z) \approx \nabla \widehat{U}_1(z)$, where $\widehat{U}_1$ is solution to the problem

$$\begin{cases} \Delta \widehat{U}_1(x) = f_1(x) & \text{in } \Omega_1, \\ \Delta \widehat{U}_1(x) = 0 & \text{in } \mathbb{R}^2 \setminus \overline{\Omega_1}, \\ \widehat{U}_1|_+ - \widehat{U}_1|_- = \xi_1 \dfrac{\partial \widehat{U}_1}{\partial \nu}\bigg|_+ & \text{on } \partial\Omega_1, \\ \dfrac{\partial \widehat{U}_1}{\partial \nu}\bigg|_- = 0 & \text{on } \partial\Omega_1, \\ |\widehat{U}_1(x)| = O(|x|^{-1}) & \text{as } |x| \to \infty. \end{cases} \tag{3.12}$$

After post-processing (3.11) using the following operator

$$\mathcal{P}_{\Omega_1} = \frac{1}{2} I - \mathcal{K}^*_{\Omega_1} - \xi \frac{\partial \mathcal{D}_{\Omega_1}}{\partial \nu},$$

see [2], we get

$$\mathcal{P}_{\Omega_1}\left[\mathrm{Im}\left(\frac{\partial u_1}{\partial \nu}\right)\right](x) \approx \delta^2 \nabla \widehat{U}_1(z)^T \,\mathrm{Im}\, M(\lambda, B) \nabla_y \left(\frac{\partial \Gamma}{\partial \nu_x}\bigg|_+\right)(x,z), \quad x \in \partial\Omega_1. \tag{3.13}$$

Therefore, as long as $\mathrm{dist}(z, \partial\Omega_2) \gg 0$, the leading order term of the post-processed measured data is not significantly affected by the presence of $\mathfrak{F}_2$.

A MUSIC-type algorithm for searching the position z and a least square method for recovering the imaginary part of the polarization tensor $M(\lambda, B)$ can be applied; see [7].

3.5. Numerical experiments

With applications in robotics in mind, and for the sake of simplicity, we can assume that the two fish populating our testing environment share the same effective thickness ξ and the same shape, which is an ellipse with semiaxes $a = 2$ and $b = 0.3$. Therefore no tail-bending has been taken into account.

For the numerical computations of the direct solutions to the transmission problems involved in the following simulations, we solved the boundary integral system of equations by relying on boundary element techniques. We adapted the codes in [77] to our framework, with many fish populating the same environment.

3.5.1. Electro-communication

We perform numerical simulations to show how $\mathfrak{F}_1$ can locate the position and the orientation of $\mathfrak{F}_2$ by using a modified version of MUSIC-type algorithm for searching the dipolar source. Firstly, let us observe that accuracy is not improved by using a multi-frequency approach when noisy measurements are considered. Instead, $\mathfrak{F}_1$ can use a MUSIC-type algorithm based on movement in order to improve the accuracy in the detection algorithm. We use the approximation (3.7).

We consider N_s positions. For each $s \in \{1, \dots, N_s\}$ let us denote by $\mathfrak{F}_2^s$ the fish at the position s. On its skin there are N_r receptors $\{x_n^s\}_{n=1}^{N_r}$. For each $s = 1, \dots, N_s$, we define the $M \times 2$ lead field matrix $\mathbf{A}_s$ as

$$\mathbf{A}_s(z) = \begin{bmatrix} \dfrac{x^s_{1,1} - z_1}{\|x^s_1 - z\|^2} & \dfrac{x^s_{1,2} - z_1}{\|x^s_1 - z\|^2} \\ \vdots & \vdots \\ \dfrac{x^s_{M,1} - z_1}{\|x^s_M - z\|^2} & \dfrac{x^s_{M,2} - z_2}{\|x^s_M - z\|^2} \end{bmatrix}. \tag{3.14}$$

Let $\mathbf{F}$ be the Multi-Static Response (MSR) matrix defined as follows

$$\mathbf{F} = \begin{bmatrix} (u_2 - H^{u_2})(x_1^1) & \dots & (u_2 - H^{u_2})(x_1^{N_s}) \\ \vdots & \ddots & \vdots \\ (u_2 - H^{u_2})(x_{N_r}^1) & \dots & (u_2 - H^{u_2})(x_{N_r}^{N_s}) \end{bmatrix}.$$

Moreover, we assume that the acquired measurements are corrupted by noise, i.e.,

$$\mathbf{F}_{noisy} = \mathbf{F} + \mathbf{X},$$

where $\mathbf{X} \sim \mathcal{N}(0, \sigma^2_{\text{noise}})$ is a Gaussian random variable with mean 0 and variance σ^2_{noise}. In our simulations we set the variance to:

$$\sigma_{\text{noise}} = (\mathbf{F}_{max} - \mathbf{F}_{min})\sigma_0,$$

where σ_0 is a positive constant called noise level, and $\mathbf{F}_{max}$ and $\mathbf{F}_{min}$ are the maximal and the minimal coefficient in the MSR matrix $\mathbf{F}$.

Let $\mathbf{F}^{\Re}_{noisy}$ be the real part of $\mathbf{F}_{noisy}$. Let $\lambda_1 \geq \lambda_2 \geq \cdots \geq \lambda_{N_r}$ be the eigenvalues of $\mathbf{F}^{\Re}_{noisy} \cdot (\mathbf{F}^{\Re}_{noisy})^T$ and let $\Phi_1, \dots, \Phi_{N_r}$ be the correspondent eigenvectors. The first eigenvalue is the one associated to the signal source and the span of the eigenvector Φ_1 is called the signal subspace. The other eigenvectors span the noise subspace.

As is well known, the MUSIC algorithm estimates the location of the dipole by checking the orthogonality between $\mathbf{A}_s(z)$ (3.14) and the noise subspace projector $\mathcal{P}_N$ [61]. This can be done for each position s.

For this purpose, we shall use a modified version of the MUSIC localizer in [68], by simply taking the maximum over the positions:

$$\mathcal{I}_2(z) = \max_{s=1,\dots,N_s} \left(\frac{1}{\lambda_{\min}(\mathbf{A}_s(z)^T \mathcal{P}_N \mathbf{A}_s(z), \mathbf{A}_s(z)\mathbf{A}_s(z)^T)} \right), \tag{3.15}$$

where $\lambda_{\min}(\cdot,\cdot)$ indicates the generalized minimum eigenvalue of a matrix pair.

We expect that the MUSIC localizer has a large peak at the location of the equivalent dipole we are searching for. Once an estimate $\widehat{z}$ of the true location has been obtained, the dipole moment can be estimated by means of the following formula:

$$\widehat{\mathbf{p}}_{est} = (\mathbf{A}(\widehat{z})^T \mathbf{A}(\widehat{z}))^{-1} \mathbf{A}(\widehat{z})^T \Phi_1. \tag{3.16}$$

i.e., the least-square solution to the linear system

$$\Phi_1 = \mathbf{A}(\widehat{z})\widehat{\mathbf{p}}. \tag{3.17}$$

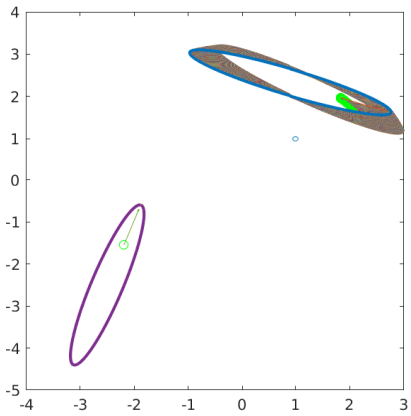

Figure 3.5.: The setting. $\mathfrak{F}_1$ is acquiring measurements at $N_s = 150$ different closely spaced positions.

Algorithm 3: MS MUSIC: Detect the presence of a conspecific from skin measurements

---

Input : The feedback, that is the total electric potential signal $u(x,t)$ recorded by the receptors on $\partial\Omega_1$.

1 Decompose the feedback u into u_1 and u_2 using signal separation techniques;
2 `MUSIC_dipoleSearch`$(u_2|_{\partial\Omega_1}, \Omega_1)$:
3 Build the (real part of the) MSR matrix $\mathbf{F}_{noisy} \in M(N_r \times N_s, \mathbb{R})$ from measurements collected during a short period;
4 Compute the eigen-decomposition of $\mathbf{F}_{noisy}\mathbf{F}_{noisy}^T = \Phi\Lambda\Phi^T$ and the noise subspace projector $\mathcal{P}_N$;
5 Evaluate the MUSIC localizer $\mathcal{I}_2$ on the nodes of a fine uniform grid $\mathcal{G}$ in the vicinity of Ω_1 ;
6 $\widehat{z} \leftarrow \arg\max_{\mathcal{G}} \mathcal{I}_2(z)$;
7 Determine $\widehat{\mathbf{p}}_{est}$ as the least-square solution to the linear system (3.17);

Output : an approximated position of the position of the electric organ of the conspecific $\mathfrak{F}_2$.

3.5.2. Tracking

Now we want to show that the dipole approximation that we assumed in the previous subsection is good enough to be used successfully for tracking purposes.

We assume the following setting for the numerical simulations. The fish $\mathfrak{F}_1$ is swimming along a fixed trajectory. Let us assume that the motion of its electric organ is described

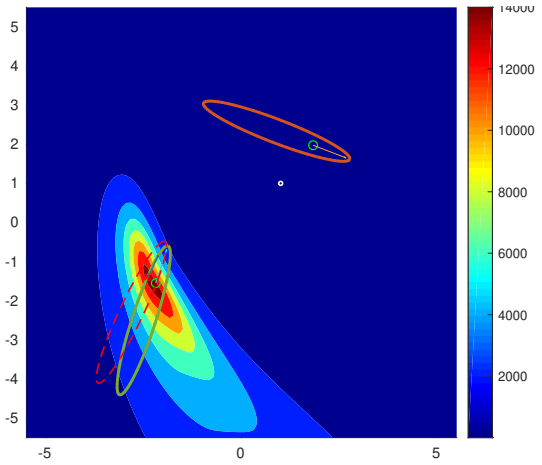

Figure 3.6.: Estimate of the position and the orientation of $\mathfrak{F}_2$, with noise level $\sigma_0 = 0.1$. The dashed red curve represents the estimated body of $\mathfrak{F}_2$, whereas the green one represents the true body of $\mathfrak{F}_2$. The white circle represents a small dielectric object placed between $\mathfrak{F}_1$ and $\mathfrak{F}_2$.

by a continuous path $F : [t_1, t_N] \longrightarrow \mathbb{R}^2$. Let $t_1 < t_2 < \cdots < t_N$ be a temporal grid on $[t_1, t_N]$ and let $t_j = s_1^j < \cdots < s_M^j = t_{j+1}$ be a grid on $[t_j, t_{j+1}]$ for $j = 1, \ldots, N-1$.

At the beginning, when $t = t_1$, $\mathfrak{F}_2$ starts following $\mathfrak{F}_1$. The tracking is performed by estimating the positions of $\mathfrak{F}_1$ at the nodes of the grid $t_1, \ldots, t_N$. Let us denote by X_n, Y_n and p_n, q_n the positions and the orientations of $\mathfrak{F}_2$ and $\mathfrak{F}_1$ at $t = t_n$, respectively. In order to obtain an estimate $\widehat{Y}_n$ of the position Y_n we can apply Algorithm 4, that employs measurements at $s_1^{n-1}, \ldots, s_M^{n-1}$ to reduce the effect of the noise. More precisely, the discrete dynamic system that describes the evolution of the positions and orientations of the two fish is as follows:

$$\begin{cases} X_n = X_{n-1} + h_n p_{n-1}, \\ p_n = \mathbf{R}(\theta_n) p_{n-1}, \\ Y_n = F(t_n), \\ q_n = F'(t_n) \approx \frac{F(t_n) - F(t_{n-1})}{h}, \end{cases} \tag{3.18}$$

where X_0 and p_0 are the initial data. Let us define $T_{n-1} := \widehat{Y}_{n-1} - X_{n-1}$, the pointing direction. The update of the orientation of $\mathfrak{F}_2$ is given by an orthogonal matrix associated with a rotation by an angle θ_n, $\mathbf{R}(\theta_n) \in O(2, \mathbb{R})$, and the turning angle is defined as

$$\theta_n := \theta_{n-1} \pm \min\left(\theta_{\max}, \widehat{T_{n-1} p_{n-1}}\right). \tag{3.19}$$

The numbers $h_1, \ldots, h_M$ incorporate the velocity of the tracking fish and should be chosen adaptively, in order to allow a variety of maneuvering capabilities such as acceleration and deceleration, as well as swimming backwards when $h_n < 0$. In order to prevent both collision and separation, we shall assume the velocity to be a function of the distance

between X_n and $\widehat{Y}_n$. $\theta_{\max}$ is the maximum turning angle. It is worth mentioning that the choice of $\theta_{\max}$ has a strong impact on the efficiency of the tracking procedure.

Algorithm 4: Real-Time Tracking: Fish-follows-Fish algorithm.

Input : Temporal grid over $[t_1, t_N]$. The maximum turning angle $\theta_{\max}$.

```
RT_Tracking(θ_max, [t_1, t_N], N, M) :
    for n ← 1, ..., N do
        X_n ← X_{n−1} + h_n p_{n−1};
        p_n ← R(θ_n) p_{n−1};
        Ŷ_n ← MUSIC_dipoleSearch(n)
    end
```

Output : Trajectory of the following fish.

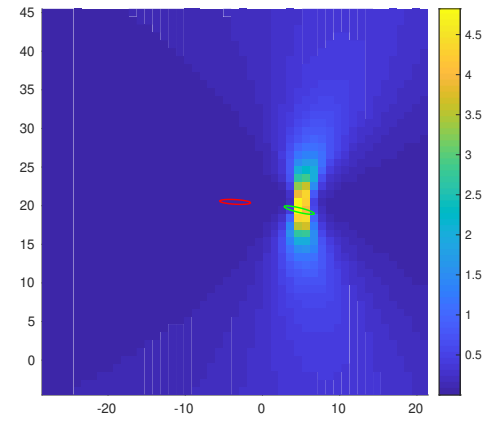

(a) $\sigma_0 = 0.01$

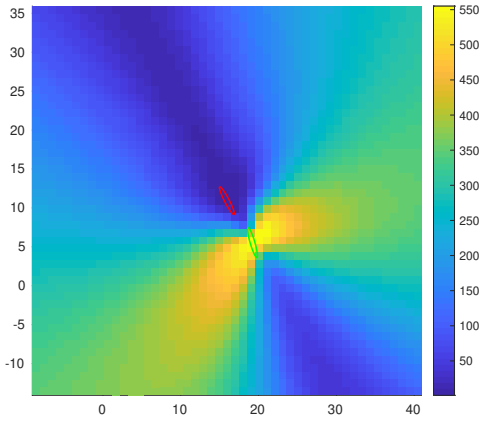

(b) $\sigma_0 = 0.1$

Figure 3.7.: Plot of the imaging functional $\mathcal{I}_2$ that the fish $\mathfrak{F}_1$ uses to track $\mathfrak{F}_2$.

The algorithm `MUSIC_dipoleSearch` employs a multi-position dipole search that uses M positions in between. In our numerical simulations, in order to have a real-time tracking procedure, we have set $M = 5$. We have set $\theta_{\max} = 10^{-1}$.

3.5.3. Electro-sensing

While the fish can sense the presence of other conspecifics at some distance, the range for active electro-sensing is much more short [52].

The effectivity of the estimated position of a small dielectric target inevitably depends on the relative distances among the fish, its conspecifics and the target. However, this seems perfectly reasonable. We have to require

1. The two fish do not get too close to each other;
2. The small dielectric target D is in the electro-sensing range of $\mathfrak{F}_1$.

If the above qualitative conditions are not met, there is no guarantee that we can get accurate results.

We perform many experiments to show that the MUSIC-type algorithm proposed in [2] works under the conditions outlined above. Based on approximation (3.13) we consider the illumination vector

$$g(z) = \left(\nabla \widehat{U}_1(z) \cdot \nabla_z \left(\frac{\partial \Gamma}{\partial \nu_x} \right)(x_1, z), \ldots, \nabla \widehat{U}_1(z) \cdot \nabla_z \left(\frac{\partial \Gamma}{\partial \nu_x} \right)(x_{N_r}, z) \right)^T,$$

and define the MUSIC localizer as follows:

$$\mathcal{I}_1(z) = \frac{1}{|(I - P)\widetilde{g}(z)|}, \tag{3.20}$$

where $\widetilde{g} = \frac{g}{|g|}$ and $\widehat{U}_1$ is the solution to (3.12).

Algorithm 5: SF MUSIC: Detection of a small dielectric target in the presence of another conspecific

---

Input : The feedback, that is the total electric potential signal $u(x,t)$ recorded by the receptors on $\partial\Omega_1$.

1 Decompose the feedback u into u_1 and u_2 using signal separation techniques ;
2 `MUSIC_target`$(u_1|_{\partial\Omega_1}, \Omega_1)$:
3 Post-process the data $\operatorname{Im} u_1|_{\partial\Omega_1}$;
4 Build the SFR $\mathbf{S}_{noise}$ for the post-processed data ;
5 Build and evaluate the MUSIC localizer $\mathcal{I}_1$ on the nodes of a fine uniform grid $\mathcal{G}$ in the vicinity of Ω_1 ;
6 $\widehat{z} \leftarrow \arg\max_{\mathcal{G}} \mathcal{I}_1(z)$;

Output : An approximated position of the target.

3.6. Concluding remarks

In this chapter, we have formulated the time-domain model for a shoal of weakly electric fish. We have shown how the jamming avoidance response can be interpreted within this mathematical framework and how it can be exploited to design communication systems, following strategies and active electro-sensing algorithms. In a forthcoming work, we plan to extend our present approach to develop navigation patterns inspired by the collective behavior of the weakly electric fish.

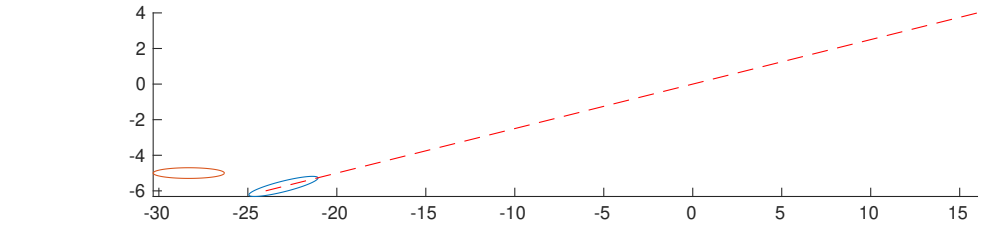

(a) Starting position.

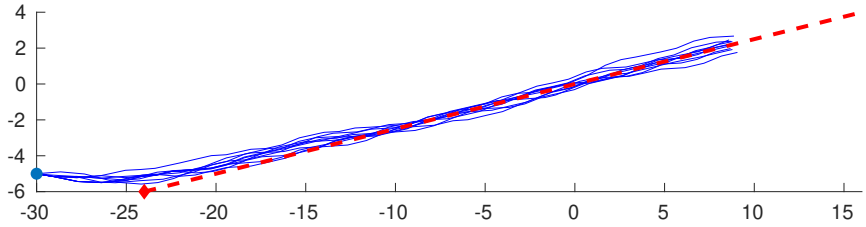

(b) $\sigma_0 = 0.01$

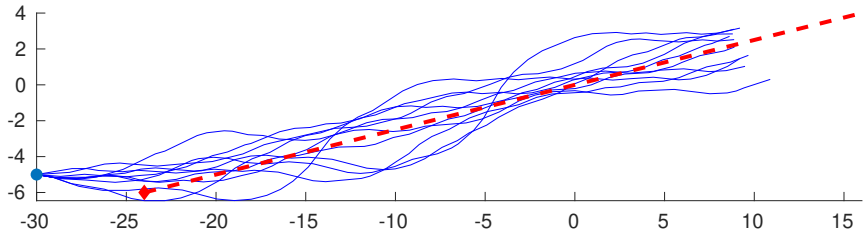

(c) $\sigma_0 = 0.05$

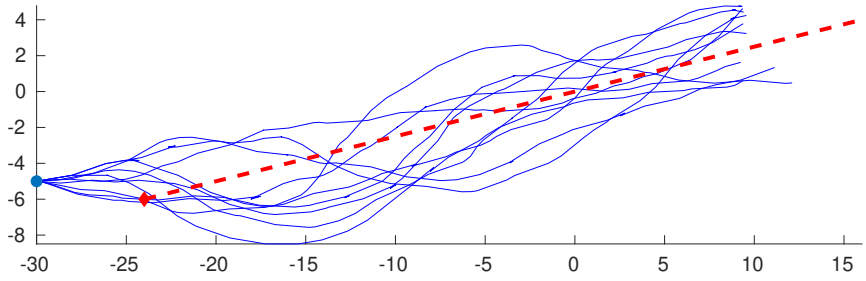

(d) $\sigma_0 = 0.2$

Figure 3.8.: Plot of the linear trajectory tracking. $N_{\text{exp}} = 10$ trials have been considered.

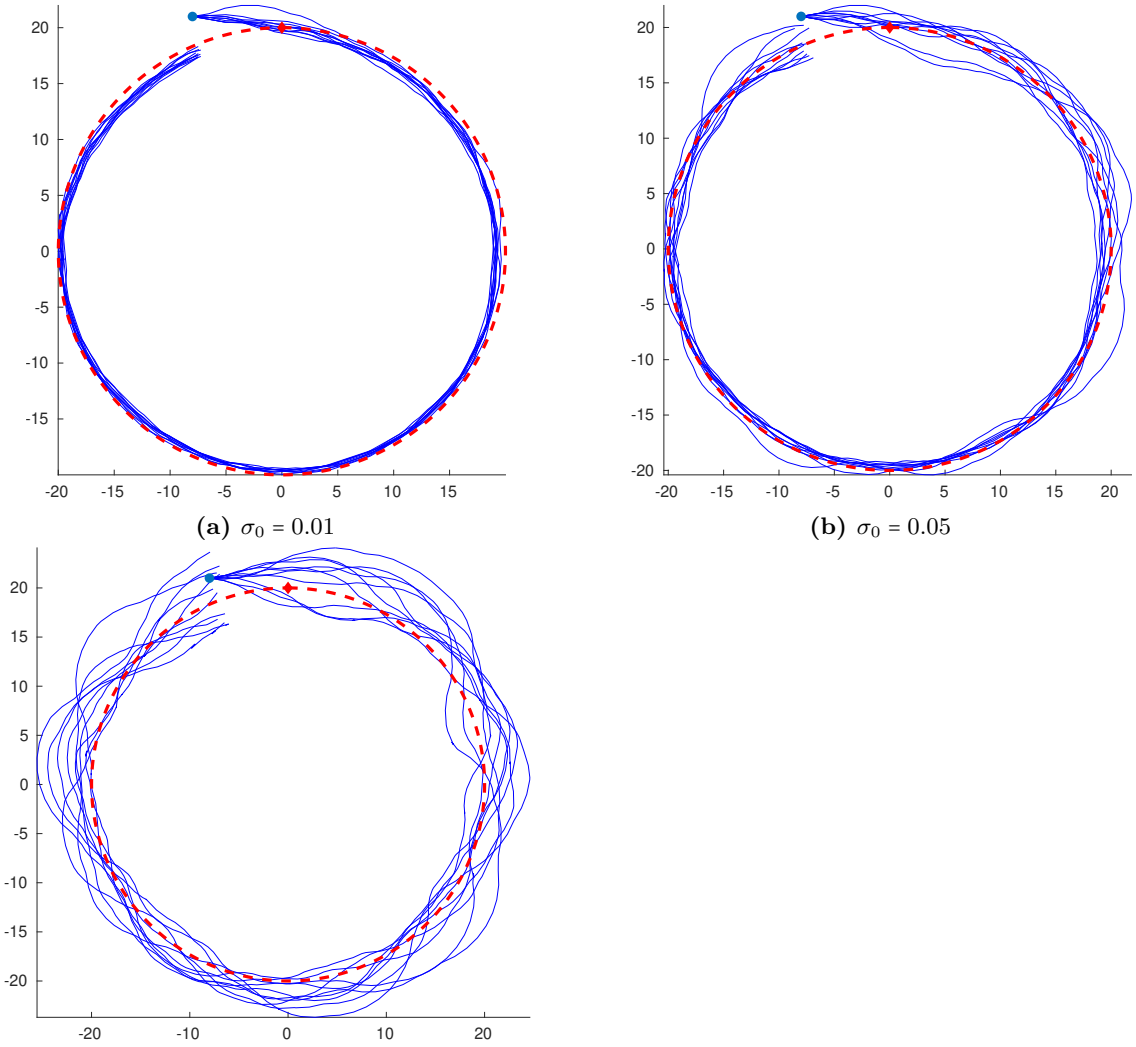

(a) $\sigma_0 = 0.01$

(b) $\sigma_0 = 0.05$

(c) $\sigma_0 = 0.2$

Figure 3.9.: Plot of the trajectory tracking when the leading fish is swimming in circle, clockwisely. $N_{\text{exp}} = 10$ trials/realizations have been considered.

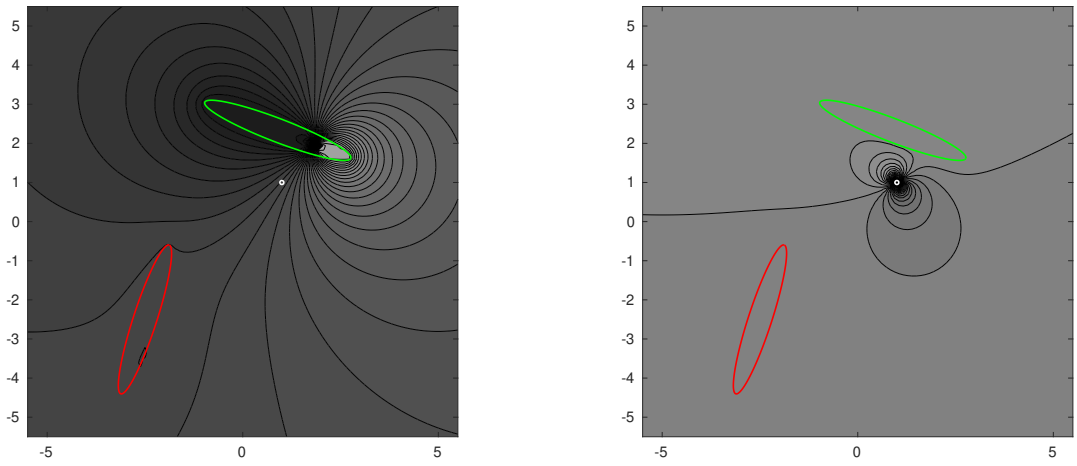

(a) Plot of $\operatorname{Re} u_1$.

(b) Plot of $\operatorname{Im} u_1$.

Figure 3.10.: Plot of the isopotential lines when $\mathfrak{F}_2$ (red) is passive (electrically silent) and $\mathfrak{F}_1$ (green) is active.

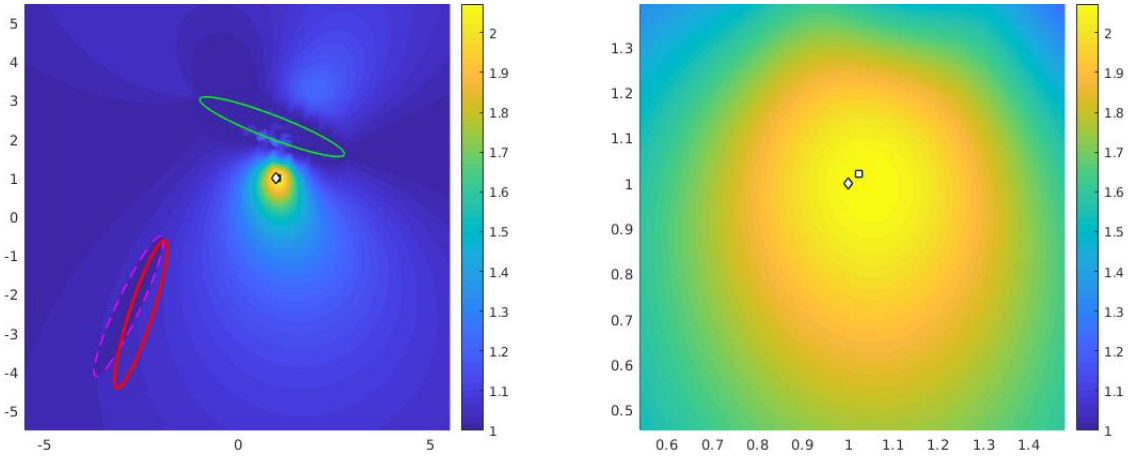

(a)

(b)

Figure 3.11.: Plot of the MUSIC imaging functional used in Algorithm 5 by using $N_r = 32$ receptors and $N_f = 100$ frequencies, with noise level $\sigma_0 = 0.1$. The square and the diamond indicate the approximation of the center and the true center of the target D, respectively. $\mathfrak{F}_1$ (green) can image the target despite the presence of $\mathfrak{F}_2$ (red), which is estimated by applying Algorithm 4.

Part II.

Bio-inspired transient echo-sensing

4. Reconstruction of a small acoustic inclusion via Time-dependent Polarization Tensors

Contents

The results presented in this chapter are contained in [32]. We aim at modeling a static bat, which is sending waves and recording the scattering echoes due to the presence of an acoustic inclusion. The scattering acoustic wave contains information that can be used to reconstruct high-frequency features of the inclusion.

The problem has to be evaluated in the frequency-domain first. Based on the layer potential techniques in [1], we derive an asymptotic expansion for the scattered field in terms of the FDPTs. Such asymptotic expansion is based on careful and precise estimates of the remainders with respect to the frequency. In particular, in the two-dimensional case, thorough estimates are needed due to the logarithmic singular behavior of the Hankel function at the origin [1, 53, 58, 79]. We require the inclusion to be small compared to the wavelength. In such a situation it is possible to expand the solution of the wave equation around the background solution [21]. Recall that high frequencies correspond exactly to small wavelengths. The idea is then to truncate the high frequencies, as in [12, 41]. This corresponds to the case of a constant frequency (CF) bat, which cannot

hear all the frequencies outside a certain range of finite values [71]. By applying the truncated Fourier transform to the frequency-dependent asymptotic expansion, we switch to the time-domain. The TDPTs are defined as the building blocks of the corresponding time-dependent asymptotic expansion.

While the leading-order term in this asymptotic formula has been derived by Ammari *et al.* [12, 41] for the three-dimensional case, the high-order ones are new. It is by exploiting the high-order terms of the time-dependent expansion that we are able to retrieve the fine shape details of an acoustic inclusion and extend the shape reconstruction methods for the frequency-domain proposed in [23]. Moreover, a valuable trait of our expansion is the fact that the TDPTs provide a proper interpretation of the multi-frequency problem, which can then be naturally tackled in the temporal domain.

This chapter is organized as follows. In Section 4.1, we recall the definitions of the boundary layer potentials in dimension $d = 2, 3$, and state some basic results that are used throughout the chapter. In Section 4.2, we describe the mathematical model concerning the Helmholtz equation, which we rewrite as a transmission problem, providing a representation formula for the solution. In Sections 4.3, 4.4 and 4.5 we perform the derivation of asymptotic expansions in dimension $d = 2$. In particular, Section 4.3 is devoted to the proof of a stability estimate for the two-dimensional transmission problem, which is used in Section 4.4 to estimate the remainder of the expansion obtained in the frequency-domain, in terms of the operating frequency ω. In Section 4.5, an expansion for the two-dimensional transient wave equation is presented. This asymptotic formula in time-domain is written in terms of the new concept of time-dependent polarization tensors (TDPTs). Translation, rotation and scaling properties for the TDPTs are also derived. In Section 4.6, we show that high-order TDPTs allow to reconstruct both the volume and the material property of a small inclusion. It is worth mentioning that, in our framework, these information can be separated and retrieved without using a near-field expansion [12, 41]. Furthermore, we adapt a well-known procedure for reconstructing fine shape details of the inclusion by using the TDPTs. This algorithm consists of a recursive optimization of a functional based on its shape derivative [24, 16, 23].

In Section 4.7, we perform numerical experiments in the two-dimensional case to validate the usage of the TDPTs. The reconstruction procedures of Section 4.6 are tested for different inclusions and acquisition settings, and the results are reported. In particular, we observe that the optimization algorithm performs well in recovering the boundary of the inclusion even with moderate level of noise.

Similar results to those of Sections 4.3, 4.4 and 4.5 are presented for the three-dimensional case in Appendix B.1.

4.1. Preliminary results

Before introducing our problem we recall some basic facts about the boundary layer potentials that we use repeatedly in the sequel.

Let us denote by Γ_ω the outgoing fundamental solution to the Helmholtz operator $\Delta + \omega^2$ in $\mathbb{R}^d$, that is [5]

$$\Gamma_\omega(x) := \begin{cases} \dfrac{i}{4} H_0^{(1)}(\omega|x|), & d = 2, \\ \dfrac{e^{i\omega|x|}}{4\pi|x|}, & d = 3. \end{cases} \tag{4.1}$$

Here, $H_0^{(1)}$ is the Hankel function of the first kind of order zero, i denotes the imaginary unit and $x \in \mathbb{R}^d$. We also consider Γ_0 defined by

$$\Gamma_0(x) := \begin{cases} \dfrac{1}{2\pi} \log|x|, & d = 2, \\ \dfrac{1}{4\pi|x|}, & d = 3. \end{cases}$$

Note that Γ_ω solves (in the sense of distributions) the equation

$$(\Delta + \omega^2)\Gamma_\omega = \delta_0 \quad \text{in } \mathbb{R}^d, \quad d = 2, 3,$$

where δ_0 is the Dirac mass at 0. Let D be a bounded Lipschitz domain in $\mathbb{R}^d$. The single- and double-layer potentials on D, $\mathcal{S}_D^\omega$ and $\mathcal{D}_D^\omega$, are defined as follows: $\phi \in L^2(\partial D)$,

$$\mathcal{S}_D^\omega[\phi](x) = \int_{\partial D} \Gamma_\omega(x - s)\phi(s)\, d\sigma(s),$$
$$\mathcal{D}_D^\omega[\phi](x) = \int_{\partial D} \frac{\partial \Gamma_\omega}{\partial \nu_s}(x - s)\phi(s)\, d\sigma(s).$$

The behavior of $\mathcal{S}_D^\omega[\phi]$ across the boundary ∂D is described by the following well-known formulas [15].

Lemma 4.1.1 *For $\phi \in L^2(\partial D)$,*

$$\mathcal{S}_D^\omega[\phi]|_+(x) = \mathcal{S}_D^\omega[\phi]|_-(x), \text{ for a.e. } x \in \partial D,$$
$$\left.\frac{\partial \mathcal{S}_D^\omega[\phi]}{\partial \nu}\right|_\pm (x) = \left(\pm\frac{1}{2}\mathcal{I} + (\mathcal{K}_D^\omega)^*\right)[\phi](x), \text{ for a.e. } x \in \partial D,$$

where the subscript $\pm$ means $\mathcal{S}_D^\omega[\phi]|_\pm(x) := \lim_{t \to 0} \mathcal{S}_D^\omega[\phi](x \pm t\nu(x))$, $\mathcal{I}$ is the identity operator and $(\mathcal{K}_D^\omega)^*$ is defined by

$$(\mathcal{K}_D^\omega)^*[\phi](x) = \int_{\partial D} \frac{\partial \Gamma_\omega(x - y)}{\partial \nu_x}\phi(y)\, d\sigma(y).$$

Note that $(\mathcal{K}_D^\omega)^*$ is the L^2-adjoint of $\mathcal{K}_D^\omega$, with

$$\mathcal{K}_D^\omega[\phi](x) = \int_{\partial D} \frac{\partial \Gamma_\omega(x - y)}{\partial \nu_y}\phi(y)\, d\sigma(y).$$

We also recall the following lemma [21, 44, 43].

Lemma 4.1.2 *There exists $\omega_0 > 0$ such that for $\omega < \omega_0$,*

a) if $d = 2$

$$\left\| \mathcal{S}_D^\omega[\phi] - \mathcal{S}_D^0[\phi] - \beta_\omega \int_{\partial D} \phi \right\|_{H^1(\partial D)} \leq C\omega^2 \ln \omega \|\phi\|_{L^2(\partial D)},$$
$$\left\| \left. \frac{\partial \mathcal{S}_D^\omega[\phi]}{\partial \nu} \right|_\pm - \left. \frac{\partial \mathcal{S}_D^0[\phi]}{\partial \nu} \right|_\pm \right\|_{L^2(\partial D)} \leq C\omega^2 \ln \omega \|\phi\|_{L^2(\partial D)},$$

where $\beta_\omega = \frac{1}{2\pi}(\ln \omega - \ln 2 + \gamma - \frac{\pi}{2} i)$, and γ is the Euler constant,

b) if $d = 3$

$$\|\mathcal{S}_D^\omega[\phi] - \mathcal{S}_D^0[\phi]\|_{H^1(\partial D)} \leq C\omega \|\phi\|_{L^2(\partial D)},$$
$$\left\| \left. \frac{\partial \mathcal{S}_D^\omega[\phi]}{\partial \nu} \right|_\pm - \left. \frac{\partial \mathcal{S}_D^0[\phi]}{\partial \nu} \right|_\pm \right\|_{L^2(\partial D)} \leq C\omega \|\phi\|_{L^2(\partial D)}.$$

Note that when $d = 2$ the single-layer potential is not, in general, invertible nor injective.

4.2. Mathematical model in the frequency domain

Let B be a bounded Lipschitz domain in $\mathbb{R}^d$ ($d = 2, 3$) such that B contains the origin and $|B| = 1$, and let $D = z + \varepsilon B$ be a small acoustic inclusion of contrast $k > 0$, $k \neq 1$, with $0 < \varepsilon < 1$. Let Γ_ω be as in (4.1). Denote by V_y the field corresponding to a time-harmonic wave generated at $y \in \mathbb{R}^d \setminus \overline{D}$,

$$V_y(x, \omega) := \Gamma_\omega(x - y),$$

where $\omega > 0$ is the operating frequency, and $x \neq y$. Moreover, we assume that $\operatorname{dist}(y, D) \gg 1$, that is, the inclusion D is far from the source.

Let v_y be the field perturbed by the presence of the inclusion D, which is the solution to

$$\nabla \cdot (\chi(\mathbb{R}^d \setminus \overline{D}) + k\chi(D))\nabla v_y + \omega^2 v_y = \delta_y, \tag{4.2}$$

with χ denoting the characteristic function, and $v_y - V_y$ satisfying the so-called Sommerfeld radiation condition, i.e.,

$$\lim_{r \to +\infty} r^{(d-1)/2} \left(\frac{\partial}{\partial r}(v_y - V_y) - i\omega(v_y - V_y) \right) = 0, \quad |x| = r. \tag{4.3}$$

Equation (4.2) can be written equivalently as the following transmission problem

$$\begin{cases} \Delta v_y + \omega^2 v_y = \delta_y, & \mathbb{R}^d \setminus \overline{D}, \\ \Delta v_y + \dfrac{\omega^2}{k} v_y = 0, & D, \\ v_y|_+ = v_y|_-, & \partial D, \\ \left.\dfrac{\partial v_y}{\partial \nu}\right|_+ = k \left.\dfrac{\partial v_y}{\partial \nu}\right|_-, & \partial D, \\ v_y - V_y \text{ satisfies condition (4.3).} \end{cases}$$

Notice that the solution v_y can be represented as follows [21]:

$$v_y(x,\omega) = \begin{cases} V_y(x,\omega) + \mathcal{S}_D^{\omega}[\psi](x), & x \in \mathbb{R}^d \setminus \overline{D}, \\ \mathcal{S}_D^{\frac{\omega}{\sqrt{k}}}[\phi](x), & x \in D, \end{cases} \tag{4.4}$$

where the pair $(\phi, \psi) \in L^2(\partial D) \times L^2(\partial D)$ is the unique solution of the following system of boundary integral equations on ∂D:

$$\begin{cases} \mathcal{S}_D^{\frac{\omega}{\sqrt{k}}}[\phi] - \mathcal{S}_D^{\omega}[\psi] = V_y, \\ k \left.\dfrac{\partial \mathcal{S}_D^{\frac{\omega}{\sqrt{k}}}[\phi]}{\partial \nu}\right|_- - \left.\dfrac{\partial \mathcal{S}_D^{\omega}[\psi]}{\partial \nu}\right|_+ = \dfrac{\partial V_y}{\partial \nu}, \end{cases} \quad \text{on } \partial D. \tag{4.5}$$

Remark 4.2.1 *The system* (4.5) *has a unique solution provided that* ω^2 *is not a Dirichlet eigenvalue for* $-\Delta$ *on* D. *This is certainly true when* $\lambda_1(D) \geq (1/|D|)^{2/d} C_d^{2/d} j_{d/2-1,1}$, *where* $j_{m,1}$ *is the first positive zero of the Bessel function* J_m, C_d *is the volume of the* d*-dimensional unit ball, and* $\lambda_1(D) > 0$ *is the smallest eigenvalue of* $-\Delta$ *on* D; *see [26, 51].*

Hereinafter, we limit our considerations to the two-dimensional problem only. For the three-dimensional case see Appendix B.1.

4.3. Stability estimates for the transmission problem

The technical estimates contained in this section will be used in the derivation of the asymptotic expansion to make the dependence of the remainder on the operating frequency explicit.

Let $D = \varepsilon B + z$, $|B| = 1$ and $D \subset \mathbb{R}^2$. We suppose that $\omega \in (0, \varepsilon^{-\gamma})$, with $0 < \gamma < 1$. Note that there exists $\varepsilon_0 > 0$ such that, for ε sufficiently small, $\varepsilon\omega \leq \varepsilon_0 < 1$, i.e., $\varepsilon\omega$ can be made arbitrarily small. The main estimate is given by the following proposition.

Proposition 4.3.1 *For each $(F,G) \in H^1(\partial D) \times L^2(\partial D)$, let $(\phi,\psi) \in L^2(\partial D) \times L^2(\partial D)$ be the unique solution of the system of integral equations*

$$\begin{cases} \mathcal{S}_D^{\frac{\omega}{\sqrt{k}}}[\phi] - \mathcal{S}_D^{\omega}[\psi] = F, \\ k \left.\dfrac{\partial \mathcal{S}_D^{\frac{\omega}{\sqrt{k}}}[\phi]}{\partial \nu}\right|_- - \left.\dfrac{\partial \mathcal{S}_D^{\omega}[\psi]}{\partial \nu}\right|_+ = G, \end{cases} \qquad \text{on } \partial D. \tag{4.6}$$

Let $\varepsilon_0 > 0$ be such that $\varepsilon\omega \le \varepsilon_0 < 1$. We have

$$\|\phi\|_{L^2(\partial D)} + \|\psi\|_{L^2(\partial D)} \le C(\varepsilon^{-1}\|F\|_{L^2(\partial D)} + \|\nabla F\|_{L^2(\partial D)} + \|G\|_{L^2(\partial D)}), \tag{4.7}$$

where C does not depend on ε and ω.

Proposition 4.3.1 states that the solution to system (4.6) depends continuously on the right-hand side of the system, i.e., (F,G).

Since the two-dimensional fundamental solutions $\Gamma_{\varepsilon\omega}(x-y)$ and $\Gamma_{\varepsilon\omega/\sqrt{k}}(x-y)$ do not converge to $\Gamma_0(x-y) = \frac{1}{2\pi}\log|x-y|$ as ε goes to zero, the proof of Proposition 4.3.1 is not immediate. The proof we present here relies on the following lemma [21, 44, 43].

Lemma 4.3.2 *For each $(f,g) \in H^1(\partial B) \times L^2(\partial B)$, let $(\phi,\psi) \in L^2(\partial B) \times L^2(\partial B)$ be the unique solution of the system*

$$\begin{cases} \mathcal{S}_B^0[\phi] + \beta_{\varepsilon\omega/\sqrt{k}} \displaystyle\int_{\partial B} \phi \, d\sigma - \mathcal{S}_B^0[\psi] - \beta_{\varepsilon\omega} \int_{\partial B} \psi \, d\sigma = f, \\ k \left.\dfrac{\partial \mathcal{S}_B^0[\phi]}{\partial \nu}\right|_- - \left.\dfrac{\partial \mathcal{S}_B^0[\psi]}{\partial \nu}\right|_+ = g, \end{cases} \qquad \text{on } \partial B. \tag{4.8}$$

Suppose there exists $\varepsilon_0 > 0$ such that $\varepsilon\omega \le \varepsilon_0 < 1$. We have

$$\|\phi\|_{L^2(\partial B)} + \|\psi\|_{L^2(\partial B)} \le C(\|f\|_{H^1(\partial B)} + \|g\|_{L^2(\partial B)}), \tag{4.9}$$

where C does not depend on ε nor ω.

Proof. We define

$$\widehat{\mathcal{S}}_B^{\varepsilon\omega}[\phi] := \mathcal{S}_B^0[\phi] + \beta_{\varepsilon\omega} \int_{\partial B} \phi \, d\sigma.$$

Hariharan and MacCamy proved that $\widehat{\mathcal{S}}_B^{\varepsilon\omega}$ is invertible for $\varepsilon\omega$ small enough [44]. In particular, a ϕ solution to

$$\widehat{\mathcal{S}}_D^{\varepsilon\omega}[\phi] = h, \quad \text{for } h \in H^1(\partial B),$$

can be represented as

$$\phi = \phi_0 + \frac{c_1 - \beta_{\varepsilon\omega}}{\beta_{\varepsilon\omega} - c_0}\phi_1,$$

where $(\phi_0, c_0) \in H^1(\partial B) \times \mathbb{R}$ solves

$$\begin{cases} \mathcal{S}_B^0[\phi_0] + c_0 = 0, \\ \int_{\partial B} \phi_0 = 1, \end{cases}$$

and $(\phi_1, c_1) \in L^2(\partial B) \times \mathbb{C}$ solves

$$\begin{cases} \mathcal{S}_B^0[\phi_1] + c_1 = h, \\ \int_{\partial B} \phi_1 = 1. \end{cases}$$

Moreover, there exists a constant K, independent of ε, ω and h, such that

$$\|\phi_0\|_{L^2(\partial B)} + |c_0| \leq K,$$

$$\|\phi_1\|_{L^2(\partial B)} + |c_1| \leq K\|h\|_{H^1(\partial B)},$$

that is

$$\|\phi\|_{L^2(\partial B)} = \|(\widehat{\mathcal{S}}_B^{\varepsilon\omega})^{-1}[h]\|_{L^2(\partial B)} \leq K\|h\|_{H^1(\partial B)}.$$

By solving system (4.8) for (ϕ, ψ), we get

$$\phi = \psi + \frac{1}{2\pi}\ln(\sqrt{k})\left(\int_{\partial B}\psi\, d\sigma\right)(\widehat{\mathcal{S}}_B^{\varepsilon\omega})^{-1}[\chi_{\partial B}] + (\widehat{\mathcal{S}}_B^{\varepsilon\omega})^{-1}[f]$$

and

$$\begin{aligned}\psi = {} & \frac{k}{2\pi(1-k)}\ln(\sqrt{k})\left(\int_{\partial B}\psi\right)\left(\frac{(k+1)}{2(k-1)}\mathcal{I} - \mathcal{K}_B^*\right)^{-1}\left(-\frac{1}{2}\mathcal{I} + \mathcal{K}_B^*\right)(\widehat{\mathcal{S}}_B^{\varepsilon\omega})^{-1}[\chi_{\partial B}] \\ & - \frac{k}{1-k}\left(\frac{(k+1)}{2(k-1)}\mathcal{I} - \mathcal{K}_B^*\right)^{-1}\left(-\frac{1}{2}\mathcal{I} + \mathcal{K}_B^*\right)(\widehat{\mathcal{S}}_B^{\varepsilon\omega})^{-1}[f] + \left(\frac{(k+1)}{2(k-1)}\mathcal{I} - \mathcal{K}_B^*\right)^{-1}[g].\end{aligned}$$

From the above expressions, it is immediate to deduce that

$$\|\phi\|_{L^2(\partial B)} + \|\psi\|_{L^2(\partial B)} \leq C(\|f\|_{H^1(\partial B)} + \|g\|_{L^2(\partial B)}),$$

where C does not depend on ε and ω. □

Now we are in position to prove Proposition 4.3.1.

Proof of Proposition 4.3.1. Let

$$\widetilde{\phi}(\tilde{x}) = \phi(\varepsilon\tilde{x} + z), \quad \tilde{x} \in \partial B,$$

and define $\widetilde{\psi}$, $\widetilde{F}$ and $\widetilde{G}$ likewise. By a change of variables, (4.6) reads as follows:

$$\begin{cases} \mathcal{S}_B^{\frac{\varepsilon\omega}{\sqrt{k}}}[\widetilde{\phi}] - \mathcal{S}_B^{\varepsilon\omega}[\widetilde{\psi}] = \varepsilon^{-1}\widetilde{F}, \\ k\dfrac{\partial \mathcal{S}_B^{\frac{\varepsilon\omega}{\sqrt{k}}}[\widetilde{\phi}]}{\partial\nu}\Big|_- - \dfrac{\partial \mathcal{S}_B^{\varepsilon\omega}[\widetilde{\psi}]}{\partial\nu}\Big|_+ = \widetilde{G}, \end{cases} \quad \text{on } \partial B.$$

Consider the operator $T : L^2(\partial B) \times L^2(\partial B) \longrightarrow H^1(\partial B) \times L^2(\partial B)$ defined by

$$T(\widetilde{\phi}, \widetilde{\psi}) := \left(\mathcal{S}_B^{\frac{\varepsilon\omega}{\sqrt{k}}}[\widetilde{\phi}] - \mathcal{S}_B^{\varepsilon\omega}[\widetilde{\psi}], k\frac{\partial \mathcal{S}_B^{\frac{\varepsilon\omega}{\sqrt{k}}}[\widetilde{\phi}]}{\partial \nu}\bigg|_- - \frac{\partial \mathcal{S}_B^{\varepsilon\omega}[\widetilde{\psi}]}{\partial \nu}\bigg|_+ \right). \tag{4.10}$$

T can be decomposed as

$$T = T_0 + T_\varepsilon,$$

where

$$T_0(\widetilde{\phi}, \widetilde{\psi}) := \left(\mathcal{S}_B^0[\widetilde{\phi}] + \beta_{\varepsilon\omega} \int_{\partial B} \widetilde{\phi} - \mathcal{S}_B^0[\widetilde{\psi}] - \beta_{\varepsilon\omega} \int_{\partial B} \widetilde{\psi}, k\frac{\partial \mathcal{S}_B^0[\widetilde{\phi}]}{\partial \nu}\bigg|_- - \frac{\partial \mathcal{S}_B^0[\widetilde{\psi}]}{\partial \nu}\bigg|_+ \right),$$

and

$$T_\varepsilon := T - T_0.$$

For $\varepsilon\omega < \varepsilon_0$, and ε_0 small enough, Lemma 4.1.2 implies that

$$\|T_\varepsilon(\widetilde{\phi}, \widetilde{\psi})\|_{H^1 \times L^2} \leq C(\varepsilon\omega)^2 \ln(\varepsilon\omega) \left(\|\widetilde{\phi}\|_{L^2} + \|\widetilde{\psi}\|_{L^2}\right),$$

where C does not depend on ε nor ω. Since T_0 is invertible [21, 44, 43], T is invertible for $\varepsilon\omega$ small enough and

$$T^{-1} = T_0^{-1} + E,$$

where the operator E satisfies

$$\|E(\varepsilon^{-1}\widetilde{F}, \widetilde{G})\|_{L^2 \times L^2} \leq C(\varepsilon\omega)^2 \ln(\varepsilon\omega) \, \|(\varepsilon^{-1}\widetilde{F}, \widetilde{G})\|_{H^1 \times L^2},$$

with C being independent of $\widetilde{F}$, $\widetilde{G}$, ε and ω. Finally, we have

$$(\widetilde{\phi}, \widetilde{\psi}) = T^{-1}(\varepsilon^{-1}\widetilde{F}, \widetilde{G}) = T_0^{-1}(\varepsilon^{-1}\widetilde{F}, \widetilde{G}) + E(\varepsilon^{-1}\widetilde{F}, \widetilde{G}) = (\widetilde{\phi}_0, \widetilde{\psi}_0) + E(\varepsilon^{-1}\widetilde{F}, \widetilde{G}).$$

By applying Lemma 4.3.2, and assuming $\varepsilon\omega$ small enough, it follows that

$$\begin{aligned} \|(\widetilde{\phi}, \widetilde{\psi})\|_{L^2 \times L^2} &\leq C\|(\varepsilon^{-1}\widetilde{F}, \widetilde{G})\|_{H^1 \times L^2} + C(\varepsilon\omega)^2 \ln(\varepsilon\omega) \, \|(\varepsilon^{-1}\widetilde{F}, \widetilde{G})\|_{H^1 \times L^2} \\ &\leq C\|(\varepsilon^{-1}\widetilde{F}, \widetilde{G})\|_{H^1 \times L^2}, \end{aligned}$$

where C does not depend on ε and ω. By scaling back, we get inequality (4.7).

□

4.4. Frequency-domain asymptotic expansion

Let D be as in the previous section, i.e., $D = \epsilon B + z$. For $x \in \partial D$, z away from the location y of the source, we consider the truncated Taylor series of the background field

$$V_{y,n}(x,\omega) := \sum_{|\alpha|=0}^{n} \frac{\partial_z^\alpha V_y(z,\omega)}{\alpha!}(x-z)^\alpha.$$

Let $(\phi_n, \psi_n) \in L^2(\partial D) \times L^2(\partial D)$ be the unique solution of

$$\begin{cases} \mathcal{S}_D^{\frac{\omega}{\sqrt{k}}}[\phi_n] - \mathcal{S}_D^{\omega}[\psi_n] = V_{y,n+1}, \\ k\dfrac{\partial \mathcal{S}_D^{\frac{\omega}{\sqrt{k}}}[\phi_n]}{\partial \nu}\Big|_- - \dfrac{\partial \mathcal{S}_D^{\omega}[\psi_n]}{\partial \nu}\Big|_+ = \dfrac{\partial V_{y,n+1}}{\partial \nu}, \end{cases} \quad \text{on } \partial D. \tag{4.11}$$

Then $(\phi - \phi_n, \psi - \psi_n)$ is the unique solution of

$$\begin{cases} \mathcal{S}_D^{\frac{\omega}{\sqrt{k}}}[\phi - \phi_n] - \mathcal{S}_D^{\omega}[\psi - \psi_n] = V_y - V_{y,n+1}, \\ k\dfrac{\partial \mathcal{S}_D^{\frac{\omega}{\sqrt{k}}}[\phi - \phi_n]}{\partial \nu}\Big|_- - \dfrac{\partial \mathcal{S}_D^{\omega}[\psi - \psi_n]}{\partial \nu}\Big|_+ = \dfrac{\partial (V_y - V_{y,n+1})}{\partial \nu}, \end{cases} \quad \text{on } \partial D.$$

By Proposition 4.3.1, we have

$$\|\phi - \phi_n\|_{L^2(\partial D)} + \|\psi - \psi_n\|_{L^2(\partial D)} \le C(\varepsilon^{-1}\|V_y - V_{y,n+1}\|_{H^1(\partial D)} + \|\nabla(V_y - V_{y,n+1})\|_{L^2(\partial D)}),$$

where C does not depend on ε and ω. By definition of $V_y - V_{y,n+1}$, we have

$$\|V_y - V_{y,n+1}\|_{L^2(\partial D)} = \left(\int_{\partial D} |V_y - V_{y,n+1}|^2 d\sigma\right)^{1/2} \le |\partial D|^{1/2}\|V_y - V_{y,n+1}\|_{L^\infty(\partial D)}.$$

Hereinafter, we assume that $\omega \in (0, \varepsilon^{-\gamma})$, with $0 < \gamma < 1$. By expanding $V_y - V_{y,n+1}$ using the chain rule together with recurrence relations of the derivative of the Hankel function and the following approximation formula [1, 53, 79]

$$|H_\nu^{(1)}(\omega|z-y|)| = O(\omega^{-1/2}) \qquad \text{as } \omega \gg 1,$$

we obtain

$$\|\phi - \phi_n\|_{L^2(\partial D)} + \|\psi - \psi_n\|_{L^2(\partial D)} \le C|\partial D|^{1/2}\varepsilon^{n+1}(1 + \omega^{n+3/2}).$$

For $x \in \mathbb{R}^2 \setminus \overline{D}$, $x \neq y$, $\operatorname{dist}(x, D) \ge c_1 > 0$, the representation formula (4.4) yields

$$v(x,\omega) - V_y(x,\omega) = \mathcal{S}_D^{\omega}[\psi_n](x) + \mathcal{S}_D^{\omega}[\psi - \psi_n](x).$$

By applying the Cauchy-Schwarz inequality, we obtain

$$\begin{aligned} |\mathcal{S}_D^{\omega}[\psi - \psi_n](x)| &\le \left[\int_{\partial D} |\Gamma_\omega(x,s)|^2 d\sigma(s)\right]^{1/2} \|\psi - \psi_n\|_{L^2(\partial D)} \\ &\le \|\Gamma_\omega(x,\cdot)\|_{L^\infty(\partial D)}|\partial D|^{1/2}\|\psi - \psi_n\|_{L^2(\partial D)}. \end{aligned}$$

Then, we have

$$v(x,\omega) - V_y(x,\omega) = \mathcal{S}_D^{\omega}[\psi_n](x) + O(\varepsilon^{n+2}(|\ln\omega| + \omega^{n+1})). \tag{4.12}$$

For each multi-index α, define $(\phi_\alpha, \psi_\alpha)$ to be the unique solution to

$$\begin{cases} \mathcal{S}_B^{\varepsilon\omega}[\phi_\alpha](\tilde{x}) - \mathcal{S}_B^{\frac{\varepsilon\omega}{\sqrt{k}}}[\psi_\alpha](\tilde{x}) = \tilde{x}^\alpha, \\ k\dfrac{\partial \mathcal{S}_B^{\varepsilon\omega}[\phi_\alpha]}{\partial\nu}\Big|_-(\tilde{x}) - \dfrac{\partial \mathcal{S}_B^{\frac{\varepsilon\omega}{\sqrt{k}}}[\psi_\alpha]}{\partial\nu}\Big|_+(\tilde{x}) = \dfrac{\partial \tilde{x}^\alpha}{\partial\nu}, \end{cases} \qquad \tilde{x} \in \partial B, \tag{4.13}$$

where $\tilde{x} = \varepsilon^{-1}(x - z)$, $x \in \partial D$. The following proposition has been proved in [20].

Proposition 4.4.1 *We claim that*

$$\begin{aligned} \phi_n(x) &= \sum_{|\alpha|=0}^{n+1} \varepsilon^{|\alpha|-1} \frac{\partial_z^\alpha V_y(z,\omega)}{\alpha!} \phi_\alpha(\varepsilon^{-1}(x-z)), \\ \psi_n(x) &= \sum_{|\alpha|=0}^{n+1} \varepsilon^{|\alpha|-1} \frac{\partial_z^\alpha V_y(z,\omega)}{\alpha!} \psi_\alpha(\varepsilon^{-1}(x-z)), \end{aligned} \tag{4.14}$$

for $x \in \partial D$ and (ϕ_n, ψ_n) defined as in (4.11).

Expansion (4.12) together with formula (4.14) yields:

$$v_y(x,\omega) - V_y(x,\omega) = \sum_{|\alpha|=0}^{n+1} \varepsilon^{|\alpha|-1} \frac{\partial_z^\alpha V_y(z,\omega)}{\alpha!} \mathcal{S}_D^{\omega}[\psi_\alpha(\varepsilon^{-1}(\cdot - z))](x) + O(\varepsilon^{n+2}(|\ln\omega| + \omega^{n+1})),$$

for $x \in \mathbb{R}^2 \setminus \overline{D}$ and $x \neq y$. Note that

$$\mathcal{S}_D^{\omega}[\psi_\alpha(\varepsilon^{-1}(\cdot - z))](x) = \int_{\partial D} \Gamma_\omega(x,s)\psi_\alpha(\varepsilon^{-1}(s-z))\, d\sigma(s) = \varepsilon \int_{\partial B} \Gamma_\omega(x, \varepsilon\tilde{s}+z)\psi_\alpha(\tilde{s})\, d\sigma(\tilde{s}).$$

By a straightforward calculation, we get $\|\Gamma_\omega(x,\cdot)\|_{C^{n+2}(\overline{D})} \leq C(1+\omega^{n+3/2})$, where C does not depend on ω. Therefore, for sufficiently small ε, we have

$$\Gamma_\omega(x, \varepsilon\tilde{s} + z) = \sum_{|\beta|=0}^{n+1} \frac{\varepsilon^{|\beta|}}{\beta!} \partial_z^\beta \Gamma_\omega(x,z)\tilde{s}^\beta + O(\varepsilon^{n+1}(1+\omega^{n+3/2})).$$

Finally, we get

$$\mathcal{S}_D^{\omega}[\psi_\alpha(\varepsilon^{-1}(\cdot - z))](x) = \sum_{|\beta|=0}^{n+1} \frac{\varepsilon^{|\beta|+1}}{\beta!} \partial_z^\beta \Gamma_\omega(x,z) \int_{\partial B} \tilde{s}^\beta \psi_\alpha(\tilde{s})\, d\sigma(\tilde{s}) + O(\varepsilon^{n+2}(1+\omega^{n+3/2})).$$

For multi-indices α and β in $\mathbb{N}^2$, the frequency dependent polarization tensors (FDPTs) $\widehat{W}_{\alpha\beta} := \widehat{W}_{\alpha\beta}(B, \varepsilon\omega, \frac{\varepsilon\omega}{\sqrt{k}})$ are defined as [23, 21]

$$\widehat{W}_{\alpha\beta} := \int_{\partial B} \tilde{s}^\beta \psi_\alpha(\tilde{s})\, d\sigma(\tilde{s}). \tag{4.15}$$

We obtain the following theorem.

Theorem 4.4.2 *Suppose that ω^2 is not a Dirichlet eigenvalue for $-\Delta$ on D and $\omega \in (0, \varepsilon^{-\gamma})$, with $0 < \gamma < 1$. The following asymptotic expansion holds:*

$$v_y(x,\omega) - V_y(x,\omega) = \sum_{|\beta|=0}^{n+1} \sum_{|\alpha|=0}^{n-|\beta|+1} \frac{\varepsilon^{|\alpha|+|\beta|}}{\alpha!\,\beta!} \partial_z^\alpha V_y(z,\omega) \partial_z^\beta \Gamma_\omega(x,z) \widehat{W}_{\alpha\beta} + O(\varepsilon^{n+2}(|\ln\omega| + \omega^{n+1})), \tag{4.16}$$

for $x \in \mathbb{R}^2 \setminus \overline{D}$.

Remark 4.4.3 *The following proposition from [21] shows the limiting behavior of $\widehat{W}_{\alpha\beta}$ as $\varepsilon \to 0$ and makes the connection between the FDPTs and the generalized polarization tensors (GPTs) $M_{\alpha\beta}$ [24, 23] explicit.*

Proposition 4.4.4 *If $|\alpha| \geq 1$ and $|\beta| \geq 1$, the harmonic sum of $\widehat{W}_{\alpha\beta}$ has the following asymptotic behavior:*

$$\sum_\alpha a_\alpha \widehat{W}_{\alpha\beta} \to \sum_\alpha a_\alpha M_{\alpha\beta} \qquad \text{as } \varepsilon \to 0.$$

4.5. Time-domain asymptotic expansion

In this section, we abandon the frequency-domain to inspect our problem in the time-domain. We define the emitted wave generated at $y \in \mathbb{R}^2 \setminus \overline{D}$ as

$$U_y(x,t) := \frac{H(t - |x-y|)}{2\pi\sqrt{t^2 - |x-y|^2}},$$

where H is the Heaviside function at 0 [69]. In particular, U_y satisfies the wave equation

$$\begin{cases} (\partial_t^2 - \Delta) U_y(x,t) = \delta_{x=y}\delta_{t=0}, & (x,t) \in \mathbb{R}^2 \times \mathbb{R}, \\ U_y(x,t) = 0 & \text{for } x \in \mathbb{R}^2 \text{ and } t \ll 0. \end{cases}$$

In the presence of a small acoustic inclusion D of contrast k (as described in Section 4.2), the perturbed wave $u_y = u_y(x,t)$, is the solution to

$$\begin{cases} \partial_t^2 u_y - \nabla \cdot (\chi(\mathbb{R}^2 \setminus \overline{D}) + k\chi(D)) \nabla u_y = \delta_{x=y}\delta_{t=0} & \text{in } \mathbb{R}^2 \times (0,\infty), \\ u_y(x,t) = 0 & \text{for } x \in \mathbb{R}^2 \text{ and } t \ll 0. \end{cases}$$

For $\rho > 0$, we define the operator P_ρ acting on tempered distributions by

$$P_\rho[\psi](t) = \int_{|\omega| \leq \rho} e^{-i\omega t} \widehat{\psi}(\omega)\, d\omega, \tag{4.17}$$

where $\widehat{\psi}$ is the Fourier transform of ψ. The operator P_ρ truncates the high-frequency components of ψ [12, 41]. Note that

$$P_\rho[U_y](x,t) = \int_{|\omega|\le\rho} e^{-i\omega t}\left(\int_{\mathbb{R}} e^{i\omega t}U_y(x,t)\,dt\right)d\omega = \int_{|\omega|\le\rho} e^{-i\omega t}\frac{i}{4}H_0^{(1)}(\omega|x-y|)\,d\omega,$$

and satisfies

$$(\partial_t^2-\Delta)P_\rho[U_y](x,t) = \delta_{x=y}\psi_\rho(t) \quad \text{in } \mathbb{R}^2\times\mathbb{R},$$

where

$$\psi_\rho(t) := \frac{2\sin\rho t}{t} = \int_{|\omega|\le\rho} e^{-i\omega t}\,d\omega.$$

From Theorem 4.4.2, we have

$$\int_{|\omega|\le\rho} e^{-i\omega t}(v_y(x,\omega)-V_y(x,\omega))\,d\omega = \sum_{|\beta|=0}^{n+1}\sum_{|\alpha|=0}^{n-|\beta|+1}\frac{\varepsilon^{|\alpha|+|\beta|}}{\alpha!\,\beta!}\int_{|\omega|\le\rho} e^{-i\omega t}\partial_z^\alpha V_y(z,\omega)\partial_z^\beta\Gamma_\omega(x,z)\widehat{W}_{\alpha\beta}\,d\omega + \int_{|\omega|\le\rho} e^{-i\omega t}R(x,\omega)\,d\omega,$$

where $R(x,\omega)$ denotes the remainder in (4.16). Suppose that $\rho = O(\varepsilon^{-\gamma})$ for some $\gamma<1$. Then

$$\int_{|\omega|\le\rho} e^{-i\omega t}R(x,\omega)\,d\omega = O\left(\varepsilon^{(n+2)(1-\gamma)}\right).$$

Notice that the following identity holds

$$\int_{|\omega|\le\rho} e^{-i\omega t}\partial_z^\alpha V_y(z,\omega)\partial_z^\beta\Gamma_\omega(x,z)\widehat{W}_{\alpha\beta}\,d\omega$$

$$= \int_{\mathbb{R}^2}\partial_z^\alpha P_\rho[U_y](z,t-\tau-\tau')\partial_z^\beta P_\rho[U_z](x,\tau)\left(\int_{|\omega|\le\rho} e^{-i\omega\tau'}\widehat{W}_{\alpha\beta}(\omega)d\omega\right)d\tau\,d\tau'.$$

This suggests the following definition.

Definition 4.5.1 *For $\rho<1/\varepsilon$ and multi-indices α and β, the two-dimensional truncated time-dependent polarization tensors (hereinafter, TDPTs), $P_\rho[W_{\alpha\beta}]$, are defined as:*

$$P_\rho[W_{\alpha\beta}](D,k,t) := \int_{|\omega|\le\rho} e^{-i\omega t}\widehat{W}_{\alpha\beta}(\omega)\,d\omega, \tag{4.18}$$

where $\widehat{W}_{\alpha\beta}$ are the two-dimensional FDPTs.

Remark 4.5.2 *The condition on the truncating threshold ρ in Definition 4.5.1, i.e., $\rho < 1/\varepsilon$, boils down to considering only the frequencies ω for which the FDPTs $\widehat{W}_{\alpha\beta}(\omega)$ are well-defined in the integral transform P_ρ.*

Remark 4.5.3 *We warn the reader that the symbol used in Definition 4.5.1 for denoting the TDPTs, i.e., $P_\rho[W_{\alpha\beta}](D,k,t)$, is an abuse of notation, since no $W_{\alpha\beta}$ has been defined; see Remark 4.5.2. However, we preferred to keep this notation to remain consistent with the definition of P_ρ given in [12, 41].*

Thus, we have proved the following theorem.

Theorem 4.5.4 *For $0 < \gamma < 1$, the following asymptotic expansion holds:*

$$\begin{aligned} &P_\rho[u_y](x,t) = P_\rho[U_y](x,t) \\ &+ \sum_{|\beta|=0}^{n+1} \sum_{|\alpha|=0}^{n-|\beta|+1} \frac{\varepsilon^{|\alpha|+|\beta|}}{\alpha!\,\beta!} \int_{\mathbb{R}} \partial_z^\beta P_\rho[U_z](x,\tau) \left(\int_{\mathbb{R}} \partial_z^\alpha P_\rho[U_y](z, t-\tau-\tau') P_\rho[W_{\alpha\beta}](\tau')\, d\tau' \right) d\tau \\ &+ O\left(\varepsilon^{(n+2)(1-\gamma)}\right), \end{aligned} \tag{4.19}$$

where $x \in \mathbb{R}^2 \setminus \overline{D}$, $D = \varepsilon B + z$, $|B| = 1$, $P_\rho[W_{\alpha\beta}]$ are the TDPTs defined in Definition 4.5.1 and $\rho = O(\varepsilon^{-\gamma})$.

In the end, Theorem 4.5.4 shows that the scattered wave can be written as a truncated expansion having the TDPTs as building blocks. Since these tensors are the Fourier transformed FDPTs, the transient expansion (4.19) provides a proper interpretation of the multi-frequency problem, which can then be naturally tackled in the temporal domain.

Moreover from Proposition 4.4.4, one can immediately show the limiting behavior of $P_\rho[W_{\alpha\beta}]$ as $\varepsilon \to 0$ and make the connection between the TDPTs and the GPTs explicit.

Proposition 4.5.5 *If $|\alpha| \geq 1$ and $|\beta| \geq 1$, the harmonic sum of $P_\rho[W_{\alpha\beta}]$ has the following asymptotic behavior:*

$$\sum_\alpha a_\alpha P_\rho[W_{\alpha\beta}] \to \frac{2\sin(\rho t)}{t} \sum_\alpha a_\alpha M_{\alpha\beta} \qquad \text{as } \varepsilon \to 0.$$

By following the proofs in [15], it is easy to derive translation, rotation, and scaling properties for the TDPTs similar to those enjoyed by the GPTs.

Proposition 4.5.6 *For translation $T = (T_1, T_2)$, angle θ with respect to the origin, and positive constant s, let*

$$D_T := \{y + T \,:\, y \in D\}, \qquad D_\theta := \{y_\theta := R(\theta)y \,:\, y \in D\}, \qquad sD := \{sy \,:\, y \in D\}.$$

For multi-indices α, β, γ and η in $\mathbb{N}^2$, let the coefficients $c^T_{\beta\eta}$, $c^T_{\alpha\gamma}$, $r^\theta_{\beta\eta}$, and $r^\theta_{\alpha\gamma}$ be such that

$$(x-T)^\alpha = \sum_{|\gamma|\le|\alpha|} c^T_{\alpha\gamma} x^\gamma, \qquad (x_{-\theta})^\alpha = \sum_{|\gamma|=|\alpha|} r^\theta_{\alpha\gamma} x^\gamma.$$

We have the following relations:

- $P_\rho[W_{\alpha\beta}](D,k,t) = \sum_{\substack{|\eta|\le|\beta|\\|\gamma|\le|\alpha|}} c^T_{\beta\eta} c^T_{\alpha\gamma} P_\rho[W_{\eta\gamma}](D_T,k,t)$;
- $P_\rho[W_{\alpha\beta}](D,k,t) = \sum_{\substack{|\eta|=|\beta|\\|\gamma|=|\alpha|}} r^\theta_{\beta\eta} r^\theta_{\alpha\gamma} P_\rho[W_{\eta\gamma}](D_\theta,k,t)$;
- $P_\rho[W_{\alpha\beta}](D,k,t) = \frac{1}{s^{|\alpha|+|\beta|-1}} P_{s^{-1}\rho}[W_{\alpha\beta}](sD,k,st)$.

4.6. Reconstruction methods

It is already known that the high-order generalized polarization tensors (GPTs) [24, 16] and the FDPTs [23] of an inclusion contain a mixture of geometric information and material parameters. In this section we aim at showing that the same holds for the TDPTs of an acoustic inclusion (4.18) by extending some of the existing methods that has been established for GPTs and FDPTs.

Firstly, formulas for determining the size, the contrast and the equivalent ellipse of an inclusion are provided in terms of $P_\rho[W_{\alpha\beta}](t)$. Secondly, the optimal control approach of [24, 16, 23] for recovering shape details of an inclusion is also adapted in order to perform with the TDPTs. Finally, a procedure for the reconstruction of the TDPTs is presented.

In what follows, without loss of generality, the location of the inclusion is supposed to be known. As a matter of fact, the location can be priorly estimated by using, for instance, a MUSIC-type algorithm; see [17].

4.6.1. Size, contrast and equivalent ellipse

We now extend the well-known procedure to obtain the equivalent ellipse representing the shape of the inclusion for $P_\rho[\mathcal{W}_{(1)}](t)$, where $\widehat{\mathcal{W}}_{(1)}$ is the matrix given by

$$\widehat{\mathcal{W}}_{(1)} := (\widehat{\mathcal{W}}_{\alpha\beta})_{|\alpha|=|\beta|=1} = \varepsilon^2 (\widehat{W}_{\alpha\beta})_{|\alpha|=|\beta|=1}.$$

Since we have

$$P_\rho[\mathcal{W}_{(1)}](D,k,t) \to \frac{2\sin(\rho t)}{t} M(D,k) \quad \text{as } \varepsilon \to 0,$$

where $M(D,k) = (M_{\alpha\beta})_{|\alpha|=|\beta|=1}$ is the polarization tensor (PT), the same procedure of [23] applies by using $P_\rho[\mathcal{W}_{(1)}](t)$ instead of $\widehat{\mathcal{W}}_{(1)}$.

Let $\mathcal{E}$ be the equivalent ellipse associated to the shape D, and let θ be its rotation angle. Then the size $|D|$ and the contrast k of the inclusion can be estimated as follows. We have

$$|D| \approx \frac{1}{\int_{|\omega|\leq\rho} e^{-i\omega t}\omega^2 d\omega} P_\rho[W_{(0,0),(0,0)}](t),$$

$$k \approx \frac{|D|(P_\rho[\mathcal{W}'_{11}] + P_\rho[\mathcal{W}'_{22}]) + (t/(2\sin(\rho t)))P_\rho[\mathcal{W}'_{22}]P_\rho[\mathcal{W}'_{11}]}{(t/(2\sin(\rho t)))P_\rho[\mathcal{W}'_{22}]P_\rho[\mathcal{W}'_{11}] - |D|(P_\rho[\mathcal{W}'_{22}] + P_\rho[\mathcal{W}'_{11}])},$$

where

$$\widehat{\mathcal{W}'}_{(1)} = R(-\theta)\widehat{\mathcal{W}}_{(1)}R(-\theta)^T,$$

with $R(-\theta)$ being the rotation by $-\theta$.

Therefore, from the TDPTs $P_\rho[W_{\alpha\beta}](t)$ we are able to recover an approximation of the volume of the inclusion, separating the information on the material property from the geometric features.

4.6.2. Fine shape details

So far, we reconstructed the contrast k, the size $|D|$ and the equivalent ellipse $\mathcal{E}$. We now reconstruct fine details of the shape of the inclusion using the new concept of high-order TDPTs.

Assuming the inclusion to be a small deformation of the reconstructed equivalent ellipse, we can recover the fine details of its shape by (recursively) minimizing over D the time-dependent discrepancy functional defined by:

$$J^{(K)}(D)(t) := \sum_{1\leq|\alpha|+|\beta|\leq K} \left| \sum_{\alpha,\beta} a_\alpha b_\beta P_\rho[W_{\alpha\beta}](D,t) - \sum_{\alpha,\beta} a_\alpha b_\beta P_\rho[W_{\alpha\beta}]^{\text{meas}} \right|^2, \tag{4.20}$$

where the coefficients a_α, b_β are chosen such that $\sum_\alpha a_\alpha x^\alpha$ and $\sum_\beta b_\beta x^\beta$ are harmonic polynomials and hence coincide with cos and sin functions on the unit circle.

We introduce the operator $\mathcal{K}_D$ given by

$$\mathcal{K}_D[\phi](x) = \frac{1}{2\pi}\int_{\partial D} \frac{\langle y-x, \nu_y\rangle}{|x-y|^2}\phi(y)\, d\sigma(y), \quad \text{for } \phi \in L^2(\partial D).$$

It is well known that the L^2-adjoint of $\mathcal{K}_D$ is

$$\mathcal{K}_D^*[\phi](x) = \frac{1}{2\pi}\int_{\partial D} \frac{\langle x-y, \nu_x\rangle}{|x-y|^2}\phi(y)\, d\sigma(y), \quad \text{for } \phi \in L^2(\partial D).$$

Notice that the ones above consist in a particular case of Lemma 4.1.1 for $\omega = 0$. Recall that, for η much smaller than ε,

$$\sum_{\alpha,\beta} a_\alpha b_\beta M_{\alpha\beta}(D_\eta, k) - \sum_{\alpha,\beta} a_\alpha b_\beta M_{\alpha\beta}(D,k) \approx \eta \int_{\partial D} h(x)\widehat{\phi}_{HF}(x) d\sigma(x),$$

where

$$\widehat{\phi}_{HF} = (k-1)\left[\left.\frac{\partial v}{\partial \nu}\right|_{-}\left.\frac{\partial u}{\partial \nu}\right|_{-} + \frac{1}{k}\left.\frac{\partial u}{\partial T}\right|_{-}\left.\frac{\partial v}{\partial T}\right|_{-}\right],$$

and

$$u = H(x) + \mathcal{S}_D\left[\left(\frac{k+1}{2(k-1)}\mathcal{I} - \mathcal{K}_D^*\right)^{-1}\left[\frac{\partial H}{\partial \nu}\right]\right](x),$$

$$v = F(x) + \mathcal{D}_D\left[\left(\frac{k+1}{2(k-1)}\mathcal{I} - \mathcal{K}_D\right)^{-1}[F]\right](x),$$

where $H = \sum_\alpha a_\alpha x^\alpha$ and $F = \sum_\beta b_\beta x^\beta$ are defined as above; see [24, 23]. From Proposition 4.5.5 we get

$$\sum_{\alpha,\beta} a_\alpha b_\beta P_\rho[W_{\alpha\beta}](D,k) \to \frac{2\sin(\rho t)}{t}\sum_{\alpha,\beta} a_\alpha b_\beta M_{\alpha\beta}(D,k) \quad \text{as } \varepsilon \to 0,$$

which yields the following approximation formula:

$$\sum_{\alpha,\beta} a_\alpha b_\beta P_\rho[W_{\alpha\beta}](D_\eta,t) - \sum_{\alpha,\beta} a_\alpha b_\beta P_\rho[W_{\alpha\beta}](D,t) \approx \eta \int_{\partial D_{\text{given}}} h(x) P_\rho[\phi_{HF}](x,t)\, d\sigma(x). \tag{4.21}$$

Note that

$$P_\rho[\phi_{HF}](x,t) = \frac{2\sin(\rho t)}{t}\widehat{\phi}_{HF}(x).$$

Therefore, we modify the initial shape D^{init} to obtain D^{mod} by the gradient descent method

$$\partial D^{\text{mod}} = \partial D^{\text{init}} - \left(\frac{J^{(n)}[D^{\text{init}}]}{\sum_j (\langle d_S J^{(n)}[D^{\text{init}}], \psi_j\rangle)^2}\sum_j \langle d_S J^{(n)}[D^{\text{init}}], \psi_j\rangle \psi_j\right)\nu,$$

where ν is the outward unit normal to D^{init} and $\{\psi_j\}$ is a basis of $L^2(\partial D^{\text{init}})$. The shape derivative of $J^{(n)}[D]$ follows immediately from the approximation formula (4.21) and is given by

$$\begin{aligned}&\langle d_S J^{(n)}[D], h\rangle_{L^2(\partial D)}\\ &= \sum_{1\le|\alpha|+|\beta|\le K}\left(\sum_{\alpha,\beta} a_\alpha b_\beta P_\rho[W_{\alpha\beta}](D,t) - \sum_{\alpha,\beta} a_\alpha b_\beta P_\rho[W_{\alpha\beta}](B,t)\right)\langle P_\rho[\phi_{HF}], h\rangle_{L^2(\partial D)}.\end{aligned}$$

As in [24, 23], we can make the optimization procedure recursively by increasing K to refine the reconstruction of the shape details of the inclusion. At each step, the initial guess for the shape is the result of the previous one. The equivalent ellipse in Section 7.2 provides a good initial guess to begin with.

4.6.3. Reconstruction of the TDPTs from multi-frequency MSR measurements

We begin by recalling how to reconstruct the FDPTs from multi-static measurements.

Let $D = \varepsilon B + z$ be a small acoustic two-dimensional inclusion of characteristic size ε, and contrast k. Let us consider two arrays: an array of M transmitters $\{y_1, \dots, y_M\}$ and another of N receivers $\{x_1, \dots, x_N\}$, both distributed around the inclusion D. For a given frequency $\omega \in [-\rho, \rho]$, let $\mathcal{A}_\omega$ be the corresponding $N \times M$ Multi-Static Response (MSR) matrix. Precisely, the (i,j)-th entry of $\mathcal{A}_\omega$ is given by

$$(\mathcal{A}_\omega)_{i,j} = v_{y_j}(x_i, \omega) - V_{y_j}(x_i, \omega), \quad i \in \{1, \dots, N\},\ j \in \{1, \dots, M\}, \tag{4.22}$$

that is, the scattered field recorded at the receiver x_i, due to the transmitter y_j.

As usual, in order to model the error in the measurements, additive Gaussian white noise $\mathcal{X}_{\text{noise}}$ is used to contaminate $\mathcal{A}$. We suppose that $\mathcal{X}_{\text{noise}} = \sigma_{\text{noise}}\mathcal{X}_0$, where σ_{noise} and $\mathcal{X}_0$ is an $N \times M$ complex random matrix with independent and identically distributed $\mathcal{N}(0,1)$ entries. Hence, the entries of $\mathcal{X}_{\text{noise}}$ are independent complex Gaussian random variables with mean zero and variance σ^2_{noise}.

In view of formula (4.16), each entry of the MSR matrix admits the following expansion

$$(\mathcal{A}_\omega)_{i,j} = \mathcal{G}_\omega(x_i, z)\widehat{\mathcal{W}}(\omega)\mathcal{G}_\omega(y_j, z)^T + O(\varepsilon^{n+2}(|\ln\omega| + \omega^{n+1})),$$

where

$$\mathcal{G}_\omega(y, z) = \left(\frac{1}{\alpha!}\partial_z^\alpha \Gamma_\omega(y, z)\right)_{|\alpha| \le n}$$

is a row vector, and

$$\widehat{\mathcal{W}} = (\widehat{\mathcal{W}}_{\alpha\beta})_{|\alpha|+|\beta| \le n} = \left(\varepsilon^{|\alpha|+|\beta|}\widehat{W}_{\alpha\beta}\right)_{|\alpha|+|\beta| \le n}$$

is the matrix containing the FDPTs, as in [23]. Then, the tensor $\widehat{\mathcal{W}}$ can be reconstructed from the measurements $\mathcal{A}_\omega$ as the least-squares solution to the following problem

$$\widehat{\mathcal{W}}(\omega)^{\text{meas}} \leftarrow \arg\min_{\mathcal{W}} \|\mathcal{G}_\omega(:, z)\widehat{\mathcal{W}}(\omega)\mathcal{G}_\omega(:, z)^T - \mathcal{A}_\omega\|_F, \tag{4.23}$$

where $\|\cdot\|_F$ denotes the Frobenius norm of a matrix; see [23], and $\mathcal{G}_\omega(:, z)$ is a matrix obtained by vertically concatenating the row vectors $\mathcal{G}_\omega(x_i, z)$ (resp. $\mathcal{G}_\omega(y_j, z)$) for all the receivers x_i (resp. transmitters y_j).

Now, by using the reconstructed FDPTs at multiple frequencies in a discrete subset of the interval $[-\rho, \rho]$ we can get an approximation for the TDPTs (4.18). More precisely, let the set of sampled frequencies S_L be a uniform discretization of the interval $[-\rho, \rho]$, i.e.,

$$-\rho = \omega_{-L} < \omega_{-L+1} < \cdots < \omega_{-1} < 0 < \omega_1 < \cdots < \omega_{L-1} < \omega_L = \rho,$$

with $\omega_{l+1} - \omega_l = \rho/L$ for every $|l| \leq L$. Then the estimator built on this sampling set of frequencies is obtained by applying the discrete Fourier transform (DFT)

$$P_\rho[\mathcal{W}_{\alpha\beta}](t)^{\text{meas}} := \frac{\rho}{L} \sum_{l=-L}^{L} e^{-i\omega_l t} \widehat{\mathcal{W}}_{\alpha\beta}(\omega_l)^{\text{meas}} . \tag{4.24}$$

Such estimator is unbiased, with variance

$$Var(P_\rho[\mathcal{W}_{\alpha\beta}]^{\text{meas}}) = \frac{\rho^2}{L^2} \sum_{l=-L}^{L} Var(\widehat{\mathcal{W}}_{\alpha\beta}(\omega_l)^{\text{meas}}) . \tag{4.25}$$

Since the remainder stated in (4.16) is singular at $\omega = 0$, caution is needed when dealing with small frequencies. In order to get the asymptotic behavior of this dispersion term (4.25) as $L \to +\infty$ we should slightly modify the choice of the range of frequencies by casting a neighborhood of $\omega = 0$ away. In particular for some small $\rho_0 > 0$ we require that $S_L \cap [-\rho_0, \rho_0] = \varnothing$, S_L being uniformly distributed in $[-\rho, -\rho_0]$ and $[\rho_0, \rho]$, separately. Hence $Var(\widehat{\mathcal{W}}_{\alpha\beta}(\omega_l)^{\text{meas}}) \leq C(\rho_0)$ for all $\omega \in S_L$. Then it is readily seen that $Var(P_\rho[\mathcal{W}_{\alpha\beta}]^{\text{meas}}) \to 0$ as $L \to +\infty$.

Note that this reconstruction presented here is indirect in the sense that we don't extract the TDPTs directly from the temporal data. Instead, the estimation is done by aggregating the results of multiple reconstructions in the frequency-domain.

4.7. Numerical illustrations

In this section, we present some numerical simulations to corroborate the theoretical results of this chapter. The simulations aim at showing that the new concept of TDPT can be successfully employed for imaging a small acoustic inclusion.

In what follows, all the experiments are carried out in the two-dimensional case. First, we perform an analysis of the computational accuracy of $P_\rho[\mathcal{W}]^{\text{meas}}$, which is reconstructed from MSR measurements using the method proposed in Section 4.6.3. Then we test the optimization procedure in Section 4.6.2 to restore the fine shape details of the inclusion.

4.7.1. Reconstruction of the TDPTs

We present computational results regarding the reconstruction of TPDTs from MSR measurements by solving (4.23). The comparison between $P_\rho[\mathcal{W}]^{\text{meas}}$, obtained from measured $\widehat{\mathcal{W}}$, with $P_\rho[\mathcal{W}]$, numerically computed by solving (4.13) and computing (4.18). For the latter, boundary elements techniques are used in the approximate evaluation of $\widehat{\mathcal{W}}$, as in [23].

Let D_1 and D_2 be two small acoustic inclusions of different shapes and same characteristic size $\varepsilon = 0.05$ and contrast $k = 3$, centered at $z_1 = [0.3, -0.1]$ and $z_2 = [0, 0.25]$, as shown in Figure 4.1.

We consider coincident arrays of transmitters and receivers to acquire the multi-static data (4.22). In particular, circular and square configurations are tested in the reconstruction of $\widehat{\mathcal{W}}$ for D_1 (Figure 4.1a) and D_2 (Figure 4.1b), respectively.

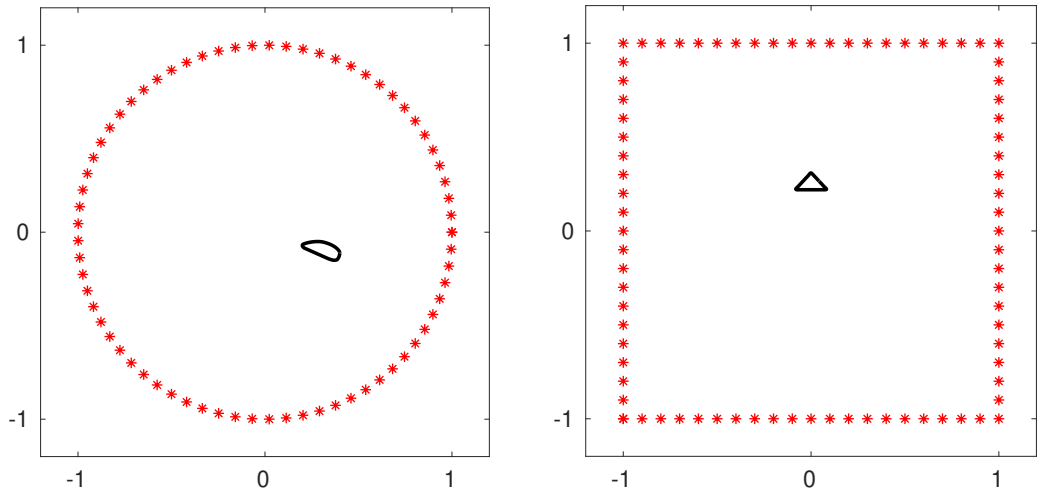

(a) $N_1 = 70$ transmitters/receivers on the unit circle, surrounding the inclusion $D_1 = \varepsilon B_1 + z_1$.

(b) $N_2 = 80$ transmitters/receivers on the unit square, surrounding the inclusion $D_2 = \varepsilon B_2 + z_2$.

Figure 4.1.: Geometries of the acquisition setting. The black curves correspond to two small inclusions with common size $\varepsilon = 0.05$ and contrast $k = 3$.

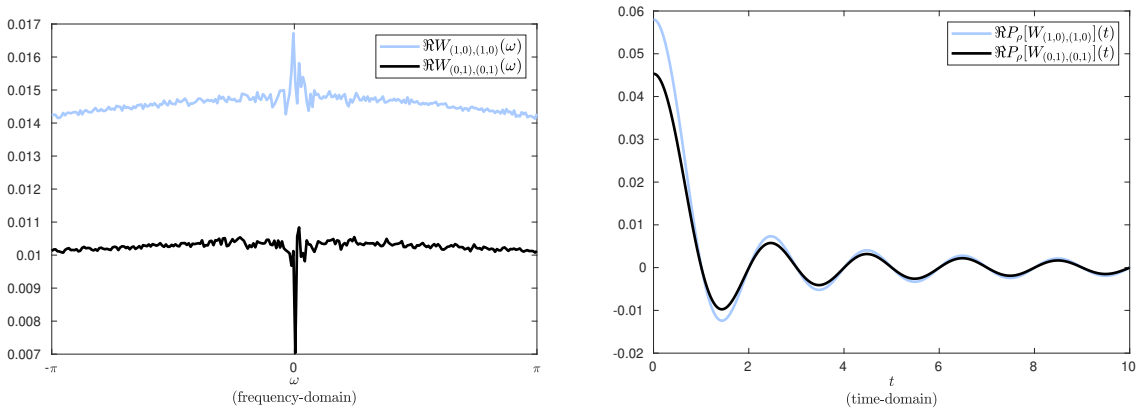

Figure 4.2.: The diagonal elements of the reconstructed first order FDPT, namely $\widehat{\mathcal{W}}_{\alpha\beta}$ with $|\alpha| = |\beta| = 1$ (on the left), and the corresponding first order TDPT, namely $P_\rho[\mathcal{W}_{\alpha\beta}]$, over the interval $[0, 5]$ (on the right). 20% of noise is considered in the reconstruction of the FDPT.

The reconstruction of the first order TDPT of D_1 with 20% of noise is reported in Figure 4.2. A uniform sampling of 2^8 frequencies within $[-\rho, \rho] = [-\pi, \pi]$ is used, and the resulting $P_\rho[\mathcal{W}_{\alpha\beta}]^{\text{meas}}$ is plotted over the interval $[0, 5]$. With this choice of ρ, the condition on the truncating threshold in Definition 4.5.1 is satisfied; see Remark 4.5.2.

An analysis of the error in the noiseless reconstruction is performed. Since the TDPTs are functions, the L^2-norm is adequate. We define the absolute and relative-error as follows:

$$\text{absErr}(T) = \|P_\rho[\mathcal{W}_{\alpha\beta}]^{\text{meas}} - P_\rho[\mathcal{W}_{\alpha\beta}]\|_{L^2(0,T)},$$

$$\text{relErr}(T) = \frac{\|P_\rho[\mathcal{W}_{\alpha\beta}]^{\text{meas}} - P_\rho[\mathcal{W}_{\alpha\beta}]\|_{L^2(0,T)}}{\|P_\rho[\mathcal{W}_{\alpha\beta}]\|_{L^2(0,T)}}.$$

The results are shown in Figure 4.3.

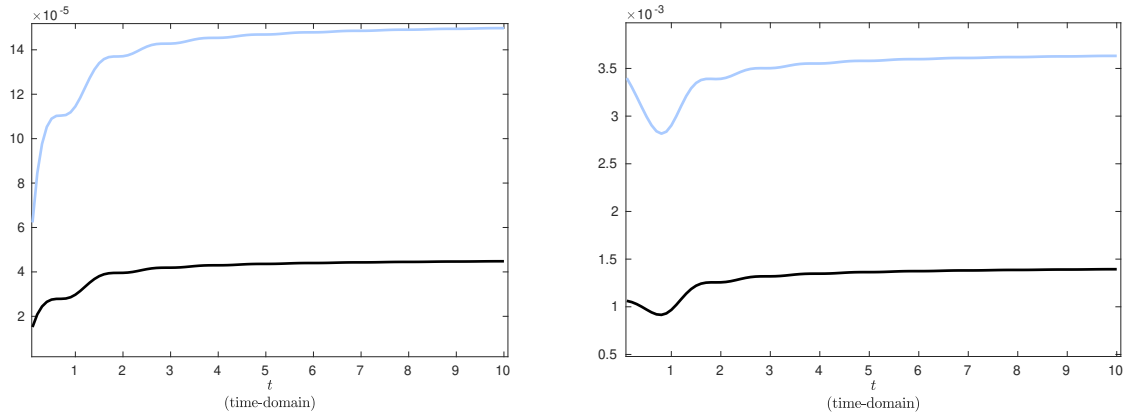

Figure 4.3.: L^2 -absolute (left) and -relative (right) errors in the noiseless reconstruction of $P_\rho[\mathcal{W}_{(1,0),(1,0)}]$ (pale blue) and $P_\rho[\mathcal{W}_{(0,1),(0,1)}]$ (black), assuming the setting shown in Figure 4.1b.

4.7.2. Reconstruction of the fine shape details

In this section, we set k to be the value found by the method proposed in Section 4.6.3, and use the equivalent ellipse as an initial guess for the optimization procedure in Section 4.6.2.

Firstly, to simulate the reconstruction of the fine details of the inclusions D_1 and D_2, we reconstruct the TDPTs up to order $n = 4$ by using measurements coming from the two different acquisition settings as in Figure 4.1. A uniform sampling of 2^6 frequencies within the range $[-\rho, \rho] = [-\pi/8, \pi/8]$ is used to this aim. This is done as described in Section 7.3. After obtaining $P_\rho[\mathcal{W}_{\alpha\beta}]^{\text{meas}}$, we feed them to the optimization algorithm of Section 4.6.2. At each step, the algorithm recursively minimizes the discrepancy function (4.20), yielding a progressive update of the shape. The equivalent ellipse is taken as initial guess.

The results after few iterations with 20% of noise are shown in Figure 4.4. The number of iterations is less than 30, and the stopping criteria we used are those stated in [23]. We can observe that details finer than the equivalent ellipse are well recovered for both the inclusions despite the fact that noisy measurements are used to reconstruct the TDPTs.

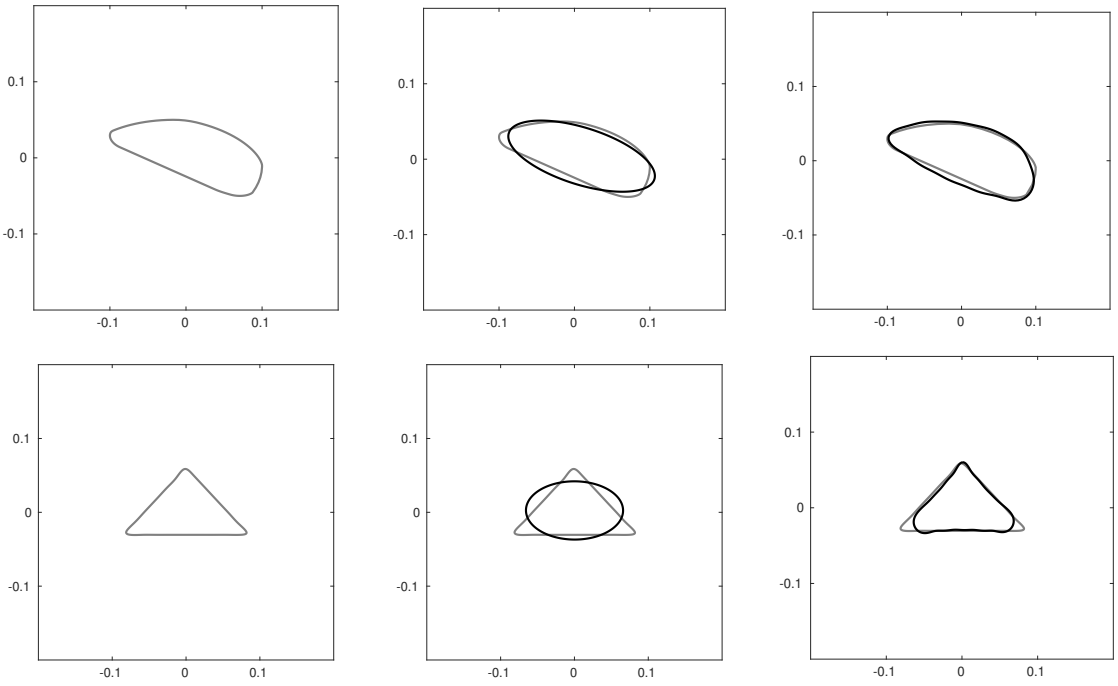

Figure 4.4.: Gray curve is the actual inclusion (left column) whereas the black curve represents the equivalent ellipse (mid column) and the reconstructed shape with 20% of noise after few iterations (right column).

4.8. Concluding remarks

In this chapter, we have presented for the first time the new concept of the TDPTs for the transient problem. These objects are the truncated Fourier transforms of the FDPTs introduced by Ammari et al. in [23]. We have shown that by operating with a range of frequencies, we can recover the high-order TDPTs from the measurements, and this yields a robust reconstruction of the fine shape details of the small acoustic inclusion. From our analysis, we deduce that already-known results involving the reconstruction of the inclusion via MSR measurements at a single frequency, when performed at multiple frequencies, can be naturally interpreted in the time-domain. For future purposes, it is expected that the TDPTs will be relevant to develop promising time-domain techniques for target classification in echolocation by extending the correspondent frequency-domain methods [25, 30] and the electro-sensing case [7, 4, 66]. Moreover, our analysis paves the way for investigating the more general situation of a bat which uses the movement to better map the surrounding environment. This worthwhile extension is of primary importance, being suitable for bio-inspired applications in robotics.

Appendices

A. Appendix

A.1. Generalized polarization tensors and boundary layer potentials

In this appendix, we briefly summarize some fundamental concepts that are essential for understanding the subject in question. For further references see [2, 14, 7, 66].

Let Ω be a simply connected bounded domain. We assume $\Omega \in C^{1,\alpha}$, for some $\alpha > 0$.

Definition A.1.1 *Denote by Γ the fundamental solution of the Laplacian in $\mathbb{R}^2$, i.e.,*

$$\Gamma(x-y) := \frac{1}{2\pi}\log|x-y|, \qquad x, y \in \mathbb{R}^2.$$

Definition A.1.2 *For any $\phi \in L^2(\partial\Omega)$, the single- and double-layer potentials on Ω are given by the following formulas:*

$$\mathcal{S}_\Omega[\phi](x) := \int_{\partial\Omega} \Gamma(x,y)\phi(y)\ d\sigma_y, \qquad x \in \mathbb{R}^2,$$

$$\mathcal{D}_\Omega[\phi](x) := \int_{\partial\Omega} \frac{\partial\Gamma}{\partial\nu_y}(x,y)\phi(y)\ d\sigma_y, \qquad x \in \mathbb{R}^2 \setminus \partial\Omega.$$

Recall that for $\phi \in L^2(\Omega)$, the functions $\mathcal{S}_\Omega$ and $\mathcal{D}_\Omega$ are harmonic functions in $\mathbb{R}^2 \setminus \partial\Omega$.

Definition A.1.3 *The operator $\mathcal{K}_\Omega$ and its L^2-adjoint $\mathcal{K}_\Omega^*$ are given by the following formulas:*

$$\mathcal{K}_\Omega[\phi](x) := \frac{1}{2\pi}\int_{\partial\Omega} \frac{(y-x)\cdot\nu(y)}{|x-y|^2}\phi(y)\ d\sigma_y, \qquad x \in \partial\Omega,$$

$$\mathcal{K}_\Omega^*[\phi](x) := \frac{1}{2\pi}\int_{\partial\Omega} \frac{(x-y)\cdot\nu(x)}{|x-y|^2}\phi(y)\ d\sigma_y, \qquad x \in \partial\Omega$$

where p.v. stands for the Cauchy principal value.

$\mathcal{K}_\Omega^*$ is also known as the Neumann–Poincaré operator.

The behavior of the single- and double-layer potentials across the boundary $\partial\Omega$ is described by the following relations [22]:

$$\mathcal{S}_\Omega[\phi]|_+ = \mathcal{S}_\Omega[\phi]|_-,$$

$$\left.\frac{\partial \mathcal{S}_\Omega[\phi]}{\partial \nu}\right|_\pm = \left(\pm\frac{1}{2}I + \mathcal{K}_\Omega^*\right)\phi,$$
$$\mathcal{D}_\Omega[\phi]|_\pm = \left(\mp\frac{1}{2}I + \mathcal{K}_\Omega\right)\phi,$$
$$\left.\frac{\partial \mathcal{D}_\Omega[\phi]}{\partial \nu}\right|_+ = \left.\frac{\partial \mathcal{D}_\Omega[\phi]}{\partial \nu}\right|_-,$$

We introduce the generalized polarization tensor (GPT).

Definition A.1.4 *Let $\alpha, \beta \in \mathbb{N}^2$ be multi-indices. We define the GPT associated with the domain Ω and the contrast $\lambda \in \left(-\frac{1}{2}, \frac{1}{2}\right)$ by*

$$M_{\alpha\beta}(\lambda, \Omega) := \int_{\partial\Omega} (\lambda I - \mathcal{K}_\Omega^*)^{-1}\left[\frac{\partial y^\alpha}{\partial \nu}\right] y^\beta \; d\sigma_y,$$

where I is the identity operator.

We can also define the contracted generalized polarization tensors (CGPTs) as follows.

Definition A.1.5 *Let $m, n \in \mathbb{N}$. We define the CGPTs by*

$$M_{mn}^{cc} = \sum_{|\alpha|=m} \sum_{|\beta|=n} a_\alpha^m a_\beta^n M_{\alpha\beta},$$
$$M_{mn}^{cs} = \sum_{|\alpha|=m} \sum_{|\beta|=n} a_\alpha^m b_\beta^n M_{\alpha\beta},$$
$$M_{mn}^{sc} = \sum_{|\alpha|=m} \sum_{|\beta|=n} b_\alpha^m a_\beta^n M_{\alpha\beta},$$
$$M_{mn}^{ss} = \sum_{|\alpha|=m} \sum_{|\beta|=n} b_\alpha^m b_\beta^n M_{\alpha\beta},$$

where the real numbers a_α^m and b_β^m are defined by the following relation

$$(x_1 + ix_2)^m = \sum_{|\alpha|=m} a_\alpha^m x^\alpha + i \sum_{|\beta|=m} b_\beta^m x^\beta.$$

A.2. Kronecker products and generalized inverses

Let us denote by $\mathcal{M}_{m,n}$ the space of $m \times n$ matrices.

Definition A.2.1 (vec operator) *Given a matrix $\mathbf{X} = \begin{bmatrix}\mathbf{x}^1 & \mathbf{x}^2 & \dots & \mathbf{x}^m\end{bmatrix} \in \mathcal{M}_{k,m}$, define the vectorization operator $vec(\cdot) : \mathcal{M}_{k,m} \to \mathcal{M}_{km,1}$ as follows:*

$$vec(\mathbf{X}) = \begin{bmatrix}\mathbf{x}^1 \\ \vdots \\ \mathbf{x}^m\end{bmatrix} \in \mathcal{M}_{km,1}. \tag{A.1}$$

Definition A.2.2 (Kronecker product) *Given* $\mathbf{X} = (x_{ij}) \in \mathcal{M}_{m,n}$ *and* $\mathbf{Y} = (y_{ij}) \in \mathcal{M}_{p,q}$, *define*

$$\mathbf{X} \otimes \mathbf{Y} = \begin{bmatrix} x_{11}\mathbf{Y} & x_{12}\mathbf{Y} & \dots & x_{1n}\mathbf{Y} \\ x_{21}\mathbf{Y} & x_{22}\mathbf{Y} & \dots & x_{2n}\mathbf{Y} \\ \vdots & \vdots & \ddots & \vdots \\ x_{m1}\mathbf{Y} & x_{m2}\mathbf{Y} & \dots & x_{mn}\mathbf{Y} \end{bmatrix} \in \mathcal{M}_{mp,nq}. \tag{A.2}$$

For all matrices $\mathbf{A}$, $\mathbf{B}$ and $\mathbf{C}$ such that the product $\mathbf{ABC}$ is well defined we have

$$\mathrm{vec}(\mathbf{ABC}) = (\mathbf{C}^\top \otimes \mathbf{A})\mathrm{vec}(\mathbf{B}). \tag{A.3}$$

We introduce a generalized Kronecker product.

Definition A.2.3 (Generalized Kronecker product [64, 57]) *Given a matrix* $\mathbf{X}$ $(M \times l)$ *and a set of* M *matrices* $\mathbf{Y}$ $(N \times r)$ *we define the matrix* $\mathbf{X} \otimes \{\mathbf{Y}_\ell\}$ $(MN \times lr\ )$ *as*

$$\mathbf{X} \otimes \{\mathbf{Y}_\ell\} := \begin{bmatrix} \mathbf{X}_{1,:} \otimes \mathbf{Y}_1 \\ \vdots \\ \mathbf{X}_{M,:} \otimes \mathbf{Y}_M \end{bmatrix}. \tag{A.4}$$

Notice that in [64] the factors are swapped compared to this definition. The reason is that, unlike us, they considered a *left* Kronecker product.

Definition A.2.4 (Generalized column-wise Kronecker product) *Given a matrix* $\mathbf{X}$ $(M \times l)$ *and a set of* M *matrices* $\mathbf{Y}_\ell$ $(N \times r)$ *we define the matrix* $\mathbf{X} \otimes_C \{\mathbf{Y}_\ell\}$ $(MN \times lr\ )$ *as*

$$\mathbf{X} \otimes_C \{\mathbf{Y}_\ell\} := \begin{bmatrix} \mathbf{X}_{:,1} \otimes \mathbf{Y}_1 & \dots & \mathbf{X}_{:,l} \otimes \mathbf{Y}_M \end{bmatrix}. \tag{A.5}$$

Definition A.2.5 (Moore–Penrose inverse) *The Moore–Penrose inverse of the matrix* $\mathbf{M}$ $(m \times p)$ *is the unique matrix* $\mathbf{G}$ $(p \times m)$ *satisfying the following four* Penrose conditions*:*

1. $\mathbf{MGM} = \mathbf{M}$,
2. $\mathbf{GMG} = \mathbf{G}$,
3. $(\mathbf{MG})^\top = \mathbf{MG}$,
4. $(\mathbf{GM})^\top = \mathbf{GM}$.

A matrix $\mathbf{G}$ satisfying (1) is called a *generalized inverse* or a *g-inverse*.

A matrix $\mathbf{G}$ satisfying (1) and (2) is called a *reflexive g-inverse*.

A matrix $\mathbf{G}$ satisfying (1) and (3) is called a *least-square g-inverse*.

A matrix $\mathbf{G}$ satisfying (1) and (4) is called a *minimum norm g-inverse*.

A.3. Reminder in the asymptotic expansion (1.5)

Let $\varepsilon = \delta/\rho$ be the length-scale. By definition, the truncation error at the receptor $x_r^{(s)}$ is given by

$$\mathbf{E}_{rs} := u^{(s)}(x_r^{(s)}) - H^{(s)}(x_r^{(s)}) - \mathcal{L}^{(s)}(\mathbb{M}^{(K)}).$$

The asymptotic behavior of $\mathbf{E}_{sr}$ in the far-field regime is assessed by the following proposition.

Proposition A.3.1 *For $\delta, \varepsilon \ll 1$ we have the following asymptotic behavior*

$$|\mathbf{E}_{rs}| = O(\varepsilon^{K+2}). \tag{A.6}$$

Proof. Hereinafter, we simplify our notation by fixing the index position s, i.e., $x_r^{(s)} = x_r$, $H^{(s)} = H$, $\mathbf{E}_{rs} = E_r$.

Let us define $H_K(x) = \sum_{|\alpha|=0}^{K} \frac{1}{\alpha!}\partial^\alpha H(z)(x-z)^\alpha$. The truncation error can be expressed as

$$E_r = \int_{\partial D} \Gamma_K(x_r - y)(\lambda I - \mathcal{K}_D^*)^{-1}[\partial_\nu H - \partial_\nu H_K]\, \mathrm{d}s_y + \int_{\partial D} (\Gamma - \Gamma_K)(x_r - y)(\lambda I - \mathcal{K}_D^*)^{-1}[\partial_\nu H]\, \mathrm{d}s_y. \tag{A.7}$$

We want to estimate each term separately.

Denote the first term by

$$E_r^{(1)} := \int_{\partial D} \Gamma_K(y; x_r, z)(\lambda I - \mathcal{K}_D^*)^{-1}\left[\frac{\partial H}{\partial \nu} - \frac{\partial H_K}{\partial \nu}\right](y)\, \mathrm{d}s_y. \tag{A.8}$$

We have

$$\begin{aligned}
\left|E_r^{(1)}\right| &\le \left| \int_{\partial D} \Gamma_K(y; x_r, z)(\lambda I - \mathcal{K}_D^*)^{-1}\left[\frac{\partial H}{\partial \nu} - \frac{\partial H_K}{\partial \nu}\right](y)\, \mathrm{d}s_y \right| \\
&\le \sup_{y \in \partial D} |\Gamma_K(y; x_r, z)| \int_{\partial D} \left| (\lambda I - \mathcal{K}_D^*)^{-1}\left[\frac{\partial H}{\partial \nu} - \frac{\partial H_K}{\partial \nu}\right](y) \right| \mathrm{d}s_y \\
&\le \|\Gamma_K(\cdot; x_r, z)\|_{L^\infty(\partial D)} \left\| (\lambda I - \mathcal{K}_D^*)^{-1}\left[\frac{\partial H}{\partial \nu} - \frac{\partial H_K}{\partial \nu}\right] \right\|_{L^2(\partial D)} |\partial D|^{1/2} \\
&\le C \|\Gamma_K(\cdot; x_r, z)\|_{L^\infty(\partial D)} \left\| \frac{\partial H}{\partial \nu} - \frac{\partial H_K}{\partial \nu} \right\|_{L^2(\partial D)} |\partial D|^{1/2} \\
&\le C' \frac{\delta}{\rho} \left\| \frac{\partial H}{\partial \nu} - \frac{\partial H_K}{\partial \nu} \right\|_{L^2(\partial D)} |\partial D|^{1/2} \\
&\le C' \frac{\delta^2}{\rho} \left\| \frac{\partial H}{\partial \nu} - \frac{\partial H_K}{\partial \nu} \right\|_{L^\infty(\partial D)} |\partial B|.
\end{aligned}$$

Now we estimate the term

$$\left\| \frac{\partial H}{\partial \nu} - \frac{\partial H_K}{\partial \nu} \right\|_{L^\infty(\partial D)}. \tag{A.9}$$

Recall the integral form of the reminder of Taylor's formula:

$$(H - H_K)(y) = \sum_{|\alpha|=K+1} \frac{1}{\alpha!} \int_0^1 (1-t)^K \partial^\alpha H(ty)\, \mathrm{d}t\, y^\alpha,$$

then

$$\left(\frac{\partial H}{\partial \nu} - \frac{\partial H_K}{\partial \nu} \right)(y) = \sum_{|\alpha|=K+1} \frac{1}{\alpha!} \left[\int_0^1 (1-t)^K \partial_\nu \partial^\alpha H(ty)\, \mathrm{d}t\, y^\alpha + \int_0^1 (1-t)^K \partial^\alpha H(ty)\, \mathrm{d}t\, \partial_\nu y^\alpha \right].$$

It is immediate to show that

$$\left| \left(\frac{\partial H}{\partial \nu} - \frac{\partial H_K}{\partial \nu} \right) \Big|_{\partial D} \right| \le C \left(\delta^{K+1} \sum_{|\alpha|=K+1} \frac{1}{\alpha!} \|\nabla \partial^\alpha H\|_{C^0(\overline{D})} + \delta^K \sum_{|\alpha|=K+1} \frac{1}{\alpha!} \|\partial^\alpha H\|_{C^0(\overline{D})} \right).$$

Assume $\rho \ge \operatorname{dist}(\partial\Omega, 0) > 1$, $\delta \ll 1$. By using formulas for the derivatives of H we get

$$\left\| \frac{\partial H}{\partial \nu} - \frac{\partial H_K}{\partial \nu} \right\|_{L^\infty(\partial D)} \le \left(\frac{C_1'}{\rho^{K+3}} + \frac{C_2'}{\rho^{K+2}} \right) \delta^{K+1} + \left(\frac{C_1}{\rho^{K+2}} + \frac{C_2}{\rho^{K+1}} \right) \delta^K, \tag{A.10}$$

hence

$$\left\| \frac{\partial H}{\partial \nu} - \frac{\partial H_K}{\partial \nu} \right\|_{L^\infty(\partial D)} = O\left(\frac{\delta^K}{\rho^{K+1}} \right).$$

Therefore

$$\left| E_r^{(1)} \right| \le C' \frac{\delta}{\rho} \left\| \frac{\partial H}{\partial \nu} - \frac{\partial H_K}{\partial \nu} \right\|_{L^2(\partial D)} |\partial D|^{1/2} \le C'' \frac{\delta^{K+2}}{\rho^{K+2}} = O(\varepsilon^{K+2}).$$

Denote the second term in (A.7) by

$$E_r^{(2)} := \int_{\partial D} (\Gamma - \Gamma_K)(x_r - y)(\lambda I - \mathcal{K}_D^*)^{-1} \left[\frac{\partial H}{\partial \nu} \right](y)\, \mathrm{d}s_y. \tag{A.11}$$

We have

$$\begin{aligned}
\left| E_r^{(2)} \right| &= \left| \int_{\partial D} (\Gamma - \Gamma_K)(x_r - y)(\lambda I - \mathcal{K}_D^*)^{-1} \left[\frac{\partial H_K}{\partial \nu} \right](y)\, \mathrm{d}s_y \right| \\
&\le \|\Gamma(x_r - \cdot) - \Gamma_K(x_r - \cdot)\|_{L^\infty(\partial D)} \int_{\partial D} \left| (\lambda I - \mathcal{K}_D^*)^{-1} \left[\frac{\partial H}{\partial \nu} \right](y) \right| \mathrm{d}s_y \\
&\le \|\Gamma(x_r - \cdot) - \Gamma_K(x_r - \cdot)\|_{L^\infty(\partial D)} \left\| (\lambda I - \mathcal{K}_D^*)^{-1} \left[\frac{\partial H}{\partial \nu} \right] \right\|_{L^2(\partial D)} |\partial D|^{1/2} \\
&\le C \|\Gamma(x_r - \cdot) - \Gamma_K(x_r - \cdot)\|_{L^\infty(\partial D)} \left\| \frac{\partial H}{\partial \nu} \right\|_{L^2(\partial D)} |\partial D|^{1/2} \\
&\le C \|\Gamma(x_r - \cdot) - \Gamma_K(x_r - \cdot)\|_{L^\infty(\partial D)} \left\| \frac{\partial H}{\partial \nu} \right\|_{L^\infty(\partial D)} |\partial D|.
\end{aligned}$$

Since $\|\Gamma(x_r - \cdot) - \Gamma_K(\cdot; x_r, z)\|_{L^\infty(\partial D)} \leq C\left(\frac{\delta}{\rho}\right)^{K+1}$, see [6], and

$$\left\|\frac{\partial H}{\partial \nu}\right\|_{L^\infty(\partial D)} \leq C\rho^{-1}, \tag{A.12}$$

we have

$$\left|E_r^{(2)}\right| = O(\varepsilon^{K+2}).$$

□

A.4. Technical estimates

A.4.1. Uniqueness results

In this section, we show that the matrix of receptors $\mathbf{G}^{(s)}$ is full column rank. We begin by observing that $\mathbf{G}^{(s)}$ is closely related to a special $N_r \times 2K$ Vandermonde matrix of the form

$$\mathbf{V}_K := \begin{bmatrix} \zeta_1 & \overline{\zeta}_1 & \zeta_1^2 & \overline{\zeta}_1^2 & \cdots & \zeta_1^K & \overline{\zeta}_1^K \\ \zeta_2 & \overline{\zeta}_2 & \zeta_2^2 & \overline{\zeta}_2^2 & \cdots & \zeta_2^K & \overline{\zeta}_2^K \\ \vdots & & \vdots & & \ddots & & \vdots \\ \zeta_{N_r} & \overline{\zeta}_{N_r} & \zeta_{N_r}^2 & \overline{\zeta}_{N_r}^2 & \cdots & \zeta_{N_r}^K & \overline{\zeta}_{N_r}^K \end{bmatrix}. \tag{A.13}$$

Matrices of this type are of interest when dealing with univariate polynomial interpolation on complex conjugate points. We introduce the map

$$\mathcal{K} : \mathbb{C} \setminus \{0\} \longrightarrow \mathbb{C} \setminus \{0\}$$

$$\mathcal{K}(z) = \overline{z}^{-1} = \frac{z}{|z|^2}.$$

$\mathcal{K}$ is known in the literature as the Kelvin transform. Then the entries of $\mathbf{V}_K$ (A.13) are defined as follows: for any receptor $z_l \in \partial\Omega$ we set $\zeta_l = \mathcal{K}(z_l) = e^{i\theta_l}/r_l$.

To relate $\mathbf{V}_K$ to $\mathbf{G}^{(s)}$ we introduce two other matrices. By employing the product defined in Definition A.2.3, consider the $2K \times 2K$ diagonal scaling matrix

$$\mathbf{C} := \mathbf{I}_K \otimes \left\{\ell^{-1}\mathbf{I}_2\right\},$$

and, by setting $J = \frac{1}{2}\begin{bmatrix} 1 & -i \\ 1 & i \end{bmatrix}$, define the complex $2K \times 2K$ block diagonal matrix:

$$\mathbf{J} := \mathbf{I}_K \otimes J.$$

It can be easily verified that $\mathbf{G}^{(s)} = -\frac{1}{2\pi}\mathbf{V}_K\mathbf{J}\mathbf{C}$.

Observe that there exists a permutation matrix $\mathbf{P}$ such that $\mathbf{V}_K\mathbf{P} = \begin{bmatrix} \mathbf{W}_K & \overline{\mathbf{W}}_K \end{bmatrix}$.

Lemma A.4.1 *Let $\mathbf{V}_{(1,\dots,2K)}$ be the square submatrix of $\mathbf{V}_K\mathbf{P}$ obtained by considering the first $2K$ rows. Then*

$$det(\mathbf{V}') = \mathrm{Re}(P(\zeta_1,\dots,\zeta_{2K},\overline{\zeta}_1,\dots,\overline{\zeta}_{2K})),$$

where $P \in \mathbb{C}[z_1,\dots,z_{2K},\overline{z}_1,\dots,\overline{z}_{2K}]$. Since $\zeta_l = x_l + iy_l$ and $\overline{\zeta}_l = x_l - iy_l$, it is clear that

$$det(\mathbf{V}') = Q(x_1,y_1,\dots,x_{2K},y_{2K}),$$

where $Q \in \mathbb{R}[x_1,y_1,\dots,x_{2K},y_{2K}]$.

The set $\mathcal{H} = \{Q = 0\}$ is an hyper-surface in the affine space $\mathbb{R}^{4K} \simeq \underbrace{\mathbb{R}^2 \times \cdots \times \mathbb{R}^2}_{2K}$.

Definition A.4.2 *A finite set of points $\mathcal{S} = \{(x_1,y_1),\dots,(x_{2K},y_{2K})\} \subset \mathbb{R}^2$, $\#\mathcal{S} = 2K$, is called a* general configuration *if the point $(x_1,y_1,\dots,x_{2K},y_{2K})$ does not lie on $\mathcal{H}$.*

Proposition A.4.3 *Suppose there are $2K$ receptors z_l such that $\zeta_l = \mathcal{K}(z_l)$ are a general configuration. Then $\mathbf{V}_K$ is of maximal rank.*

Proof. Without loss of generality, let $\zeta_1,\dots,\zeta_{2K}$ be a general configuration. From Lemma A.4.1 it follows that $\det(\mathbf{V}')$ is a real multivariate polynomial, and it does not vanish when evaluated at the points $\zeta_1,\dots,\zeta_{2K}$. □

Remark A.4.4 *By an abuse of definition, a set of points $\{z_l\}_l$ such that $\{\mathcal{K}(z_l)\}_l$ is a general configuration, shall be called a general configuration likewise.*

A.4.2. Moore-Penrose inverse of S

For $\ell \in \mathbb{N}$, let $r_\ell(\gamma)$ be the following rotation matrix:

$$r_\ell(\gamma) := \begin{bmatrix} \cos(\ell\gamma) & \sin(\ell\gamma) \\ -\sin(\ell\gamma) & \cos(\ell\gamma) \end{bmatrix}.$$

If we assume that the body of the fish lies in a thin annulus around the orbit of radius ρ while swimming around the target, then the form of the design matrix can be simplified. In this case, if (1.16) is used, the information on the fish concerning its geometry and its electric field can be separated from the "kinematics". Easy calculations show that

$$\mathbf{G}^{(s)} = \mathbf{G}^{(1)}(\mathbf{I}_K \otimes \{r_1(\ell(s-1)\gamma)\}),$$

$$\mathbf{Z}_{s,:} = \mathbf{Z}_{1,:}(\mathbf{I}_K \otimes \{r_1((1+\ell)(s-1)\gamma)\}),$$

where

$$\mathbf{Z}_{1,:} = \begin{bmatrix} \cos(2\overline{\theta}_1) & \sin(2\overline{\theta}_1) & \cos(3\overline{\theta}_1) & \sin(3\overline{\theta}_1) & \dots & \cos((K+1)\overline{\theta}_1) & \sin((K+1)\overline{\theta}_1) \end{bmatrix}.$$

Moreover, given $\alpha_s = \alpha_0 + (s-1)\gamma$ angle of $\mathbf{p}_s$, we have

$$\mathbf{P}_K^{(s)} = \mathbf{I}_K \otimes \left\{(-1)^{\ell+1} r_1(\alpha_0 + (s-1)\gamma)\right\}.$$

Hereinafter, we assume that the fish moves with its electric organ along on a circular orbit of radius ρ.

Recall that

$$\mathbf{S} = \mathbf{S}_{dip} + \mathbf{S}_{SL}.$$

By using the rotational symmetry of the configuration and the notation hereabove, we rewrite $\mathbf{S}_{dip}$ and $\mathbf{S}_{SL}$ as follows:

$$\begin{aligned}(\mathbf{S}_{dip})_{s,:} &= \mathbf{Z}_{s,:}\mathbf{P}_K^{(s)\top}\mathbf{D}_{2,K+1} \\ &= \mathbf{Z}_{1,:}(\mathbf{I}_K \otimes \{r_1((1+\ell)(s-1)\gamma)\}_\ell)(\mathbf{I}_K \otimes \{(-1)^{\ell+1} r_1(-\alpha_0 - (s-1)\gamma)\}_\ell)\mathbf{D}_{2,K+1} \\ &= \mathbf{Z}_{1,:}(\mathbf{I}_K \otimes \{(-1)^{\ell+1} r_1(-\alpha_0 + \ell(s-1)\gamma)\}_\ell)\mathbf{D}_{2,K+1},\end{aligned}$$

and

$$(\mathbf{S}_{SL})_{s,:} = -\mathbf{u}\mathbf{G}^{(1)}(\mathbf{I}_K \otimes \{r_1(\ell(s-1)\gamma)\}_\ell).$$

Here, $\mathbf{D}_{2,K+1}$ is given as in Section 3.2 by

$$\mathbf{D}_{2,K+1} = \mathbf{I}_K \otimes \{\rho^{-(\ell+1)}\mathbf{I}_2\}_\ell.$$

Finally,

$$\mathbf{S}_{dip} = (\mathbf{I}_M \otimes \mathbf{Z}_{1,:}) \begin{bmatrix} \mathbf{I}_K \otimes \{(-1)^{\ell+1} r_1(-\alpha_0)\}_\ell \\ \vdots \\ \mathbf{I}_K \otimes \{(-1)^{\ell+1} r_1(-\alpha_0 + \ell(M-1)\gamma)\}_\ell \end{bmatrix} \mathbf{D}_{2,K+1},$$

and

$$\mathbf{S}_{SL} = (\mathbf{I}_M \otimes -\mathbf{u}\mathbf{G}^{(1)}) \begin{bmatrix} \mathbf{I}_K \otimes r_1(0) \\ \vdots \\ \mathbf{I}_K \otimes \{r_1(\ell(M-1)\gamma)\}_\ell \end{bmatrix}.$$

Hereinafter, we assume that $\partial^\alpha \mathcal{S}_{\Omega_s}(z)$ is non-zero for each $|\alpha| \le K$. In the far field regime this assumption guarantees that the GPTs can be retrieved up to order K. It will become clear soon that this condition also makes $\mathbf{S}_{SL}$ full column rank, allowing to compute its Moore–Penrose inverse as

$$\mathbf{S}_{SL}^\dagger = (\mathbf{S}_{SL}^\top \mathbf{S}_{SL})^{-1}\mathbf{S}_{SL}^\top.$$

We have the following lemma.

Lemma A.4.5 *For $1 \le k \le 2K$ and $M \gg 1$, we have*

$$\|(\mathbf{S}_{SL}^\dagger)_{k,:}\|_F \lesssim \frac{\lceil k/2 \rceil \rho^{\lceil k/2 \rceil}}{\sqrt{M}}. \tag{A.14}$$

Proof. Let us denote the $1 \times 2K$ row vector $-\mathbf{u}\mathbf{G}^{(1)}$ by $\mathbf{w}$. We need to compute $\mathbf{S}_{SL}^{\top}\mathbf{S}_{SL}$, that is

$$\begin{bmatrix}\mathbf{I}_K \otimes r_1(0) & \dots & \mathbf{I}_K \otimes \{r_1(-\ell(M-1)\gamma)\}_\ell\end{bmatrix}(\mathbf{I}_M \otimes \mathbf{w}^{\top})(\mathbf{I}_M \otimes \mathbf{w})\begin{bmatrix}\mathbf{I}_K \otimes r_1(0)\\ \vdots \\ \mathbf{I}_K \otimes \{r_1(\ell(M-1)\gamma)\}_\ell\end{bmatrix}.$$

Since $(\mathbf{I}_M \otimes \mathbf{w}^{\top})(\mathbf{I}_M \otimes \mathbf{w}) = \mathbf{I}_M \otimes \mathbf{w}^{\top}\mathbf{w}$, the product $\mathbf{S}_{SL}^{\top}\mathbf{S}_{SL}$ boils down to

$$\mathbf{S}_{SL}^{\top}\mathbf{S}_{SL} = \sum_{s=1}^{M}(\mathbf{I}_K \otimes \{r_1(-\ell(s-1)\gamma)\}_\ell)\mathbf{w}^{\top}\mathbf{w}(\mathbf{I}_K \otimes \{r_1(\ell(s-1)\gamma)\}_\ell).$$

Notice that the receptor $x_l^{(1)}$ is $x_l^{(1)} = r_l e^{i\theta_l^{(1)}}$. Since $\rho - \eta \le r_i \le \rho + \eta$, for some η small, we assume that $x_l^{(1)} = \rho e^{i\theta_l^{(1)}}$. As a consequence, we can factorize $\mathbf{G}^{(1)}$ as

$$\mathbf{G}^{(1)} = \widetilde{\mathbf{G}}^{(1)}(\mathbf{I}_K \otimes \{\ell^{-1}\rho^{-\ell}\mathbf{I}_2\}_\ell),$$

where $\widetilde{\mathbf{G}}^{(1)}$ is a Vandermonde-type matrix with nodes on the unit disk $|z| = 1$.

We obtain

$$\mathbf{w}^{\top}\mathbf{w} = (\mathbf{I}_K \otimes \{\ell^{-1}\rho^{-\ell}\mathbf{I}_2\}_\ell)(\widetilde{\mathbf{G}}^{(1)})^{\top}\mathbf{u}^{\top}\mathbf{u}\widetilde{\mathbf{G}}^{(1)}(\mathbf{I}_K \otimes \{\ell^{-1}\rho^{-\ell}\mathbf{I}_2\}_\ell).$$

It is immediate to see that

$$\mathbf{S}_{SL}^{\top}\mathbf{S}_{SL} = \mathbf{D}_{1,K}\mathbf{C}\left(\sum_{s=1}^{M}(\mathbf{I}_K \otimes \{r_1(-\ell(s-1)\gamma)\}_\ell)\widetilde{\mathbf{w}}^{\top}\widetilde{\mathbf{w}}(\mathbf{I}_K \otimes \{r_1(\ell(s-1)\gamma)\}_\ell)\right)\mathbf{C}\mathbf{D}_{1,K},$$

where

$$\mathbf{D}_{1,K} := \mathbf{I}_K \otimes \{\rho^{-\ell}\mathbf{I}_2\}_\ell, \qquad \widetilde{\mathbf{w}} = -\mathbf{u}\widetilde{\mathbf{G}}^{(1)}.$$

Let us denote $\mathbf{S}_{SL}\mathbf{D}_{1,K}^{-1}\mathbf{C}^{-1}$ by $\widetilde{\mathbf{S}}_{SL}$.

To prove estimate (A.14), we rely on the following inequality:

$$\|(\mathbf{S}_{SL}^{\dagger})_{k,:}\|_F \le \|(\mathbf{C}^{-1}\mathbf{D}_{1,K}^{-1})_{k,:}\|_F \, \|(\widetilde{\mathbf{S}}_{SL}^{\top}\widetilde{\mathbf{S}}_{SL})^{-1}\|_F \, \|\widetilde{\mathbf{S}}_{SL}^{\top}\|_F. \tag{A.15}$$

By a straightforward calculation, it is immediate to see that

$$\|(\mathbf{C}^{-1}\mathbf{D}_{1,K}^{-1})_{k,:}\|_F \le \lceil k/2 \rceil \, \rho^{\lceil k/2 \rceil}, \tag{A.16}$$

and

$$\|\widetilde{\mathbf{S}}_{SL}^{\top}\|_F \le \sqrt{M} \max_{1 \le m \le M} \|(\widetilde{\mathbf{S}}_{SL})_{m,:}\|_F \lesssim \sqrt{M}. \tag{A.17}$$

Finally, we investigate the Frobenius norm of $(\widetilde{\mathbf{S}}_{SL}^{\mathsf{T}}\widetilde{\mathbf{S}}_{SL})^{-1}$. For $1 \le j \le K$, we observe that

$$\begin{aligned}\left(\widetilde{\mathbf{S}}_{SL}^{\mathsf{T}}\widetilde{\mathbf{S}}_{SL}\right)_{2j-1:2j,\,2j-1:2j} &= \sum_{s=1}^{M} r_1(-j(s-1)\gamma)\begin{bmatrix}\widetilde{w}_{2j-1}\\ \widetilde{w}_{2j}\end{bmatrix}\begin{bmatrix}\widetilde{w}_{2j-1} & \widetilde{w}_{2j}\end{bmatrix} r_1(j(s-1)\gamma)\\ &= U^{\mathsf{H}}\left(\sum_{s=1}^{M}\begin{bmatrix}e^{-ij(s-1)\gamma} & 0\\ 0 & e^{ij(s-1)\gamma}\end{bmatrix}\begin{bmatrix}y_{2j-1}\\ y_{2j}\end{bmatrix}\begin{bmatrix}y_{2j-1}\\ y_{2j}\end{bmatrix}^{\mathsf{H}}\begin{bmatrix}e^{ij(s-1)\gamma} & 0\\ 0 & e^{-ij(s-1)\gamma}\end{bmatrix}\right)U\\ &= U^{\mathsf{H}}\begin{bmatrix}M|y_{2j-1}|^2 & \frac{1-e^{-2ijM\gamma}}{1-e^{-2ij\gamma}}(y_{2j}\overline{y}_{2j-1})\\ \frac{1-e^{2ijM\gamma}}{1-e^{2ij\gamma}}(y_{2j-1}\overline{y}_{2j}) & M|y_{2j}|^2\end{bmatrix}U,\end{aligned}$$

where

$$\begin{bmatrix}y_{2j-1}\\ y_{2j}\end{bmatrix} = U\begin{bmatrix}\widetilde{w}_{2j-1}\\ \widetilde{w}_{2j}\end{bmatrix}, \qquad U = \frac{1}{\sqrt{2}}\begin{bmatrix}1 & i\\ 1 & -i\end{bmatrix}.$$

For $1 \le j < k \le K$, we have

$$\begin{aligned}\left(\widetilde{\mathbf{S}}_{SL}^{\mathsf{T}}\widetilde{\mathbf{S}}_{SL}\right)_{2j-1:2j,\,2k-1:2k} &= \sum_{s=1}^{M} r_1(-j(s-1)\gamma)\begin{bmatrix}\widetilde{w}_{2j-1}\\ \widetilde{w}_{2j}\end{bmatrix}\begin{bmatrix}\widetilde{w}_{2k-1} & \widetilde{w}_{2k}\end{bmatrix} r_1(k(s-1)\gamma)\\ &= U^{\mathsf{H}}\begin{bmatrix}\frac{1-e^{-i(j-k)M\gamma}}{1-e^{-i(j-k)\gamma}}(y_{2j-1}\overline{y}_{2k-1}) & \frac{1-e^{-i(j+k)M\gamma}}{1-e^{-i(j+k)\gamma}}(y_{2j}\overline{y}_{2k-1})\\ \frac{1-e^{i(j+k)M\gamma}}{1-e^{i(j+k)\gamma}}(y_{2j-1}\overline{y}_{2k}) & \frac{1-e^{i(j-k)M\gamma}}{1-e^{i(j-k)\gamma}}(y_{2j}\overline{y}_{2k})\end{bmatrix}U.\end{aligned}$$

Therefore, $\widetilde{\mathbf{S}}_{SL}^{\mathsf{T}}\widetilde{\mathbf{S}}_{SL}$ can be written as follows:

$$\widetilde{\mathbf{S}}_{SL}^{\mathsf{T}}\widetilde{\mathbf{S}}_{SL} = \mathbf{U}^{\mathsf{H}}(M\mathbf{D}+\mathbf{R})\mathbf{U},$$

where

$$\mathbf{D} := \begin{bmatrix}|y_1|^2 & & 0\\ & \ddots & \\ 0 & & |y_{2K}|^2\end{bmatrix}, \qquad \mathbf{R} := \widetilde{\mathbf{S}}_{SL}^{\mathsf{T}}\widetilde{\mathbf{S}}_{SL} - \mathbf{D}, \qquad \mathbf{U} := \mathbf{I}_K \otimes U.$$

Notice that requiring $\mathbf{D}$ to be invertible is equivalent to saying that each $|y_j|$, and thus each $\widetilde{w}_j$, is non-zero. For this reason, the initial assumption on $\partial^{\alpha}\mathcal{S}_{\Omega_s}(z)$ implies that $\mathbf{D}$ is invertible (see [7]) and thus, for M large enough, $\mathbf{S}_{SL}$ is full column rank. Since $\|\mathbf{R}\|_F = O(1)$, we have [33]

$$\mathbf{U}(\widetilde{\mathbf{S}}_{SL}^{\mathsf{T}}\widetilde{\mathbf{S}}_{SL})^{-1}\mathbf{U}^{\mathsf{H}} = \frac{1}{M}\left(\mathbf{D}+\frac{1}{M}\mathbf{R}\right)^{-1} = \frac{1}{M}\mathbf{D}^{-1} + O\left(\frac{1}{M^2}\right).$$

Since $\mathbf{U}$ is unitary, $\|\mathbf{U}(\widetilde{\mathbf{S}}_{SL}^{\mathsf{T}}\widetilde{\mathbf{S}}_{SL})^{-1}\mathbf{U}^{\mathsf{H}}\|_F = \|(\widetilde{\mathbf{S}}_{SL}^{\mathsf{T}}\widetilde{\mathbf{S}}_{SL})^{-1}\|_F$. Hence

$$\|(\widetilde{\mathbf{S}}_{SL}^{\mathsf{T}}\widetilde{\mathbf{S}}_{SL})^{-1}\|_F \lesssim \frac{1}{M}. \tag{A.18}$$

Finally, inequality (A.15) together with estimates (A.16), (A.17) and (A.18) shows that $\|(\mathbf{S}_{SL}^{\dagger})_{k,:}\|_F$ satisfies (A.14). □

We are now ready to estimate the dependency of $(\mathbf{S}^\dagger)_{k,:}$ on M and ρ. For ρ large enough, we observe that the leading order term of $(\mathbf{S}^\dagger)_{k,:}$ is $(\mathbf{S}_{SL}^\dagger)_{k,:}$.

Since

$$\mathbf{S} = \mathbf{S}_{dip} + \mathbf{S}_{SL},$$

we have [33]

$$\mathbf{S}^\dagger = (\mathbf{S}_{dip} + \mathbf{S}_{SL})^\dagger = \mathbf{S}_{SL}^\dagger - \mathbf{S}_{SL}^\dagger \mathbf{S}_{dip} \mathbf{S}_{SL}^\dagger + \sum_{\ell=2}^{\infty} (-1)^\ell (\mathbf{S}_{SL}^\dagger \mathbf{S}_{dip})^\ell \mathbf{S}_{SL}^\dagger.$$

It is immediate to prove the following lemma.

Lemma A.4.6 *For $1 \le k \le 2K$, we have*

$$(\mathbf{S}^{\,\dagger})_{k,:} = (\mathbf{S}_{SL}^{\,\dagger})_{k,:} + O(\rho^{\lceil k/2 \rceil - 1}).$$

Proof. Let us denote the matrix $\mathbf{S}_{dip}\mathbf{D}_{2,K+1}^{-1}$ by $\widetilde{\mathbf{S}}_{dip}$. Observe that both $\widetilde{\mathbf{S}}_{SL}$ and $\widetilde{\mathbf{S}}_{dip}$ are independent of ρ. We have

$$\begin{aligned}
\|(\mathbf{S}_{SL}^\dagger)_{k,:}\mathbf{S}_{dip}\mathbf{S}_{SL}^\dagger\|_F &= \|(\mathbf{C}^{-1}\mathbf{D}_{1,K}^{-1})_{k,:}\widetilde{\mathbf{S}}_{SL}^\dagger \widetilde{\mathbf{S}}_{dip}\mathbf{D}_{2,K+1}\mathbf{C}^{-1}\mathbf{D}_{1,K}^{-1}\widetilde{\mathbf{S}}_{SL}^\dagger\|_F \\
&= \rho^{-1}\|(\mathbf{C}^{-1}\mathbf{D}_{1,K}^{-1})_{k,:}\widetilde{\mathbf{S}}_{SL}^\dagger \widetilde{\mathbf{S}}_{dip}\mathbf{C}^{-1}\widetilde{\mathbf{S}}_{SL}^\dagger\|_F \\
&\lesssim \rho^{\lceil k/2 \rceil - 1}.
\end{aligned}$$

□

A.5. Transferable Belief Model

In this appendix we present some basic definitions from evidence theory. In particular, we shall consider the Transferable Belief Model (TBM); see [72]. This theory does not require any underlying probability space.

In the context of dictionary classification, the frame of discernment is usually modeled as a finite set $\mathscr{C} = \{c_1, c_2, \ldots, c_N\}$, which is called a *dictionary*.

A belief function is a function $\mathsf{bel} : 2^{\mathscr{C}} \longrightarrow [0,1]$ such that the following hold

1. $\mathsf{bel}(\varnothing) = 0$;
2. for all $A_1, A_2, \ldots, A_n \in 2^{\mathscr{C}}$,

$$\mathsf{bel}(A_1 \cup A_2 \cup \cdots \cup A_n) \ge \sum_i \mathsf{bel}(A_i) - \sum_{i>j} \mathsf{bel}(A_i \cap A_j) - \ \ldots \ -(-1)^n \mathsf{bel}(A_1 \cap A_2 \cap \cdots \cap A_n)\ ; \tag{A.19}$$

3. $\mathsf{bel}(\mathscr{C}) \le 1$.

A basic belief assignment (BBA) m is a function $\mathsf{m} : 2^{\mathscr{C}} \longrightarrow [0,1]$ such that

$$\sum_{A \in 2^{\mathscr{C}}} \mathsf{m}(A) = 1.$$

The value $\mathsf{m}(A)$ for $A \in 2^{\mathscr{C}}$ is called the basic belief mass (BBM) given to A. This is a part of the agent's belief that supports A, and that, due to lack of information, does not support any strict subset of A. If $\mathsf{m}(A) > 0$ then A is called focal set. Observe that it is allowed to allocate positive BBM to $\varnothing$, i.e., $\mathsf{m}(\varnothing) > 0$.

The BBA related to a belief function bel is the function $\mathsf{m} : 2^{\mathscr{C}} \longrightarrow [0,1]$ such that:

$$\begin{aligned} \mathsf{m}(A) &= \sum_{B \in 2^{\mathscr{C}},\, \varnothing \neq B \subseteq A} (-1)^{|A|-|B|} \mathsf{bel}(B), \quad \text{for all } A \in 2^{\mathscr{C}},\ A \neq \varnothing, \\ \mathsf{m}(\varnothing) &= 1 - \mathsf{bel}(\mathscr{C}). \end{aligned} \tag{A.20}$$

Moreover, there is a one-to-one correspondence between m and bel via the following formula

$$\mathsf{bel}(A) = \sum_{B \in \mathscr{C},\, \varnothing \neq B \subseteq A} \mathsf{m}(B), \quad \text{for all } A \in 2^{\mathscr{C}},\ A \neq \varnothing, \tag{A.21}$$

that is, $\mathsf{bel}(A)$ is obtained by summing all BBMs given to subsets $B \in 2^{\mathscr{C}}$ with $B \subseteq A$, and it quantifies the total amount of justified specific support given to A.

Let m_1 and m_2 be two BBAs, we define the TBM conjunctive combination of the two as

$$(\mathsf{m}_1 \textcircled{\cap} \mathsf{m}_2)(A) = \sum_{B \cap C = A} \mathsf{m}_1(B)\mathsf{m}_2(C). \tag{A.22}$$

In the TBM model, from a decision-making point of view, we need to resort to a probability distribution in order to select the most reliable hypothesis in $\mathscr{C}$. Such a function is called a *pignistic probability*, and is defined as

$$\mathrm{BetP}(c) = \sum_{A \subseteq \mathscr{C}, c \in A} \frac{\mathsf{m}(A)}{|A|}. \tag{A.23}$$

The term *pignistic* stresses the fact that the only purpose of these probabilities is that of forcing a decision.

B. Appendix

B.1. The results in the three-dimensional case

For the sake of completeness, in this appendix we focus on the three-dimensional case ($d = 3$). In doing so, we note that the derivation of the asymptotic expansion in time-domain can be carried out similarly to the two-dimensional case (see Sections 4.3, 4.4 and 4.5). Only minor changes in the proofs are required.

In the sections below, we aim at stressing the differences from the proofs which are given for the two-dimensional case.

B.1.1. Stability estimates for the Helmholtz equation

Let $D = \varepsilon B + z$, $|B| = 1$ and $D \subset \mathbb{R}^3$. Let ω, $0 < \gamma < 1$, and $\varepsilon_0 > 0$ be as in Section 4.3. As in the two dimensional case, the main estimate is given by Proposition 4.3.1. However, while the proof that we presented for the two-dimensional case resort to Lemma 4.3.2, in the three-dimensional case it can be proved more directly. We sketch the proof below, highlighting the changes with respect to the previous argument.

Proof. The skeleton of the proof is the same as for the two-dimensional case. The operator T is introduced as in (4.10), and it is decomposed as follows

$$T = \widetilde{T}_0 + \widetilde{T}_\varepsilon,$$

where, this time, $\widetilde{T}_0$ is defined as

$$\widetilde{T}_0(\widetilde{\phi}, \widetilde{\psi}) := \left(\mathcal{S}_B^0[\widetilde{\phi}] - \mathcal{S}_B^0[\widetilde{\psi}], k \frac{\partial \mathcal{S}_B^0[\widetilde{\phi}]}{\partial \nu}\bigg|_- - \frac{\partial \mathcal{S}_B^0[\widetilde{\psi}]}{\partial \nu}\bigg|_+ \right),$$

and

$$\widetilde{T}_\varepsilon := T - \widetilde{T}_0.$$

Then, the argument proceeds as in the two-dimensional case. □

B.1.2. Frequency-dependent asymptotic expansion

By using the same techniques of Section 4.4, the frequency-dependent asymptotic expansion in $\mathbb{R}^3$ is readily obtained.

Theorem B.1.1 *Suppose that ω^2 is not a Dirichlet eigenvalue for $-\Delta$ on D and $\omega \in (0, \varepsilon^{-\gamma})$, with $0 < \gamma < 1$. The following asymptotic expansion holds:*

$$v_y(x,\omega) - V_y(x,\omega) = \sum_{|\beta|=0}^{n+1} \sum_{|\alpha|=0}^{n-|\beta|+1} \frac{\varepsilon^{|\alpha|+|\beta|+1}}{\alpha!\,\beta!} \partial_z^\alpha V_y(z,\omega) \partial_z^\beta \Gamma_\omega(x,z) \widehat{W}_{\alpha\beta} + O(\varepsilon^{n+3}(1+\omega^{n+2})),$$

for $x \in \mathbb{R}^3 \setminus \overline{D}$, where $\widehat{W}_{\alpha\beta}$ are the FDPTs defined as in (4.15).

It is worth noticing that the leading-order term of the scattered field derived in [12, 41] can be recovered from Theorem B.1.1. In particular, we have

$$v_y(x,\omega) - V_y(x,\omega) = \varepsilon^3 \nabla_z V_y(z,\omega) M(k,B) \nabla_z \Gamma_\omega(x,z) + O(\varepsilon^4 \omega^3),$$

where $M(k,B) = (m_{ij})_{i,j}$ is the polarization tensor (PT) given by

$$m_{ij} = \int_{\partial B} \xi_j \left(\frac{(k+1)}{2(k-1)} \mathcal{I} - \mathcal{K}_B^* \right)^{-1} [\nu_i](\xi)\, d\sigma(\xi),$$

$\nu = (\nu_1, \nu_2, \nu_3)$ is the outward unit normal to ∂B, $\xi = (\xi_1, \xi_2, \xi_3)$, and k is the contrast.

B.1.3. Time-domain asymptotic expansion

In the three-dimensional case, the emitted wave generated at $y \in \mathbb{R}^3 \setminus \overline{D}$ is defined as

$$U_y(x,t) := \frac{\delta_0(t - |x-y|)}{4\pi|x-y|},$$

where δ_0 is the Dirac mass at 0. It is readily seen that U_y satisfies

$$\begin{cases} (\partial_t^2 - \Delta) U_y(x,t) = \delta_{x=y} \delta_{t=0}, & (x,t) \in \mathbb{R}^3 \times \mathbb{R}, \\ U_y(x,t) = 0 & \text{for } x \in \mathbb{R}^3 \text{ and } t \ll 0. \end{cases}$$

For $u_y = u_y(x,t)$, we consider the wave equation

$$\begin{cases} \partial_t^2 u_y - \nabla \cdot (\chi(\mathbb{R}^3 \setminus \overline{D}) + k\chi(D)) \nabla u_y = \delta_{x=y} \delta_{t=0} & \text{in } \mathbb{R}^3 \times (0,\infty), \\ u_y(x,t) = 0 & \text{for } x \in \mathbb{R}^3 \text{ and } t \ll 0. \end{cases}$$

For $\rho > 0$, let P_ρ be the operator defined in (4.17). Since

$$\widehat{U}_y(x,\omega) := \int_{\mathbb{R}} e^{i\omega t} U_y(x,t)\, dt = \frac{e^{i\omega|x-y|}}{4\pi|x-y|} = V_y(x,\omega),$$

it follows that

$$P_\rho[U_y](x,t) = \frac{\psi_\rho(t-|x-y|)}{4\pi|x-y|},$$

and $P_\rho[U_y]$ satisfies

$$(\partial_t^2 - \Delta) P_\rho[U_y](x,t) = \delta_{x=y}\psi_\rho(t) \text{ in } \mathbb{R}^3 \times \mathbb{R}.$$

Moreover, we have that

$$P_\rho[u_y](x,t) = \int_{|\omega|\le\rho} e^{-i\omega t} v_y(x,\omega)\, d\omega,$$

where v_y is the solution to the three-dimensional problem in the frequency domain.

Similarly to the two-dimensional case, we define the TDPTs as a truncated Fourier transform of FDPTs.

Definition B.1.2 *For $\rho < 1/\varepsilon$ and multi-indices α and β, the three-dimensional TDPTs, $P_\rho[W_{\alpha\beta}]$, are defined as follows:*

$$P_\rho[W_{\alpha\beta}](x,t) = \int_{|\omega|\le\rho} e^{-i\omega t} \widehat{W}_{\alpha\beta}\, d\omega, \tag{B.1}$$

where $\widehat{W}_{\alpha\beta}$ are the FDPTs given by (4.15).

We refer to Remarks 4.5.2 and 4.5.3, where the given definition and notation are clarified.

Proceeding as in Section 4.5, the following expansion of $P_\rho[u_y - U_y](x,t)$ in terms of the TDPTs is readily obtained.

Theorem B.1.3 *For $0 < \gamma < 1$, the following asymptotic expansion holds:*

$$\begin{aligned} &P_\rho[u_y](x,t) = P_\rho[U_y](x,t) \\ &+ \varepsilon \sum_{|\beta|=0}^{n+1} \sum_{|\alpha|=0}^{n-|\beta|+1} \frac{\varepsilon^{|\alpha|+|\beta|}}{\alpha!\,\beta!} \int_{\mathbb{R}} \partial_z^\beta P_\rho[U_z](x,\tau) \left(\int_{\mathbb{R}} \partial_z^\alpha P_\rho[U_y](z, t-\tau-\tau') P_\rho[W_{\alpha\beta}](\tau')\, d\tau' \right) d\tau \\ &+ O\left(\varepsilon^{(n+3)(1-\gamma)}\right), \end{aligned}$$

where $x \in \mathbb{R}^3 \setminus \overline{D}$, $D = \varepsilon B + z$, $|B| = 1$, $P_\rho[W_{\alpha\beta}]$ are the TDPTs defined in Definition (B.1.2) *and $\rho = O(\varepsilon^{-\gamma})$.*

References

[1] M. Abramowitz and I. Stegun. *Handbook of Mathematical Functions*. National Bureau of Standards, Washington D.C., 1964.

[2] H. Ammari, T. Boulier, and Josselin Garnier. Modeling active electrolocation in weakly electric fish. *SIAM Journal on Imaging Sciences*, 6(1):285–321, 2013.

[3] H. Ammari, M. Putinar, Andries Steenkamp, and Faouzi Triki. Identification of an algebraic domain in two dimensions from a finite number of its generalized polarization tensors. *Mathematische Annalen*, 375(3-4):1337–1354, 2019.

[4] H. Ammari and H. Wang. Time-domain multiscale shape identification in electro-sensing. *Imaging, Multi-scale and High Contrast Partial Differential Equations, Contemp. Math.*, 660:23–44, 2016.

[5] Habib Ammari. *Biomedical Imaging Modalities*. Springer Berlin Heidelberg, Berlin, Heidelberg, 2008.

[6] Habib Ammari, Thomas Boulier, Josselin Garnier, Wenjia Jing, Hyeonbae Kang, and Han Wang. Target identification using dictionary matching of generalized polarization tensors. *Foundations of Computational Mathematics*, 14(1):27–62, Feb 2014.

[7] Habib Ammari, Thomas Boulier, Josselin Garnier, and Han Wang. Shape recognition and classification in electro-sensing. *Proceedings of the National Academy of Sciences*, 111(32):11652–11657, 2014.

[8] Habib Ammari, Thomas Boulier, Josselin Garnier, and Han Wang. Mathematical modelling of the electric sense of fish: the role of multi-frequency measurements and movement. *Bioinspiration & Biomimetics*, 12(2):025002, jan 2017.

[9] Habib Ammari, Yat Tin Chow, and Hongyu Liu. Localized sensitivity analysis at high-curvature boundary points of reconstructing inclusions in transmission problems, 2019.

[10] Habib Ammari, Yat Tin Chow, and Jun Zou. Phased and phaseless domain reconstructions in the inverse scattering problem via scattering coefficients. *SIAM Journal on Applied Mathematics*, 76(3):1000–1030, 2016.

[11] Habib Ammari, Youjun Deng, Hyeonbae Kang, and Hyundae Lee. Reconstruction of inhomogeneous conductivities via the concept of generalized polarization tensors. *Annales de l'I.H.P. Analyse non linéaire*, 31(5):877–897, 2014.

[12] Habib Ammari, Pierre Garapon, Lili Guadarrama Bustos, and Hyeonbae Kang. Transient anomaly imaging by the acoustic radiation force. *Journal of Differential Equations*, 249(7):1579–1595, 2010.

[13] Habib Ammari, Josselin Garnier, Laure Giovangigli, Wenjia Jing, and Jin-Keun Seo. Spectroscopic imaging of a dilute cell suspension. *Journal de Mathématiques Pures et Appliquées*, 105(5):603–661, 2016.

[14] Habib Ammari, Josselin Garnier, Wenjia Jing, Hyeonbae Kang, Mikyoung Lim, Knut Sølna, and Han Wang. *Mathematical and Statistical Methods for Multistatic Imaging*. Springer International Publishing, Cham, 2013.

[15] Habib Ammari, Josselin Garnier, Wenjia Jing, Hyeonbae Kang, Mikyoung Lim, Knut Sølna, and Han Wang. *Target Identification and Tracking*. Springer International Publishing, Cham, 2013.

[16] Habib Ammari, Josselin Garnier, Hyeonbae Kang, Mikyoung Lim, and Sanghyeon Yu. Generalized polarization tensors for shape description. *Numerische Mathematik*, 126, 12 2011.

[17] Habib Ammari, Ekaterina Iakovleva, and Dominique Lesselier. A music algorithm for locating small inclusions buried in a half-space from the scattering amplitude at a fixed frequency. *Multiscale Modeling & Simulation*, 3(3):597–628, 2005.

[18] Habib Ammari and Hyeonbae Kang. High-order terms in the asymptotic expansions of the steady-state voltage potentials in the presence of conductivity inhomogeneities of small diameter. *SIAM Journal on Mathematical Analysis*, 34(5):1152–1166, 2003.

[19] Habib Ammari and Hyeonbae Kang. Properties of the generalized polarization tensors. *Multiscale Modeling & Simulation*, 1(2):335–348, 2003.

[20] Habib Ammari and Hyeonbae Kang. Springer Berlin Heidelberg, Berlin, Heidelberg, 2004.

[21] Habib Ammari and Hyeonbae Kang. Boundary layer techniques for solving the helmholtz equation in the presence of small inhomogeneities. *Journal of Mathematical Analysis and Applications*, 296(1):190–208, 2004.

[22] Habib Ammari and Hyeonbae Kang. *Polarization and Moment Tensors: With Applications to Inverse Problems and Effective Medium Theory*. Springer, New York, 2007.

[23] Habib Ammari, Hyeonbae Kang, Eunjoo Kim, and June-Yub Lee. The generalized polarization tensors for resolved imaging part ii: Shape and electromagnetic parameters reconstruction of an electromagnetic inclusion from multistatic measurements. *Math. Comput.*, 81, 04 2012.

[24] Habib Ammari, Hyeonbae Kang, Mikyoung Lim, and Habib Zribi. The generalized polarization tensors for resolved imaging. part i: Shape reconstruction of a conductivity inclusion. *Math. Comput.*, 81, 01 2012.

[25] Habib Ammari, Minh Phuong Tran, and Han Wang. Shape identification and classification in echolocation. *SIAM Journal on Imaging Sciences*, 7(3):1883–1905, 2014.

[26] M.S. Ashbaugh and R.D. Benguria. Isoperimetric inequalities for eigenvalues of the laplacian. In *Spectral Theory and Mathematical Physics: A Festschrift in Honor of Barry Simon's 60th Birthday*, volume 76, pages 105–139. Proceedings of Symposia in Pure Mathematics, 2007.

[27] C. Assad. *Electric field maps and boundary element simulations of electrolocation in weakly electric fish*. PhD thesis, 1997.

[28] David Babineau, Andre Longtin, and John Lewis. Modeling the electric field of weakly electric fish. *The Journal of experimental biology*, 209:3636–51, 10 2006.

[29] Yang Bai, Izaak D Neveln, Michael Peshkin, and Malcolm A MacIver. Enhanced detection performance in electrosense through capacitive sensing. *Bioinspiration & Biomimetics*, 11(5):055001, aug 2016.

[30] Lorenzo Baldassari. Scattering coefficients of inhomogeneous objects and their application in target classification in wave imaging. *European Journal of Applied Mathematics*, 31(4):553–573, 2020.

[31] Lorenzo Baldassari and Andrea Scapin. Multi-scale classification for electrosensing. *SIAM Journal on Imaging Sciences*, 14(1):26–57, 2021.

[32] Lorenzo Baldassari and Andrea Scapin. Reconstruction of a small acoustic inclusion via time-dependent polarization tensors. *IMA Journal of Applied Mathematics*, 02 2021. hxaa045.

[33] Adi Ben-Israel. On error bounds for generalized inverses. *SIAM Journal on Numerical Analysis*, 3, 12 1966.

[34] Eric Bonnetier, Faouzi Triki, and Chun-Hsiang Tsou. On the electro-sensing of weakly electric fish. *Journal of Mathematical Analysis and Applications*, 464(1):280–303, 2018.

[35] R. Budelli and A.A. Caputi. The electric image in weakly electric fish: perception of objects of complex impedance. *Journal of Experimental Biology*, 203(3):481–492, 2000.

[36] Hamstra R.H. Bullock, T.H. and H Scheich. The jamming avoidance response of high frequency electric fish. *J. Comp. Physiol.*, 77:23–48, 1972.

[37] Angel Ariel Caputi. The bioinspiring potential of weakly electric fish. *Bioinspiration & Biomimetics*, 12(2):025004, feb 2017.

[38] M. G. Christensen and A. Jakobsson. Optimal filter designs for separating and enhancing periodic signals. *IEEE Transactions on Signal Processing*, 58(12):5969–5983, 2010.

[39] O.M. Curet, N.A. Patankar, G.V. Lauder, and M.A. Maciver. Aquatic manoeuvering with counter-propagating waves: A novel locomotive strategy. *J. R. Soc. Interface*, 8:1041–1050, 2011.

[40] Assem Deif. The generalized inverse of a perturbed singular matrix. *Zeitschrift Fur Angewandte Mathematik Und Physik - ZAMP*, 34:291–300, 05 1983.

[41] S. Gdoura and L. Guadarrama-Bustos. Transient wave imaging of anomalies: a numerical study. *Mathematical and Statistical Methods for Imaging, Contemporary Mathematics*, 548:31–43, 2011.

[42] T. Greville. Some applications of the pseudoinverse of a matrix. *SIAM Review*, 2(1):15–22, 1960.

[43] S.I. Hariharan and R.C. MacCamy. A boundary element method for a two-dimensional interface problem in electromagnetics. *Numer. Math.*, 42:311–322, 1983.

[44] S.I. Hariharan and R.C. MacCamy. Low frequency acoustic and electromagnetic scattering. 1983.

[45] B. He, T. Musha, Y. Okamoto, S. Homma, Y. Nakajima, and T. Sato. Electric dipole tracing in the brain by means of the boundary element method and its accuracy. *IEEE Transactions on Biomedical Engineering*, BME-34(6):406–414, 1987.

[46] W. Heiligenberg. Theoretical and experimental approaches to spatial aspects of electrolocation. *J. Comp. Physiol.*, 103:247–272, 1975.

[47] W. Heiligenberg. Principles of electrolocation and jamming avoidance in electric fish. In *Studies of Brain Function*, 1977.

[48] W. Heiligenberg, C. Baker, and J. Bastian. The jamming avoidance response in gymnotoid pulse-species: A mechanism to minimize the probability of pulse-train coincidence. *Journal of comparative physiology*, 124:211–224, 2004.

[49] Shogen K. Matsuo T. et al. Hoshimiya, N. The apteronotus eod field: Waveform and eod field simulation. *J. Comp. Physiol.*, 135:283–290, 1980.

[50] Van-Nam Huynh, Nguyen Thanh Tri, and Cuong Anh Le. Adaptively entropy-based weighting classifiers in combination using dempster-shafer theory for word sense disambiguation. *Comput. Speech Lang.*, 24:461–473, 2010.

[51] E. Krahn. Über minimaleigenschaften der kugel in drei und mehr dimensionen. *Acta Comm. Univ. Tartu (Dorpat)*, pages 1–44, 1926.

[52] Bernd Kramer. *Electroreception and communication in fishes*, volume 42 of *Progress in Zoology*. Gustav Fischer, Stuttgart, 1996.

[53] N.N. Lebedev. *Special Functions and their Applications*.

[54] Chen Ling, L. House Jonathan, Krahe Rüdiger, and E. Nelson Mark. Modeling signal and background components of electrosensory scenes. *Journal of Comparative Physiology A*, 191:331–345, 2005.

[55] M. A. MacIver, N. M. Sharabash, and M. E. Nelson. Prey-capture behavior in gymnotid electric fish: Motion analysis and effects of water conductivity. March 2001.

[56] M.A. Maciver. *The computational neuroethology of weakly electric fish: Body modeling, motion analysis, and sensory signal estimation.* PhD thesis, 2001.

[57] Ana Marco, José-Javier Martínez, and Raquel Viaña. Least squares problems involving generalized kronecker products and application to bivariate polynomial regression. *Numerical Algorithms*, Sep 2018.

[58] G. Matviyenko. On the evaluation of bessel functions. *Appl. Comput. Harmon. Anal.*, 1:116–135, 1993.

[59] D. Mercier, G. Cron, T. Denoeux, and M. Masson. Fusion of multi-level decision systems using the transferable belief model. In *2005 7th International Conference on Information Fusion*, volume 2, pages 8 pp.–, July 2005.

[60] V.M. Mondéjar-Guerra, R. Muñoz-Salinas, M.J. Marín-Jiménez, A. Carmona-Poyato, and R. Medina-Carnicer. Keypoint descriptor fusion with dempster–shafer theory. *International Journal of Approximate Reasoning*, 60:57 – 70, 2015.

[61] J. C. Mosher, P. S. Lewis, and R. M. Leahy. Multiple dipole modeling and localization from spatio-temporal meg data. *IEEE Transactions on Biomedical Engineering*, 39(6):541–557, 1992.

[62] Federico Pedraja, Rossana Perrone, Ana Silva, and Ruben Budelli. Passive and active electroreception during agonistic encounters in the weakly electric fish gymnotus omarorum. *Bioinspiration & Biomimetics*, 11(6):065002, oct 2016.

[63] Brian Rasnow, Christopher Assad, Mark E. Nelson, and James M. Bower. Simulation and measurement of the electric fields generated by weakly electric fish. In D. S. Touretzky, editor, *Advances in Neural Information Processing Systems 1*, pages 436–443. Morgan-Kaufmann, 1989.

[64] P. Regalia and M. Sanjit. Kronecker products, unitary matrices and signal processing applications. *SIAM Review*, 31(4):586–613, 1989.

[65] Phillip A Regalia and Mitra K Sanjit. Kronecker products, unitary matrices and signal processing applications. *SIAM review*, 31(4):586–613, 1989.

[66] Andrea Scapin. Electro-sensing of inhomogeneous targets. *Journal of Mathematical Analysis and Applications*, 472(2):1872 – 1901, 2019.

[67] Andrea Scapin. Electrocommunication for weakly electric fish. *Inverse Problems & Imaging*, 14:97, 2020.

[68] K. Sekihara, D. Poeppel, A. Marantz, H. Koizumi, and Y. Miyashita. Noise covariance incorporated meg-music algorithm: a method for multiple-dipole estimation tolerant of the influence of background brain activity. *IEEE Transactions on Biomedical Engineering*, 44(9):839–847, 1997.

[69] A. Shlivinski, E. Heyman, and A. Devaney. Time domain radiation by scalar sources: Plane wave to multipole transform. *Journal of Mathematical Physics*, 42:5915–5919, 2001.

[70] Fenton M.B. Simmons, J.A. and M.J. O'Farrell. Echolocation and pursuit of prey by bats. *Science*, 203:16–21, 1979.

[71] J.A. Simmons. Perception of echo phase information in bat sonar. *Appl. Comput. Harmon. Anal.*, 204:1336–38, 1979.

[72] Philippe Smets. The nature of the unnormalized beliefs encountered in the transferable belief model. In Didier Dubois, Michael P. Wellman, Bruce D'Ambrosio, and Phillipe Smets, editors, *Uncertainty in Artificial Intelligence*, pages 292 – 297. Morgan Kaufmann, 1992.

[73] Philippe Smets and Robert Kennes. *The Transferable Belief Model*, pages 693–736. Springer Berlin Heidelberg, Berlin, Heidelberg, 2008.

[74] G. von der Emde. Active electrolocation of objects in weakly electric fish. *Journal of Experimental Biology*, 202(10):1205–1215, 1999.

[75] G. von der Emde, S. Schwarz, L. Gomez, R. Budelli, and K. Grant. Electric fish measure distance in the dark. *Nature*, 395:890–894, 1998.

[76] Gerhard von der Emde and Steffen Fetz. Distance, shape and more: recognition of object features during active electrolocation in a weakly electric fish. *Journal of Experimental Biology*, 210(17):3082–3095, 2007.

[77] H. Wang. Shape identification in electro-sensing. https://github.com/yanncalec/SIES, 2013.

[78] Wei Wang, Jindong Liu, Guangming Xie, Li Wen, and Jianwei Zhang. A bio-inspired electrocommunication system for small underwater robots. *Bioinspiration & Biomimetics*, 12(3):036002, mar 2017.

[79] G.N. Watson. *A Treatise on the Theory of Bessel Functions*. Cambridge University Press, Cambridge, 1944.

[80] L. Xu, A. Krzyzak, and C. Y. Suen. Methods of combining multiple classifiers and their applications to handwriting recognition. *IEEE Transactions on Systems, Man, and Cybernetics*, 22(3):418–435, May 1992.

[81] Jie Zhou, Yunmin Zhu, X. Rong Li, and Zhisheng You. Variants of the greville formula with applications to exact recursive least squares. *SIAM Journal on Matrix Analysis and Applications*, 24(1):150–164, 2002.